STATUS OF THESIS

Title of thesis	STUDIES OF NOVEL AMINO ACID POLYMERIZED IONIC LIQUIDS FOR CARBON DIOXIDE CAPTURE

I MAISARA SHAHROM BINTI RAJA SHAHROM

hereby allow my thesis to be placed at the Information Resource Center (IRC) of Universiti Teknologi PETRONAS (UTP) with the following conditions:

1. The thesis becomes the property of UTP
2. The IRC of UTP may make copies of the thesis for academic purposes only.
3. This thesis is classified as

[ ] Confidential

[/] Non-confidential

If this thesis is confidential, please state the reason:

_____
_____
_____

The contents of the thesis will remain confidential for _____ years.

Remarks on disclosure:

_____
_____
_____

Endorsed by

_____ _____

Signature of Author | Signature of Supervisor

Permanent address:_____ | Name of Supervisor

No 6, Jalan Chemor Makmur 3, Desa | Assoc. Prof. Dr. Cecilia Devi Wilfred

Chemor Makmur, 31200 Chemor,

Perak

Date : | Date :

UNIVERSITI TEKNOLOGI PETRONAS

STUDIES OF NOVEL AMINO ACID POLYMERIZED IONIC LIQUIDS FOR CARBON DIOXIDE CAPTURE

by

MAISARA SHAHROM BINTI RAJA SHAHROM

The undersigned certify that they have read, and recommend to the Postgraduate Studies Programme for acceptance this thesis for the fulfillment of the requirements for the degree stated.

Signature: _____

Main Supervisor: Assoc. Prof. Dr. Cecilia Devi Wilfred

Signature: _____

Co-Supervisor: Assoc. Prof. Dr. Chong Fai Kait

Signature: _____

Head of Department: Assoc. Prof. Dr Hanita binti Daud

Date: _____

STUDIES OF NOVEL AMINO ACID POLYMERIZED IONIC LIQUIDS FOR CARBON DIOXIDE CAPTURE

by

MAISARA SHAHROM BINTI RAJA SHAHROM

A Thesis

Submitted to the Postgraduate Studies Programme

as a Requirement for the Degree of

DOCTOR OF PHILOSOPHY

FUNDAMENTAL OF APPLIED SICENCES

UNIVERSITI TEKNOLOGI PETRONAS

BANDAR SERI ISKANDAR,

PERAK

OCTOBER 2017

DECLARATION OF THESIS

Title of thesis | STUDIES OF NOVEL AMINO ACID POLYMERIZED IONIC LIQUIDS FOR CARBON DIOXIDE CAPTURE

I MAISARA SHAHROM BINTI RAJA SHAHROM

hereby declare that the thesis is based on my original work except for quotations and citations which have been duly acknowledged. I also declare that it has not been previously or concurrently submitted for any other degree at UTP or other institutions.

Witnessed by

Signature of Author

Signature of Supervisor

Permanent address:
No 6, Jalan Chemor Makmur 3,
Desa Chemor Makmur, 31200
Chemor, Perak

Name of Supervisor
Assoc. Prof. Dr. Cecilia Devi Wilfred

Date :

Date :

DEDICATION

My beloved mom and dad

Misalmah Ujang & Raja Shahrom Raja Kamarudin

My supportive husband

Mohd Nor Hilmy Md Dali

My addorable kids

Aimy Delisha & Adib Daniel.

ACKNOWLEDGEMENTS

Alhamdulillah, thank to the Almighty Allah S.W.T for His blessing and for giving me strength and guidance for me to complete this research as my PhD studies. Without His permission, I am not able to complete this research and finished this perfectly. I would like to record my gratitude to my supervisor Assoc. Prof. Dr. Cecilia Devi Wilfred and my co-supervisor Assoc. Prof. Dr. Chong Fai Kait and Prof. Dr. Yatimah Alias (Universiti Malaya) for their supervision and guidance from the very early stage of this research and throughout this PhD journey. It is an exhausting, emotional and struggle journey but somehow this giving me extraordinary experiences throughout the work.

My grateful thank to my beloved family especially my husband Mohd Nor Hilmy bin Md Dali, my daughter Aimy Delisha and my son Adib Daniel. Special dedicated for my mom Misalmah bt Ujang, my dad Raja Shahrom bin Raja Kamarudin, all my family member thank you very much for your prayers, moral support, great sacrifice, patience and encouragement for the completion of this work. Words fail me to express my appreciation to them. Their continuous support, love, confidence, encouragement, passions give me strength to complete this study. It is a pleasure to convey my gratitude to all member Center of Research in Ionic Liquids (CORIL), post doctorial, research officers, friends, students and lecturers. Thank you for their research attitude and consistent guidance throughout this work. Special thanks to our previous post doctorial, Dr Mohd Farid Ismail for his contribution on DFT calculation. To Fundamental and Applied Sciences Department (FASD), Centralized Analytical Laboratory (CAL), Chemical Engineering (CE) staff in UTP, thank you for their kind support for this period and their assistance for analyzing samples. I would like to thank everybody who was important to the successful realization of thesis, as well as expressing my apology that I could not mention personally one by one.

ABSTRACT

The existing processes for CO_2 removal in natural gas is by using alkanolamine which caused several drawbacks *i.e.*, high vapour pressure, corrosive nature and high energy input for regeneration. Therefore a new solvent to replace the alkanolamine is highly needed. Ionic liquids (ILs) are regarded as a potential option because they have negligible vapour pressure under ambient conditions and higher thermal stability. Much higher absorption capacity can be achieved if the CO_2 is chemically absorbed instead of physically. Amino acid have been used as anions due to the functionality of amine group and known as Amino Acid Ionic Liquids (AAILs). However, AAILs suffer the problem of having high viscosities. Amino Acid Polymerized Ionic Liquids (AAPILs), are much easier to handle in solid form with higher CO_2 capacity. In this research, eight different types of amino acids using arginine [Arg], lysine [Lys], histidine [Hist], taurine [Tau], proline [Pro], serine [Ser], alanine [Ala] and glycine [Gly] are synthesized. Different types of cations and alkyl chain length on the cation were also studied. The results showed that the highest CO_2 sorption capacity was obtained with [VBTMA][Arg] with 0.83 mol/mol and this increased to 1.14 mol/mol at 1 atm, 298 K after polymerization. Arginine, [Arg] comprises of multiple numbers of amine, thus accessability for CO_2 to react with amine is an advantage. By increasing the pressure to 10 bar, the CO_2 sorption increased to 2.77 mol/mol. The sorption decreased at higher temperature and full desorption occurred at 80 ^{o}C. The AAPILs also can be reusable with 86 % sorption capacity on fifth sorption. FTIR showed the formation of carbamic acid species after CO_2 sorption, hence proving the chemisorption occurred in AAPILs. From the BET model, it was confirmed that physical adsorption with multilayer formation occurred in AAPILs. Therefore, both chemisorption and physisorption are involved in AAPILs. CO_2 sorption capacity increases gradually with water. The selectivity of AAPILs towards different types of gases showed higher CO_2 sorption capacity with 12.9 wt%

compared to CH_4 (1.3 wt%) and N_2 (0.8 wt%). The degradation temperature and glass transition temperature also increase after polymerization. Four adsorption isotherm models were applied for the CO_2 adsorption *e.g.* Freundlich, Langmuir, Dubinin Raduschkevich and Temkin isotherm. The Freundlich model provides the best fit to the experimental data. The adsorption was also modeled through various kinetic models *e.g.* pseudo first order, pseudo second order, Elovich's kinetic model and an intra-particle diffusion model. It was found that pseudo first order model was well fitted with the kinetic data. Thermodynamic analysis proves that the CO_2 sorption is spontaneous process (ΔG -3.16 kJ/mol) and exothermic in nature with ΔH is -30.3 kJ/mol. According to DFT calculation, CO_2 that attached with one primary amine in argininate shows that ΔH calculated is -30.4 kJ/mol which good agreement with experimental ΔH. This proves it follows 1:1 mechanism. As a conclusion, AAPILs is a good alternative to replace the usage of alkanolamine (0.5 mol/mol) to capture CO_2 in natural gas. The presence of amino acids as anion makes the AAPILs greener and easier to handle. In industry, this will be beneficial due to non volatile, reusable and low energy input for regeneration.

.

ABSTRAK

Pada masa kini, proses penyingkiran karbon dioksida (CO_2) dalam gas asli adalah dengan menggunakan alkanolamina. Walaubagaimanapun, ianya memberikan beberapa kesan buruk seperti tekanan wap yang tinggi, sifat menghakis dan memerlukan tenaga yang tinggi untuk penggunaan semula. Oleh itu, pelarut terbaru diperlukan bagi menggantikan penggunaan alkanolamina ini. Cecair ionik (ILs) merupakan alternatif terbaru kerana ILs mempunyai sifat tekanan wap yang rendah dan kestabilan terma yang tinggi. Lebih banyak penyerapan CO_2 pada ILs boleh berlaku pada penyerapan kimia berbanding fizikal. Asid amino dipilih sebagai anion dan dikenali sebagai asid amino cecair ionik (AAILs). Walaubagaimanapun, AAILs yang terhasil mempunyai kelikatan yang tinggi oleh itu dengan pempolimeran AAILs dikenali sebagai asid amino polimer cecair ionik (AAPILs), yang bersifat pepejal dan mudah untuk dikendalikan. Lapan jenis asid amino digunakan sebagai anion seperti arginina [Arg], lysina [Lys], histidina [Hist], taurina [Tau], prolina [Pro], serina [Ser], alanina [Ala] dan glysina [Gly]. Jenis kation dan pengaruh panjang rantai alkil juga turut dikaji. Keputusan menunjukkan penyerapan CO_2 yang tertinggi adalah pada [VBTMA][Arg] dengan 0.83 mol/mol dan meningkat pada 1.14 mol/mol setelah dipolimerkan, poly[VBTMA][Arg]. Ini adalah kerana [Arg] mempunyai bilangan kumpulan amino yang banyak oleh itu tindak balas antara CO_2 dan amino adalah tinggi. Apabila tekanan meningkat kepada 10 bar, penyerapan CO_2 juga meningkat kepada 2.77 mol/mol tetapi berkurangan pada suhu setinggi 80 ^{o}C apabila terjadi nyahserapan sepenuhnya. AAPILs juga boleh diguna semula dengan peratus penyerapan sebanyak 86% pada penyerapan kali ke 5. Bagi menentukan mekanisma penyerapan, pencirian FTIR menunjukkan wujud kumpulan asid karbamik yang terhasil dari tindak balas CO_2 dan kumpulan amino pada AAPILs yang membuktikan berlakunya penjerapan kimia. BET model pula menunjukkan penyerapan fizikal turut berlaku dengan pembentukkan multilapisan pada AAPILs.

Penambahan air pada AAPILs juga menunjukkan penyerapan CO_2 meningkat. AAPILs turut selektif dalam penyerapan gas di mana penyerapan CO_2 adalah tertinggi sebanyak 12 wt% berbanding gas metana (CH_4) (1.3 wt%) dan gas nitrogen (N_2) (0.8 wt%). Kestabilan terma juga menunjukkan suhu degradasi dan suhu peralihan kaca meningkat pada AAPILs. Ini menunjukkan setelah pempolimeran AAPILs berlaku, peningkatan pada penyerapan CO_2 dan kestabilan terma dapat dilihat. Pada tekanan yang tinggi, penyerapan fizikal juga berlaku oleh itu empat isoterma penyerapan dijalankan menggunakan model Freundlich, Langmuir, Dubinin Raduschkevich dan model Temkin. Model Freundlich merupakan model terbaik di mana memberikan pekali regresi terbaik. Kinetik penyerapan CO_2 juga dikaji menggunakan empat model kinetik iaitu pseudo tertib pertama, pseudo tertib kedua, model kinetik Elovich dan model difusi intra-partikel. Daripada pekali regresi, pseudo tertib pertama menunjukkan model kinetik terbaik. Selain itu, analisis termodinamik membuktikan bahawa penyerapan CO_2 adalah secara spontan (ΔG -3.16 kJ/mol) dan eksotermik dengan ΔH -30.3 kJ/mol. Menurut pengiraan DFT, satu mol CO_2 yang bertindak balas dengan satu mol arginina memberikan pengiraan ΔH sebanyak -30.4 kJ/mol di mana nilai entalpi ini sama dengan nilai entalpi eksperimen lalu membuktikan mekanisma 1:1 tercapai. Kesimpulannya, AAPILs merupakan alternatif terbaik dalam menggantikan penggunaan alkanolamina (0.5 mol/mol). Dengan menggunakan organik asid amino sebagai anion, ILs yang terhasil adalah lebih hijau dan lebih mudah diurus disebabkan oleh AAPILs yang bersifat pepejal. Di industri, ini adalah sangat baik disebabkan oleh sifat AAPILs yang tidak meruap, boleh diguna semula dengan lebih tinggi penyerapan CO_2 dapat dicapai.

In compliance with the terms of the Copyright Act 1987 and the IP Policy of the university, the copyright of this thesis has been reassigned by the author to the legal entity of the university,

Institute of Technology PETRONAS Sdn Bhd.

Due acknowledgement shall always be made of the use of any material contained in, or derived from, this thesis.

© Maisara Shahrom Raja Shahrom, 2017
Institute of Technology PETRONAS Sdn Bhd
All rights reserved.

TABLE OF CONTENT

ABSTRACT vii
ABSTRAK ix
LIST OF FIGURES xvi
LIST OF TABLES xviii
CHAPTER 1: INTRODUCTION 1
1.1 Carbon dioxide (CO_2) Removal from Natural Gas 1
1.2 CO_2 Emissions 2
1.3 CO_2 Capture Technologies 3
1.3.1 CO_2 removal by amines 3
1.3.2 CO_2 removal by membrane 4
1.3.3 CO_2 removal by solid sorbents 6
1.4 Ionic Liquids (ILs) 8
1.5 Ionic Liquids (ILs) for CO_2 capture 9
1.6 Novelty of Amino Acid Polymerized Ionic Liquids (AAPILs) 10
1.7 Problem Statements 11
1.8 Objectives 12
1.9 Scope of Studies 12
1.10 Thesis Outline 13
CHAPTER 2: LITERATURE REVIEW 15
2.1 Physical Properties of Ionic Liquids (ILs) 15
2.1.1 Thermal properties of ILs 19
2.2 Review on CO_2 Sorption 22
2.2.1 CO_2 sorption on alkanolamine 22
2.2.2 CO_2 sorption on room temperature ionic liquids (RTILs) 24
2.2.3 CO_2 sorption on task specific ionic liquids (TSILs) 27
2.2.4 CO_2 sorption on amino acid ionic liquids (AAILs) 30
2.2.5 CO_2 sorption on polymerized ionic liquids (PILs) 39
CHAPTER 3: RESEARCH METHODOLOGY 44
3.1 Materials 49
3.2 Synthesis of Ionic Liquids, RTILs 49

3.2.1 Synthesis of (vinylbenzyl)tritethylammonium chloride, [VBTEA][Cl] 49
3.2.2 Synthesis of (vinylbenzyl)tributylammonium chloride, [VBTBA][Cl] 50
3.2.3 Synthesis of (vinylbenzyl)methylimidazolium chloride, [VBMI][Cl] 50
3.2.4 Synthesis of (vinylbenzyl)methylpiperidinium chloride, [VBPPN][Cl] 50
3.3 Synthesis of the monomers, AAILs 51
3.3.1 Anion exchange from Cl^- to OH^- 51
3.3.2 Neutralization with amino acid 51
3.4 Synthesis of amino acids polymerized ionic liquids (AAPILs) 52
3.5 Characterization of Ionic Liquids 53
3.5.1 Structure analysis 53
3.5.2 Density 54
3.5.3 Water content 54
3.5.4 Chloride content 54
3.5.5 Thermal stability 54
3.5.6 Surface morphology 55
3.5.7 Surface Area and Porosity (SAP) Analyzer 55
3.6 CO_2 sorption measurement 55
3.6.1 Adsorption Isotherm Measurement 57
3.7 COSMO-RS 59
3.8 Density Functional Theory (DFT) Study of Amine Molecular 60
3.8.1 Thermochemistry output 61
CHAPTER 4: RESULTS AND DISCUSSION 64
4.1 Identification and Structural Analysis of AAILs and AAPILs 64
4.2 Functional Group Identification 67
4.3 Physical Properties 69
4.4 Synthesis attempts of different backbone for polymerization 71
4.5 Thermal stability on AAILs and AAPILs 75
4.5.1 Effect of anion on thermal stability 75
4.5.2 Effects of cation on thermal stability 76

4.6 Morphology Micrograph 78
4.7 Carbon Dioxide Sorption 80
4.7.1 Comparison of CO_2 sorption capacities with MEA, RTILs, AAILs and AAPILs 80
4.7.2 Effects of anion on CO_2 sorption 83
4.7.2.1 Activity coefficient at infinite dilution, $\gamma s\infty$ by COSMO-RS 86
4.7.2.2 σ-Profile of CO_2 and anions, [Arg] and [Ala] 87
4.7.3 Effects of cation on CO_2 sorption 89
4.7.4 Effect of pressure 91
4.7.4.1 The Brunauer-Emmett-Teller (BET) Model 92
4.7.5 Effect of Temperature 94
4.7.6 Recyclability of AAPILs 96
4.8 Adsorption Isotherm 98
4.9 Thermodynamic analysis 103
4.10 Kinetic Studies on poly[VBTMA][Arg] at different temperature 106
4.10.1 Pseudo-first order kinetic model 107
4.10.2 Pseudo second order kinetic model 108
4.10.3 Elovich kinetic model 110
4.10.4 Intra-particle diffusion kinetic model 111
4.11 Evaluation of activation energy 113
4.12 Density Functional Theory (DFT) on Thermochemistry Calculation 114
4.13 Proposed Mechanism of poly[VBTMA][Arg] with CO_2 117
4.14 Characterization of AAPILs after CO_2 sorption 119
4.15 Effect of water to AAPILs 121
4.16 Comparison of gas solubility in poly[VBTMA][Lys] 123
CHAPTER 5: CONCLUSIONS AND RECOMENDATIONS 126
5.1 Conclusions 126
5.2 Recommendations 128
APPENDIX A: NMR SPECTRUMS OF ALL AAPILS AND THEIR MONOMERS 153
APPENDIX B: FTIR SPECTRUMS OF ALL AAPIL SYNTHESIZED AND CALIBRATION CURVE FOR CHLORIDE CONTENT 166

APPENDIX C: TGA AND DSC THERMOGRAM 174
APPENDIX D: SEM MICROGRAPHS.....179
APPENDIX E: CO_2 SORPTION DATA.....186

LIST OF FIGURES

Figure 1.1: Reaction of amine and CO_2 3
Figure 1.2: Schematic of a gas separation membrane [6]. 5
Figure 1.3: Cations and anions usually used in ionic liquids synthesis 8
Figure 2.1: Design of amino acids for functionalised ILs 16
Figure 2.2: Proposed mechanism of [EMIM][OAc] 26
Figure 2.3: Proposed mechanism of CO_2 absorption by ether functionalized ILs. 29
Figure 2.4: Proposed mechanism of CO_2 absorption by acid functionalized ILs 30
Figure 2.5: The pathway for the formation of the $[N_{66614}][Lys]$-CO_2 [105] 32
Figure 2.6: Proposed mechanism of [aemmim][tau] with CO_2 [119] 33
Figure 2.7: Proposed CO_2 absorption process by $[aEMMIM][BF_4]$ [120] 33
Figure 2.8: The formation of carbamate 36
Figure 3.1: Synthesis route of [VBTEA][Cl] 49
Figure 3.2: Synthesis route for [VBMI][Cl] 50
Figure 3.3: Synthesis route of [VBPPN][Cl] 51
Figure 3.4: Synthesis route of the monomers, AAILs with [VBTMA] as cation 52
Figure 3.5: Polymerization of AAILs to AAPILs 53
Figure 3.6: Schematic diagram for gas absorption/adsorption cell 57
Figure 3.7: Flowchart of the KS SCF procedure 62
Figure 3.8: Flowchart for overall methodology 63
Figure 4.1: FTIR spectrum for [VBTMA][Gly] and poly[VBTMA][Gly] 67
Figure 4.2: Ion Chromatogram of chloride, on [VBTMA][OH] 70
Figure 4.3: Different backbone of AAPILs 72
Figure 4.4: ^{1}H-NMR for (a) [METMA][Cl] and (b) [METMA][Gly] 73
Figure 4.5: ^{1}H-NMR for (a) [ABIM][Gly] (b) polymerized [ABIM][Gly] 74
Figure 4.6: TGA analysis for [ABIM][Gly] 74
Figure 4.7: SEM images for AAPILs synthesized 79
Figure 4.8: CO_2 sorption on AAILs, AAPILs, RTILs and MEA 81
Figure 4.9: Degradation temperature on poly[VBTMA][Pro] at 6h and 24h 82
Figure 4.10: CO_2 sorption on poly[VBTMA][Pro] at 6h and 24h reaction times 83

Figure 4.11: CO_2 sorption on AAPILs with different anions 86
Figure 4.12: σ-profile of CO_2, [Arg] and [Ala] as computed by COSMO-RS 88
Figure 4.13: CO_2 sorption on different cation with fixed [Lys] anion at 1 bar, 298 K 89
Figure 4.14: CO_2 sorption on different of alkyl chain length 90
Figure 4.15: CO_2 sorption with increasing pressure at 298 K 91
Figure 4.16: BET physisorption isotherm on poly[VBTMA][Arg] at higher pressure93
Figure 4.17: BET isotherm model plot 94
Figure 4.18: CO_2 sorption at different temperatures.....95
Figure 4.19: CO_2 sorption on poly[VBTMA][Arg] at different temperature 96
Figure 4.20: Recylability of poly[VBTMA][Arg] 97
Figure 4.21: FTIR spectrum on poly[VBTMA][Arg].....98
Figure 4.22: Adsorption isotherms a) Freundlich b) Langmuir c) Dabunin-Radushkevic and d) Temkin isotherm by linear regression method for poly[VBTMA][Arg] at 298 K, 313 K and 333 K. 100
Figure 4.23: Thermodynamic parameters by using van Hoff's equation 104
Figure 4.24: Kinetic plot of pseudo first order model at various temperatures. 108
Figure 4.25: Kinetic plot of pseudo second order model at various temperatures. ...109
Figure 4.26: Elovich plot of CO_2 sorption at various temperatures.....111
Figure 4.27: Intra-particle diffusion model at different temperatures 112
Figure 4.28: Fitting of Arrhenius equation 113
Figure 4.29: Proposed mechanism of AAILs with CO_2 [68] 117
Figure 4.30: Proposed mechanism of poly[VBTMA][Arg] with CO_2 118
Figure 4.31: FTIR before and after CO_2 sorption of poly[VBTMA][Arg].....119
Figure 4.32: Carbamic acid formed at argininate 120
Figure 4.33: Effect of water to AAPILs.....122
Figure 4.34: Comparison of gases on poly[VBTMA][Lys] at 1 bar, 303 K.....124

LIST OF TABLES

Table 1.1: Chemical compositions in crude natural gas [1] 2
Table 1.2: CO_2 permeability and selectivity of polymeric membranes [6] 6
Table 2.1: Absorption capacity of CO_2 by mixture of imidazole-based ILs [109] 25
Table 2.2: Absorption capacity of aqueous solutions of 15% ILs + 15% MDEA 34
Table 2.3: Literature data for CO_2 sorption by AAILs. 37
Table 2.4: Literature data for CO_2 sorption in PILs 43
Table 3.1: Polymer name and monomer structure 45
Table 3.2: The non-linear and linearized equation of the isotherm models 58
Table 4.1: ^{1}H-NMR peaks for AAILs and AAPILs 64
Table 4.2: FTIR peaks, intensity and functional groups of AAPILs 68
Table 4.3: Physical properties of AAPILs synthesized 70
Table 4.4: Degradation temperature (T_d) and glass transition temperature (T_g) 75
Table 4.5: Thermal stability on AAPILs with different cation and fixed [Lys] anion 77
Table 4.6: Textural analysis before and after CO_2 sorption on poly[VBTMA][Lys] . 80
Table 4.7: CO_2 absorption on AAILs and AAPILS with fixed [VBTMA] cation 84
Table 4.8: Activity coefficient, $\boldsymbol{\gamma s}\infty$ of CO_2 in ILs 87
Table 4.9: CO_2 sorption of different cation with [Lys] as anion 90
Table 4.10: CO_2 sorption on AAPILs at different pressure 91
Table 4.11: CO_2 sorption on poly[VBTMA][Arg] at different temperature 95
Table 4.12: Adsorption isotherm parameters at 298 K, 313 K and 333 K 101
Table 4.13: Thermodynamics parameters of CO_2 adsorption 105
Table 4.14: Kinetic parameter of Pseudo first order 108
Table 4.15: Kinetic parameter of Pseudo second order 109
Table 4.16: Kinetic parameters of Elovich isotherm 111
Table 4.17: Kinetic parameters of CO_2 sorption onto poly[VBTMA][Arg] 112
Table 4.18: Molecular structures and enthalpy reaction of argininate and CO_2 115
Table 4.19: Polarizabilities (α) and gas sorption of each gas 124

NOMENCLATURE

CO_2	Carbon dioxide
ILs	Ionic liquids
AAILs	Amino acid ionic liquids
AAPILs	Amino acid polymerized ionic liquids
PILs	Polymerized ionic liquids
DSC	Differential Scanning Coulomatric
TGA	Thermogravimetric Analyzer
FTIR	Fourier Transform Infra Red
COSMO-RS	Conductor-like Screening Model for Realistic Solvents
DFT	Density functional theory
^{1}H-NMR	Proton- Nuclear Magnetic Resonance
AA	Amino acid
RTILs	Room temperature ionic liquids
TSILs	Task specific ionic liquids
MEA	monomethanolamine
DEA	diethanolamine
MDEA	methyldiethanolamine
[apbim]	1-(3-propyamino)-3-butylimidazolium
[PF_6]	Hexafluorophosphate
[BF_4]	Tetrafluoroborate
[Tf_2N]	bis(trifluoromethylsulfonyl)amide
[VBTMA]	Vinylbenzyltrimethylamoonium
[METMA]	Methacryloyloxylethyltrimethylammonium
[VBMI]	Vinylbenzylimidazolium
[VBPPN]	Vinylbenzylpiperidinium
[VBTEA]	Vinylbenzyltriethylammonium
[VBTBA]	Vinylbenzyltributylammonium
[BIEMA]	2-(1-butylimidazolium-3-yl)ethyl methacrylate
[Gly]	Glycinate
[Ala]	Alanate

[Ser]	Serinate
[Pro]	Prolinate
[Tau]	Taurinate
[Hist]	Histidinate
[Lys]	Lysinate
[Arg]	Argininate
[aP_{443}]	(3-aminopropyl)tributylphosphonium
[Trp]	Tryptophan
[Tyr]	Tyrosine
[phe]	Phenylalanine
[Val]	Valine
[Leu]	Leusine
[bis(mim)C_6]	Bishexymethyllimidazolium
[hmim]	1-hexyl-3-metylimidazolium
[bmim] / [C_4mim]	1-butyl-3-methylimidazolium
[N_{111}-C_6-mim]	Trimethelammoniumhexylimidazolium
[P_{4444}]	Tetrabutylphosphonium
[P_{66614}]	trihexyl(tetradecyl)phosphonium
[TFMS]	Trifluoromethanesulfonate
[PTS]	p-toluenesulfonate
[DADMA]	(diallyldimethylammonium
[Ac]	Acetate
[TFAc]	Trifluoroacetate
[MS]	Methanesulfonate
[HFB]	Heptaflurobutyrat
[Bz]	Benzoate
[NH_2-emim]	Amine-ethylmethylimidazolium
[CH_3COO]	Acetate
[EMIM][OAc]	Ethylmethylimidazolium acetate
[C_4py]	Tetramethylpyridinium
[Dca]	Dicyanamide
[C_2Omim]	1-ethylether-3-methylimidazolium
[Cmmim]	1-acetic acid-3-methylimidazolium

[EDTAH]	Ethylenediamine-proton
[MEAH]	Monoethanaolamine-proton
[TETAH]	Triethylenetetraamine-proton
[N_{66614}]	trihexyl(tetradecyl)ammonium
[aemmim]	1-aminoethyl-2, 3-dimethylimidazolium
[N_{1111}]	Tetramethylammonium
[N_{2222}]	Tetraethylammonium
[C_2Ohmim]	1-hydroxyethyl-3-methylimidazolium
[HHim]	1,3-bis(2-hydroxylethyl)-imidazolium
[EEim]	1,3-Bis(2-methoxy-2-oxyl ethyl) imidazolium
[MABI]	1-(2- methacryloyloxy)ethyl-3-butylimidazolium
[VBBI]	Vinylbenzylbutylimidazolium
[ABIM]	1-allyl-3-butylimidazolium

LIST OF SYMBOLS

T_g	Glass transition temperature (^oC)
T_d	Degradation temperature (^oC)
Z	Compressibility factor (bar.K)
P_{eq}	Pressure equilibrium (bar, atm)
K_L	Langmuir constant (g/mmol)
K_F	Freundlich constant ($mmol^{1-(1/n)}.g^{1/n}.g^{-1}$)
q_m	Maximum adsorption capacity (bar, atm)
q_e	Amount adsorb (mmol/g)
λ	D-R constant (mol^2/J^2)
ω	Polanyi potential
K_T	Temkin constant (cm^3/g.bar)
R^2	Correlation coefficient
ΔS	Change of entropy (kJ/mol.K)
ΔH	Change of enthalpy (kJ/mol)
ΔG	Gibbs energy (kJ/mol)
ε	Relative error (%)
q_t	Adsorb capacity at particular time (mmol/g)
K_1	Pseudo first order rate constant (1/min)
K_2	Pseudo second order rate constant (1/min)
α	Initial adsorption rate / polarizabilities (cm^3)
n	Freundlich constant (dimensionless)
R_L	Dimensionless separation factor
β	Extent of surface coverage
σ	Sigma
γ_s^∞	Activity coefficient infinite dilution

CHAPTER 1

INTRODUCTION

1.1 Carbon dioxide (CO_2) Removal from Natural Gas

Natural gas is the gas produced from hydrocarbon reservoirs which comes from the reservoir along with the oil. It consists largely of methane (CH_4), ethane (C_2H_6), propane (C_3H_8) and butane (C_4H_{10}), some higher alkanes (C_5H_{12} and above), nitrogen (N_2), oxygen (O_2), carbon dioxide (CO_2) and hydrogen sulphide (H_2S). It is used as an industrial and domestic fuel, and also used as reactant in chemical synthesis to make carbon black, carbon nanotube and others [1]. Natural gas itself might be considered a very interesting gas because of colorless, shapeless and odourless in its pure form. Natural gas is of great importance not only as a source of energy, but also as a raw material for the petrochemical industry [2]. It is a combustible mixture of hydrocarbon gases and gives off energy when it burned [1, 3].

However, the challenge in natural gas processing is that many raw natural gases are contaminated with undesired components such as H_2S and CO_2 [4]. Therefore, the removal of acid gases (CO_2, H_2S and other sulphur components) is warranted [1, 5]. CO_2, H_2S and any other acid gases must be removed from natural gas because in the presence of water, these impurities can form acids that corrode pipelines and any other components [6]. In addition, CO_2 provides no heating value and must be removed to meet gas quality specifications before distribution to users [4].

In Malaysia, before purification process, the natural gas consists of several gaseous and impurities as shown in Table 1.1. Removal of acid gases from raw natural gas has to be performed not only because of environmental restrictions but also technological problems during gas transportation and commercialization. There are regulation of processing and transportation that requires the removal of these

contaminants [7]. The maximum level of CO_2 in natural gas permitted to customers by pipeline is typically less than 3% although local contracts may stipulate quality specifications different to these values [4]. The captured CO_2 can be pumped back into the reservoir which reduces the atmospheric pollution by impurities like H_2S and the emissions of greenhouse gases as CO_2 [8].

Table 1.1: Chemical compositions in crude natural gas [1]

Chemical Name	Chemical Formula	Percentage (wt %)
Methane	CH_4	40-50
Ethane	C_2H_6	5-10
Propane	C_3H_8	1-5
Carbon dioxide	CO_2	20-3
Hydrogen sulphide	H_2S	0-1

1.2 CO_2 Emissions

CO_2 emissions from fossil fuel combustion (coal, oil and natural gas) for energy production are also the main source of energy-related emissions [9]. This CO_2 emissions are another economical challenge [10]. Approximately 25% of the total CO_2 emissions in the world are produced from combustion for electricity generation. According to Karadas *et al.* [11], the CO_2 emissions value will increase from 19.4 % in 2005 to 25% in 2030, which is at a rate 2.1% per year due to the combustion of fossil fuel.

Although the characteristics of CO_2 capture from natural gas and from flue gas of conventional fossil fuel fired power plants are very different, it is clear that both problems are closely related. Thus, similar approaches are frequently used for both cases. Therefore, high performance technologies with new cost effective for capturing CO_2 are being researched [6, 8, 9, 12]. The main strategies for natural gas processing are identical to those used in CO_2 capture technologies [7].

1.3 CO_2 Capture Technologies

The current technologies for CO_2 capture and separation mainly include solvents, membrane and sorbents [4]. The mechanism for CO_2 capture depends on the chemistry and the capturing approaches or the absorbent materials [13].

1.3.1 CO_2 removal by amines

Mostly alkanolamines, such as monoethanolamine (MEA), diethanolamine (DEA) and methyldiethanolamine (MDEA) are being used for CO_2 capture through carbamate or carbonate formation. Amines are so effective for CO_2 capture because of their properties such as high reactivity with CO_2, high absorbing capacity (in terms of mass of CO_2) and CO_2 selectivity [14].

The absorption of CO_2 in amine based is mostly acid-base chemistry [5]. Amines readily react with acids to form acid-base salts [15]. This structural characteristic plays the major role in the acid gas removal capabilities of the various amine solvents [3, 16].

Figure 1.1 shows the formation of carbamate spesies after reaction of amine and CO_2. In Equation 1.1 shows a direct reaction between CO_2 and amine to form zwitterions. These zwitterions react with a base to lose its proton. This base can be any base such as amine, OH^- and H_2O as shown in Equation 1.2.

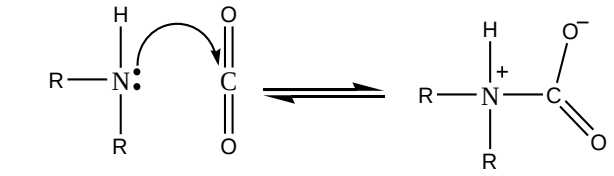

1.1

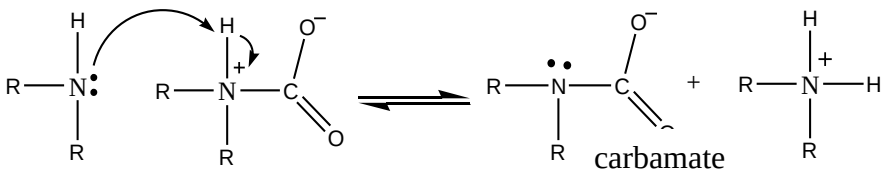

1.2

Figure 1.1: Reaction of amine and CO_2

The “carbamate reaction” occurred in Equation 1.2, only occurs with primary and secondary amines. The stoichiometry of the carbamate reaction indicates that 2 mol of

amine react with 1 mol of CO_2. Thus, the capacity of CO_2 captured is limited to 0.5 mol CO_2 per mol amine [8].

However, the carbamate can undergo partial hydrolysis as shown in Equation 1.3 to form bicarbonate and regenerate free amine. Thus, CO_2 loading greater than 0.5 moles is possible through the hydrolysis of the carbamate intermediate to bicarbonate [17].

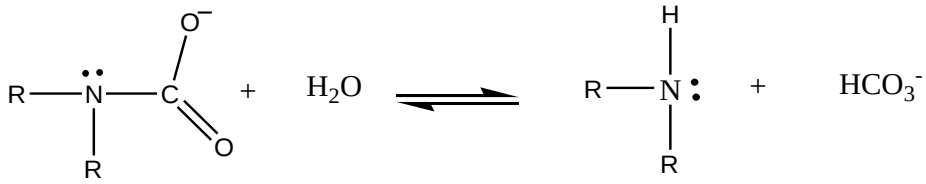

1.3

However, there are drawbacks linked with amines such as high vapour pressure, corrosive in nature and requires high energy input for regeneration. The high vapour pressure allows emission of amine gases into the air upon heating. These gases are unstable in nature thus giving them the possibility of producing dangerous toxins such as nitrosamine, nitrasmine and amides [18-21]. Nitrosamines are of the most concern as they are cryogenic and toxic to humans even at low levels. The amines itself are also corrosive especially MEA which corrodes the equipment. The regeneration process leads to high energy consumption in order to break the chemical bonds formed between the CO_2 and amine [22]. The intensive energy use to break the chemical bonds between the absorbents and the absorbed CO_2 in the regeneration step is ΔH = -80 to -64 kJ/mol for bicarbonate formation or -101 kJ/mol for carbamate formation. This represents a high operation expense due to the energy cost related to the regeneration step [23].

1.3.2 CO_2 removal by membrane

CO_2 removal from natural gas also uses membranes or a thin barrier that allows passage of certain substances. The membrane acts as a filter to remove one or more gas components from a mixture [6, 24]. Some are used in an industrial scale and have the possibility of being implemented into the process of CO_2 capture [6, 22]. Membrane separation technology is based on the interaction of specific gases with the membrane material by a physical or chemical interaction. Membranes with immobilized amine or alkali carbonate solutions attach to amine functionality can be

classified as a chemical absorption process. By modifying the material, the rate at which the gases pass through can be controlled [22].

There are two characteristics that describe the performance of a membrane which is permeability and selectivity. Permeability is defined as the volume of a gas species passing through the membrane per unit time and area. Selectivity quantifies a membranes preference to pass one gas species over another. This permeability and selectivity of membranes are strongly dependent upon gas stream characteristic (*i.e.* velocity, gas component molecular weight and kinetic diameter) [6]. Figure 1.2 shows a general schematic of a gas separation membrane.

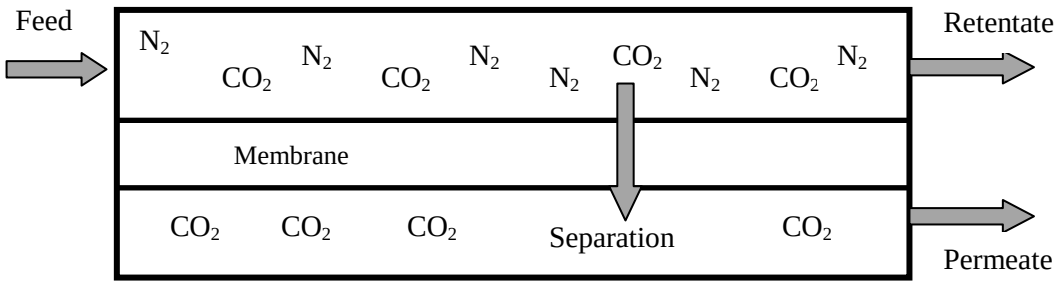

Figure 1.2: Schematic of a gas separation membrane [6].

Gas mixtures can be separated with porous and nonporous membranes.The porous membrane acts as a boundary between gas and liquid, whereby a non-porous membrane allows selective and controlled transfer of a species from one phase to another phase which separated by membrane. By using non porous hollow fibers, the separation is normally regarded as a rate governed membrane separation process. This kind of polymeric membrane requires a pressure upstream for removal efficiency which restricts the application. Meanwhile, for the porous membrane, the driving forces, transport mechanisms, and basis for selectivity reside in the two contacting phases, either liquid/liquid or gas/liquid. The selectivity is governed by the partitioning characteristics between the two phases. Therefore, under certain conditions, the membrane pore size can also influence the solute selectivity [25].

Polymeric membranes generally is non porous and gas permeation is described by the solution diffusion mechanism. This is based on the solubility of specific gases within the membrane and their diffusion through the dense membrane matrix. The separation is not just dependent upon molecular size but also relies on the chemical

interaction between the gases and the polymer [24]. It also exhibit high CO_2 permeability but low selectivity. This can be controlled by altering the pressure, temperature and polymer concentration during membrane synthesis. This polymeric membrane is susceptible to aging, plasticization and degradation at higher temperature [18].

There are variety of polymeric membranes which provide good permeability and selectivity towards CO_2 in CO_2/N_2 gas streams [26]. These includes polyimides, polycarbonates, polyethyleneoxide (PEO), polyacetylenes, polyaniline, poly(arylene ethers), polyarylates, polyphenylene ethers and polysulfone. The CO_2 permeability and selectivity of the most popular polymeric membranes is shown in Table 1.2.

Table 1.2: CO_2 permeability and selectivity of polymeric membranes [6]

Material	CO_2 permeability (barrer)	CO_2/N_2 selectivity
polyarylate	5-85	10-30
polycarbonate	5-110	15-26
Polyimide	5-450	5-55
polysulfone	5-110	10-33

Generally, polyimide has high permeability and CO_2 selectivity which makes them more attractive as a membrane compared to the others [6].

1.3.3 CO_2 removal by solid sorbents

A variety of materials have been studied as CO_2 sorbents through chemical reactions and physical adsorptions [18]. Aqueous amine solution exhibit disadvantages such as low contact area between gas and liquid, low CO_2 loading and severe adsorbent corrosion. Therefore, solid adsorption process may be an alternative to achieve the CO_2 capture purpose [20]. There are variety of solid adsorbents for CO_2 capture including microporous and mesoporous materials which is carbon-based sorbents such as activated carbon and carbon molecular sieves, zeolites, metal oxides and others.

Carbonaceous adsorbents such as activated carbon have been widely used for CO_2 capture due to their wide availability, low cost, high thermal stability and low

sensitivity to moisture. However, in a range of 50-120 ^{o}C, the carbonaceous materials exhibit low selectivity in operation due to high sensitivity in temperature. Studies showed that activated carbon and charcoal were shown to exhibit moderate adsorption selectivity for CO_2/N_2 at low pressures below 1 atm [27].

Zeolites are amongst the most widely reported physical adsorbents for CO_2 capture. It largely affected by their size, charge density and chemical composition of cations in their porous structures [28]. The interaction between CO_2 molecules and modified basic sites are through the formation of covalent bonding [29]. Although CO_2 adsorption can be enhanced by these approaches, there exist several drawbacks. The result showed that the CO_2 adsorption capacity and the CO_2/N_2 selectivity are relatively low. Besides the CO_2 adsorption capacity greatly declines in the presence of moisture in gas because of their highly hydrophilic character, thus a high regeneration temperature (above 300 ^{o}C) is needed [30].

Metal oxides (such as CaO and MgO) are promising capture materials given their ability to retain high adsorption capacities at temperatures above 300 ^{o}C. This operation defined as carbonation-calcination cycle: the carbonation reaction of CO_2 with solid CaO at 600 – 650 ^{o}C precipitates calcium calbonate ($CaCO_3$), while the reverse calcinations reaction regenerates the oxide at 800 – 850 ^{o}C [31]. However, the degradation of adsorbents has been observed after several cycles. To improve oxide materials, metals containing lithium such as Li_2ZrO_3 and Li_4SiO_4 have recently attracted attention for their high CO_2 adsorption capacities [32].

Metal-organic frameworks (MOFs) also have attracted significant interest in the recent years due to their remarkably high surface area, controllable pore structures and tunable pore surface properties. These properties can be easily tuned by changing the metallic clusters or the organic ligands. MOFs exhibit exceptional CO_2 adsorption capacity to deal with pure CO_2 at high pressures. However, their adsorption capacities are dramatically reduced when they are exposed to a gas mixture [33]. Although carbonaceous and MOFs materials seem to be as promising CO_2 adsorbents, the operations are at high pressures and low temperatures. It also showed that low selectivity is the major drawback for most physical adsorbents.

1.4 Ionic Liquids (ILs)

Ionic liquids (ILs) are a new class purely ionic salt-like materials that are liquid at room temperature with a low melting point (below 100 ^{o}C) are commonly composed of ions with combinations of organic cations and organic / inorganic anions. Therefore, ILs have been highly promoted as "*designer solvents*" as they can be designed by appropriate combinations of various cations and anions which increases their potential applications [34]. Over the last few years, ILs have been popularly used as solvents for organic synthesis and also been used as media for extraction processes and also known as greener solvents as they will replace volatile organic solvents in several chemical reactions [35, 36].

The first ionic liquid was discovered during World War I, in 1914, in the field of explosives research. It was ethylammonium nitrate with a melting point of 12 ^{o}C [37]. Nowadays, around 10^{18} ILs have been predicted and could be synthesized by combining different ions [38].

Chemically, the ionic liquids are composed of an organic asymmetric cation such as imidazolium, ammonium, phosphonium, or pyridinium species with one or more alkyl groups attached to the nitrogen or carbon atoms [39]. The most employed anions which influence the ionic liquids properties commonly used halides, mineral acid anions, and polyatomic inorganics species like PF_6^-, BF_4^- [40] as shown in Figure 1.3.

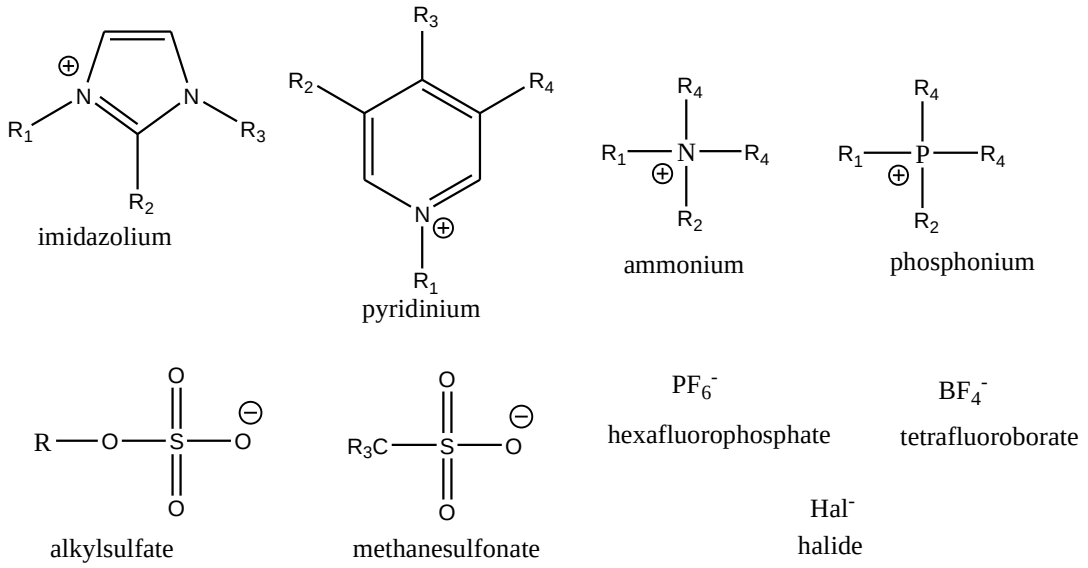

Figure 1.3: Cations and anions usually used in ionic liquids synthesis

The physical and chemical properties of the ionic liquids are determined by the nature of cation and anion. Therefore it is possible to achieve specific chemical properties by tuning the combinations of cations and anions [41]. Some properties such as thermal stability and miscibility depend on the anion while others such as viscosities, surface tension and density depend on the alkyl chain in the cation and/or shape or symmetry [42].

The use of ILs to replace conventional materials has received considerable attention as they are potentially safer and cleaner due to their extremely low vapor pressure, if the ionic liquids are properly chosen [43]. ILs have been extensively studied in different areas such as batteries [44, 45], green solvents [46, 47], CO_2 capture [48, 49], biopolymer dissolution [50-54] and others applications such as [42] liquid-liquid extraction [55, 56] or in membrane separations [57-59].

1.5 Ionic Liquids (ILs) for CO_2 capture

Among the many potential absorbents studied, ILs are regarded as a potential option for CO_2 capture because they typically have negligible vapour pressure under ambient conditions [60, 61]. The physico-chemical properties such as viscosity and density can usually be tuned to suit the intended use [21].

There are a large number of experimental studies on ILs for CO_2 capture. Brennecke *et al.* [59, 62-64], were the first to report on CO_2 solubility in imidazolium and pyridinium ILs. They found that ILs that contains fluoroalkyl chains on either cation or anion improves CO_2 solubility in contrast to less fluorinated ILs. These fluorinated ILs have high stability and low reactivity and thus have many excellent properties. However, these ILs only applicable for physical adsorption therefore higher pressure needed for capturing CO_2 [59]. Thus, with fluoro groups in ILs, they are poorly biodegradable and less environmentally benign [65].

Much higher absorption capacity can be achieved if the CO_2 is chemically absorbed instead of physically [66]. Bates *et al.* [67] prepared ILs with functionalized amino group tethered at the cation. Thus, the mechanism 2:1 (ILs : CO_2) applied and the maximum CO_2 capacity can be up to 0.5 mol/mol at 1 bar pressure. Goodrich *et al*. [68] suggested that 1:1 (ILs : CO_2) mol ratio can be achieved when the amine is tethered to anion instead of cation. They used amino acid as anion is known as Amino

Acid Ionic Liquids (AAILs) and achieved CO_2 capacity with 1 mol/mol [69-71]. However, these AAILs suffer the problem of having high viscosities since AAILs with amine functionalized either in cation or anion increases the van der Waals interactions, hence increasing the number of hydrogen bonds [72]. This higher viscosities would slow the absorption kinetics and causes higher operational cost [73].

Polymerized ionic liquids (PILs) have recently attracted attention due to the solid material formed after polymerization of ILs. This would overcome the viscosities problem in ILs. PILs also exhibiting higher CO_2 adsorption compared to the monomeric ILs [40, 74-78]. This is because PILs have larger free volume which can trap a larger amount of CO_2. The properties of PILs also can be customized by varying the combination of polycation-anion pair [79]. The capacity of CO_2 capture depends on the type of polycation, polymer backbone, anion and substituents [80]. The polycation type is considered a decisive factor in CO_2 capture performance, with ammonium-based having high CO_2 capacity than imidazolium-based PILs [80, 81]. Most of the PILs reported in literature are using inorganic anions *i.e.* $[PF_6]$ and $[BF_4]$ which make them difficult to be applied to industry [81]. In addition, these PILs only have a physical adsorption with low CO_2 capacity.

1.6 Novelty of Amino Acid Polymerized Ionic Liquids (AAPILs)

ILs with amine functionalized are synthesized by using amino acids as anion which is known as Amino Acid Ionic Liquids (AAILs). These AAILs are expected to give high CO_2 sorption capacity since the functionalized amine would enhance the CO_2 capacity by chemical absorption. By using amino acid with multiple numbers of amine group *i.e* arginine and lysine, it is expected to give higher CO_2 sorption capacity as they are more amines reacting with CO_2.

To overcome the viscosities of AAILs, these AAILs are then subjected to polymerization. These ILs are known as Amino Acid Polymerized Ionic Liquids (AAPILs). The AAPILs are formed in solid where they are much easier to be handled compared in liquid form. The AAPILs are a new type of PILs with amine functionalized tethered to the anion. Chemical absorption are dominant instead of only physical adsorption as other authors reported [74, 75, 82, 83]. Thus, the CO_2

sorption capacities as expected to be higher in AAPILs than in monomeric form, AAILs.

In addition, amino acid is a greener organic anion that replaces the use of inorganic anion in PILs *i.e.* [PF_6] and [BF_4] which may form HF gas. Thus, AAPILs would be a potential solvent to replace the alkanolamine which only limited to 0.5 mol/mol.

1.7 Problem Statements

The increasing carbon dioxide (CO_2) content in natural gas reserves discovered around the world is one of the major issues facing the industry nowadays. Therefore, CO_2 must be removed from natural gas in order to increase the heating value of the gas, prevent corrosion of gas process equipment and crystallization of CO_2 during the cryogenic process (liquefaction process) and to meet pipeline specifications. RTILs have been proposed as promising alternative for capturing CO_2. The common disadvantages for all ILs, is the higher viscosity which slow the adsorption kinetics and causes higher operational cost.

Polymerized ILs, (PILs) which could be formed by polymerizing the ILs monomer, will incorporate macromolecular structure with ILs. This would enhance the CO_2 sorption as compared to monomer ILs. The available data of PILs on CO_2 sorption are basically on [PF_6] and [BF_4] based anion polymers which make it difficult to apply in industry as they form toxic HF gas. Although PILs have been known to be used as CO_2 adsorbents, there are some limitations in adsorption capacity seen for PILs. The PILs suffer from relatively low CO_2 adsorption capacities due to physical adsorption mechanism. Therefore, much higher adsorption capacity can be achieved if the CO_2 is chemically absorbed instead of physically [68]. Therefore, by synthesize new AAPILs, a green ILs formed with functionalized amine tethered in anion would expect to give higher CO_2 sorption capacities. This is because, after polymerization the CO_2 sorption capacity increases due to involvement of physical adsorption as well with chemical absorption. In addition, the AAPILs are in solid form thus easier to handle than in liquid form.

1.8 Objectives

The objectives of this study are:

1. To synthesize and characterize Amino Acid Polymerized Ionic Liquids (AAPILs)

2. To study the chemical absorption and physical adsorption in AAPILs for CO_2 sorption

3. To study the effect of amine functionality on amino acid as anions for CO_2 sorption

4. To propose the absorption mechanism between AAPILs and CO_2

1.9 Scope of Studies

The scope of this research is to synthesize and characterize amino acids polymerized ionic liquids (AAPILs) for CO_2 capture. A number of cations (ammonium, piperidinium and imidazolium based) and anions (glycine, alanine, serine, proline, taurine, histidine, lysine and arginine) will be synthesized. The different alkyl chain length on cation (methyl, ethyl and butyl) will also be studied for CO_2 capture.

This study has been divided to four stages. The first is to study the monomer (AAILs) in terms of thermal stability and CO_2 sorption at 1 bar and 298 K. The effect of polymerization on thermal stability is studied between the monomers and polymers.

Secondly, these AAILs will undergo polymerization to form AAPILs. These AAPILs are believed to enhance the CO_2 sorption and thermal stability of the monomer (AAILs). The performance of AAPILs in terms of CO_2 sorption is expected to be improved. The effect of changing the cation and anion will be carried out at 1 bar and 298 K. The screening process was done at ambient pressure to study the mechanism.

Thirdly, the best AAPILs will be subjected to higher pressure (up to 10 bar) and temperature (298 K to 353 K) to study the adsorption and desorption of CO_2. The characterization before and after CO_2 sorption will be studied by using FTIR in order to confirm the chemical absorption occurred in AAPILs. Several amino acids are used to study the effect of amine functionality as anion. This study will proceed with COSMO-RS to study the chemical potential between CO_2 and anions. To confirm the physical adsorption, BET model is carried out to determine the physical adsorption isotherm.

At the fourth stage, is the effectiveness of AAPILs on recyclability, selectivity of gases and addition of water in AAPILs towards CO_2 sorption are determined. Since ILs is known to be expensive, the recyclability of AAPILs is studied. The selectivity of AAPILs with different type of gases (CO_2, methane and nitrogen) would be studied to confirm the separation of gas in natural gas.

Generally, the isotherm and thermodynamic studies on CO_2 absorption are also important to study the enthalpy, entropy, Gibbs energy and activation energy on AAPILs. To confirm the enthalpy in the experimental is same with the calculated enthalpy, the DFT in thermodynamic analysis will be carried out to confirm the reaction between amine with CO_2. Once the reaction between amine and CO_2 is confirmed, the mechanism between AAPILs and CO_2 can be proposed.

1.10 Thesis Outline

Chapter Two is the literature review on the main topic of this thesis. This review includes two parts. First part is related in the field of synthesis, physical properties and thermal stability of ILs. The second part provides a review on related research work in the field on the solubility of CO_2 in RTILs, TSILs and PILs.

Chapter Three is the research experimental and methods. The details on materials and procedure to synthesize AAILs and AAPILs followed by details experimental procedure are explained. All the characterization of these AAILs and AAPILs synthesized is also explained.

Chapter Four presents the results from the characterization of AAILs and AAPILs synthesized. Chapter Four also includes CO_2 sorption of the AAILs and AAPILs and

the effects of: polymerization, changing the anion, cation, alkyl chain length of cation, effect of pressure, BET model, temperature, activity coefficient, adsorption isotherm, kinetic studies, DFT calculation, proposed mechanism, addition of water, selectivity of gas and reusability of AAPILs are also studied. Chapter Five is the conclusion followed by recommendations for future works in AAPILs for CO_2 capture.

CHAPTER 2

LITERATURE REVIEW

This chapter is divided into two main parts. First is the synthesis part which provides a review on related work in the field of synthesis, the physical properties (densities and viscosities) of ILs and thermal stability (decomposition temperature, T_d and glass transition temperature, T_g) of ILs. The second part provides a review on related research work in the solubility of CO_2 in alkanolamine, RTILs, TSILs, AAILs and PILs. The effect of different factors such as alkyl chain length and functional groups, cations and anions, effects on polymerization on the CO_2 sorption is also reported.

2.1 Physical Properties of Ionic Liquids (ILs)

Ionic liquids (ILs) are special salts consist of bulky organic cations and inorganic / organic anions. This ILs are composed entirely of ions and strongly resemble ionic melts that may be produced by heating metallic salts [84]. New ionic solvents could be made by coupling different positive and negative ions for countless reactions. Therefore this led to the possibility of customizing the design of ionic solvents for a specific application. Physical and chemical properties such as density, conductivity, viscosity, lewis acidity, hydrophobicity and hydrogen bonding capability of the ionic solvents can be changed by varying the structure of the component ions to obtain the desired solvent properties [42].

Holbery *et al.* (2003), reported the major factors influencing the low melting point in ILs are charge size, charge distribution of ions and the asymmetric extent of the cation [85]. Generally, larger ions results in a decrease in melting point due to the delocalization of charge, less charge density and therefore reduced Columbic attraction between the ions. The failure of the ions to fit into crystal lattice owing to

the sizes of the ions involved, described as "*packing inefficiency*" has been anticipated as a key factor in rationalizing the low melting points of some ionic liquids [86]. Large anions with many degrees of freedom reduce crystallization until lower melting points are obtained [87].

ILs also can be made up by mixing of acid and base and known as protic ILs. The attentions of protic ILs have been explored since the potential cost is lower. Protic ILs was produced by proton transfer from acid to base. Vijayarhagavan *et al.* (2013), have studied the protic ILs for CO_2 capture [88]. The results showed that the sorption process with protic ILs included a chemical reaction and it is comparable with 30 wt% MEA. However, the mass transfer coefficient magnitudes lower than MEA which is might be due to the higher viscosity of ILs and its impact on CO_2 diffusivity. Thus it is explain that the viscosity of ILs gives major impact on the CO2 sorption capacity.

Amino acids have both a carboxylic acid residue and an amine group in a single molecule; therefore, they can be used as either anions or cations. These groups are useful in their ability to introduce functional groups to the ILs. The properties of the resulting AAILs depend on the side groups of the amino acids involved. The advantages by using amino acids are their low cost, high biodegradability and high biological activity. Since the AA contains both an amino group and carboxylic acid in a single molecule, with various side groups and a chiral carbon atom, AAs are the best candidates to act as a platform for functional ILs as shown in Figure 2.1 [73]. However, with this functionalized groups, the AAILs suffer the problem of having high viscosity as they have larger van der Waals force and a tendency of forming numbers of hydrogen bonds.

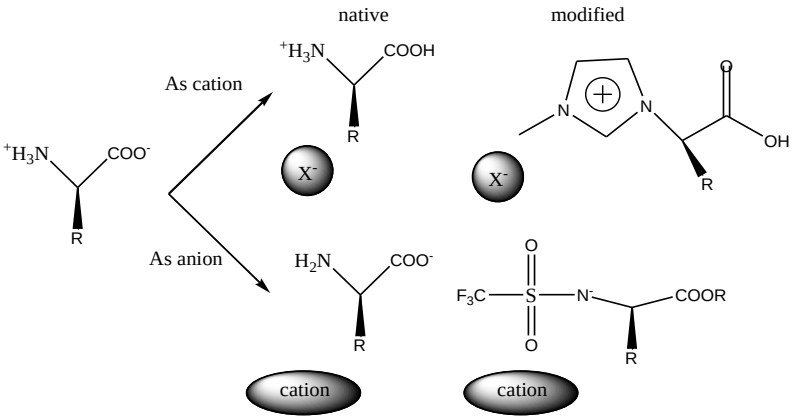

Figure 2.1: Design of amino acids for functionalised ILs

However, this ILs can be proposed as hydrophilic or hydrophobic ILs by tailoring the cation and anion. Usually the hydrophobic ILs reported as replacements for hydrophobic organic solvents. Hydrophobic ILs, mostly contains fluorinated anions such as hexafluorophosphate, PF_6^- or bis(trifluoromethylsulfonyl)imide, Tf_2N^-. This is because fluorine would weaken the electrostatic interaction force through a reduction of anionic charge density thus making this salt hydrophobic [89]. These hydrophobic ILs generally undergo phase separation with water which provides a liquid-liquid extraction system as well as yielding heterogeneous reaction media.

Since tendency of functional groups in amino acid to made a hydrogen bond with water is higher, Kagimoto *et al.* [90], worked on synthesized hydrophobic AAILs. It were first prepared by Fukumoto and Ohno [72] by using 1-ethyl-3-methylimidazolium as cation, ([emim]) with 20 different natural amino acids as anion. However, [emim][AA]s showed a decomposition temperature around 200 ^oC. To overcome this, Kagimoto *et a.l* [90] used phosphonium cations because of good thermal stability and electrochemical thermal stability. They synthesized a series of AAILs ($[P_{n,n,n,m}][AA]$) with $n \geq 6$, showed a hydrophobic ILs and underwent phase separation with water. The results also showed that water content in the ILs depended on the amino acid side chains and the alkyl chain length of the cation [91].

To study the densities in AAILs, Kagimoto *et al.* [90], reported that the density depends mainly on the number of carbon atoms, regardless the symmetry of the cations. The density decreased with increasing alkyl chain length or having only an alkyl group on the side chain length on the amino acids. This is because the elongation the alkyl side chains of $[AA]^-$ increases the free volume of the ILs thereby decreasing the density [71]. However, with introduction of functional groups including the carboxyl group, hydroxyl group and aromatic ring, the density of salts increases through effects the hydrogen bonding and π-π stacking. This is agrees with Zhang *et al.* [71] showed $[AA]^-$ with grafting functional group increases the densities than *n*-alkyl chains [71].

The amine-functionalized ILs especially tertiary amine-functionalized ILs has lower densities compared to the non-functionalized ILs [92]. The density of the ILs depends also on several factors such as electrostatic interactions between positive and negative, molecular mass, size and shape (symmetry) of the ions and on the dispersion forces or van der Waals forces of attraction between molecules. By changing the alkyl

chain length, the density of ILs can be controlled. The combination of cation and anion need to be careful because some properties *i.e.* density, viscosity and hydrophilicity are affected by the alkyl groups of ions [93-95]. This is supports by Goodrich *et al*. [96] that increasing the alkyl chain length on either cation or anion, the density will decrease. They synthesized AAILs with $[P_{66614}]$ as cation and amino acids as anion. The density was observed to decrease in the order [Gly] > [Ala] > [Sar] > [Val] > [Leu] > [Ile].

For the dicationic ILs, their densities were observed to increase linearly with a decrease in temperature and higher than the density of water and traditional solvents. The densities of AA-DILs were higher than AAILs phosphonium based but lower than amine functionalized imidazolium type ILs and traditional-DILs. The densities of $[bis(mim)C_6][Tf_2N]_2$ are higher than $[N_{111}\text{-}C_6\text{-}mim][Tf_2N]_2$ due to the symmetrical DIL which had a higher density than their asymmetrical analogs due to symmetry effects in its molecular structure [97].

However the main problem with ILs, it suffers a problem of having high viscosities due to nature of liquids. The viscosity of AAILs mainly depends by the strength of both the van der Waals interaction force and hydrogen bonding. Generally, the viscosity increases with elongation of the alkyl chains [90]. According to Zhang *et al*. (2009), by tethering dual amine groups in cation and anion, the viscosities of the $[aP_{4443}][AA]$ are large mainly because the larger size of $[aP_{4443}]^+$ leads to increasing number of van der Waals interactions [71]. Two amine groups may increase the number of hydrogen bonds. By increasing the chain length of $[AA]^-$ it decreases the mobility of the ionic liquids leading to an increase of viscosities as follows [Gly] < [Ala] < [Val] < [Leu] (713.9 < 758.0 < 888.2 < 1193.8 mPa at 25 ^oC). The presence of large ring in the $[AA]^-$ anion also decreases the mobility of the ILs leading to increase in the viscosities such as $[Trp]^-$,$[Tyr]^-$ and $[His]^-$ are all above 2000 mPa s at 25 ^oC. The grafting of an SH or OH functional group onto the $[AA]^-$ anion increases the viscosity due to tendency to form hydrogen bonds for example $[Cys]^-$, $[Ser]^-$ and $[Thr]^-$ compared to $[AA]^-$ without functional group.

It was well known that the viscosities of traditional monocationic ILs were usually low especially when pairing with $[Tf_2N]$, $[PF_6]$ or [TfO] anion. However, when introducing amine groups onto the cation or anion, the viscosities increase with nearly four times. For dicationic ILs (DIL), the viscosities of $[bis(mim)C_2][Gly]_2$ was 2586

cP at 30 ^{o}C which was the lowest for DIL, but still higher than some monocationic functionalized counterparts. Furthermore, the viscosities of DILs were largely dependence on their molecule structures. The longer alkyl side chain of the amino acids and alkyl link-chain of the dication, the higher their viscosities became [97].

This is supports by Muhammad *et al*. (2011), that the structures of AA anions have pronounced effect on the viscosities of the AAILs [98]. This might be because of the increase in the internal resistance, for mobility of the AAILs. The functional group in AA anions also contributes to the increases of viscosity of AAILs due to its tendency to form hydrogen bonds. The interaction such as hydrogen bonding, van der Waals interactions and size of amino acids were found to increase following the order [emim][gly] < [emim][ala] < [emim][ser] < [emim][pro].

Therefore, due to their liquid nature, ILs lack mechanical stability and may not be able for certain application when a solid material is needed. Poly ionic liquids (PILs) which is in solid form is one of the alternatives to overcome the viscosity problem in ILs. PILs is a species with monomer repeating unit connected through a polymeric backbone to form a macromolecular architecture [83]. The properties of PILs are strongly related to both polymer backbone and ILs structure. The structure of the cation and anion (ion type and substitute groups on cation) determine the physicochemical properties of ILs. Unlike the ILs or ILs/polymer mixture, where both cation and anion are mobile, PILs are restricted in mobility compared to their counter ions [99].

The major advantages by forming PILs are easier to handle, enhanced stability, improved processability, flexibility, durability to improve control over meso to nano structure. PILs can be prepared by polymerization of cation or anion which resulting in macromolecular with repeating charge (cationic or anionic) units. Two common groups being examined when approaching for the preparation of PILs are acryloyl (or methacryloyl) and vinyl groups [40].

2.1.1 Thermal properties of ILs

The studies of thermal stability of ILs are needed to ensure the stability of ILs for capturing CO_2 at higher temperature. Kagimoto *et al.* (2010), reported that for symmetric cations, the glass transition temperature (T_g) decreased with increasing

alkyl chain length up to carbon number 8, [$P_{8,8,8,8}$] [90]. This reduction in T_g has been attributed to the disruption of crystal packing and the flexibility increase due to alkyl chains and also reduction in lattice energy. However, the T_g increases again when n=10 due to increase in van der Waals interaction force. The T_g of AAILs with long alkyl chain depends more on the flexibility of the alkyl chain rather than the side chain structure of the amino acids [90].

ILs thermal stability is ruled by intermolecular interactions. The three most important ones are hydrogen bond, Coulombic interactions (occurred between anionic and cationic charges) and van der Waals interactions. However the degradation temperature (T_d) decreases with substitution of the alkyl chain where it induces a higher molecular volume of the cation and also the presence of fluorine atom [100].

AAILs with phosphonium cation have greater thermal stability than other AAILs by different cations. It is suggested that dealkylation of the cation took place during the thermal decomposition. The results also showed that the T_d of AAILs-imidazolium based is lower than corresponding amino acids. For example the decomposition temperature of [emim][Ala] is 212 ^{o}C and alanine is 297 ^{o}C. However, for phosphonium cation with alanine as anion, the decomposition temperature is 288 ^{o}C . These is clear that the cations decompose before amino acids [90]. According to Zhang *et al.* (2009), ionic liquids with [aP_{4443}][AA] have glass transition temperature from -69.7 to -29.6 ^{o}C, lower than those of [emim][AA] [71]. For example the differences of T_g between anions of [Asp], [Gln], [Glu] and [Arg] from [emim][AA] and [aP_{4443}][AA] are 58.9, 40.4, 40.3 and 38.3 ^{o}C, respectively.

As well as the cation $[aP_{4443}]^{+}$, the structures of $[AA]^{-}$ also have a big effect on the T_g and T_d values. The T_g values decrease in the order [aP_{4443}][Gly] (-69.7 ^{o}C) < [aP_{4443}][Ala] (-67.3 ^{o}C) < [aP_{4443}][Val] (-62.5 ^{o}C) < [aP_{4443}][Leu] (-61.4 ^{o}C) which corresponds to an increasing length of the alkyl side chain of the $[AA]^{-}$. For thermal decomposition, the active functional groups on $[AA]^{-}$ and the high negative charge density of $[AA]^{-}$ lower the thermal decomposition temperatures of the [aP_{4443}][AA]. For example for $[AA]^{-}$ anion like $[Cys]^{-}$ (202 ^{o}C), $[Tyr]^{-}$ (231 ^{o}C), $[Thr]^{-}$ (245 ^{o}C) and $[Ser]^{-}$ (254 ^{o}C) are functionalised by SH or OH moieties have lower thermal decomposition temperature. For $[AA]^{-}$ structures with ring in their side-chains and low negative charge densities, for example [His], [Phe], [Pro] and [Trp] have high T_d values with 300, 282, 280 and 277 ^{o}C respectively. For anion [Val], [Lys], [Ile],

[Leu], [Ala] and [Gly] all T_d are above 280 ^oC because the anions have only alkyl side chains which also results in a low negative charge density [71].

Goodrich *et al.* (2011), found that cation [P_{66614}] is a very stable with a decomposition temperature as high as 420 ^oC when paired with stable anion [60]. This might be because of asymmetry of the [P_{66614}] cation which increases in stability compared to smaller cation, [P_{4444}]. By studying the decomposition temperature with various anions, it was found that the decomposition temperature decrease in order of [Tau] > [Gln] > [Pro] > [Met] > [Lys] > [Thr] > [Asn]. For glass transition temperature, the T_g for $[P_{66614}]^+$, varied from -86 to -69 ^oC lower than the values for the same anions with [emim], [P_{4444}], [aP_{4443}] cations [96].

Thermal properties for dicationic ILs (DILs) showed the T_g increase with alkyl side-chain length of the amino acid when DILs had the same dications, due to the van der Waals force between alkyl side chains. In DILs with the same alkyl link chain length, the T_g of DIL with asymmetric structure was nearly 6 ^oC lower than symmetric structure. For T_d, the alkyl side chain length of amino acids and the alkyl link-chain length of the dication also had a great influence on thermal stability. For example, DILs $[Bis(mim)C_4]^{2+}$ was 40 ^oC higher than $[bis(mim)C_2]^{2+}$ with same anions. This shows that increase of alkyl chain length of dication could enhance T_d [97].

In PILs, thermal stability showed that T_d of PILs on [TFMS], [PTS], [BF_4] and [Tf_2N] as anions were higher than chloride as anion which indicates that increased thermal stability. However, PILs with [Ac], [TFAc], [MS], [HFB], [Bz] and [NO_3] anions, the thermal stability decreased. This indicates that anion plays a key role in determining thermal stability. In T_g, the T_g for poly[DADMA][Cl] was found to be at 204 ^oC. By using inorganic anion, poly[DADMA][NO_3], the T_g reduced slightly to 197 ^oC. For PILs with organic anion, the T_g was reduced to 90-117 ^oC. This lowering in T_g, by a particular anion attributed to the larger size of the anion in PILs. The increased anion size may not render as efficient chain packing as [Cl] as anion of smaller size. This lead to lowering the of interchain interactions in the formed PIL than poly[DADMA][Cl]. This resulted in lowering the T_g temperature [74]. This is agreed by Tang *et al*. [82] that anions in PILs such as [BF_4] have a strong plasticizing effects thus improve flexibility of polymer chains, facilitate the segmental motion and reduce T_g of the PILs.

For PILs imidazolium based, the initial decomposition temperatures of PILs were up to nearly 300 ^{o}C under N_2 atmosphere. For glass transition temperature, the DSC curves of PILs with different anions showed that PILs- PF_6 and PILs-BF_4 were 68 ^{o}C and 135 ^{o}C respectively with no melting endotherm observed in DSC traces [76].

2.2 Review on CO_2 Sorption

The most common technology for CO_2 absorption in industry is using alkanolamine such as primary monoethanolamine (MEA), diethanolamine (DEA) and methyldiethanolamine (MDEA). These amines have been constantly synthesized to ascertain their capability in CO_2 capture. It can capture CO_2 up to 0.5 mol/mol. However, this caused a serious several drawbacks such as high volatility, corrosive in nature and higher cost for regeneration. Therefore, alternative to replace the usage of alkanolamine is highly needed. ILs has been proposed as a good replacement for alkanolamine since it is low volatility, low vapor pressure and high solubility with CO_2. This efficiency of CO_2 sorption by using ILs can be enhanced by tethering the amine group either cation or anion. The interaction between this amine and CO_2 would increase the CO_2 sorption capacity due to the chemical absorption. It has been reported that by tethering the amine on anion, the CO_2 sorption capacity can be as high as 1.0 mol/mol due to the formation of carbamic acid. However, the higher viscosity in ILs may attribute to the low efficiency and slow absorption kinetic thus difficult to apply in industry. Therefore by polymerized the ILs resulted in solid form with amine functionalized as anion seems promising for capturing CO_2 in natural gas.

2.2.1 CO_2 sorption on alkanolamine

Specifically, the desired properties of the amine include fast kinetic, absorption-desorption rate, absorption capacity and ability to reach 90% capture efficiency [101]. In recent times, polyamines have been discovered to have a very good CO_2 absorption capacity, high mass transfer and high reaction kinetics (mainly to the presence of multiple amine groups). It has been used as a promoter or activator in high absorption capacity solvents to enhance their CO_2 capture efficiency. The polyamines that contain primary or secondary amine group are usually used for enhancing amine-CO_2

kinetics whereas tertiary amino group will not be used as rate promoters due to their slow CO_2 absorption pathway [102].

Many studies have been devoted to improve CO_2 absorption and selectivity by chemical modification on the surface of solid materials possessing high surface area. The basic organic group (amine) and inorganic metal oxide (alkali metal or alkali-earth metal) are of particular interest. Amine-based adsorbents have widely been studied and exhibited the advantage as low heat of regeneration over aqueous amines due to the low heat capacity of solid supports. Their low CO_2 adsorption capacity and high cost, however, are the major challenges to commercialize [103].

Yang *et al.* (2015), have studied the use of perfluorinated silica-stabilized with with dry alkanolamines (DA_f) for CO_2 capture. DA_f display high operational CO_2 capture efficiency with 98 wt% as compared to bulk MEA with only 60 wt%. This lower absorption of bulk MEA is due to mass transport arising from the large increase of viscosity due to carbamate salt formation. DA_f also exhibit extraordinary recyclability with a negligible decrease in absorption capacity over at least ten absorption-regeneration cycles. Moreover, the amine component of the DA_f is also isolated by the silica particles from pipelines and other corrosion sensitive materials [104].

Kim *et al.* (2013) have studied the CO_2 absorption by aqueos alkanolamines solution with different structures which is MEA 30wt%, DEA 30 wt%, TEA 30wt% and AMP 30 wt%. All the experimental absorbents showed higher CO_2 loadings with lower reaction temperature. While a primary amine, MEA, and a secondary amine, DEA, showed CO_2 loading limited to 0.6 (mol CO_2/mol amine), a sterically hindered amine, AMP showed higher CO_2 loading with 0.8 (mol CO_2/mol amine). This is because, AMP formed unstable carbamate and hydrolysis easily occurred, leading to the formation of free amines and bicarbonate ions. Therefore, AMP had higher CO_2 loadings compared to those for unhindered primary and secondary amines. However, the slopes of the graphs of MEA and DEA rapidly increased at CO_2 loadings higher than a certain value, whereas TEA and AMP yielded curves with gentle slopes. These results show that the carbamate reactions, which major reactions of primary and secondary amines, occur quickly, while the unstable carbamate reactions and

subsequent bicarbonate formation that appear in tertiary and sterically hindered amines occur slowly [15].

However, there are drawbacks linked with amines such as high vapour pressure, corrosive in nature and requires high energy input for regeneration. The high vapour pressure allows emission of amine gases into the air upon heating. The amines itself are also corrosive especially MEA which corrodes the equipment. The regeneration process leads to high energy consumption in order to break the chemical bonds formed between the CO_2 and amine [22]. However, the major drawback which limits the potential in using MEA in the capture process is the high energy for regeneration of MEA which could be as high as 3.3-4.4 GJ/ton CO_2. It has been reported that the amount of regeneration energy could account for 70-80 % of the entire operating cost of CO_2 capture plant [101].

2.2.2 CO_2 sorption on room temperature ionic liquids (RTILs)

ILs are promising candidates as absorbents for CO_2 removal because of their high thermal stability, negligible vapor pressure and tunable physicochemical properties [105]. Many research groups have carried out research on solubility of CO_2 in ILs [52, 53, 97, 106, 107]. Brennecke *et al.* (2003), were the first to report on CO_2 solubility. They reported that ILs with fluoroalkyl improves CO_2 solubility compared to non-fluorinated ILs [59, 62-64]. The anion plays a key role in determining CO_2 solubility in ILs and through physical adsorption with CO_2, less energy is needed for the regeneration of ILs [59]. The enthalpy required is less than 20 kJ/mol to release the physically adsorbed CO_2 in regeneration step, which is only a quarter of the energy consumed in amine-based method [65].

There were a number of factors that controlled the CO_2 solubility in the ILs which both cation and anion are related. The anion played the biggest role in CO_2 solubility. Anions that contain fluoroalkyl groups were found to have some of the highest CO_2 solubilities. As the number of fluoroalkyl groups increased, the CO_2 solubility also increased. For the cations, there are two factors that influenced the CO_2 solubility. The biggest effect was seen in increasing of alkyl chain length on the cation. For a given cation, the CO_2 solubility increased with increasing alkyl chain length [52, 108]. This might be due to entropic reasons that by increasing alkyl chain length, the

density of ILs decreases. Therefore, there are more free volume within the longer chain ILs [59].

Table 2.1: Absorption capacity of CO_2 by mixture of imidazole-based ILs [109]

Ionic liquids	Exp value (mol/mol)
[bmim][BF_4]	0.0212
[bmim][BF_4] + [NH_2-emim][BF_4]	0.0698
[bmim][Tf_2N]	0.0378
[bmim][Tf_2N] + [NH_2-emim][BF_4]	0.0747
[bmim][CH_3CO_2]	0.0316
[bmim][CH_3CO_2] + [NH_2-emim][BF_4]	0.0291
[NH_2-emim][BF_4]	0.0610

Mei *et al.* (2012), have studied the CO_2 sorption performance by imidazole based ILs mixtures [110]. It was showed that better CO_2 absorption capacity obtained for the mixtures of [bmim][BF_4] or [bmim][Tf_2N] with [NH_2-emim][BF_4] than single IL. However, the CO_2 sorption reduced after [NH_2-emim][BF_4] was mixed with [bmim][CH_3CO_2]. The reason might be that two kinds on ionic liquids interacted each other. Table 2.1 shows the results of CO_2 sorption capacity for the mixture of ILs. The mixtures containing anion [Tf_2N] and [BF_4] shows better CO_2 sorption which might result from the fluorination [64]. The regeneration performance of the ILs mixtures also shows good result where 10 times of absorption/desorption cycles still shows the quality of mixture remained basically unchanged.

Blath *et al.* (2012), have studied the absorption ability of carbon dioxide in ILs with basic anion like acetate, privalate, lactate and benzoate and imidazolium as cation [111]. The ILs showed chemisorptions due to a formation of carboxylate at the imidazolium ring. This is confirmed by ^{13}C NMR analysis where the peaks can be related with the carbon atoms of the imidazolium ring. For CO_2-treated [EMIM][OAc], two new peaks can be found at 154.44 ppm which represents the carbon atom from CO_2, which is bound to the C2 atom of the imidazolium ring by forming the carboxylate. The second peaks at 141.63 ppm and stands for the C2 atom itself, which is linked to the carboxylate group. The unbound C2 carbon atoms to carboxylate can be found at 138.15 ppm. This mechanism discussed in Figure 2.2. For

the anions, they found that acetate gave the best absorption. For benzoate anions, the steric hindrances due to the benzol ring can effects the deprotonation step in reaction mechanism. For privalate anion, the extra CH_3 groups can also alter the chemisorptions ability slightly. This can lead to higher Henry's law contants compared to [EMIM][OAc].

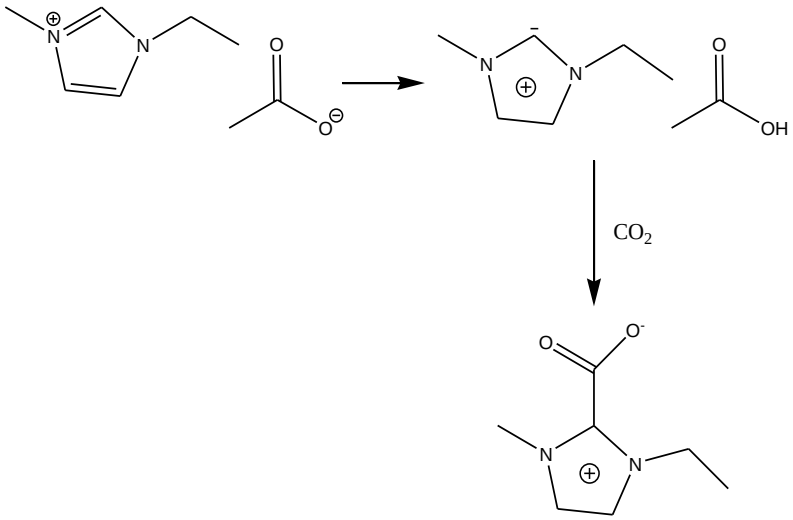

Figure 2.2: Proposed mechanism of [EMIM][OAc]

Yunus *et al*. (2012), have studied the solubility of CO_2 in pyridinium based ILs with several anions and different of alkyl chain length (butyl, octyl, decyl) [112]. The results showed that the CO_2 absorption increases as alkyl chain length increased. This is due to the behaviour of entropic rather than enthalpic reasons, where increasing the cation alkyl chain length will decrease the density of the ILs and subsequently increasing free volume in the ILs for the absorption of CO_2 gas by space filling mechanism. For fluorinated anion, the solubility of CO_2 increases in the order of $[C_4py][Dca] < [C_4py][TfAc] < [C_4py][Tf_2N]$. This trend follows the order of fluorination presents in the anion and also the molar mass of the ILs. It can be concluded that an increase in the length of fluroalkyl leads to an increase in CO_2 solubility.

Anthony *et al*. (2005), have studied the anion effect of gas solubilities in ILs [64]. The results showed that water and benzene were most soluble, followed by nitroux oxide and carbon dioxide, ethylene, ethane and oxygen. Carbon monoxide solubility was below the detection limit. This results showed that gases with large dipole moments (*e.g.* water) or quadrupole moments (*e.g.* CO_2 and N_2O), and those with chance for specific interactions (*e.g.* hydrogen bonding) have the highest solubilties in

ILs. Whereas, the solubility of nonpolar gases are correlate well with polarizability. However, carbon monoxide does not follow this trend, which indicated that these factors cannot fully describe behaviour of gases in ILs. For the anions, it can be seen that [Tf_2N] anion increases all gas solubilities compared to [BF_4] and [PF_6]. By changing the cation from imidazolium to quaternary ammonium or pyrolidinium with [Tf_2N] as anions, it gave little difference in CO_2 and O_2 solubility.

Husson *et al.* (2010), have studied the effect of water on CO_2 sorption by [emim][Tf_2N] [113]. It is observed that the solubility decreases with the mole fraction concentration of water (0.28 mole fraction) from 2.63×10^{-2} for the pure ILs to 1.88×10^{-2} which the reduction approximately 30% on the CO_2 solubility. The viscosities of the mixtures of [emim][Tf_2N] with water (0.300 mole fraction, 303 K) resulted approximately 40 % lower than pure ILs. It concluded that the viscosity of the ILs medium can be significantly reduced while maintaining the same order of magnitude for the low pressure of CO_2 solubility. This is because the viscosities can considerable modifying the transport of the gas in liquid medium. Thus it can substantially affect the characteristics of the ILs medium as an absorbent for carbon dioxide.

In the event of conventional ionic liquids, carbon dioxide is absorbed by occupying free space between the ions, thus high pressure is needed in the physical adsorption process. However, the adsorption capacity is relatively low [21].

2.2.3 CO_2 sorption on task specific ionic liquids (TSILs)

Owing to the limitations in adsorption capacity seen for RTILs in physical adsorption mechanism, an attention now focused on a new concept where the advantages of ILs are combined with the incorporation of functional groups to allow chemical binding of CO_2 to the absorbents. They are some functional groups that can enhance the CO_2 sorption capacity such as carboxylate functionality, amine functionality and combined functionality. The CO_2 should bind to the functional group in a thermodynamic sense and the kinetics should be sufficient enough for this process to operate at a fast enough absorption rates. Therefore, the absorption step must not be too exothermic so the removal of CO_2 in regeneration step can be conducted without high energy requirements. This is because, by using conventional amines like MEA, DEA or MDEA have high relatively large exothermic sorption enthalpies (above -80 kJ/mol).

Thus, by functionalize ILs exhibiting less exothermic sorption enthalpy would be very attractive [21].

The remarkable properties of ILs for CO_2 sorption are mostly decided by cations, anions and factors associated with structural modification of duo. As reported, anion plays the biggest role in CO_2 sorption which anions with fluoroalkyl groups were found to have the highest CO_2 solubility. By increasing the quantity of fluoroalkyl groups, the CO_2 solubility also increased. Whereas in the case of cations, there were two factors that controlled the CO_2 solubiliy in ILs. First is when the alkyl chain length on the cation increased and the second factor was to attach a functional group like ether to cation. This is to create a greater free volume or by incorporating a CO_2-philic carbonyl functional moiety such as amine, alcohol, carboxylic and nitrile. This promising strategy leads to the synthesis of TSILs [65, 108].

Much higher absorption capacity can be achieved if the CO_2 is chemically absorbed instead of physically [66]. Bates *et al.* (2002), prepared ILs with ions incorporating amino- functional groups for this purpose, for example 1-(3-propyamino)-3-butylimidazolium-tetrafluoroborate, [apbim][BF_4], where the primary amine is covalently tethered at the cation [67]. This IL absorbed 0.5 mol CO_2 / mol IL at P(CO_2) = 1 atm and room temperature during 3 hour exposure period. Since then, a number of other researchers [60, 68, 70, 71, 96, 114, 115] have also studied CO_2 absorption in amine-functionalized cation and anion ILs. Some of the best performing materials are the di-amino functional protic ILs, which have absorption capacities >12 wt% [88, 116].

Sharma *et al.* (2012), have studied the series of ether functionalized on imidazolium cation based ILs, [C_2Omim][X] [117]. Among the functionalized ILs, ether functionalized have been paid much attraction due to their attractive physical and chemical properties which include air and moisture stability, selective, thermally stable, long life operational and a promising candidate for CO_2 capture. The results showed that ether functionalized shows significantly high absorption capacity for CO_2 which reached about 0.9 mol CO_2 per mol ILs at 1.6 bar, 303 K. The CO_2 absorption results shows that the absorption of CO_2 in ether functionalized is a chemical process which follows 1:1 mechanism and forms a carbamic acids. The detailed mechanism is presented in Figure 2.3.

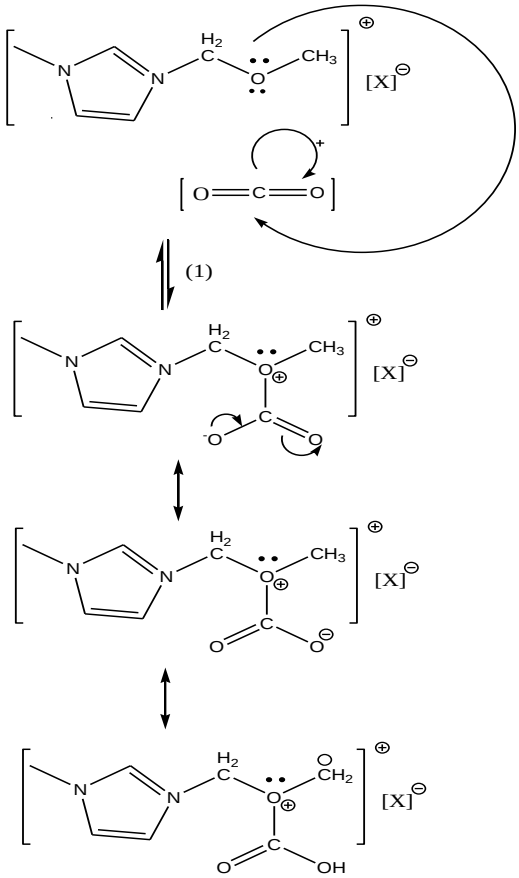

Figure 2.3: Proposed mechanism of CO_2 absorption by ether functionalized ILs.

Figure 2.3 shows that the lone pair of electrons on oxygen atom of the ether group attacks as a nucleophile on the carbon atom of CO_2 and lead to formation of carboxylic acid. This indicates the predominance of 1:1 mechanism, where the CO_2 reacts with one mole ILs to form a carbamic acid. This interaction of CO_2 with ILs are shown on FTIR spectra where two new peaks appeared around 1700 cm^{-1} and 1405 cm^{-1} for (-C=O str) and (-O-H in plane bend) of the carboxylic acid. These peaks confirm the chemical process between ether functionalized and CO_2.

On 2012, Sharma *et al*. (2012), also reported that acid functionalized ILs, [Cmmim][X] for CO_2 sorption also reaches 0.9 mol CO_2 per mol at 1.6 bar , 303 K. The reason it is not achieved the maximum capacity maybe due to the high viscosity of ILs where the formation of hydrogen bonding network increases rapidly [108]. The mechanism indicates that the lone pair of electrons on oxygen atom of the acid group attack as a nucleophile on the carbon atom of CO_2 and lead to the formation of

anhydride. This type of mechanism also called 1:1 mechanism where 1 mole of CO_2 reacts with 1 mole of ILs. The detailed mechanism is presented in Figure 2.4.

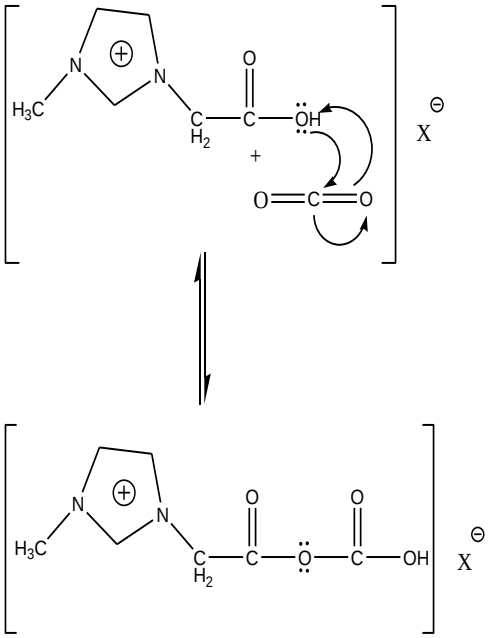

Figure 2.4: Proposed mechanism of CO_2 absorption by acid functionalized ILs

Hu *et al.* (2014), have studied the CO_2 sorption with amino group ILs. The results showed that the more amine groups in ILs led to higher CO_2 sorption capacities [118]. The CO_2 results showed that [TETAH][BF_4] gave higher CO_2 sorption as high as 0.96 mol/mol than [EDTAH][BF_4] with 0.487 mol/mol and [MEAH][BF_4] with only 0.246 mol/mol. This indicates that the greater number of an amine group in cation, the more CO_2 is absorbed. They also found out that factors such as temperature, gas flow rate and water content also had the most significant impact on the CO_2 sorption capacity. ILs [TETAH][BF_4] with 0% water gave 0.96 mol/mol. But when the water content of [TETAH][BF_4] reached 40%, CO_2 sorption capacity increased to 2.04 mol/mol. They suggested that reaction between CO_2 and H_2O, generate more H^+, thus enhancing the absorption of CO_2. Therefore, it shows that with the addition of water, the CO_2 sorption capacity increases since the water also reduces the viscosities of ILs.\

2.2.4 CO_2 sorption on amino acid ionic liquids (AAILs)

Amine functionalized-anion ILs have also been studied, mainly using amino acids as the anion [69-71]. Amino Acid Ionic Liquids (AAILs) were first prepared by

Fukumoto and Ohno [72] by using 1-ethyl-3-methylimidazolium as cation, ([emim]) with 20 different natural amino acids as anion [73].

Goodrich *et al.* (2011), suggested that 1:1 (CO_2: IL) mol ratio can be achieved when the amine is tethered to the anion instead of the cation [96]. The uptake of CO_2 by this chemical mechanism is described in Equations 2.1 and 2.2; since $[AA]^-$ have structure of $[H_2N\text{-}CHR\text{-}COO^-]$, they are represented here as $R^- NH_2$.

$$CO_2 + R^- NH_2 \rightleftharpoons R^- N^+ H_2 COO^- \quad (2.1)$$

$$R^- N^+ H_2 COO^- + R^- NH_2 \rightleftharpoons R^-NHCOO^- + R^-NH_3^+ \quad (2.2)$$

Theoretical calculations showed that the dianion formed in the Equation 2.2 is chemically unstable therefore the reaction would expect to terminate at Equation 2.1 upon addition of CO_2 to AAILs. This indicates a potential absorption stoichiometry of 1:1 (CO_2: IL). However the exact mechanism is still under debate. At higher pressures, there is an increased uncertainty where there is increased capacity due to physical adsorption, but at low pressures, chemical absorption is dominant. Calculations showed that tethering the amine to the cation favored the formation of the carbamate, reflecting the electrostatic stability of the zwitterions product. However, by tethering the amine to the anion favored the carbamic acid, reflecting the instability of the product dianion. These trends are most pronounced when the charge center and amine are in close proximity [68].

Sistla *et al*. (2014), have reported that AAILs with butylmethylimidazolium, [bmim], as cation gave CO_2 absorption within the range 0.32 – 0.62 mole CO_2 per mole IL at 2 bar pressure and 298 K [70]. The result showed that [bmim] [Arg] has the highest CO_2 absorption with 0.62 mol CO_2 / mol IL followed by [bmim] [Lys] (0.48 mol /mol) and [bmim] [His] (0.45 mol/mol). This shows that AAILs with more than one amine site show higher CO_2 absorption capacity than AAILs with only one amine group tethered to the anion. This is also agreed by Saravanamurugan *et al.* (2014), that AAILs based on naturally amino acids *i.e.* lysine (Lys), histidine (Hist), asparagines (Asn), glutamine (Gln) that contain one amine group in addition to the amino-acid functionality [105]. An absorption capacity of 2.1 mol/mol was measured for $[N_{66614}]$[Lys]. This suggested that both amine groups in lysine, reacted completely

with CO_2 to form $[N_{66614}][Lys]$-CO_2 as shown in Figure 2.5. The CO_2 absorption resulted in the formation of carbamic acids by reaction of CO_2 with amine groups by 2:1 mechanism.

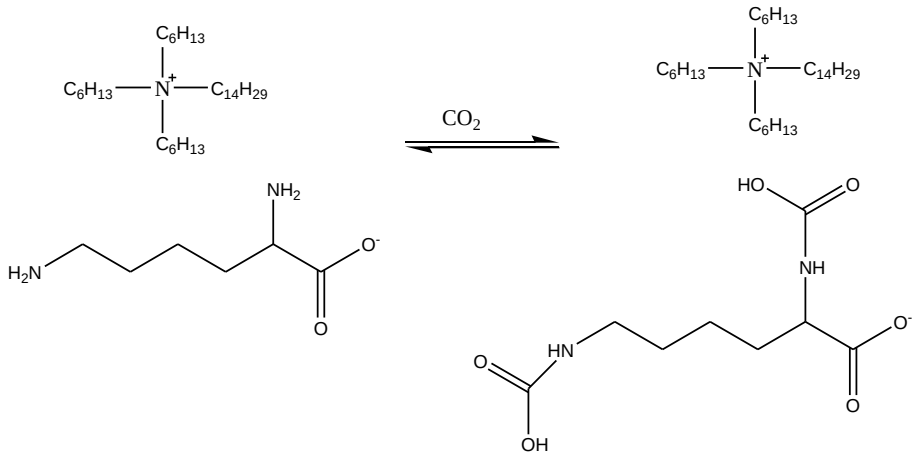

Figure 2.5: The pathway for the formation of the $[N_{66614}][Lys]$-CO_2 [105]

Gurkan *et al.* (2010), [68] and Goodrich *et al.* (2011) also studied the CO_2 absorption in AAILs by using trihexyltetradecyl phosphonium $[P_{66614}]$ as cation and methionine and proline as anions [96]. The results showed CO_2 absorption at 0.88 mol CO_2 / mol IL at 1 bar pressure. Therefore, they have shown that phosphonium-based AAILs can react with CO_2 in 1:1 stoichiometry.

Zhang *et al.* (2012), studied CO_2 capture with dual amino functionalized phosphonium ionic liquids (3-aminopropyl)tributyllphosphonium amino acids, $[aP_{4443}][AA]$ [71]. The result showed that the absorption of CO_2 was less than 0.2 mol/mol after 2 hour exposure because of high viscosities. However, after immobilizing these ILs on porous SiO_2, the results showed that the absorption of CO_2 was close to 1:1 by mol in about 80 minutes. These AAILs often suffer the problem of having high viscosity and also have lower thermal stability than general ILs.

Xue *et al.* (2011), have synthesized dual amino ionic liquids, with amino-functionalized imidazolium cation and taurine as anion; [aemmim][tau] [119]. Taurine (Tau), had been chosen since it is cheap, easily obtained and naturally occurring amino acid with a better stability than most of other amino acids. They found that CO_2 absorption capacity reached 0.9 mol CO_2 / mol IL at ambient pressure and 303 K. Since there are two amines tethered to the anion and the cation in [aemmim][tau], so the maximum absorption capacity may reaches 1.5 mol CO_2 per mol of [aemmim][tau] as shown in Figure 2.6. The interactions of carbon dioxide and

[aemmim][tau] shows that the absorption is chemical process. In FTIR, carbamate peak C=O appeared at 1661 cm^{-1} after absorption.

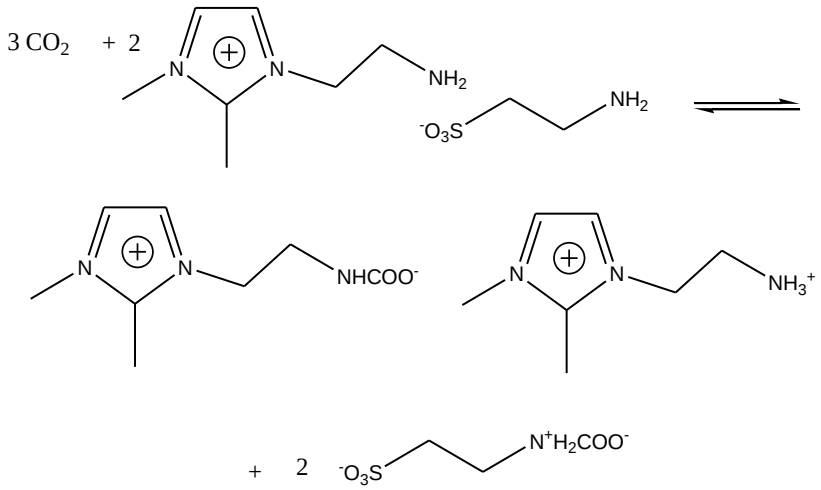

Figure 2.6: Proposed mechanism of [aemmim][tau] with CO_2 [119]

Chen *et al.* (2013), have investigate the physical and chemical interactions between CO_2 and amine functionalized ILs which is [aEMMIM][BF_4] [120]. The results showed that there are both physical and chemical interactions between amine-functionalized ILs and CO_2. They observed that 21% of [aEMMIM][BF_4] interacted with CO_2 chemically at 1:1 (CO_2/IL) which lead to 94% contribution to the solubility. Whereas 79% of [aEMMIM][BF_4] interacted physically leading to 6% contribution. The CO_2 sorption process by [aEMMIM][BF_4] are shown in Figure 2.7. The high viscosity of [aEMMIM][BF_4] resulted the difficult diffusion of CO_2 through [aEMMIM][BF_4] which prevents it from interacting chemically with CO_2.

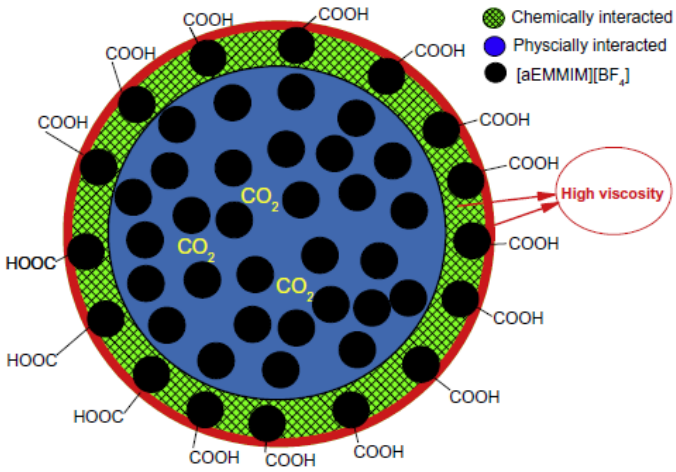

Figure 2.7: Proposed CO_2 absorption process by [aEMMIM][BF_4] [120]

Feng *et al.* (2010), have studied the absorption of CO_2 in aqueous solution of functionalized ionic liquids with MDEA [17]. They used lysine and glycine as anion and ammonium based as cation with different of alkyl chain length. It had been found that adding amino acid as anion greatly reinforced the CO_2 absorption of MDEA aqueous solution. The results showed that by using 15% AAILs + 15% MDEA had higher absorption rate and larger uptake capacity than total 30% amines. Table 2.2 shows the absorption capacity of aqueous solutions of 15% AAILs + 15% MDEA. Table 2.2 shows that the lysine based ILs was much higher than glycine based ILs which results from the two amine groups in one lysine molecule.

Table 2.2: Absorption capacity of aqueous solutions of 15% ILs + 15% MDEA

Absorbent	Mol CO_2 / mol amines
15% $[N_{1111}][Gly]$ + 15% MDEA	0.562
15% $[N_{2222}][Gly]$ + 15% MDEA	0.643
15% $[N_{1111}][Lys]$ + 15% MDEA	0.694
15% $[N_{2222}][Lys]$ + 15% MDEA	0.740
15% MEA + 15% MDEA	0.363

Zhang *et al.* (2013), have studied the absorption of CO_2 by amino acid-functionalized and traditional dicationic ionic liquids, (DILs) [97]. The results showed that CO_2 absorption capacities of pure AA-DILs were enhanced compared to monocationic ILs to give a carbamate precipitate at ambient pressure and 40 ^oC. They also studied the effect by addition of water to DILs which it might give an efficient manner for CO_2 gas capture through mixing these DILs with water. The results showed that by adding at least 60% water in $[bis(mim)C_4][Pro]_2$, the viscosity decreased hence the performance of CO_2 gas capture was enhanced largely.

Goodrich *et al.* (2011), studied the CO_2 sorption on amine functionalized anion-ILs [60]. The cation used was phosphonium based, $[P_{66614}]$, and amino acids as anion. The result showed that all AAILs synthesized rise above 0.5 mol/mol indicates the 1:1 mechanism was dominant. For $[P_{66614}][Lys]$ rises above 1 mol/mol, but in [Lys], there are two amines so its theoretical limit for the 1:1 absorption mechanism is 2 mol/mol. They also studied the effect of water on AAILs for CO_2 sorption. For $[P_{66614}][Pro]$

with 4 wt% of water, capacity of CO_2 sorption appears to be slightly decreased at lower pressures but at higher pressures it become equivalent. However, when large amount of water quantities are present, it can be seen that the water seems to have substantial impact on CO_2 sorption capabilities of ILs. They tested when 14 wt% of water are present on $[P_{66614}][Met]$, the CO_2 capacity reduced by approximately 0.2 mol/mol at 0.25 bar and by 0.1 mol/mol at 1 bar.

A hydrophilic AAILs, $[C_2OHmim][Gly]$ has been synthesized to enhance the process of MEA for CO_2 capture [61]. They studied the CO_2 capture into different mole ratios of MEA/$[C_2OHmim][Gly]$. The results showed that the capacity of MEA solution was 0.430 mol/mol and for $[C_2OHmim][Gly]$ was higher at 0.545 mol/mol. By increasing the amount of $[C_2OHmim][Gly]$, the CO_2 absorption also increased. When the mole ratio of MEA and $[C_2OHmim][Gly]$ was 7:3, the capacity of mixed solution was 0.534 mol CO_2/mol absorbent was almost the same as pure $[C_2OHmim][Gly]$. Therefore, further increase of $[C_2OHmim][Gly]$ seems no significant enhancement on the CO_2 capture. The results indicated that the interaction of MEA/$[C_2OHmim][Gly]$ on CO_2 absorption involved a mutual promoting relationship that enhanced the absorption capacity. As reported in most research, [69, 121], In the system for MEA solution, (MEA denoted as RR'NH) reacts with CO_2 through the formation of zwitterion as intermediate:

$$CO_2 + RR'NH_2 \rightleftharpoons RR'NH^+ COO^-$$

Then the zwitterions undergo the deprotonation by a base B (base catalyst), where B is a base that could be an amine, OH-, or H_2O.Thereby, these results in the formation of carbamate:

$$RR'NH^+ COO^- + B \rightleftharpoons RR'N COO^- + BH^+$$

Meanwhile the hydrophilic AAILs, $[C_2OHmim][Gly]$, also reacts with CO_2 which the reaction is similar to that between MEA and CO_2. In the system of AAILs, the base B is mostly $[C_2OHmim][Gly]$. Therefore, in the system of MEA/$[C_2OHmim][Gly]$ solution, both of the two components could react with CO_2 and they would compete each other.

To study the effect of water in ILs, McDonald *et al*. (2014), reported that CO_2 capture by AAILs are largely impacted with the presence of water [91]. The amino acid as anions plays only a transitory role in the CO_2 capture in the first minutes of exposure to wet CO_2 stream. The carbamate formed by the amine-functionalized in

amino acids reacts with CO_2. This carbamate releases the covalently bounded with CO_2 thus forming mixture of carbonate and bicarbonate.

Munoz *et al*. (2009), have come out with the mechanism when AAILs react with CO_2 [122]. The combination of CO_2 with the absorbents gives rise to a carbamate as shown in Figure 2.8. In Figure 2.8 shows that when amino acids dissolved in water, exist as a zwitterionic form (II-A) which means, that the amino group is protonated and hence not able to react with CO_2. Therefore, equimolecular amount of base was added to free the amino group in aqueous solution (III-A). This amino interacts with CO_2 to form a complex (IV-A) by an equilibrium reaction. Then, a basic group is needed to remove a proton to give the final carbamate (V-A). It should be noted that not only amino groups can react with CO_2, but other groups that present in the system are also capable.

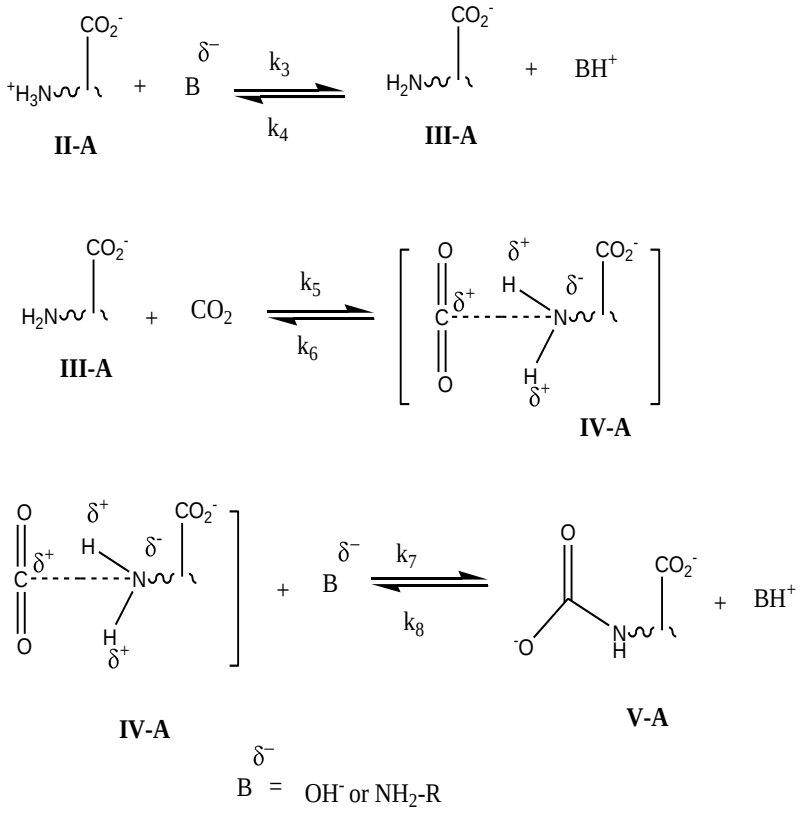

Figure 2.8: The formation of carbamate

If the pH of solution is higher than 7, hydroxide ions react with CO_2 to give hydrogen carbonate ions as shown in Equation 2.3 which can react again with hydroxide ions (Equation 2.4). Thus two hydroxide ions react very fast with one CO_2 molecule to give a system where only carbonate ions are theoretically present at the

end of the process. On the other hand, carbonate ions react with CO_2 molecules (Equation 2.5) to give hydrogen carbonate species.

$$CO_2 + OH \leftrightarrow HCO_3^- \quad 2.3$$

$$HCO_3^- + OH^- \leftrightarrow CO^{2-}_3 + H_2O \quad 2.4$$

$$CO_2 + CO^{2-}_3 + H_2O \leftrightarrow 2HCO_3^- \quad 2.5$$

Thus, in the first absorption, CO_2 is transformed into carbamate as shown in Figure 2.8 and into carbonate and hydrogen carbonate ions. After the first desorption, the carbamate formation is reversed but some of the carbonate and hydrogen carbonate ions remain in the system and therefore, the CO_2 removal is not completely achieved in desorption process. Hence, in second absorption, the CO_2 can only become a carbamate thus indicates lower absorption [122].

Table 2.3 shows a literature data on CO_2 sorption in AAILs. The result shows that most of the AAILs absorb CO_2 at low pressure (1 to 2 bar) and ambient temperature (298 K to 313 K). The results showed that AAILs able to capture CO_2 up to 1 mol/mol thus indicates that mechanism 1:1 between AAILs and CO_2 is achieved. This value is higher than alkanolamine which limited only 0.5 mol/mol. By using amine functionalized anion, AAILs, able to absorb CO_2 higher than RTILs since chemical absorption is involved in AAILs rather than physical adsorption in RTILs. However, by tethering amine either cation or anion, it will create a liquid with high viscosity thus it is difficult to handle.

Table 2.3: Literature data for CO_2 sorption by AAILs.

AAILs	P (bar), T (K)	Mol CO_2 / mol ILs	Wt %	Ref.
[bmim] [Arg]	2 bar, 298 K	0.62	8.74	[70]
[bmim] [Lys]	2 bar, 298 K	0.48	7.44	[70]
[bmim] [His]	2 bar, 298 K	0.45	6.76	[70]
[bmim] [Met]	2 bar, 298 K	0.42	6.44	[70]
[bmim] [Leu]	2 bar, 298 K	0.38	6.22	[70]
[bmim] [Gly]	2 bar, 298 K	0.38	7.85	[70]
[bmim] [Val]	2 bar, 298 K	0.39	6.73	[70]

AAILs	P (bar), T (K)	Mol CO_2 / mol ILs	Wt %	Ref.
[bmim] [Ala]	2 bar, 298 K	0.39	7.56	[70]
[bmim] [Pro]	2 bar, 298 K	0.32	5.56	[70]
[aemmim] [Tau]	1 bar, 303 K	0.9	15.0	[119]
[aP_{4443}] [Gly]	1 bar, 298 K	0.20	2.77	[71]
[aP_{4443}] [Ala]	1 bar, 298 K	0.18	2.38	[71]
[aP_{44433}] [Val]	1 bar, 298 K	0.13	1.59	[71]
[aP_{4443}] [Leu]	1 bar, 298 K	0.10	1.18	[71]
[Emim][Lys]+48.7wt%	1 bar, 313 K	0.87	3.83	[123]
[Emim][Gly]+ 48.7wt%	1 bar, 313 K	0.49	2.16	[123]
[Emim] [Ala] + 48.7 wt% PMMA	1 bar, 313 K	0.45	1.98	[123]
[Emim] [Arg] + 48.7 wt% PMMA	1 bar, 313 K	0.52	2.28	[123]
20% $C_2(N_{112})_2$ Gly_2	1 bar, 298 K	0.66	3.62	[43]
40% $C_2(N_{112})_2$ Gly_2	1 bar, 298 K	0.44	4.85	[43]
80% $C_2(N_{112})_2$ Gly_2	1 bar, 298 K	0.28	4.74	[43]
20% $C_2(N_{114})_2$ Gly_2	0.97bar,298K	0.66	3.25	[43]
40% $C_2(N_{114})_2$ Gly_2	0.97bar,298K	0.40	4.52	[43]
80% $C_2(N_{114})_2$ Gly_2	0.97bar,298K	0.28	4.49	[43]
[P_{66614}] [Met]	1 bar, 298 K	0.88	6.14	[124]
[P_{66614}] [Pro]	1 bar, 298 K	0.90	6.63	[68]
[Bis(mim)C_2] [Gly] $_2$	1 bar, 313 K	1.00	12.93	[114]
[Bis(mim)C_2] [Pro] $_2$	1 bar, 313 K	1.05	10.98	[114]
[Bis(mim)C_4] [Gly] $_2$	1 bar, 313 K	1.10	13.73	[114]
[Bis(mim)C_4] [Pro] $_2$	1 bar, 313 K	0.98	9.61	[114]
[P_{66614}] [Gly]	1 bar, 298 K	1.26	9.93	[96]
[P_{66614}] [Ala]	1 bar, 298 K	0.66	5.08	[96]
[P_{66614}] [Sar]	1 bar, 298 K	0.91	7.0	[96]
[P_{66614}] [Ile]	1 bar, 298 K	0.97	6.95	[96]
[P_{66614}] [Pro]	1 bar, 298 K	0.88	6.49	[96]

AAILs	P (bar), T (K)	Mol CO_2 / mol ILs	Wt %	Ref.
$[P_{66614}]$ [Met]	1 bar, 298 K	0.88	6.14	[96]
$[P_{66614}]$ [Lys]	1 bar, 298 K	1.37	9.58	[60]
$[P_{66614}]$ [Tau]	1 bar, 298 K	0.80	5.79	[60]

2.2.5 CO_2 sorption on polymerized ionic liquids (PILs)

In CO_2 separations, ILs have been proposed as alternatives for CO_2 capture media since it is in solid form thus easier to handle. Tang *et al.* (2005), is the first group who reported on PILs for CO_2 sorption. They found out that polymers from ILs monomers had higher CO_2 sorption capacity than RTILs [80]. PILs were shown to exhibit several times higher than their monomeric forms or commonly used ILs. In PILs, they have much faster CO_2 sorption and desorption rates than others RTILs [74].

Since then, PILs have recently attracted attention for CO_2 absorption [40, 74-78]. This is due to larger free volume in PILs which can trap a larger amount of CO_2. The properties of PILs also can be customized by varying the combination of polycation-anion pair [79]. The capacity of CO_2 capture depends on the type of polycation, polymer backbone, anion and substituents [80]. The polycation type is considered a decisive factor in CO_2 capture performance, ammonium-based PILs having capacity than imidazolium-based PILs [80, 81]. By comparing the backbone of cation, PILs with a polystyrene backbone, vinylbenzyltrimethylammonium ([VBTMA]), gave higher CO_2 sorption than those with a polymethylmethacrylate, ([MATMA]) backbone.This is because the structures with polystyrene backbone in cation exhibit higher adsorption capacity and the larger substituent on imidazolium cation pose hindrance and lower the adsorption. [81].

The result showed that poly[VBTMA][BF_4] had a higher CO_2 sorption capacity than poly[MATMA][BF_4] [82]. This is probably because of polystyrene backbone was more rigid than [MATMA]. They also studied on the effects of alkyl chain length and observed that with long alkyl chain, it may reduced the CO_2 sorption due to steric effects in cation may hinder the interaction. The anions in PILs also played an important factor. The results showed that poly[VBTMA][BF_4] had strong interaction with CO_2 hence gave higher CO_2 sorption capacity. However, with [PF_6] and [Tf_2N]

anion, CO_2 sorption capacity decreased slightly and showed a very low CO_2 sorption capacity. This is contrasts to the RTILs that in PILs, fluorine atom not a decisive factors in determining CO_2 sorption.

Tang *et al*. (2005), also reported that PILs able to adsorb CO_2 even at low pressure [81]. The results showed that poly[VBTMA][BF_4] and poly[MATMA][BF_4] took up 0.102 and 0.079 mol/mol respectively at 0.78 bar pressure and 298 K. Their monomers showed no measureable sorption of CO_2 because of crystalline structures in low pressure. In PILs, it took only several minutes to reach 90% capacity and less than 60 minutes for equilibrium. The specific surface area for poly[VBTMA][BF_4] was 0.46 m^2/g and 20.5 m^2/g for poly[MATMA][BF_4]. This is due to a non porous structures in poly[VBTMA][BF_4] thus gave lower specific surface area while poly[MATMA][BF_4] was porous due to the uneven structure thus gave a larger surface area. Therefore, they proposed that the CO_2 sorption in PILs involves absorption (the bulk) and adsorption (the surface).

The rates of adsorption and desorption of PILs is fast as compared to RTILs. This might be because of the bulk adsorption phenomenon appears to govern the capture progress. RTILs with polymerizable entities show higher permeability, solubility and diffusivity values for CO_2, N_2 and CH_4. These PILs structures can capture almost double the amount of CO_2 compared to the RTILs. However, with longer alkyl chains on PILs cation, may pose a steric hindrance between CO_2-cation interaction. This may shrink the microvoid volume which resulting from plasticization and rigidity due to crosslinking, thus decreasing the CO_2 sorption capacity [125].

CO_2 sorption of the PILs was much faster than RTILs. It took only 4 min for Poly[VBIT] and Poly[VBIH] and 3 min for Poly[BIMT] to reach their 90% sorption capacities and about 30 min to reach their full capacities. In contrast, it took more than 400 min for the monomers, BIMT and [bmim][BF_4] to reach their equilibrium [80]. The fast of adsorption and desorption rates in PILs might be because of polymers are solids at room temperature. The calculated of CO_2 adsorption assuming a monolayer of polymer particles surface showed only 4% of the measured total of CO_2 sorption capacities. This indicates that the bulk of polymer particles played a major role in CO_2 sorption. Therefore, CO_2 adsorption involves more on adsorption in the bulk but less adsorption in the surface [80].

Yu *et al.* (2013), have prepared a new porous polymeric particles, *i.e.* poly[VBTEA][Cl], poly[VBTEA][BF_4] and poly[VBTEA][PF_6] which prepared from crosslinking polymerization of 4-vinylbenzyltriethylammonium with *N,N*-methylenebisacrylamide *via* inverse suspension polymerization [78]. To get polymer microparticles with porous structure and larger special surface area, PEG 600 used as porogen since it can be conveniently removed to form pores. The apparent porosities are estimated to be 55 %, 69.7 % and 64.3 % respectively. The porous polymeric microparticles exhibited high CO_2 sorption capacity of poly[VBTEA][PF_6] with 14.04 mg/g, poly[VBTEA][BF_4] with 11.84 mg/g and poly[VBTEA][Cl] with 10.40 mg/g.

Privalova *et al.* (2013), reported that poly[BIEMA][PF_6] showed higher CO_2 soprtion at 0.029 mol/mol followed with poly[BIEMA][BF_4] with 0.022 mol/mol [79]. Contrary to RTILs, the presence of F atoms in PILs seems to be not a decisive factor to enhance CO_2 sorption. Poly[BIEMA][OTf^-] and poly[BIEMA][NTf_2^-] showed only 0.019 and 0.018 mol/mol respectively. This is due to the bulky anions in [OTf^-] [NTf_2] may decrease the spare volume thus prevent the CO_2 penetration towards polycation.

Wilke *et al.* (2012), have study to enhance the CO_2 sorption by mesoporous PILs via a hard templating of silica nanoparticles [126]. They studied whether the presence of pronounced specific surface area can increase the capacity CO_2 uptake even more. It was found that the highest uptake for mesoporous PILs (mpPIL) is 0.46 mmol/g, higher than PILs with 0.13 mmol/g and the monomeric species only 0.02 mmol/g at 273 K, 1 bar pressure. PILs have known as powerful CO_2 adsorbents and usually it is found that PILs shows a higher CO_2 uptake compared to the monomer analogues. The mesoporous PILs showed a significantly faster CO_2 adsorption than nonporous PILs. It also showed that the adsorption into the bulk PIL is much slower at 30 h, than mesostructured PILs only takes 5 min. Hence, the beneficial effect of the additional specific surface area was proven while maintaining and increasing the favourable interactions of the ILs with CO_2. The presence of large mesopores can significantly boost the mass transfer through the system which is beneficial for many applications.

Bhavsar *et al*. (2012), studied the effect of anion on CO_2 sorption. The cation used was poly[DADMA] and the anion used was a different types of counter ions such as organic anion; carboxylates (Ac, TFAc, HFB, Bz), sulfonates (MS, TFMS, PTS) and inorganic anions (BF_4, NO_3, Cl) [74]. The CO_2 sorption coefficient (S_{CO2}) on various

carboxylate based PILs was increased on order of [TFAc] < [HFB] < [Bz] < [Ac] by following the order of increasing their basicity (PKa of conjugate acid: [TFAc]=0.0 < [HFB]=0.4 < [Bz]=4.2 < [Ac]=4.8. This behaviour of PILs is similar to ILs where by increasing basicity of anion, the CO_2 sorption also increased. However, for sulfonated anions, S_{CO2} followed the order of [TFMS] > [PTS] ≈ [MS] where pKa of conjugate acids for [TFMS]=-13, [PTS]=-2.8 and [MS]=-2.0. Thus basicity of the anion may not solely responsible for increasing the CO_2 sorption in PILs. Besides basicity, fractional free volume (FFV) in polymer matrix may also compete for governing the CO_2 sorption. For PILs containing inorganic anion (Cl, NO_3 and BF_4), The results also showed that S_{CO_2} and selectivities for S_{CO_2}/S_{H_2} and S_{CO_2}/S_{N_2}, increased with increasing molar mass of the anion. However, this parameter of molar mass was not applicable in case of PILs with carboxylated and sulfonated anions.

Xiong *et al.* (2012), studied PILs which prepared by melt condensation polymerization with stannous octoate as catalyst. The results showed that the CO_2 sorption capacities for PILs are higher than in ILs [76]. For Poly[EEIm][PF_6] and poly[EEIm][BF_4] took up 0.042 and 0.045 mol/mol higher than the monomer with only 0.021 and 0.01 mol/mol respectively. However in the case of [HHIm] [PF_6] provided the highest CO_2 sorption capacity with 0.1 mol/mol. In particular, PF_6- improved the CO_2 solubility in ILs and PILs. These results suggested that the association of CO_2 with the anion was the best indicator of CO_2 solubility in imidazolium-based ILs. It can be seen that the [HHIm][PF_6] presented the highest CO_2 solubility among all the ILs and PILs. This may be due to the association of CO_2 with the anion and the hydrogen bonding interactions between the hydroxyl groups of [HHIm][PF_6] and CO_2 [76].

Sorption rate for these PILs is really fast compared to RTILs. It took several minutes for them to reach 95%, to their equilibrium where as for RTILs, [MABI][BF_4] and [bmim][BF_4] took 400 min to reach equilibrium. The fast sorption of PILs is affected neither by particle size nor by surface area. When replacing the [BF_4] in poly[VBBI][BF_4] with [Cl] anion, poly[VBBI][Cl] showed slower sorption rate even with the same magnitude of particle size suggesting that the fast CO_2 sorption is characteristic of PILs [80, 82].

The isothermal process of CO_2 sorption in PILs was found to be well fitting into dual-mode sorption model which describe the gas solubility in glassy polymer. This

suggests that the CO_2 sorption into PILs had two parts. One dissolved into matrix and the second adsorbed into microvoids following Langmuir hole-filling process. With the same backbone and similar anion, the CO_2 sorption is found to decrease in order of ammonium > pyridinium > phosphonium > imidazolium cations. By comparing the computed values of Henry's law constant (k_D) and the affinity constant for Langmuir mode, it is found to be in same order of magnitude. This is showed that the ammonium cation has the strongest interaction with CO_2 whereas the imidazolium has the weakest. Ammonium based PILs has a high saturation capacity C_H for Langmuir mode, suggesting a high fraction of microvoids compared to imidazolium-based ones [82].

Table 2.4: Literature data for CO_2 sorption in PILs

PILs	P (bar), T (K)	Mol /mol	Ref
Poly[VBTMA][PF_6]	0.789 bar, 295 K	0.11	[81]
Poly[VBTMA][Tf_2N]	0.789 bar, 295 K	0.029	[81]
Poly[VBTMA][Sac]	0.789 bar, 295 K	0.027	[81]
Poly[MATMA][BF_4]	0.789 bar, 295 K	0.080	[81]
Poly[VBTMA][BF_4]	0.789 bar, 295 K	0.102	[81]
Poly[VBTEA][BF_4]	0.789 bar, 295 K	0.049	[81]
Poly[VBTBA][BF_4]	0.789 bar, 295 K	0.031	[81]
Poly[VBIH][BF_4]	0.789 bar, 295 K	0.028	[80]
Poly[VBIT][BF_4]	0.789 bar, 295 K	0.022	[80]
Poly[BIEMA][BF_4]	1 bar, 298 K	0.022	[79]
Poly[BIEMA][PF_6]	1 bar, 298 K	0.029	[79]
Poly[BIEMA][OTf]	1 bar, 298 K	0.019	[79]
Poly[EEIm][PF_6]	1 bar, 298 K	0.042	[76]
poly[EEIm][BF_4]	1 bar, 298 K	0.045	[76]

Table 2.4 shows a literature data on CO_2 sorption on PILs reported. It can be seen that all PILs have low CO_2 sorption capacities (average 0.05 mol/mol) at low pressure (up to 1 bar). This is due to low physical adsorption capacities occurred in most PILs as compared to AAILs. Therefore, by tethering the amine functional in PILs may enhance the CO_2 sorption capacities and would overcome the viscosity problem in ILs.

CHAPTER 3

RESEARCH METHODOLOGY

It is important to understand the major factors that affect the CO_2 solubility in ILs and to produce ILs that has high potential for CO_2 sorption. ILs that contains functional group either in cation or anion or both may enhance the CO_2 sorption in ILs.

In this study, twelve amino acid polymerized ionic liquids (AAPILs) have been synthesized where the monomers are amino acids ionic liquids (AAILs) which will be polymerized by using radical initiator AIBN. Amino acids were used as anion with amine functional groups in their amino acids structure. By tethering the amine groups in anion, it can enhance the CO_2 sorption by following the mechanism of 1:1 as suggested by Goodrich *et al.* (2011) [96]. The anions are glycine [Gly], alanine [Ala], serine [Ser], proline [Pro], taurine [Tau], histidine [Hist], lysine [Lys] and arginine [Arg].

These anions have been chosed to study the amine functionality for reaction with CO_2 as amino acid [Gly], [Ala], [Ser], [Pro] and [Tau] contain one functional amine and for [Hist], [Lys] and [Arg] contain several additional amines which expected to give higher CO_2 uptake. In addition, these types of amino acids are usually used for CO_2 sorption as reported in literature. The cations are vinylbenzyltrimethylammonium [VBTMA], vinylbenzyltriethylammonium [VBTEA], vinylbenzyltributylammonium [VBTBA], vinylbenzylmethylimidazolium [VBMI] and vinylbenzylmethylpiperidinium [VBPPN]. The structures for all the AAPILs synthesized are structured in Table 3.1.

Table 3.1: Polymer name and monomer structure

No	Polymer name	Polymer Abbreviation	Polymer structure
1	Poly[vinylbenzyltrimethylammonium][Glycinate]	Poly[VBTMA][Gly]	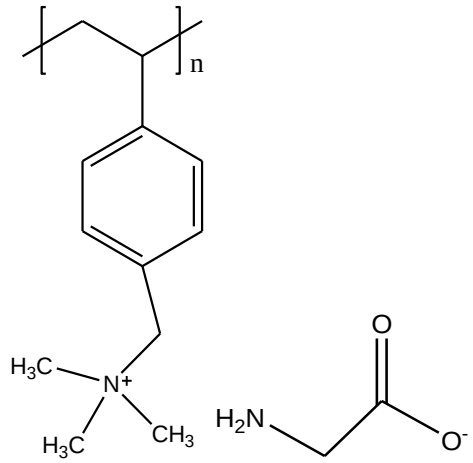
2	Poly[vinylbenzyltrimethylammonium][Alanate]	Poly[VBTMA][Ala]	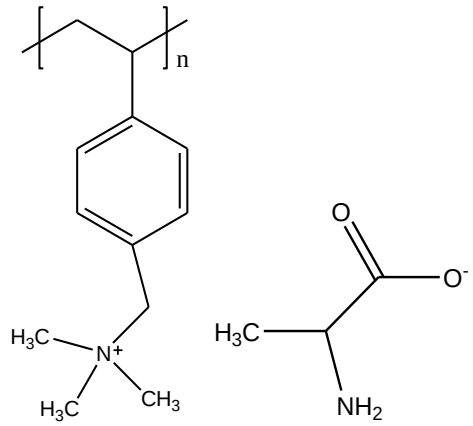
3	Poly[vinylbenzyltrimethylammonium][Serinate]	Poly[VBTMA][Ser]	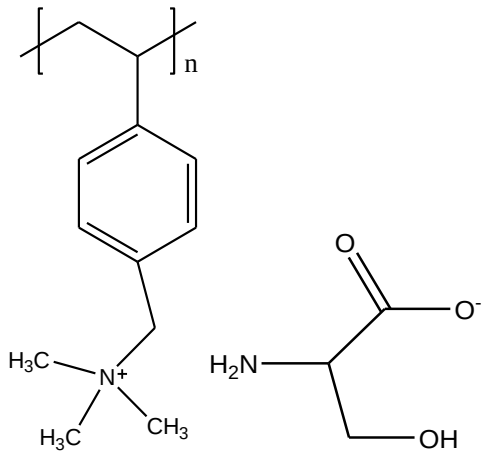

No	Polymer name	Polymer Abbreviation	Polymer structure
4	Poly[vinylbenzyltrimethylammonium][Prolinate]	Poly[VBTMA][Pro]	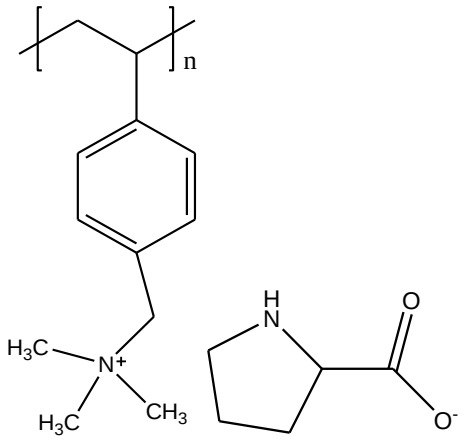
5	Poly[vinylbenzyltrimethylammonium][Taurinate]	Poly[VBTMA][Tau]	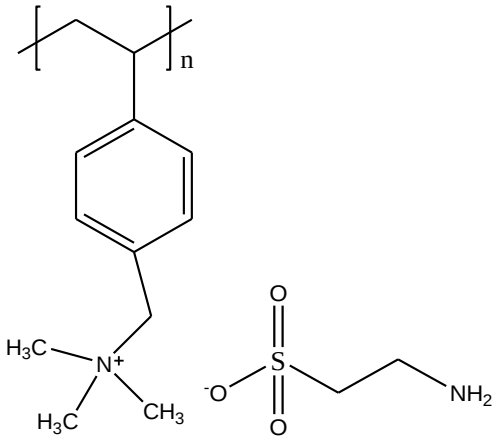
6	Poly[vinylbenzyltrimethylammonium][Histidinate]	Poly[VBTMA][Hist]	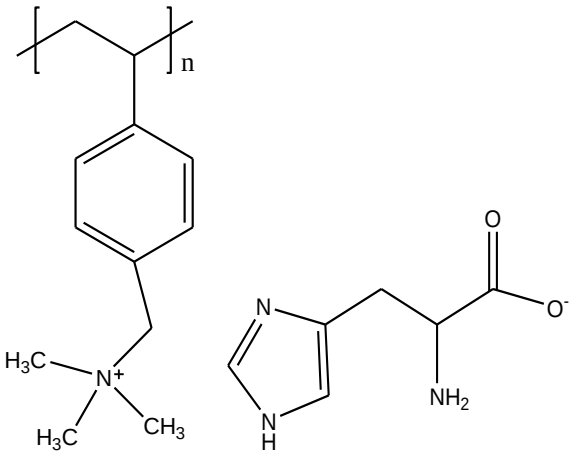

No	Polymer name	Polymer Abbreviation	Polymer structure
7	Poly[vinylbenzyltrimethylammonium][Lysinate]	Poly[VBTMA][Lys]	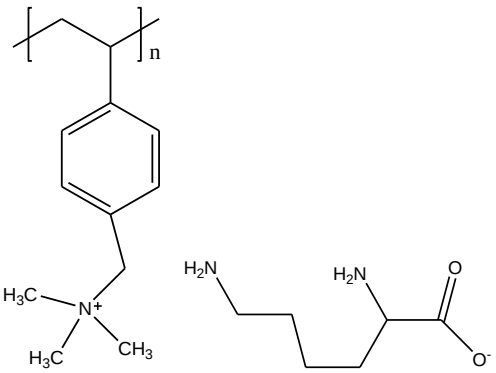
8	Poly[vinylbenzyltrimethylammonium][Arginate]	Poly[VBTMA][Arg]	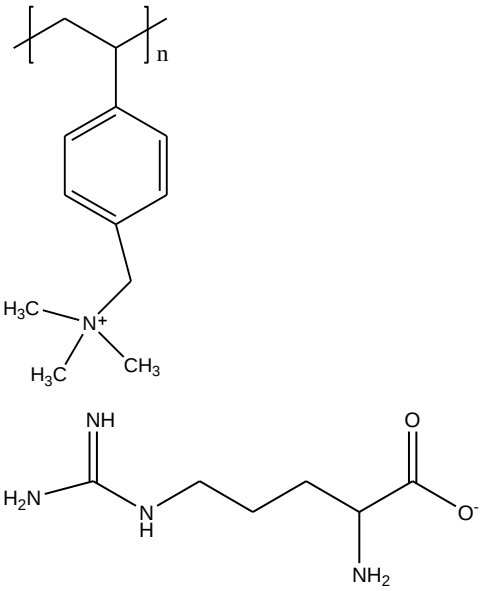
9	Poly[vinylbenzyltriethylammonium][Lysinate]	Poly[VBTEA][Lys]	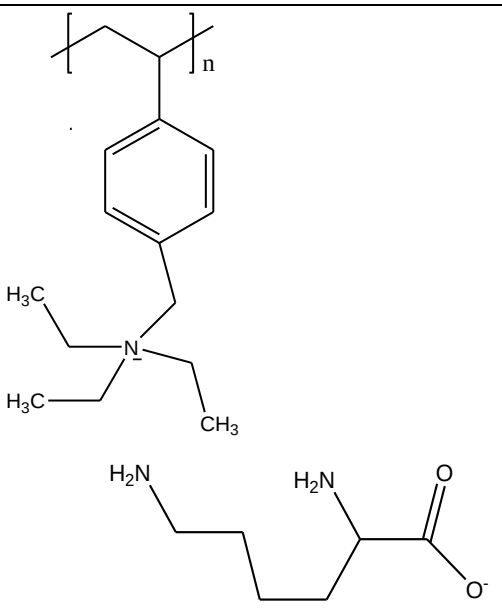

No	Polymer name	Polymer Abbreviation	Polymer structure
10	Poly[vinylbenzyltributylammonium][Lysinate]	Poly[VBTBA][Lys]	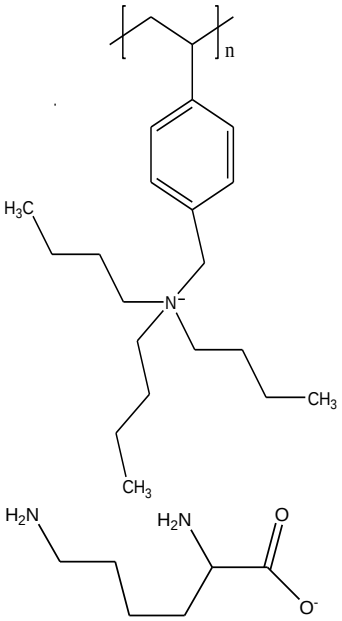
11	Poly[vinylbenzylmethylimidazolium][Lysinate]	Poly[VBMI][Lys]	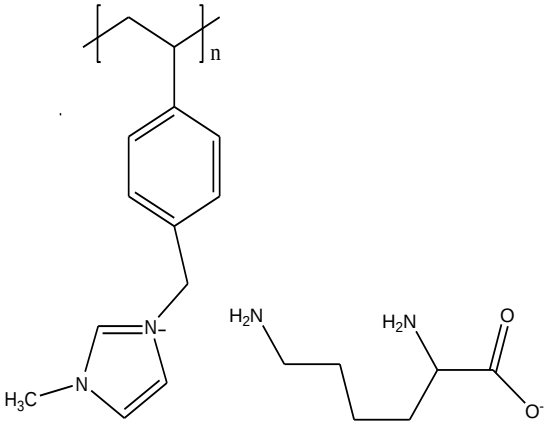
12	Poly[vinylbenzylmethylpiperidinium][Lysinate]	Poly[VBPPN][Lys]	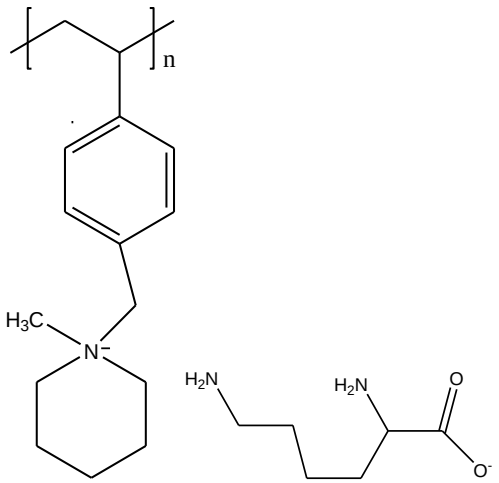

3.1 Materials

The chemicals used in the synthesis of AAPILs were (vinylbenzyl)trimethylammonium chloride 99%, 4-vinylbenzyl chloride, 2,6-di-tert-butyl-4-methylphenol (DBMP) 99.0%, glycine, L-alanine, L-serine, L-proline, L-histidine, lysine, L-arginine and anion exchange resin used was Amberlyst A-26 (hydroxide, OH^- form) which was purchased from Sigma Aldrich, Malaysia. 1-methylimidazole, 1-methylpiperidine, triethylamine 99.5%, tributylamine 99.5%, taurine, methanol, ethanol, diethylether, ethyl acetate and acetonitrile are purchased from Merck, Malaysia. Radical initiator used was α, α'-Azobisisobutyronitrile (AIBN) was purchased from R&M, Malaysia. All chemicals used in synthesis and purification are used without any further purifications. Purified gases were supplied by Linde Gases Sdn. Bhd Malaysia were used for the CO_2 measurement. The grades of gases used are carbon dioxide (CO_2) with purity 99.9%, methane (CH_4) with purity 99.99% and nitrogen (N_2) with purity 99.9%.

3.2 Synthesis of Ionic Liquids, RTILs

3.2.1 Synthesis of (vinylbenzyl)tritethylammonium chloride, [VBTEA][Cl]

4-vinylbenzyl chloride (79.36 g, 0.52 mol), triethylamine (50.59 g, 0.5 mol) and 0.4 g of DBMP were added in dried 250 ml three necked flask. The reaction mixture is stirred under nitrogen at 50 ^oC for two days. The white solid formed [VBTEA][Cl] is washed with diethylether and filtered and further dried under vacuum at 60 ^oC for 2 days. The synthesis route is shown in Figure 3.1.

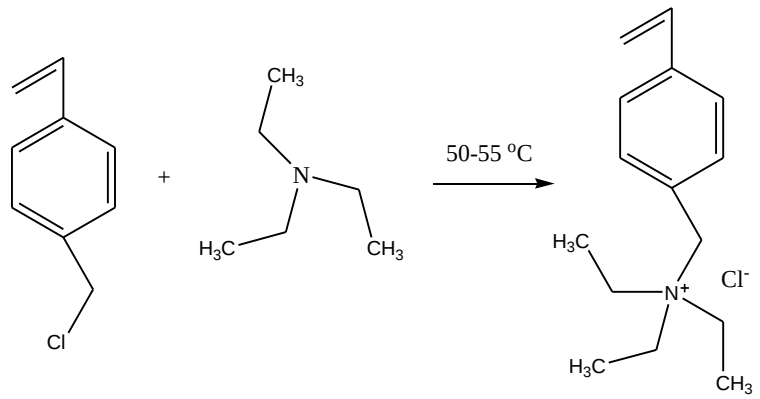

Figure 3.1: Synthesis route of [VBTEA][Cl]

3.2.2 Synthesis of (vinylbenzyl)tributylammonium chloride, [VBTBA][Cl]

Similar procedure used as describe in 3.2.1 to synthesized [VBTBA][Cl] by replacing triethylamine with tributylamine. The white solid formed is washed with diethylether, filtered and dried in vacuum oven at 60 ^{o}C for 2 days.

3.2.3 Synthesis of (vinylbenzyl)methylimidazolium chloride, [VBMI][Cl]

4-vinylbenzyl chloride (79.36 g, 0.52 mol), 1-methylimidazole (41.05 g, 0.5 mol), methanol and 0.4 g of DBMP were added in dried 250 ml three necked flask. The reaction mixture is stirred under nitrogen at 50 ^{o}C for two days. The yellow color viscous liquid is washed with diethylether and ethyl acetate. Two layers are formed. The upper layer was decanted and this was repeated for 3 times to remove any excess reactant. The solvents are removed by using rotary evaporator at 50 ^{o}C with reduced pressure. It was further dried by using vacuum oven for 2 days. The synthesis route is shown in Figure 3.2.

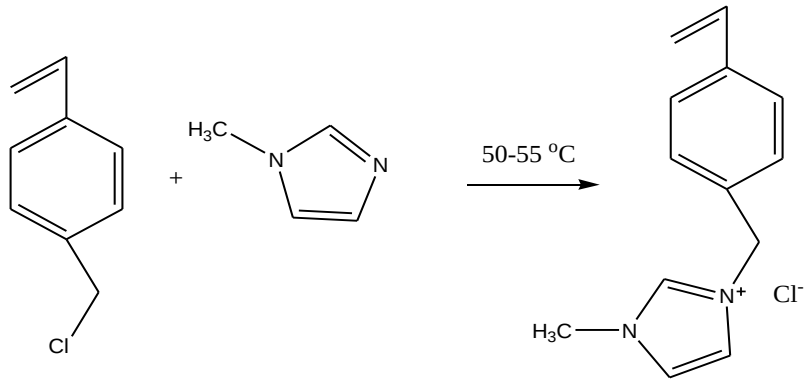

Figure 3.2: Synthesis route for [VBMI][Cl]

3.2.4 Synthesis of (vinylbenzyl)methylpiperidinium chloride, [VBPPN][Cl]

4-vinylbenzyl chloride (79.36 g, 0.52 mol), 1-methypiperidine (49.59 g, 0.5 mol), methanol and 0.4 g of DBMP were added in dried 250 ml three necked flask. The reaction mixture is stirred under nitrogen at 50 ^{o}C for two days. The white solid formed is washed with diethylether and ethyl acetate, followed with filtration. The excess of solvents was removed by using rotary evaporator at 50 ^{o}C with reduced pressure. It was further dried by using vacuum oven for 2 days. The synthesis route is shown in Figure 3.3.

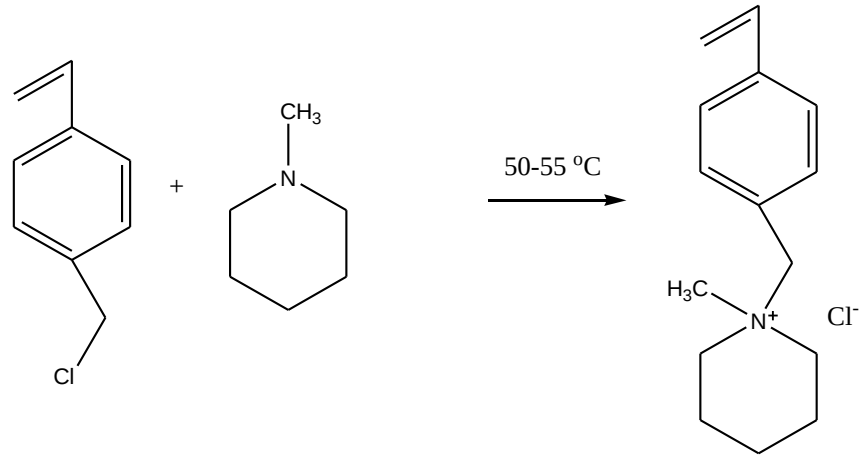

Figure 3.3: Synthesis route of [VBPPN][Cl]

3.3 Synthesis of the monomers, AAILs

All the starting material from [VBTMA][Cl], [VBTEA][Cl], [VBTBA][Cl], [VBMI][Cl] and [VBPPN][Cl] are subjected to anion exchange from Cl^- to OH^- and proceeded to neutralization process with amino acids.

3.3.1 Anion exchange from Cl^- to OH^-

10 g of the starting materials, [VBTMA][Cl] was dissolved in 200 ml of ethanol (or any solvents/water) until it was fully dissolved. The ILs solution was poured in a column chromatography filled with anion exchange resin, Amberlyst A26 (OH^- form). The resin, was filled into a column and aqueous [VBTMA][Cl] was passed through the resin. The resulting [VBTMA][OH] was collected dropwise with 1 drop in 10-15 seconds. The [VBTMA][OH] was then tested for residual Cl^- by silver nitrate ($AgNO_3$). The absence of Cl^- in the solution was confirmed with no white precipitate form. Similar procedure was used to exchange the Cl^- to OH^- for all the starting material.

3.3.2 Neutralization with amino acid

[VBTMA][OH] was neutralized with equimolar of amino acid (glycine, alanine, serine, proline, taurine, histidine, lysine or arginine). The amino acid was added to the

solution of [VBTMA][OH] and stirred for 1 day. The solvents (ethanol) were removed by using rotary evaporator 50 ^{o}C at low pressure. The excess of amino acids was precipitated out by adding proportions of acetonitrile and methanol in 7:3 ratio which gave white powder. This was then filtered out. The AAILs solution was further continued with rotary evaporator to remove all the solvents. The AAILs produced is a viscous ILs and store in a sample bottle and sealed. Similar procedure was used in neutralization process for [VBTEA], [VBTBA], [VBMI] and [VBPPN] cation. The synthesis route to synthesize the monomers is shown in Figure 3.4.

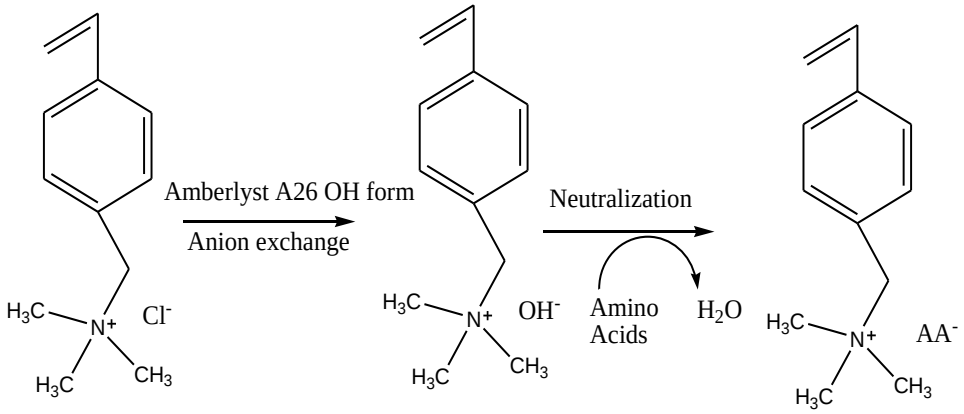

AA^- = glycine, alanine, serine, proline, taurine, histidine,lysine or arginine

Figure 3.4: Synthesis route of the monomers, AAILs with [VBTMA] as cation

3.4 Synthesis of amino acids polymerized ionic liquids (AAPILs)

In polymerization process, 10 g of the monomer [VBTMA][AA] (or any other cation), 100 mg AIBN and 5 ml of methanol are charge into three necked flask under nitrogen atmosphere and stirred. The flask is immersed in an oil bath at 65 ^{o}C for 1 day. The solid formed in flask was taken out and washed with methanol and dried in vacuum oven at 80 ^{o}C for 3 days. Similar procedure was used for the other cations and anions. The synthesis route to synthesized AAPILs from the monomer, AAILs, is shown in Figure 3.5

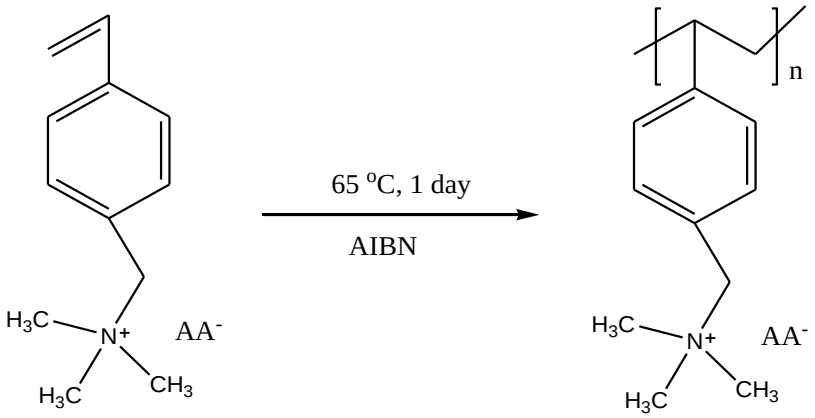

Figure 3.5: Polymerization of AAILs to AAPILs

3.5 Characterization of Ionic Liquids

The structures of all the starting materials were confirmed by using ^{1}H-NMR. The characterization of AAILs and AAPILs was carried out using ^{1}H-NMR, FTIR, Ultrapycnometer, Karl Fischer Coulomter, Ion Chromatography, Thermogravimetric analyzer, Differential Scanning Coulometric, SEM and BET. The CO_2 sorption was carried out using gas absorption/adsorption cell.

3.5.1 Structure analysis

^{1}H-NMR spectra was recorded on a Bruker Avance DRX-400 spectrometer operating at 400 MHz with deuterated methanol as solvents. The chemical shifts (δ) are reported in ppm. Multiplicities are abbreviated as follows; s for singlet, d for doublet, t for triplet, m for multiplet and br for broad.

FTIR was used to confirm the functional groups in AAPILs synthesized. FTIR was used to see the difference in functional groups before and after CO_2 sorption for AAPILs synthesized. FTIR spectra were recorded using Shimadzu FTIR in the region of 600-4000 cm^{-1} using Diamond Attenuated Total Reflactance (DATR measurement mode).

3.5.2 Density

The density of the synthesized AAPILs was determined by Ultrapycnometer 1000 Version 2.2 instrument using Argon gas. This instrument is designed for measuring the true volume and density of powders, foams and bulk solids. The samples ran for 6 times and the average is recorded with standard deviation ± 0.01 g/cm^3.

3.5.3 Water content

Water content for AAPILs was determined by Karl Fischer Coulometer model Mettler Toledo DL 39 attached with a Stromboli sample charger and the samples were heated to 150 ^oC to determine the moisture in AAPILs solid.

3.5.4 Chloride content

The chloride content of [VBTMA][OH] was determined by ion chromatography (IC) Metrohm Model 761 Compact. The equipment used was equipped with Metrosep A Supp 5-150 (6.10006.520) (4.0 mm x 150 mm) analytical column and a Metrosep A Supp 4/5 guard column (4.0 mm x 5 mm). The eluent used is a mixture of 3.2 mM Na_2CO_3 and 1.0 mM $NaHCO_3$. The data was analyzed with the aid of Metrodata IC Net 2.3 software.

3.5.5 Thermal stability

Thermal properties, degradation temperature (T_d), were measured using thermogravimetric analyzer (TGA) model Perkin Elmer Pyris 1, with heating rate of 40 ^oC/min and flow rate of nitrogen 20 ml/min. Glass transition temperature (T_g) was measured by differential scanning coulometric (DSC), Mettler Toledo model DSC 1 with heating rate 20 ^oC/min and flowrate of nitrogen 20 ml/min in temperature range from -130 ^oC to 130 ^oC. It was then cooled from ambient temperature to -130 ^oC using liquid nitrogen. Then isothermal at -130 ^oC for 2 minutes and continued with heating from -130 ^oc to 130 ^oC. The isothermal process was repeated for 2 minutes and the steps for second cycle were repeated for reproducibility.

3.5.6 Surface morphology

The morphology of AAPILs synthesized was determined by Scanning Electron Microscope (SEM), Variable Pressure Field Emmision Scanning Electron Microscope VPFESEM) model Zeiss Supra55VP. This morphology is to determine the topology structure of the sample whether the AAPILs have porous or nonporous structure. The magnification used is (300 to 5.00KX), working distance (3-6 mm) and accelerating voltage (2 to 5 kV).

3.5.7 Surface Area and Porosity (SAP) Analyzer

Surface area, pore size and pore volume of AAPILs before and after CO_2 sorption determined using surface area and porosity analyzer (Micromeritics TriStar II 3020). The SAP was calibrated using carbon black provided by Micromeritics. Before the measurement, 0.2 g sample in a sample cell was pretreated and degassed at 150 ^{o}C using N_2 for 3 hours. The purpose of this pretreatment is to remove any trapped moisture and impurities before the actual measurement. After the pretreatment process, the sample cell was tighten to the SAP system and immersed in a dewar filled with liquid N_2. The relative pressure (P/P_o) was set at 0.005-0.990, and the measurement completed in 8 hours.

3.6 CO_2 sorption measurement

The accuracy when measuring CO_2 solubility might be influence by the purity of the gas since it will affect the results. Therefore, completely degassing the solvent prior to measurement is the most important step to ensure that the absorbed gas measured during the experiment is the true gas solubility.

In this research, all CO_2 absorption studies were measured by using a gas adsorption/absorption cell as shown in Figure 3.6. The system used is a volumetric type based on pressure drop method. Before the measurement, leakage test was done at 10 bar to ensure there was no pressure drop caused by the gas leakage from the equipment and also to avoid the inaccuracy during the measurement. The equipment was also tested using monoethanolamine (MEA) as control and compares the result

with literature data. The result shown 0.47 mol/mol slightly lower than the reported in literature which is 0.55 mol/mol [14].

For the measurement procedure, the sample was first dried overnight in the oven at 110 ^{o}C to remove any moisture before the adsorption. Initially, the pressure was adjusted by using valve A and valve B to obtain the desired pressure in the CO_2 storage tank (bomb). The cell was vacuumed for 15 minutes to remove any gas in the system. Then, 0.5-1.0 g of sample was placed in the sample cell and tightly attached to the system. Once the desired temperature and pressure were stable, the CO_2 was introduced to the ILs by releasing valve B and the pressure drop was recorded until the cell's pressure remained stable. The calculation to determine the mole of CO_2 captured is shown in Equation 3.1.

$$n = \frac{P_{ini} \cdot V_{tot}}{Z_{ini} \cdot R \cdot T_{ini}} - \frac{P_{eq}(V_{tot} - V_{sample})}{Z_{eq} \cdot R \cdot T_{eq}} \qquad 3.1$$

where n = mol CO_2 captured, P_{ini} is the pressure obtained in the absence of a sample after expansion of the gas sample from the bomb into the whole system , V_{tot}= total of volume system (110 ml), Z_{ini}=compressibility factor (P_{ini}× T_{ini}), Z_{eq}=compressibility factor (P_{eq} × T_{eq}), P_{eq}=equilibrium pressure, V_{sample}=sample volume, R=0.0821 atm.L/mol.K, T_{ini}=initial temperature and T_{eq}=equilibirum temperature. The volume sample was measured by divided the mass of sample with density of the sample. The volume from valve A to valve B is 86.33 ml including the bomb volume. The compressibility factor was taken by using the *Peng-Robinson* equation of state (EOS). This EOS is use to predicting the vapour pressure and volumetric behaviour of single component systems and the phase behaviour and volumetric behaviour of the binary, ternary and multicomponent system. The *Peng Robinson* (1976) equation is shown at Equation 3.2.

$$\mathrm{Z} = \frac{\mathrm{V}}{\mathrm{V} - \mathrm{b}} - \frac{a \;\; T \;\; V}{RT[V \;\; V + b \;\; + b \;\; V - b \;\;]} \qquad 3.2$$

Where Z is the compressibility factor ($Z = PV/RT$) where T is the temperature, V is volume, P is pressure and R is the molar universal gas constant. Parameter a is a measure of the attractive forces between the molecules, and the parameter b is the co volume occupied by the molecules. The a and b parameters can be obtained from the critical properties of the fluid. The *Peng-Robinson* (PR) equation of state slightly improves the prediction of liquid volumes and predicts a critical compressibility

factor of Z_c=0.307. This equation can be used to accurately predict the vapour pressures of pure substances and equilibrium ratios of mixtures. The advantage of this equation is that they can accurately represent the relation among the pressure, temperature and phase compositions in binary or multicomponent systems. To ensure the experimental data, all the experiments were repeated three times and standard deviation of CO_2 absorption data was less than 2 %.

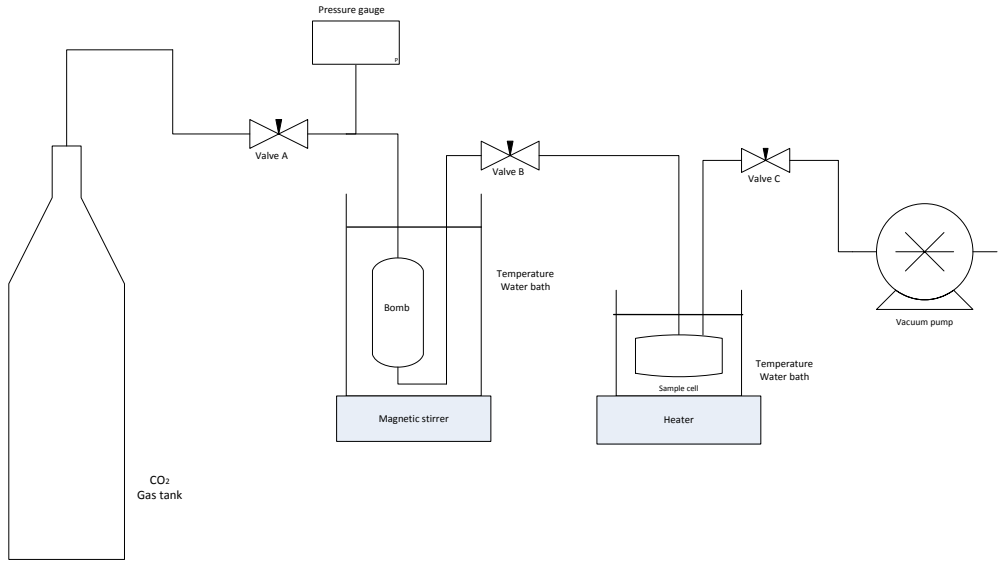

Figure 3.6: Schematic diagram for gas absorption/adsorption cell

3.6.1 Adsorption Isotherm Measurement

Adsorption equilibrium is established when an adsorbate (gas) containing phase has been contacted with the adsorbent for sufficient time [127]. The interaction between adsorbate and adsorbent can be described by adsorption isotherm. This can explain the adsorption mechanism pathways, expression of the surface properties and capacities of adsorbents of adsorption systems [128].

The adsorption isotherm was carried out by studying the CO_2 sorption on AAPILs at various pressures (1, 3, 5, 7 and 10 bar) and at temperatures 298 K, 313 K and 333 K. Only the best AAPILs on capturing CO_2 capacity would proceed for the adsorption isotherm measurement. In this work, adsorption isotherm was carried out using Langmuir, Freundlich, Dubinin Radushkevich and Temkin isotherms and the best fitted model to describe the adsorption process was determined by the correlation coefficients (R^2) value [128].

Langmuir isotherm is commonly used for isotherm modelling and originally used to describe gas adsorption on AAPILs. Thus, this isotherm is the simplest model of physical adsorption which assumes monolayer adsorption where once a molecules occupies a site, no further adsorption can take place, no interaction between adsorbed adsorbate even on the adjacent site, and the enthalpy of adsorption is the same for each molecules [129].

The Freundlich equation is an empirical model that considers heterogeneous adsorptive energies on the adsorbent surface. In Freundlich isotherm, the adsorption is not restricted to the formation of monolayer [130]. This model can be applied to multilayer adsorption with non uniform distribution of adsorption heat and affinities over the heterogenous surface [131].

Dubinin-Radushkevich isotherm is an empirical model for the adsorption of subcritical vapors onto micropore solids which follows a pore filling mechanism [127]. This isotherm generally applied to the adsorption mechanism with a Gaussian energy distribution onto heterogenous surface [132].

The Temkin isotherm is usually used for heterogenous surface energy system (non uniform distribution of sorption heat) [133]. This isotherm also account for the adsorbent-adsorbate interactions. The model assumes that heat of adsorption (function of temperature) in the layer would decrease linearly rather than logarithmic coverage [132]. The non-linear and linearized equation of these isotherm models are summarized in Table 3.2.

Table 3.2: The non-linear and linearized equation of the isotherm models

Isotherm	Non-linear equation	Liner equation
Langmuir	$q_e = \frac{q_m K_L P_e}{1 + K_L P_e}$	$\frac{P_e}{q_e} = \frac{1}{K_L q_m} + \frac{P_e}{q_m}$
Freundlich	$q_e = K_F . P_e^{\frac{1}{n}}$	$log\, q_e = log\, K_F + \frac{1}{n}\ logP_e$
Dubinin-Radushkevich	$q_e = q_m e^{-\lambda \omega^2}$	$ln\, q_e = ln\, q_m - \lambda \omega^2$
Temkin	$q_e = B(ln\, K_T P_e)$	$q_e = B\ ln\, K_T + B\ ln\, P_e$

Whereby for Langmuir: q_e is amount of CO_2 adsorbed per unit weight of adsorbent at equilibrium (mmol/g), q_m is maximum adsorption capacity (mmol/g), P_e

is equilibrium pressure (bar), K_L is Langmuir constant related to the free energy of adsorption (g/mmol). For Freundlich; K_F ($mmol^{1-(1/n)} . g^{1/n} . g^{-1}$) and n (dimensionless) is Freundlich constant related to the adsorption capacity and intensity. For Dubinin-Radushkevich; ω (J/mol) is the Polanyi potential (equivalent to RT ln (1+1/Pe)), λ is D-R constant (mol^2/J^2). For Temkin; K_T (cm^3/g.bar) is Temkin constant and B=(RT/b_T) where b_T (J/mol).

3.7 COSMO-RS

The Conductor-like Screening Model for Real Solvents (COSMO-RS) is a well established method for the prediction of thermodynamic properties and phase behavior of pure chemical species and mixtures [134]. This COSMO-RS is used to predict qualitatively the gas solubility in ILs at the correct order of magnitude compared with the experimental data. This tool relies on combining the chemical calculations obtained by uni-molecular quantum theory and statistical thermodynamic principles. COSMO-RS methodology consists on processing the screening charge density, σ on the surface of molecules to calculate the chemical potential and activity coefficient of each species in the solution [135]. In this study, COSMO-RS is used to evaluate the CO_2-capture ability of selected ILs having different combinations of cations and anions using the σ-profile analysis and σ-potential of the species involved. The solubility prediction of ILs by using COSMO-RS consists of two steps. The first step is a generation of COSMO-RS cation and anion files. The files were genereted using BP functional B88-p86 with a triple–ξ valence polarized basis set *(TZVP)* and the resolution of identity standard (*RI*) approximation using the *TURBOMOLE 6.1* program package [136]. The second steps involves a statistical thermodynamics and were performed using COSMO*therm*. The parameterization *BP_TZVP_C30_1301 (COSMOlogic GmbH & Co KG.Leverkusen, Germany)* [137], which is required for the calculation of physicochemical data and contains intrinsic parameters of COSMO*therm* and element specific parameters, was adopted. The chemical potential, μ_i is related to activity coefficient of component *i*, by

$$\gamma_i = \exp\left(\frac{\mu_i - \mu_i^o}{RT}\right) \qquad 3.2$$

Where μ_i^o the chemical potential of the pure compound *i*, *R* is is the ideal gas constant and *T* the absolute temperature. In all calculations, ILs are always treated as equimolar mixture of cation and anion thus the scale by a factor of 0.5. The best predictions were obtained with the lowest energy conformations or with global minimum for both cation and anion. Thus in this work, the lowest energy conformations of all the species involved were used in the COSMO-RS calculations [134, 136, 138].

3.8 Density Functional Theory (DFT) Study of Amine Molecular

Density Functional Theory (DFT) modeling is to understand the role of amine in reactivity towards CO_2 by studying the variations in amine-CO_2 reaction energy of systematically different amines [139]. The present work focuses on the relationship between molecular properties of amines and their influence on the amine-CO_2 interactions. Molecular modeling within the framework of density functional theory (DFT) was used to evaluate the reaction energy to form the product species associated with the amine-CO_2 system [140, 141]. Conceptual DFT was used to relate electronic structure properties of the amines to trends in their reactivity, with the purpose of providing the foundational understanding to design of amine with target reactivities towards CO_2 [142].

The energy and electronic structure of the molecular systems were computed with DFT calculations using Gaussian 09 with the *B3LYP* functional and *6-31G** basis set. This *B3LYP* functional is sufficient to establish trends in molecular reactions of systems of the size considered in this study. Energy and electronic descriptor calculations were performed for a subset of the amines studied with a larger basis set *6-31G**, with no changes to the energy correlations, indicating that the level of theory with using *6-31G** was sufficient for the trends observed [143]. This functional and basis set is on average the best choice of a model chemistry for most systems and it is particular good for organic molecules, but less so for metal containing compounds [142]. The basic algorithm for the solution of DFT consists in self consistent loop at iteration, *n*:

The flowchart procedure of Kohn-Sham Self Consistent Field, KS SCF is shown in Figure 3.7 [144]. For instance, step 1 is to choose a basis set which is *6-31G**. After choose the molecular geometry, the overlap integrals and the kinetic energy and nuclear-attraction integrals are computed. To evaluate the remaining integrals, the initial density must to be guess to contstruct the V_{xc} and to evaluate the remaining integrals in each KS matrix element. New orbitals are determined from solution of the secular equation, the density is determined from those orbitals and it is compared to the density from the preceeding iteration. Once convergence of the SCF is achieved, the energy is computed by plugging the final density to optimize the molecular geometry. At this point, either the calculation is finished, or, of geometry optimization is the goal, a determination of whether the structure corresponds to a stationary point is made [144].

3.8.1 Thermochemistry output

The behavior of the molecules is governed by the empirically determined laws of thermodynamics such as enthalpy, entropy, free energy and others. The experimental convention for assigning a zero to an enthalpy or free energy scale is that this is the value that corresponds to the heat or free energy of formation associated with every element in its most stable, pure form under standard conditions (273 K, 1 atm). Thus, the meaning of an experimental heat of formation or enthalpy of formation for a molecule is the molar enthalpy change associated with removing each of the atoms in the molecule from its elemental standard state and assembling them into molecule [144].To determine a standard state molecular thermodynamic quantity, the computed energy difference between the molecule and its constituent atoms is added to the experimental thermodynamic value determined for the identical atoms [145]. The usual way to calculate enthalpies of reaction is to calculate heats of formation and take the appropriate sums and difference as shown in Equation 3.3. The overall flowchart for the methodology is shown in Figure 3.8.

$$\Delta_r H^o\ 298\ K = \sum_{products} \Delta_f H^o_{prod}\ 298\ K - \sum_{reactants} \Delta_f H^o_{react}\ 298\ K \qquad 3.3$$

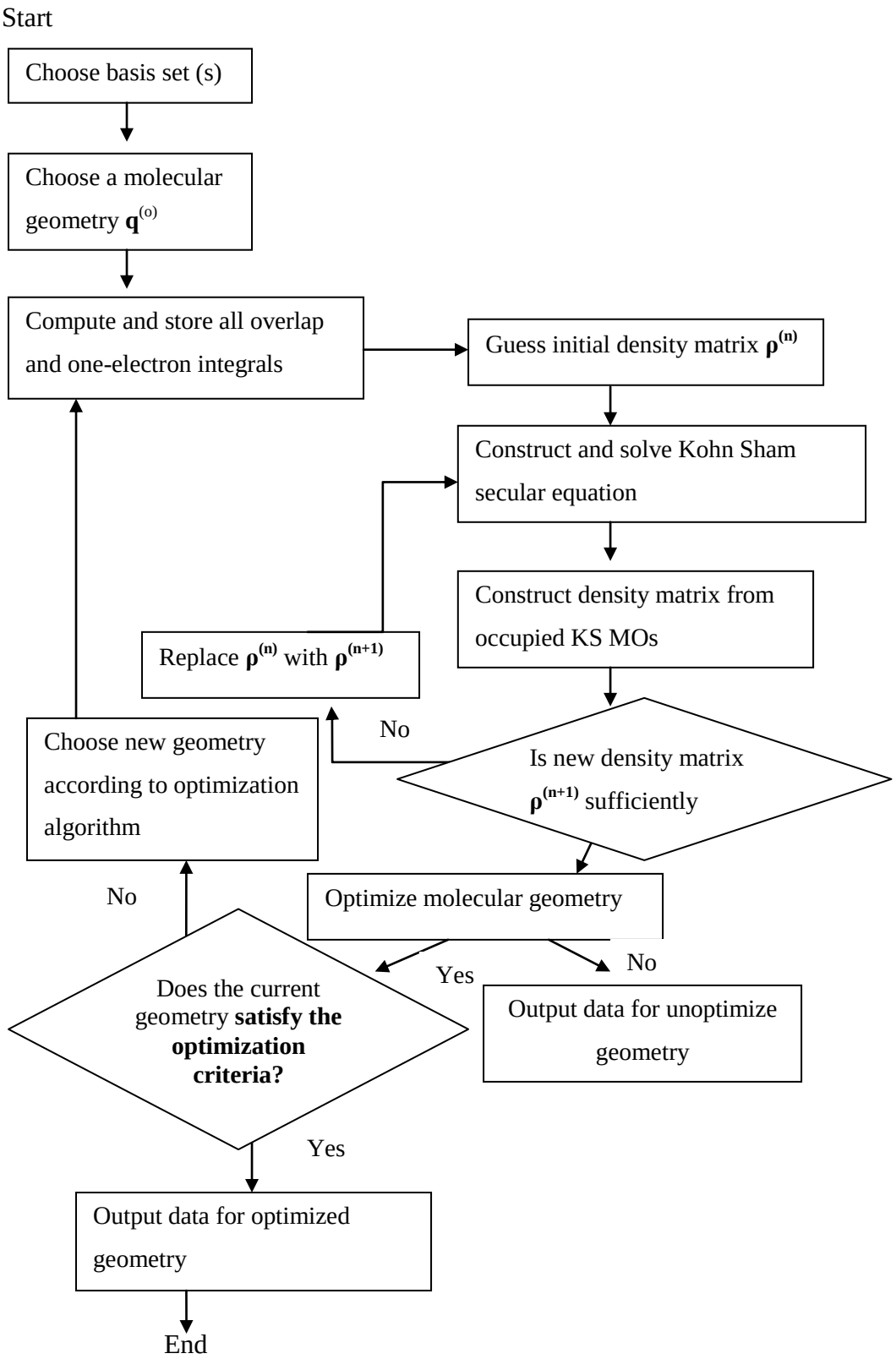

Figure 3.7: Flowchart of the KS SCF procedure

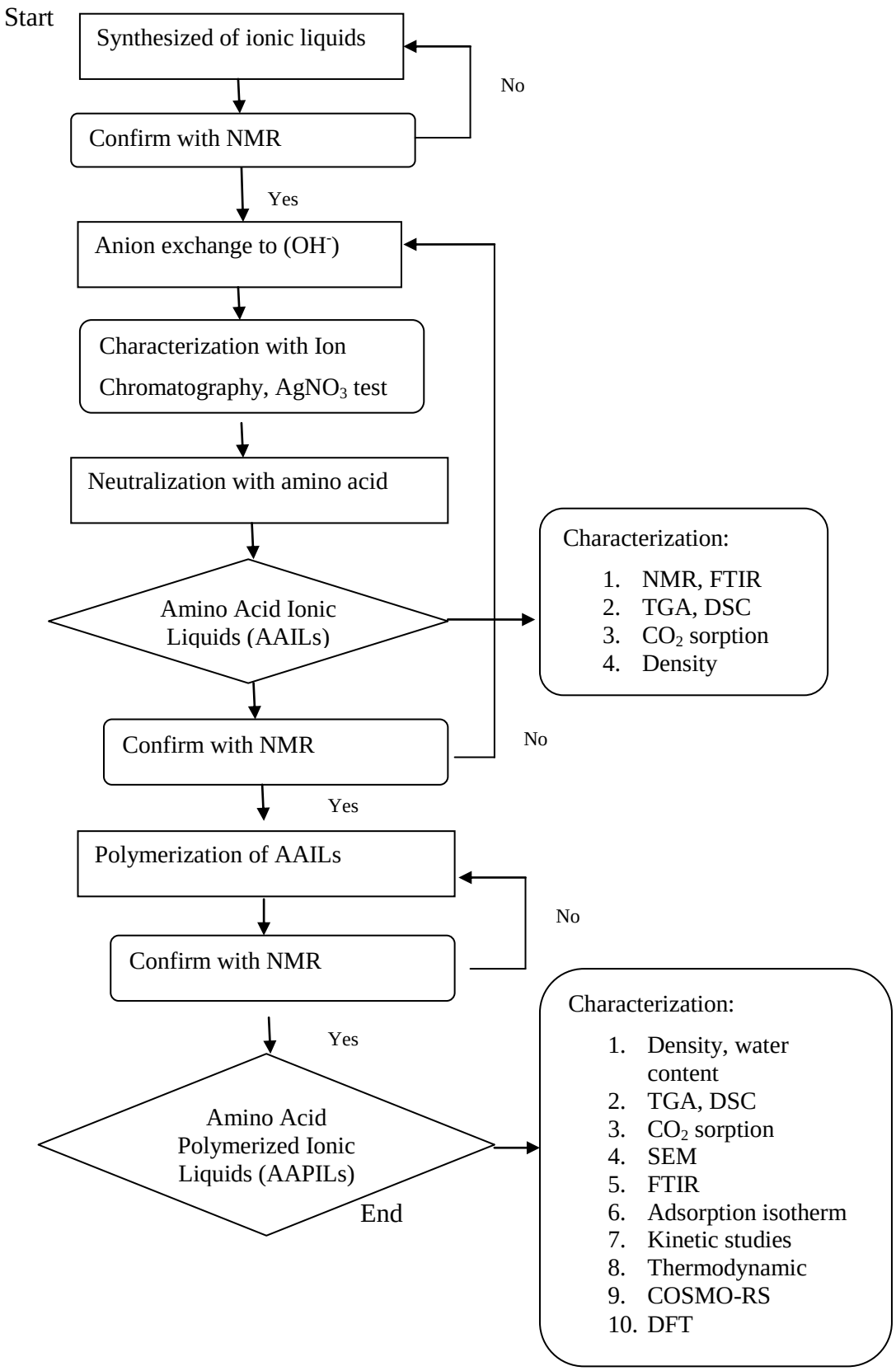

Figure 3.8: Flowchart for overall methodology

CHAPTER 4

RESULTS AND DISCUSSION

The characterization of AAPILs includes structure analysis such as ^{1}H-NMR and FTIR to confirm the structure synthesized. The chloride content and water content to ensure the purity of the synthesized AAPILs. Morphology analysis used to study the surface and porosity, the thermal stability such as degradation temperature and glass transition temperature to study the stability of AAPILs with temperature. All AAILs and AAPILs synthesized are further studied for CO_2 sorption.

4.1 Identification and Structural Analysis of AAILs and AAPILs

The ^{1}H-NMR result shows that the vinyl protons are seen at around 5.40 to 6.85 ppm in all monomers and as expected they do not appear in the polymeric compound; instead aliphatic protons are observed at 1.53 to 2.22 ppm. This indicates that the vinyl compounds were successfully polymerized. The benzylic protons and methyl protons on ammonium in the monomers also experienced upfield shifts, perhaps due to the effect of the neighboring cationic backbones in the polymer. All ^{1}H-NMR spectrum are shown in Appendix A. The ^{1}H-NMR peaks are shown in Table 4.1.

The polymerization of the monomer [VBTMA][Gly] successfully occurred when the vinyl group on the monomer has been shifted to upfield due to long alkyl group presence in the polymer. After polymerization also can be seen that all peaks of the monomers become broad due to the polymerization and low dissolution between polymer and solvent.

Table 4.1: ^{1}H-NMR peaks for AAILs and AAPILs

Sample	Cations	Anions
[VBTMA][Gly]	3.14 (s, 9H), 4.56 (s, 2H), 5.40 (d, 1H), 5.95 (d, 1H), 6.85 (q, 1H), 7.57 (d, 2H), 7.61 (d, 2H)	3.17 (d, 2H)
Poly[VBTMA][Gly]	1.53 (br, 2H), 2.05 (br, 1H), 3.12 (s, 9H), 4.52 (br, 2H), 6.61 (br, 2H), 7.28 (br, 2H)	3.19 (d, 2H)
[VBTMA][Ala]	3.14 (s, 9H), 4.55 (s, 2H), 5.40 (d, 1H), 5.91 (d, 1H), 6.85 (q, 1H), 7.57 (d, 2H), 7.63 (d, 2H)	1.30 (d, 3 H), 3.33 (q, 1H)
Poly[VBTMA][Ala]	1.62 (br, 2H), 2.17 (br, 1H), 3.05 (s, 9H), 4.52 (br, 2H), 6.56 (br, 2H), 7.26 (br, 2H)	1.37 (d, 3H), 3.43 (q, 1H)
[VBTMA][Ser]	3.14 (s, 9H), 4.55 (s, 2H), 5.40 (d, 1H), 5.95 (d, 1H), 6.85 (q, 1H), 7.57 (d, 2H), 7.63 (d, 2H)	3.31 (t, 1H), 3.65 (t, 1H), 3.80 (t, 1H)
Poly[VBTMA][Ser]	1.53 (br, 2H), 2.18 (br, 1H), 3.06 (s, 9H), 4.52 (br, 2H), 6.59 (br, 2H), 7.28 (br, 2H)	3.39 (t, 1H), 3.71 (t, 1H), 3.83 (t, 1H)
[VBTMA][Pro]	3.15 (s, 9H), 4.57 (s, 2H), 5.40 (d, 1H), 5.95 (d, 1H), 6.85 (q, 1H), 7.59 (d, 2H), 7.63 (d, 2H)	1.87 (m, 2H), 1.96 (m, 1H), 2.23 (m, 1H), 2.99 (m, 1H), 3.22 (m, 1H), 3.72 (m, 1H)
Poly[VBTMA][Pro]	1.53 (br, 2H), 2.06 (br, 1H), 3.06 (br, 9H), 4.53 (br, 2H), 6.59 (br, 2H), 7.25 (br, 2H)	1.90 (m, 2H), 2.01 (m, 1H), 2.24 (m, 1H), 3.02 (m,1H), 3.33 (m, 1H), 3.78 (m, 1H)
[VBTMA][Tau]	3.14 (s, 9H), 4.56 (s, 2H), 5.40 (d, 1H), 5.95 (d, 1H), 6.85 (q, 1H), 7.58 (d, 2H), 7.627 (d, 2H)	2.98 (t, 2H), 3.08 (t, 2H)
Poly[VBTMA][Tau]	1.53 (br, 2H), 2.29 (br 1H), 3.06 (s, 9H), 4.59 (br, 2H), 6.72 (br, 2H), 7.40 (br, 2H)	2.99 (t, 2H), 3.13 (t, 2H)
[VBTMA][Hist]	3.12 (s, 9H), 4.53 (s, 2H), 5.40 (d, 1H), 5.95 (d, 1H), 6.85 (q, 1H), 7.55 (d, 2H), 7.62 (d, 2H)	2.83 (q, 1H), 3.10 (q, 1H), 3.50 (q, 1H), 6.89 (s, 1H), 7.59 (s, 1H)
Poly[VBTMA][Hist]	1.53 (br, 2H), 2.26 (br, 1H), 3.02 (s, 9H), 4.52 (br, 2H), 6.67 (br, 2H), 7.23 (br, 2H)	2.82 (q, 1H), 3.13 (q, 1H), 3.52 (q, 1H), 6.89 (s, 1H), 7.60 (s, 1H)

Sample	Cations	Anions
[VBTMA][Lys]	3.13 (s, 9H), 4.53 (s, 2H), 5.41 (d, 1H), 5.95 (d, 1H), 6.86 (q, 1H), 7.56 (d, 2H), 7.63 (d, 2H)	1.45 (m, 2H), 1.50 (m, 2H), 1.62 (m, 1H), 1.75 (m, 1H), 2.67 (t, 2H), 3.2 (t, 1H)
Poly[VBTMA][Lys]	1.52 (br,2H), 2.15 (br, 1H), 2.84 (s, 9H), 4.23 (br, 2H), 6.55 (br, 2H), 7.08 (br, 2H)	1.26 – 1.52 (m, 6H), 2.60 (t, 2H), 3.16 (t, 1H)
[VBTMA][Arg]	3.13 (s, 9H), 4.54 (s, 2H), 5.41 (d, 1H), 5.96 (d, 1H), 6.86 (q, 1H), 7.56 (d, 2H), 7.64 (d, 2H)	1.63-1.73 (m, 4H), 3.19 (t, 2H), 3.25 (t, 1H)
Poly[VBTMA][Arg]	1.58 (br, 2H), 2.26 (br, 1H), 3.03 (s, 9H), 4.44 (br, 2H), 6.67 (br, 2H), 7.23 (br, 2H)	1.56-1.69 (m, 4H), 3.18 (t, 2H), 3.24 (t, 1H)
[VBTEA][Lys]	1.59 (t, 9H), 3.37 (q, 6H), 4.51 (s, 2H), 5.4 (d, 1H), 5.97 (d, 1H), 6.86 (q, 1H), 7.55 (d, 2H), 7.63 (d, 2H)	1.58-1.60 (m, 4H), 1.71-1.75 (m, 2H), 2.66 (t, 2H), 3.22 (t, 1H),
Poly[VBTEA][Lys]	1.46 (br, 9H), 1.68 (br, 2H), 2.35 (br, 1H), 3.23 (br, 6H), 4.48 (br, 2H), 6.71 (br, 2H), 7.26 (br, 2H)	1.46 (br, 2H), 1.64-1.68 (br, 4H), 2.58 (t, 2H), 3.23 (m, 1H)
[VBTBA][Lys]	1.1 (t, 9H), 1.4 (m, 6H), 1.87 (m, 6H), 3.37 (t, 6H), 4.57 (s, 2H), 5.42 (d, 1H), 5.98 (d, 1H), 6.86 (q, 1H), 7.51 (d, 2H), 7.65 (d, 2H)	1.35-1.5 (m, 4H), 1.58 (m, 1H), 1.74 (m, 1H), 2.66 (t, 2H), 3.22 (t, 1H)
Poly[VBTBA][Lys]	1.42 -1.52 (br, 23H), 2.23 (br, 1H), 3.08 (br, 6H), 4.29 (br, 2H), 6.55 (br, 2H), 7.09 (br, 2H)	1.42-1.52 (br, 6H), 2.27 (t, 2H), 3.12 (t, 1H)
[VBMI][Lys]	3.884 (s, 3H), 5.30 (d, 1H), 5.49 (s, 2H), 5.88 (d, 1H), 6.77 (q, 1H), 7.47 (d, 2H), 7.51 (d, 2H), 7.77 (s, 1H), 7.88 (s, 1H), 10.01 (s, 1H)	1.274 (br, 6H), 2.46 (t, 2H), 2.83 (t, 1H)
Poly[VBMI][Lys]	1.26 (br, 2H), 2.43 (br, 1H), 3.89 (br, 3H), 5.41 (br, 2H), 6.37 (br, 2H), 7.42 (br, 2H), 7.72 (br, 1H), 7.79 (br, 1H), 10.54 (br, 1H)	1.26 (br, 6H), 2.51 (br, 2H), 2.90 (t, 1H)
[VBPPN][Lys]	1.75 (m, 1H), 1.85 (m, 1H), 2.10 (m, 4H), 3.02 (s, 3H), 3.44 (t, 2H), 3.44 (t, 2H), 4.58 (s, 2H), 5.39 (d, 1H), 5.96 (d, 1H), 6.86 (q, 1H), 7.57 (d, 2H), 7.63 (d, 2H)	1.41 (m, 2H), 1.5 (m, 2H), 1.6 (m, 1H), 1.75 (m, 1H), 2.66 (m, 2H), 3.21 (t, 1H)
Poly[VBPPN][Lys]	1.80 (br, 2H), 1.89 (br, 2H), 1.95 (br, 5H), 2.99 (s, 3H), 3.2 (t, 2H), 3.37 (t, 2H), 4.55 (s, 2H), 6.64 (br, 2H), 7.3 (br, 2H)	1.64 (m, 6H), 2.90 (br, 2H), 3.37 (d, 1H)

4.2 Functional Group Identification

FTIR characterization was carried out to study the presence of functional group in AAPILs. Figure 4.1 shows the comparison of FTIR spectrum, absorbance vs wavelength between the monomer of [VBTMA][Gly] and it's polymer, poly[VBTMA][Gly].

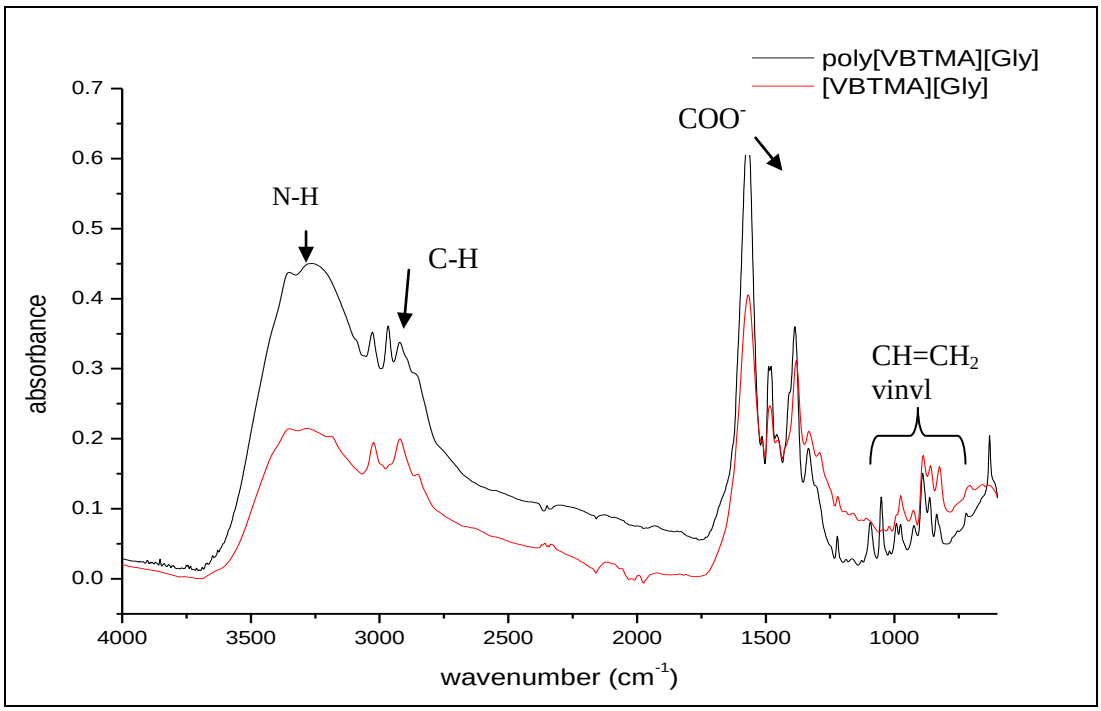

Figure 4.1: FTIR spectrum for [VBTMA][Gly] and poly[VBTMA][Gly]

In Figure 4.1, the region 3300 cm^{-1} showed the presence of N-H amides. Region 3000-2900 cm^{-1} is typical for C-H. Peak 1570 cm^{-1} for COO^- group overlapped with N-H in amino acid. Therefore, at 1479 cm^{-1} is for benzene ring in aromatic compound and peak 1386 cm^{-1} is distinct for C-N group. The vinyl compound $CH=CH_2$ shows absorption at region 1000 cm^{-1} to 990 cm^{-1}. This region appears in the monomer [VBTMA][Gly] but not in the polymer. This is shows that [VBTMA][Gly] is completely polymerized to poly[VBTMA][Gly].

Table 4.2 shows the FTIR peaks with functional group which confirmed the expected structure of the AAPILs. FTIR spectrums of AAPILs were shown in Appendix B. The characteristic FTIR peaks corresponding to C=O of the COO^- anion which mainly overlap with –NH from the amino acids at around 1610 – 1560 cm^{-1} with strong intensity. Broad peaks at around 3520 - 3320 cm^{-1} correspond to –NH of amines and the C-N stretch is observed at 1420 – 1375 cm^{-1}. Based on Table 4.2

confirms the functional group presence in all AAPILs. The intensities are abbreviated as follows: *br* for broad, *s* for strong, *vs* for very strong and *m* for medium.

Table 4.2: FTIR peaks, intensity and functional groups of AAPILs

Sample	Peaks (cm^{-1}) and intensity	Groups
Poly[VBTMA][Gly]	3280 *(br,s)* 3024-2921 *(s)* 1567 *(vs)* 1381 *(m)*	-NH_2 primary C-H region NH overlap COO^- salts C-N stretch
Poly[VBTMA][Ala]	3269 *(br, m)* 3023-2919 *(m)* 1573 *(vs)* 1357 *(m)*	NH_2 primary C-H NH overlap COO^- salts C-N stretch
Poly[VBTMA][Ser]	3269 *(br, m)* 3023-2919 *(w)* 1573*(vs)*	-NH_2 primary overlap with -OH C-H region NH overlap COO^- salts
Poly[VBTMA][Pro]	3278 *(br, m)* 2964, 2869 *(m)* 1580*(vs)* 1376 *(vs)*	-NH aromatic -CH region NH overlap COO^- salts C-N stretch
Poly[VBTMA][Tau]	3375 *(br, m)* 3031 *(w)* 2923 *(w)* 1585 *(br, m)* 1483 *(m)* 1178 *(vs)* 1033 *(vs)*	-NH_2 primary -NH_3^+ amino acids -CH_2 NH_2 alkyl amides Benzene ring (aromatic) SO_2 symmetric stretch C-NH_2 primary aliphatic amines
Poly[VBTMA][Hist]	3336 *(m)* 3028 *(m)* 2923, 2860 *(m)* 1581 *(vs)* 1404 *(m)*	-NH aromatics =CH aromatics -CH_2, -CH_3 compound NH overlap COO^- salts C-N stretch
Poly[VBTMA][Lys]	3353 *(br, m)* 2920, 2856 *(m)* 1579 *(s)* 1388 *(m)*	-NH_2 primary -CH_3 and –CH_2 aliphatic NH overlap COO^- salts C-N stretch
Poly[VBTMA][Arg]	3178 *(br, m)* 2925,2858 *(m)* 1558 *(vs)* 1390 *(s)*	-NH_3^+ amino acids -CH_3 and –CH_2 aliphatic NH overlap COO^- salts C-N stretch

Sample	Peaks (cm^{-1}) and intensity	Groups
Poly[VBTEA][Lys]	3353 *(br, m)* 2932, 2865 *(s)* 1562 *(vs)* 1512 *(s)* 1403 *(m)* 1324 *(m)*	-NH_2 primary -CH_3 and –CH_2 aliphatic NH overlap COO^- salts NH bend COO^- stretch C-H bend
Poly[VBTBA][Lys]	3356 *(br, m)* 2931, 2865 *(m)* 1572 *(vs)* 1516 *(s)* 1406 *(m)* 1349 *(m)*	-NH_2 primary -CH_3 and –CH_2 aliphatic NH overlap COO^- salts NH bend COO^- stretch C-N stretch
Poly[VBMI][Lys]	3280 *(br, m)* 2927, 2858 *(m)* 1655 *(m)* 1561 *(vs)* 1388 *(s)* 1161 *(s)*	-NH secondary -CH_3 and –CH_2 aliphatic C=C conj NH overlap COO^- salts C-N stretch -C-N aromatic amines
Poly[VBPPN][Lys]	3353 *(br, s)* 2934, 2865 *(m)* 1562 *(vs)* 1399 *(s)*	-NH_2 primary -CH_3 and –CH_2 aliphatic NH overlap COO^- salts C-N stretch

4.3 Physical Properties

The physical properties of AAPILs include chloride content, density and water content.

Chloride content of [VBTMA][OH] was determined by ion chromatography (IC) Metrohm model 761 compact. The result of chloride content for [VBTMA][OH] was negligible, which was 0.008 µS/cm. This showed that ionic liquids [VBTMA][Cl] was successfully exchange to hydroxide, [VBTMA][OH] by using anion exchange resin, Amberlyst A26 hydroxide (OH) form. This concentration of chloride is sufficiently low for application and should not have any effect on the physical properties of AAPILs. Figure 4.2 shows the ion chromatogram of chloride, Cl^- and the calibration curve is shown in Appendix B-14.

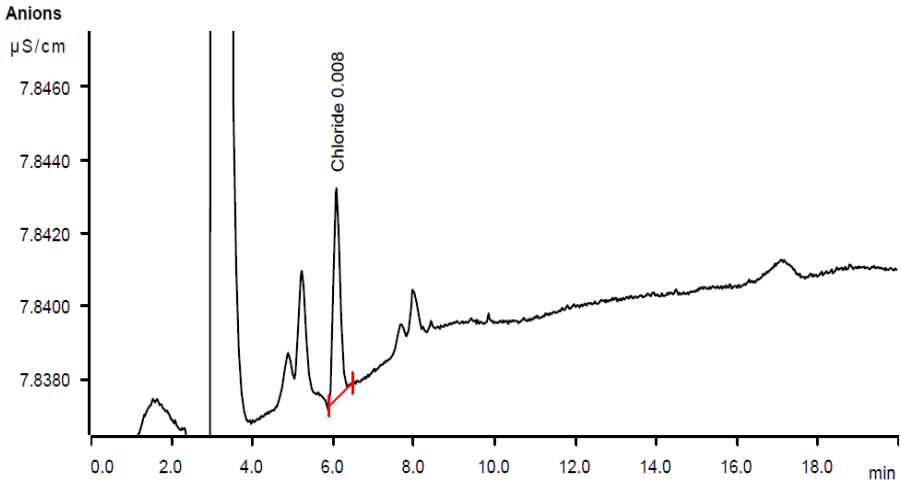

Figure 4.2: Ion Chromatogram of chloride, on [VBTMA][OH]

Physical properties such as water content, density, yield percentage (yield %), physical appearance, color and state form are shown in Table 4.3.

Table 4.3: Physical properties of AAPILs synthesized

AAPILs	Density (g/cm^3)	Water content (%)	Yield (%)	Color	Form
Poly[VBTMA][Gly]	0.8071	1.227	77.8	Yellowish	Solid
Poly[VBTMA][Ala]	0.7975	1.096	72.99	Yellowish	Solid
Poly[VBTMA][Ser]	0.7668	1.806	81.15	Brownish	Solid
Poly[VBTMA][Pro]	0.7685	1.285	60.31	Brownish	Solid
Poly[VBTMA][Tau]	0.8732	1.261	66.67	Yellowish	Solid
Poly[VBTMA][Hist]	0.8409	0.931	69.62	Yellowish	Solid
Poly[VBTMA][Lys]	0.7107	2.441	69.64	Yellowish	Solid
Poly[VBTMA][Arg]	0.7459	1.267	60.17	Yellowish	Solid
Poly[VBTEA][Lys]	1.0987	1.145	69.9	Brownish	Solid
Poly[VBTBA][Lys]	1.1216	1.524	71.6	Yellowish	Solid
Poly[VBMI][Lys]	1.2759	1.374	62.8	Brownish	Solid
Poly[VBPPN][Lys]	1.2870	1.286	66.2	Brownish	Solid

Table 4.3 shows the water content for most of the AAPILs is less than 2% except poly[VBTMA][Lys]. This water content of AAPILs was sufficiently high since the

amino acid can form hydrogen bonding with water though small amount of water was difficult to remove. The yield percentage of all AAPILs synthesized is low which within the range 60 – 70 %. This might be because of the long synthesize route from quartenization to anion exchange, neutralization and polymerization step make the loss of yield.

The densities were in the range of 0.7 – 0.8 g/cm^3 in [VBTMA] based. These densities are lower than the monomeric forms reported in literature [70, 71, 98] due to the increment in free volume [3]. According to Zhang *et al.* [71], densities are also influenced by elongating the alkyl side chains of the $[AA]^-$ which increases the free volume of ILs therefore decreasing the density. For example the density follows the order [Gly] > [Ala] > [Ser] > [Arg] > [Lys]. However the [Tau] anion shows a higher density of 0.8732 g/cm^3 due to the heavier functional group of O=S=O in structure. Aromatic functionality also influences the density such that [Hist] and [Pro] have densities higher than the other anions with longer alkyl side chains.

When changing the alkyl chain length from [VBTMA] to [VBTEA] and [VBTBA], it can be seen that the densities increases from 0.7107 g/cm^3 on poly[VBTMA][Lys] to 1.0987 g/cm^3 on poly[VBTEA][Lys] and 1.1216 on poly[VBTBA][Lys]. This is similar reported in literature [3, 82] that densities on poly[VBTMA][BF_4] is 1.035 g/cm^3 and increases to 1.225 g/cm^3 on poly[VBTEA][BF_4]. By changing the cation from ammonium to imidazolium and piperidinium based, the density increases.. Poly[VBMI][Lys] shows higher density with 1.2759 g/cm^3 and poly[VBPPN][Lys] with 1.2870 g/cm^3. This might be because of the presence of aromatic functionality on imidazolium and piperidinium which increases the density.

4.4 Synthesis attempts of different backbone for polymerization

Different type of backbones were synthesized which is vinylbenzyltrimethylammonium [VBTMA], methacryloyloxyethyltrimethylammonium [METMA] and allybutylimidazolium [ABIM] as shown in Figure 4.3.

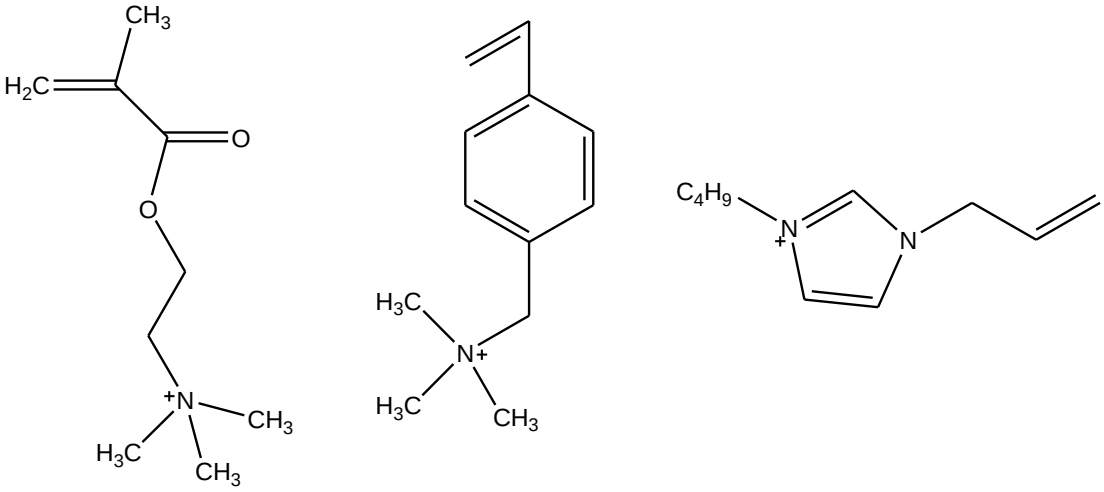

[METMA] [VBTMA] [ABIM]

Figure 4.3: Different backbone of AAPILs

However, only vinyl backbone, [VBTMA], was successfully synthesized. For [METMA] backbone, the problem arised during anion echange from [METMA][Cl] to [METMA][Gly]. This could be due to the anion exchange from Cl^- to OH^-.

From the ^{1}H-NMR spectra in Figure 4.4, can be seen that the methylmethacrylate group for [METMA][Gly] was disintegrated due to the reaction between OH^- with methylmethacrylate group thus form methacrylic acid. Therefore, [METMA] backbone is not suitable for process of anion exchange from chloride to hydroxide.

(a)

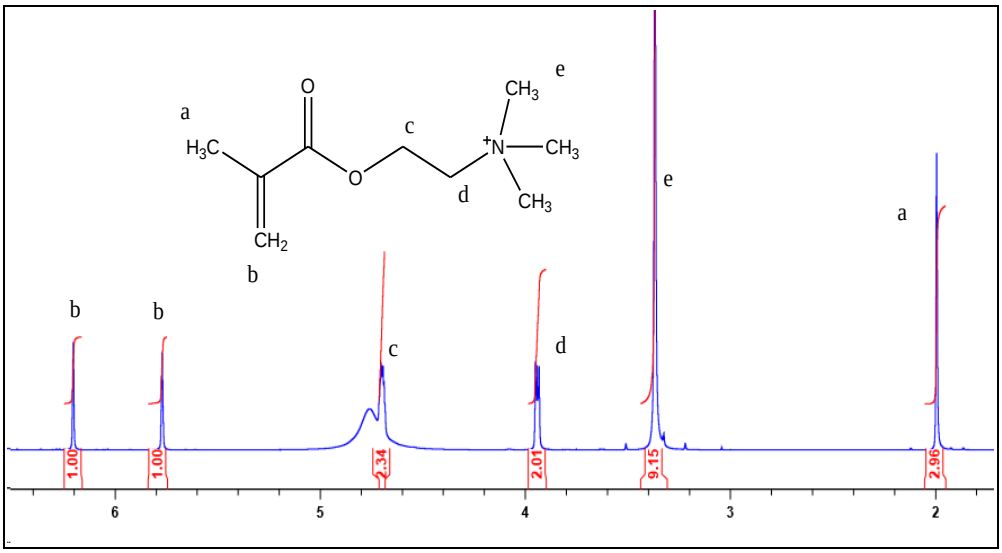

(b)

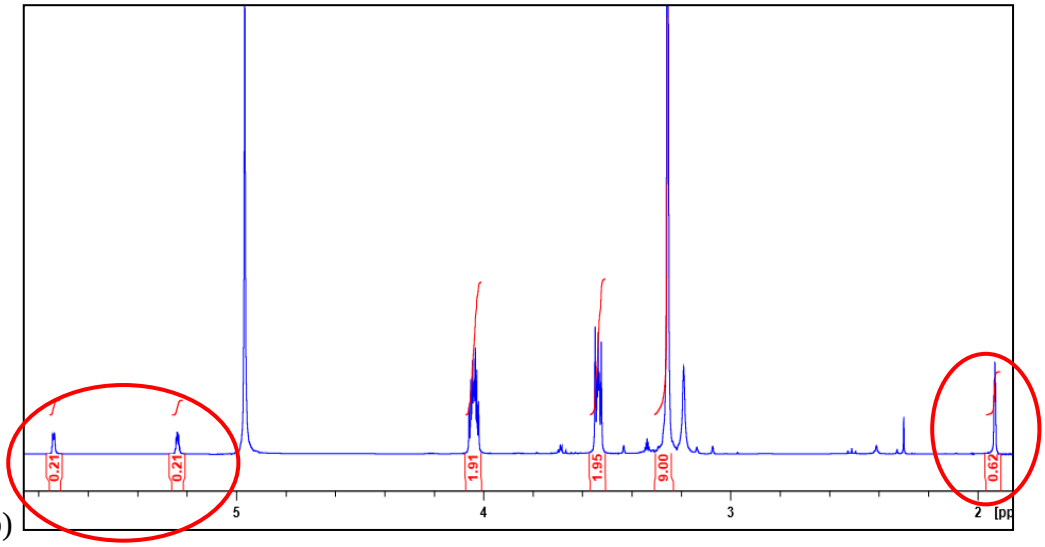

Figure 4.4: ^{1}H-NMR for (a) [METMA][Cl] and (b) [METMA][Gly]

For [ABIM] backbone, the polymerization of [ABIM] was failed and blackish color solution was formed and it seems like decompose occurred. Figure 4.5 shows ^{1}H-NMR with low integration after polymerized which explain the unsuccessful polymerization. It is believed that decomposition of [ABIM][Gly] occurred during polymerization at 65 ^{o}C as shown in Figure 4.6 Therefore, in this study only vinylbenzylic backbone were studied with various cations and anions.

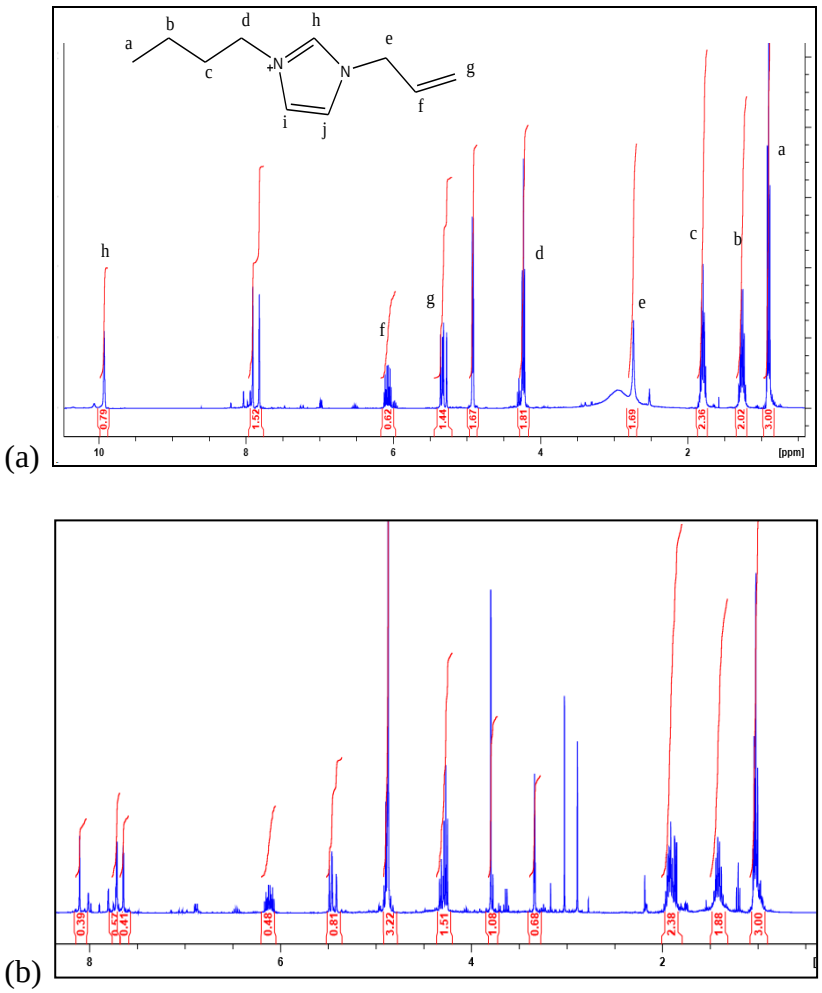

Figure 4.5: ^{1}H-NMR for (a) [ABIM][Gly] (b) polymerized [ABIM][Gly]

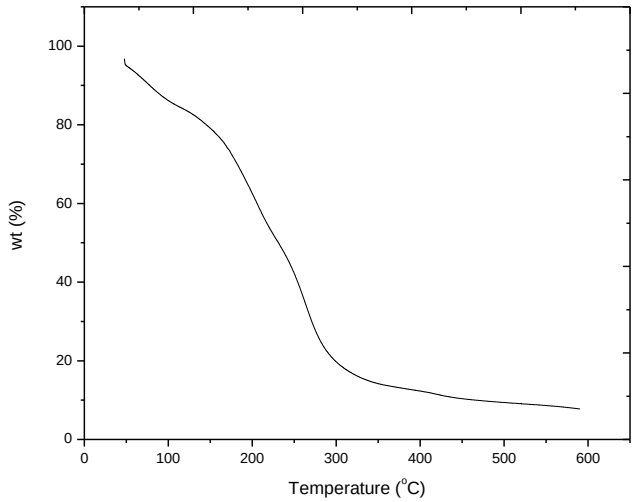

Figure 4.6: TGA analysis for [ABIM][Gly]

4.5 Thermal stability on AAILs and AAPILs

Thermal stability is an important factor that determines the applicability of ILs for high temperature application. The stability of AAPILs can be determines in a function of temperature. In thermal stability, degradation temperature (T_d) and glass transition temperature (T_g) were studied. In order to evaluate the effect of structure on AAILs and AAPILs, T_d and T_g were studied which includes the effect of changing the anion, cation and alkyl chain length.

4.5.1 Effect of anion on thermal stability

To study the effect of anions on thermal stability, [VBTMA] cation was varied with different anions, [Gly], [Ala], [Ser], [Pro], [Tau], [Hist], [Lys] and [Arg]. Table 4.4 shows the thermal stability for AAILs and AAPILs synthesized with different of anions and fixed [VBTMA] cation. TGA and DSC thermogram for the AAILs and AAPILs were shown in Appendix C.

Table 4.4: Degradation temperature (T_d) and glass transition temperature (T_g)

AAILs	T_d (^{o}C)	T_g (^{o}C)	AAPILs	T_d (^{o}C)	T_g (^{o}C)
[VBTMA] [Gly]	174	-68.3	Poly[VBTMA][Gly]	192	-46.5
[VBTMA] [Ala]	172	-57.2	Poly[VBTMA][Ala]	194	-34.7
[VBTMA] [Ser]	184	-66.2	Poly[VBTMA][Ser]	211	-38.5
[VBTMA] [Pro]	192	-46.1	Poly[VBTMA][Pro]	200	-26.5
[VBTMA] [Tau]	185	-51.5	Poly[VBTMA][Tau]	202	-23.9
[VBTMA] [Hist]	162	-14.6	Poly[VBTMA][Hist]	192	3.5
[VBTMA] [Lys]	166	-39.9	Poly[VBTMA][Lys]	191	-1.7
[VBTMA] [Arg]	170	-27.1	Poly[VBTMA][Arg]	185	-5.9

Table 4.4 shows that degradation temperature, T_d of AAILs with different anions varied from 162 ^{o}C to 192 ^{o}C. This is lower than the values for the same anions with different cations reported by Goodrich *et al*. (2011), [96] by using $[P_{66614}]^+$ as cations

and $[aP_{4443}]^+$ as reported by Zhang *et al*. (2009) [71]. As well as cation, the structures of $[AA]^-$ also have a big effect on T_d and T_g values. The $[AA]^-$ with active functional groups and have high negative charge density would lower the T_d values [71]. Anions with amine functional groups; [His], [Lys] and [Arg] have low T_d values from 162 to 170 ^oC than anions with single amine groups; [Ala], [Gly], [Ser], [Tau] and [Pro] which have high T_d values from 172 to 192 ^oC.

From Table 4.4, it can also be seen that after polymerization all T_d of AAILs increases about 10 to 30 ^oC. Polymerization increased the thermal stability of AAILs. Similar with AAILs, it also shows that anions play a significant role in determining the T_d values. Polymerization helped to increase the thermal stability of AAILs. Same trend can be observed in AAPILs where anions [Arg], [Lys] and [Hist] have low T_d values from 185 to 192 ^oC and anions [Gly], [Ala], [Pro], [Tau] and [Ser] have higher T_d values from 192 to 211 ^oC.

In contrast with T_d values, better flexibility of $[AA]^-$ with short and linear alkyl side chains lowers the T_g values. Anions [Gly], [Ser], [Ala] have lower T_g values from -46.5 to -34.7 ^oC. These anions have smaller side chain which lowers the T_g values. On the other hand, anions with ring in the side chain, long alkyl side chain of $[AA]^-$ have higher T_g values from -26.5 to 3.5 ^oC corresponding to [Pro], [Tau], [Arg], [Lys] and [Hist] anions. For [Pro] anion, it has pentagonal ring as a side chain and for anions [Tau], [Arg] and [Lys], these anions have longer alkyl side chain and contain numbers of functional group. For [Hist], it has longer alkyl side chain as well with aromatic ring in a side chain therefore, the T_g is higher than others. Similar trends can be observed with monomers where [Gly], [Ser], [Ala] have lower T_g than [Tau], [Pro], [Lys], [Arg], and [Hist]. These trends of T_d and T_g corresponds to findings by Zhang *et al*. [71] with using $[aP_{4443}]^+$ as cation.

Similar with T_d values, after polymerization, the T_g values increases with 30 to 40 ^oC. This increasing trend of T_d and T_g are due to strong intermolecular bonds in polymers chain, which have higher value of cohesive energy density [146].

4.5.2 Effects of cation on thermal stability

To study the effect of cation on thermal stability of AAILs, lysinate [Lys] anion was varied with different of cation; [VBTMA], [VBTEA], [VBTBA], [VBMI] and

[VBPPN]. The trend of T_d on AAILs with different of cation follows [VBMI] (217 ^oC) > [VBPPN] (185 ^oC) > [VBTMA] (166 ^oC).

By changing the alkyl chain length on cation, it can be seen that the T_d increases from methyl, [VBTMA] (166 ^oC) < ethyl [VBTEA] (195 ^oC) < butyl [VBTBA] (203 ^oC). Cao *et al*. [147] reported that increasing the side chain of the cation will result in decreasing the ILs thermal stability. This reduction in the T_d could be due either to the decrease in intermolecular interaction or to the initial decomposition of the alkyl substituent. However, there were exceptions as reported by many researchers. Nawshad *et al.* (2014), [148] reported that T_d increases as increasing alkyl chain length from methyl to butyl due to increase of mass loss. Similar observation trend supports by Zhang *et al*. (2013), [114] that $[bis(mim)C_4]^{2+}$ was 40 ^oC higher than $[bis(mim)C_2]^{2+}$ when paired with same $[AA]^-$ anion due to the asymmetric structures of the cation that increased the thermal stability.

By polymerizing the AAILs, the T_d increased compared to monomers as shown in Table 4.5. This correspond to the trend reported by Zhang *et al*. (2013) and Cao *et al*. (2014) [95, 147], that imidazolium is more stable ILs than ammonium cation. After polymerization, imidazolium still gave the highest degradation temperature than others cation. This might be due to the imidazole structure is resistant to ring fission during thermal rearrangement at higher temperature [149-151].

Table 4.5: Thermal stability on AAPILs with different cation and fixed [Lys] anion

AAILs	T_d (^oC)	T_g (^oC)	AAPILs	T_d (^oC)	T_g (^oC)
[VBTMA][Lys]	166	-74.0	Poly[VBTMA][Lys]	191	-1.7
[VBTEA][Lys]	195	-38.4	Poly[VBTEA][Lys]	214	-33.6
[VBTBA][Lys]	203	-25.4	Poly[VBTBA][Lys]	218	-43.2
[VBMI][Lys]	217	-44.4	Poly[VBMI][Lys]	227	-33.3
[VBPPN][Lys]	185	-50.5	Poly[VBPPN][Lys]	202	-44.4

For T_g value, the results showed the T_g on AAILs increases as alkyl chain length increase. This is because the T_g was associated with the cohesive force between the ions which mainly determined by the molar volume. At low molar volume, the force is dominated by attractive Coulomb forces between the ions which decrease with

increasing molar volume. At larger molar volumes, van der Waals starts to dominate which lead to increasing T_g. The molar volume increases with increasing of alkyl chain length attached to cation can significantly increase T_g values [152]. Thus, via the influence on cohesive forces and the value of T_g in the van der Waals regime, the alkyl chain plays an important role in the molecular mobility. According to Michael *et al.* [152], the T_g increase with increasing alkyl chain length until, n=10.

On the contrary with polymerized, AAPILs, the T_g decreases with increasing of alkyl chain length. This caused by higher surface area of the polymer due to amorphous structure thus lower the T_g values. These T_g results give a good indication of the degree of amorphous nature of the polymer and further the surface area of polymer. The T_g results also shows an indication that AAPILs are amourphous as there is no melting or crystalline peak in DSC plot. Tang *et al.* (2009) [82] reported that the plasticization reduces the T_g leads to decrement in microvoid fraction of the PILs. This trends also similar reported with Mohamed *et al.* (2011) [3] that T_g for poly[VBTMA][NO_3] (167 ^oC) is higher compared to poly[VBTEA][NO_3] (105 ^oC). The reduction of T_g has been attributed to increases of flexibility due to long alkyl chains and also the reduction in lattice energy [90].

After polymerization, the T_g increases compared to the monomer. The polymerization of AAILs enhanced the thermal stability. It can be concluded that the structure of the anions are the factors that influences the thermal stability of AAILs and AAPILs. By changing the anion, the thermal stability is greatly affected than cation modification [147].

4.6 Morphology Micrograph

All the SEM micrograph can be seen in Appendix D. From the Appendix D, the SEM micrographs showed that some of AAPILs synthesized *i.e.* poly[VBTMA][Gly], poly[VBTMA][Ser] and poly[VBTMA][Pro] showed an even surface where as other AAPILs showed an uneven surfaces thus gave higher surface area.

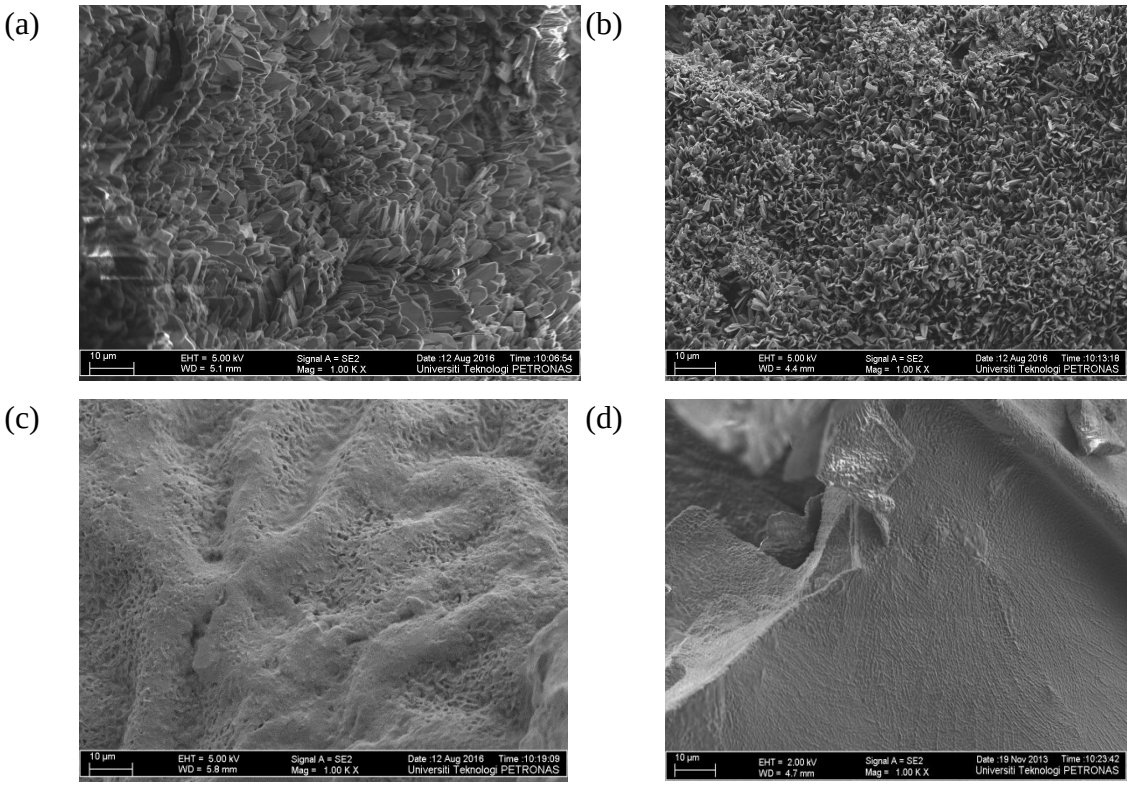

Figure 4.7: SEM images for AAPILs synthesized

Figure 4.7 shows SEM images for (a) poly[VBTMA][Tau], (b) poly[VBTMA][Hist], (c) poly[VBTMA][Lys] and (d) poly[VBTMA][Gly]. These AAPILs are predicted to give higher CO_2 sorption as their surface area can host CO_2. However Poly[VBTMA][Gly] showed even structure. If the topology structure by means of surface area of AAPILs plays a great role in CO_2 sorption capacity, then these three AAPILs (a,b and c) should gave higher CO_2 sorption than poly[VBTMA][Gly] as their surface area to host the CO_2 is higher than poly[VBTMA][Gly].

Table 4.6 shows the BET analysis before and after CO_2 sorption. It can be seen that after CO_2 sorption, the BET surface area and pore volume are lower than before CO_2 sorption due to physical adsorption occurred in the surface of poly[VBTMA][Lys]. In physical adsorption, the CO_2 are trapped in the pore hence it gives lower pore volume and decreases the surface area. However, most of AAPILs are non porous solid therefore, only poly[VBTMA][Lys] applicable for BET analysis. AAPILs with uneven surface give higher surface area plays a role in physical adsorption with CO_2.

Table 4.6: Textural analysis before and after CO_2 sorption on poly[VBTMA][Lys]

	Before CO_2	After CO_2
BET surface area (m^2/g)	2.360	1.284
Pore volume (cm^2/g)	0.003	0.002

4.7 Carbon Dioxide Sorption

Carbon dioxide sorption of the AAILs and AAPILs is measured with standard methods. The polymerization, anion, cation, alkyl chain length of cation, pressure, temperature, presense of water, comparison of gases and recyclability of AAPILs were studied. Tables of all CO_2 sorption can be found in Appendix E.

4.7.1 Comparison of CO_2 sorption capacities with MEA, RTILs, AAILs and AAPILs

To compare the efficiency of RTILs, AAILs and AAPILs towards CO_2 sorption, the CO_2 sorption were studied at 1 bar and 298 K by using the gas adsorption/absorption cell. Figure 4.8 shows the CO_2 uptake of the AAILs ([VBTMA][Arg]), AAPILs (Poly[VBTMA][Arg]), RTILs ([BMIM][Cl]) and with MEA as a control sample.

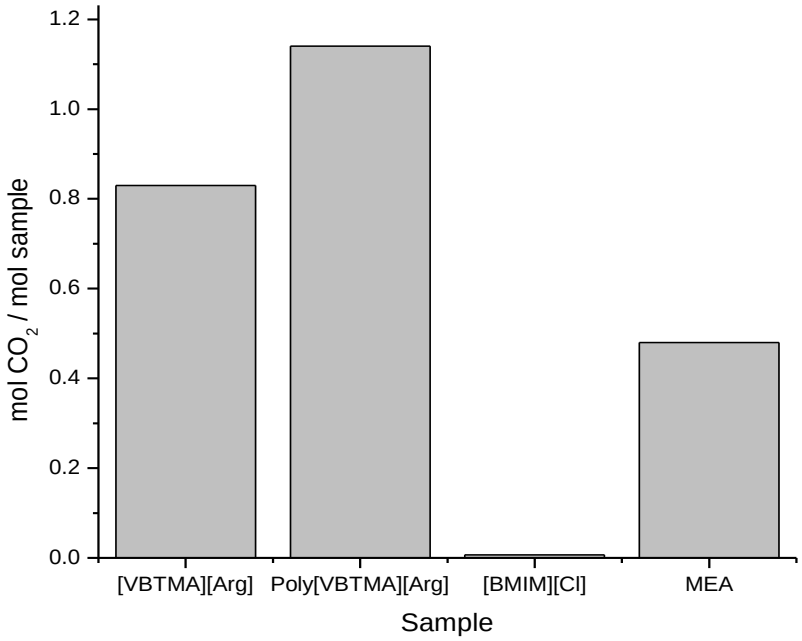

Figure 4.8: CO_2 sorption on AAILs, AAPILs, RTILs and MEA

From Figure 4.8 can be seen that the MEA sorption data obtained is 0.47 mol/mol slightly lower than that reported in the literature (0.55 mol/mol) for a THF solution of MEA [14]. MEA was run as control sample to ensure that results from the equipment for CO_2 sorption are reliable. In Figure 4.8 shows that the comparison of CO_2 sorption by using different type of samples *i.e.* MEA, RTILs, AAILs and AAPILs.

The results showed that CO_2 sorption for the AAILs is much higher with 0.83 mol/mol compared with [BMIM][Cl] with 0.03 mol/mol as the latter is exhibits only physical adsorption. This result confirms that ILs with amine functionality tethered to the anion exhibit enhanced CO_2 sorption due to a chemical absorption mechanism.

Polymerization of the AAILs led to an increase in CO_2 uptake. This has been suggested is due to the increased free volume in the polymer material. The high surface area of the powdered polymer samples enhanced the rate of CO_2 uptake. The highest absorption achieved for Poly[VBTMA][Arg] was 1.14 mol/mol. These values are higher than those reported by Tang *et al.* (2005) [81], (poly[VBTMA][BF_4] gave 0.102 mol/mol) , indicating the substantial role of the amino acid anions in the absorption. Poly[VBTMA][Arg] achieved 76% capacity in

30 min higher than [VBTMA][Arg], [BMIM][Cl] and MEA with 67 %, 25 % and 36 % sorption capacity respectively.

However, since AAPILs are not fully dissolved in any solvent, therefore the degree of polymerization (DP) is difficult to be measured. According to Osman *et al*. (2011) [3], reaction time during polymerization process would give different molecular weight with 11,518 (6 hours) and 21,531 (12 hours). Therefore, poly[VBTMA][Pro] was synthesized at two different polymerization times at 6 hours and 24 hours. Their degradation temperatures, T_d were measured as shown in Figure 4.9.

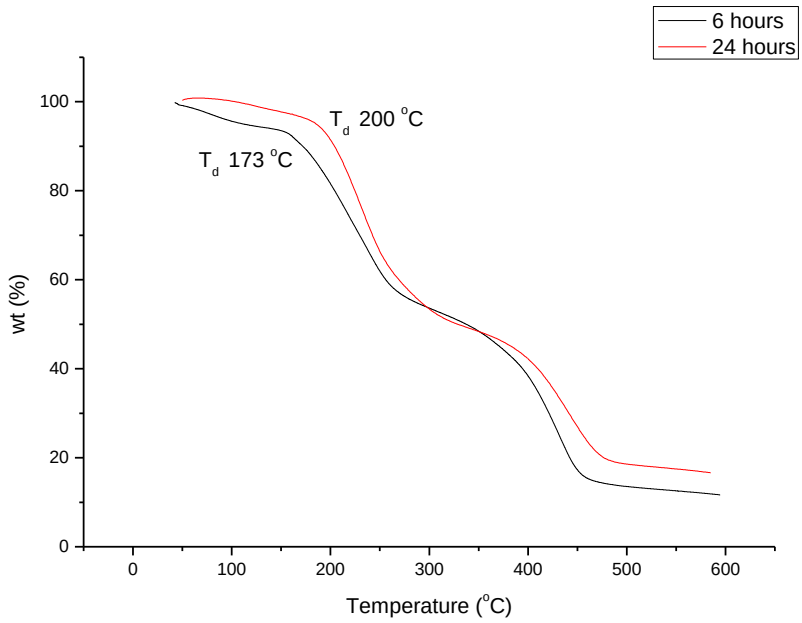

Figure 4.9: Degradation temperature on poly[VBTMA][Pro] at 6h and 24h

From Figure 4.9, the T_d on poly[VBTMA][Pro] at 24 hour reaction was 200 ^{o}C which is higher than T_d temperature at 6 hour (173 ^{o}C). In general, polymer with higher DP gave higher T_d. Thus, this indicates that these two batches of poly[VBTMA][Pro] is having different number of DP. However, even though the DP is different, these two batches of poly[VBTMA][Pro] still shows almost similar CO_2 sorption capacity with 0.60 mol/mol (6 h) and 0.62 mol/mol for 24 h as shown in Figure 4.10. This is because, the capacity of CO_2 sorption on polymer only depended on the monomer regardless the DP of polymer.

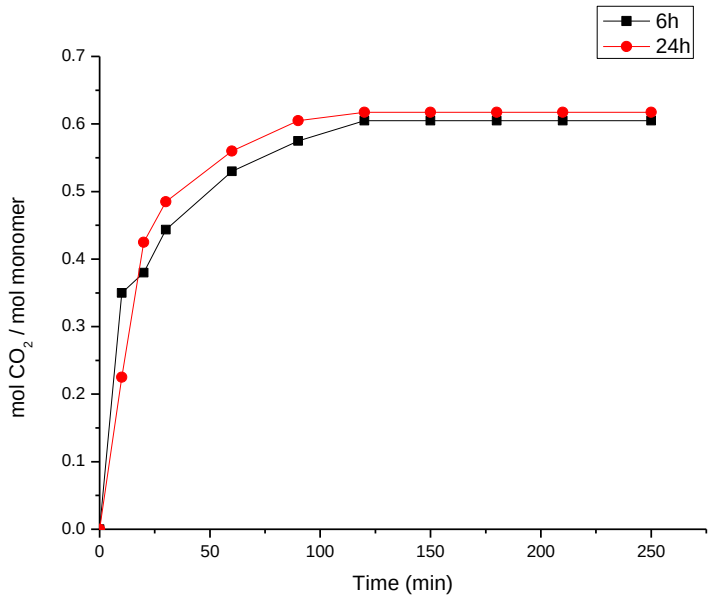

Figure 4.10: CO_2 sorption on poly[VBTMA][Pro] at 6h and 24h reaction times

4.7.2 Effects of anion on CO_2 sorption

The solubility of a gas is governed by a combination of factors namely: polarizability of the gas, the dispersion forces and the interactions between the gas and solvent. The relative influence of each of these factors differs with the nature of the gas and the solvent involved. Several studies reported that CO_2 solubility in ILs depends primarily on the strength of interaction of CO_2 with anion [153].

To study the effect of anion type on AAPILs and AAILs, the CO_2 sorption capacity with [VBTMA] and various anions were studied at 1 bar pressure at 298 K. Table 4.7 shows the CO_2 uptake on all AAILs and AAPILs synthesized.

In AAPILs, [Arg] and [Lys] have higher CO_2 sorption with 1.14 mol/mol and 1.13 mol/mol respectively. Followed with [Hist], [Ser], [Tau], [Pro], [Gly], [Ala]. This is mainly because arginine, [Arg], comprises of two primary amines and two secondary amines and [Lys] comprises of two primary amines. Thus, the accessibility of CO_2 to react with one or more of these amine sites is an advantage [70].

Table 4.7: CO_2 absorption on AAILs and AAPILS with fixed [VBTMA] cation

AAILs	Mol CO_2 / mol monomer	wt %	AAPILs	Mol CO_2 / mol monomer	wt %
[VBTMA][Gly]	0.47	8.32	Poly[VBTMA][Gly]	0.60	10.63
[VBTMA][Ala]	0.29	4.84	Poly[VBTMA][Ala]	0.56	9.05
[VBTMA][Ser]	0.39	6.07	Poly[VBTMA][Ser]	0.68	10.56
[VBTMA][Pro]	0.38	5.72	Poly[VBTMA][Pro]	0.62	9.30
[VBTMA][Tau]	0.44	6.50	Poly[VBTMA][Tau]	0.64	9.34
[VBTMA][Hist]	0.46	6.10	Poly[VBTMA][Hist]	0.80	10.62
[VBTMA][Lys]	0.66	9.05	Poly[VBTMA][Lys]	1.13	15.68
[VBTMA][Arg]	0.83	10.49	Poly[VBTMA][Arg]	1.14	14.23

Histidine, [Hist] which has one primary amine and one secondary amine in a ring, has less accessibility for CO_2 with 0.80 mol/mol. [Gly], [Ala], [Ser], [Pro] and [Tau] which has one amine group gave 0.60, 0.56, 0.68, 0.62 and 0.64 mol/mol respectively. The CO_2 sorptions in all AAPILs are higher and all are above 0.5 mol/mol whereas [Arg] and [Lys] obtained more than 1.0 mol/mol which achieved the mechanism of 1:1.

For poly[VBTMA][Arg], it is higher with 37% from the monomer, [VBTMA][Arg]. The trend for AAILs are almost similar with AAPILs, where [Arg] has the highest CO_2 sorption with 0.83 mol/mol and [Lys] with 0.66 mol/mol followed with [Gly], [Hist], [Tau], [Ser], [Pro] and [Ala]. This is lower than AAPILs since in AAPILs, both physical and chemical absorption are involved. When amine is attached to the anion of the IL, carbamate species forms, but there is a possibility that the negatively charged functionality on the anion can take up the proton released upon CO_2 capture thus forming carbamic acid [68]. The CO_2 can be absorbed with a stoichiometry of up to 1:1, meaning much more efficient use of the IL. The uptake of CO_2 by this chemical mechanism is described in Equations 4.1 and 4.2. Amino acids $[AA]^-$ have structure of $[H_2N\text{-}CHR\text{-}COO^-]$, they are represented here as $R^- NH_2$.

$$CO_2 + R^- NH_2 \leftrightarrow R^- N^+H_2COO^- \quad 4.1$$

$$R^- N^+H_2COO^- + R^- NH_2 \leftrightarrow R^- NHCOO^- + R^- NH_3^+ \quad 4.2$$

Theoretical calculations showed that the dianion formed in the equation 4.2 is chemically unstable therefore the reaction would expect to terminate at equation 4.1 upon addition of CO_2 to AAILs. This indicates a potential absorption stoichiometry of 1:1 (CO_2: IL). Since several of the AAILs show CO_2 uptake > 0.5 mol/mol, *e.g* [VBTMA][Arg] at 0.83 mol/mol, as hypothesized that maximum of 1:1 may be achievable.

These results are similar in the literature that AAILs with more than one amine site have shown higher CO_2 sorption capacity than the AAILs with only one primary amine group. Sistla *et al.* [70], reported that [bmim][Arg] shown more CO_2 sorption with 0.62 mol/mol followed with [bmim][Lys] with 0.48 mol/mol due to the availability of more accessible amine groups. Saravanamurugan *et al*. [105] reported that ammonium based, $[N_{66614}]$[Arg] shows high CO_2 sorption with 1.0 mol / mol.

The interaction between the PILs with CO_2 can be explained based on the anion. It was suggested anion has a significant role in governing the CO_2 sorption [74]. This is because, amino acids *i.e.* [Arg], [Lys] and [Hist] are basic amino acids because they contain basic side chains. The interaction of anions and CO_2 is expected to be stronger than non amino acids anions [70]. Figure 4.11 shows the CO_2 sorption of AAPILs with different anions at 1 bar, 298 K.

It can be concluded that with bigger number of amine group in ILs structure, the more CO_2 have been absorbed [118]. The CO_2 interactions between cation/anion with CO_2, also depends on the intermolecular forces and also accessibility of amine group.

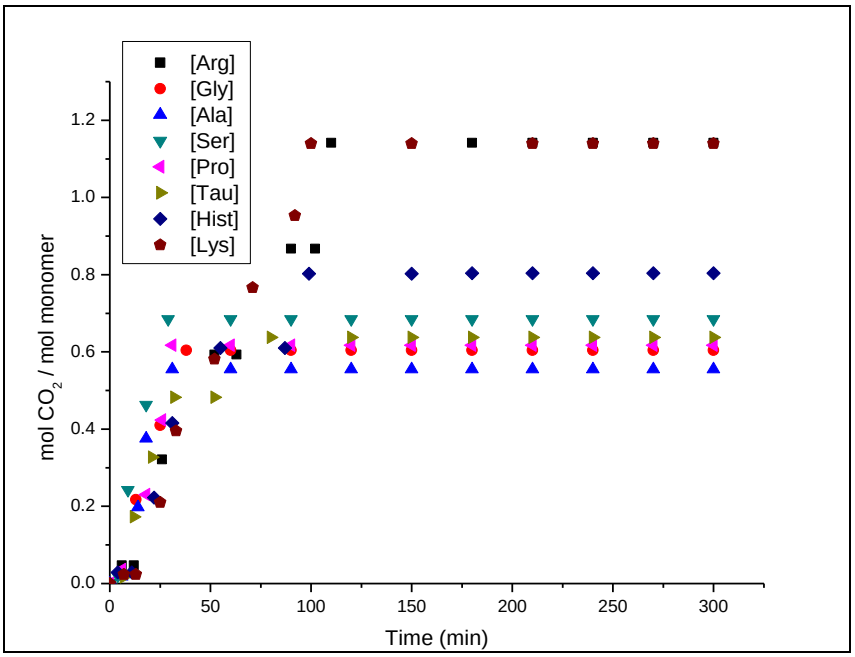

Figure 4.11: CO_2 sorption on AAPILs with different anions

With the aim of understanding the CO_2-ILs interaction, the knowledge of CO_2 behaviour in the pure state as well in the mixtures of ILs is important. This is to confirm the interaction between CO_2-ILs. Therefore, the molecular behavior of CO_2 and the type of molecular interactions can be explained by activity coefficient and σ-profiles by using COSMO-RS.

4.7.2.1 Activity coefficient at infinite dilution, γ_s^∞ by COSMO-RS

To understands the ILs-CO_2 interaction, activity coefficient, $\boldsymbol{\gamma_s^\infty}$ was carried out to evaluate the effect of the structural characteristics of ILs on the activity coefficient of CO_2 at infinite dilution in ILs, $\boldsymbol{\gamma_s^\infty}$. The activity coefficient, $\boldsymbol{\gamma_s^\infty}$ of CO_2 towards the ILs can be determined by COSMO-RS predictions as presented in Table 4.8. In addition, the experimental data were used to evaluate the reliability of the COSMO-RS model is describing the $\boldsymbol{\gamma_s^\infty}$ of these systems [154]. During the calculations, the cation and anion of ILs were treated as equimolar mixture, thus it allows to study the contribution of each counterion on their affinity toward the CO_2 molecule [155]. The lowest energy conformation gives the best prediction [154].

Table 4.8: Activity coefficient, γ_s^{∞} of CO_2 in ILs

ILs	Activity coefficient, γ_s^{∞}	CO_2 sorption (mol/mol)
[VBTMA][Arg]	0.2799	0.83
[VBTMA][Lys]	0.2816	0.66
[VBTMA][Gly]	0.2841	0.47
[VBTMA][Hist]	0.3020	0.46
[VBTMA][Ala]	0.3049	0.29

The lower activity coefficient will lead to higher interaction between the solute and solvent thus give higher CO_2 sorption. The solubility trend of CO_2 and anions observed is similar to the activity coefficient trend described above. Based on Table 4.8, can be seen that decreasing interaction with CO_2 is [VBTMA][Arg] > [VBTMA][Lys] > [VBTMA][Gly] >[VBTMA][Hist] > [VBTMA][Ala]. This trend has a good agreement with experimental results that [VBTMA][Arg] showed the highest CO_2 sorption capacity with 0.83 mol/mol and [VBTMA][Ala] gave the least CO_2 sorption capacity with 0.29 mol/mol. The interaction between CO_2 and anions, [Arg] and [Ala] can be explained by σ-profile [136].

4.7.2.2 σ-Profile of CO_2 and anions, [Arg] and [Ala]

COSMO-RS allows analyzing the behavior of a molecule in both its pure and mixture states. Therefore, the quantum chemical calculations, COSMO-RS use 3D molecular surface polarity distributions to calculate the thermodynamic properties of compounds [138]. Data can be easily envisioned in the histrogram function called σ profile. Figure 4.12 present the σ-profile for the studied CO_2 and anions, [Arg] and [Ala].

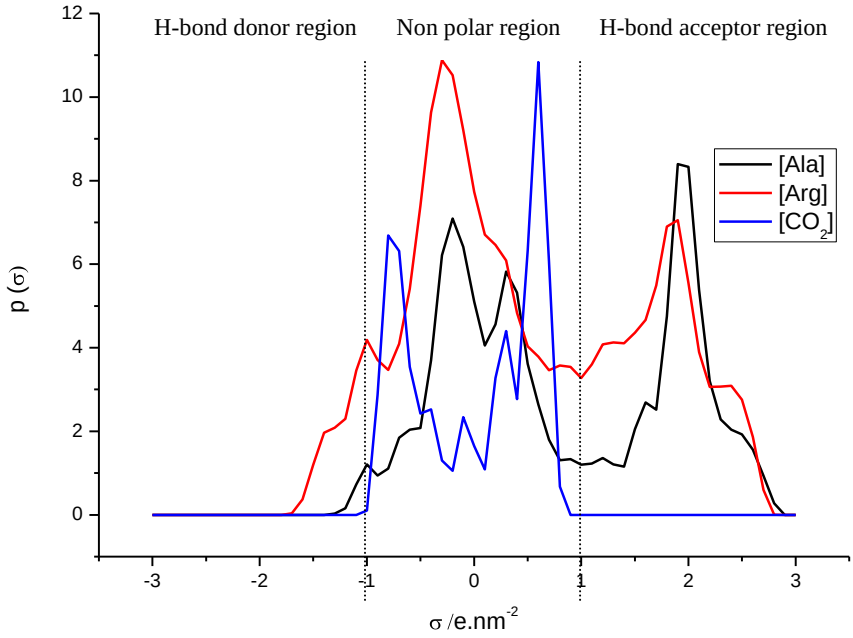

Figure 4.12: σ-profile of CO_2, [Arg] and [Ala] as computed by COSMO-RS

From Figure 4.12, the COSMO-RS histogram is generally divided into three main regions. The first region is hydrogen bond donor region where $\sigma < -1$ e.nm^{-2}. The second region is between $-1 < \sigma < 1$ e.nm^{-2} and it is related to the non-polar behavior of molecule. The third region is molecule's ability to act as hydrogen bond acceptor where it lies at $\sigma > 1$ e.nm^{-2} [156]. In Figure 4.12, the σ-profile of CO_2 presents a series of peaks within the non-polar region only. This indicates that CO_2 is highly non-polar.

Thus, a general rule can be drawn from the σ-profile that CO_2 is likely to interact with nonpolar groups of other molecules due to *'like dissolve like'* interaction between solute and solvent [156]. From Figure 4.12 can be seen that [Arg] is highly non polar compared to [Ala]. Therefore, the interaction between [Arg] with CO_2 is higher compared to [Ala]. This explains the higher solubility of CO_2 in [Arg]. In addition, the anions, [Arg] and [Ala] also has a peak in H-bond acceptor ($\sigma > 1$ e.nm^{-2}) and H-bond donor ($\sigma < -1$ e.nm^{-2}) due to the presence of COO^- and NH_2 in amino acids respectively.

Hence, it can be concluded that nonpolarity plays a significant role in the interaction of ILs with CO_2 [134, 138, 156]. Thus the affinity of CO_2 is increasing

toward more non polar ILs. Therefore, ILs with high polarity display less interaction toward CO_2 [137, 156, 157].

4.7.3 Effects of cation on CO_2 sorption

To study the effect of cation on CO_2 sorption capacity, the sorption of AAPILs with fixed anion, lysinate, [Lys] and various cation *i.e.* ammonium, [VBTMA], imidazolium [VBMI], and piperidinium [VBPPN] were studied at pressure 1 bar, 298 K. Lysinate [Lys] has been chosen because [Lys] and [Arg] both showed tredemendously CO_2 uptake. The results are shown in Figure 4.13 and Table 4.9.

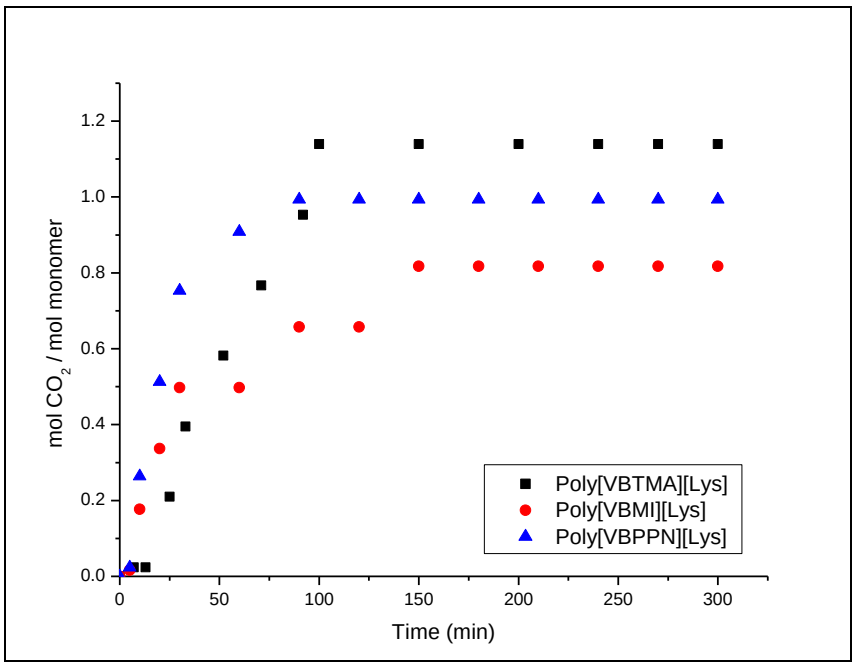

Figure 4.13: CO_2 sorption on different cation with fixed [Lys] anion at 1 bar, 298 K

At equilibrium, poly[VBTMA][Lys] absorp 1.13 mol/mol, higher than poly[VBPPN][Lys] with 0.99 mol/mol and poly[VBMI][Lys] with 0.82 mol/mol. It can be seen that ammonium cation gave higher CO_2 sorption than piperidinium while imidazolium have the least CO_2 sorption. This follows the trend reported by Tang *et al.* [82], where ammonium gave higher CO_2 sorption and imidazolium gave the lowest CO_2 sorption. This suggesting that ammonium cation had the strongest interaction with CO_2 and imidazolium cation had the weakest [82].

Table 4.9: CO_2 sorption of different cation with [Lys] as anion

AAILs	Mol CO_2/mol monomer	Wt%	AAPILs	Mol CO_2/mol monomer	Wt%
[VBTMA][Lys]	0.66	9.05	Poly[VBTMA][Lys]	1.13	15.68
[VBTEA][Lys]	0.62	7.45	Poly[VBMI][Lys]	0.82	10.44
[VBTBA][Lys]	0.62	6.60	Poly [VBPPN][Lys]	0.99	12.11
[VBMI][Lys]	0.44	5.63	Poly[VBTEA][Lys]	0.87	10.7
[VBPPN][Lys]	0.65	7.78	Poly[VBTBA][Lys]	0.72	7.63

By changing the alkyl chain length of ammonium from methyl, to ethyl and butyl, it can be seen that the CO_2 sorption decreases as shown in Figure 4.14.

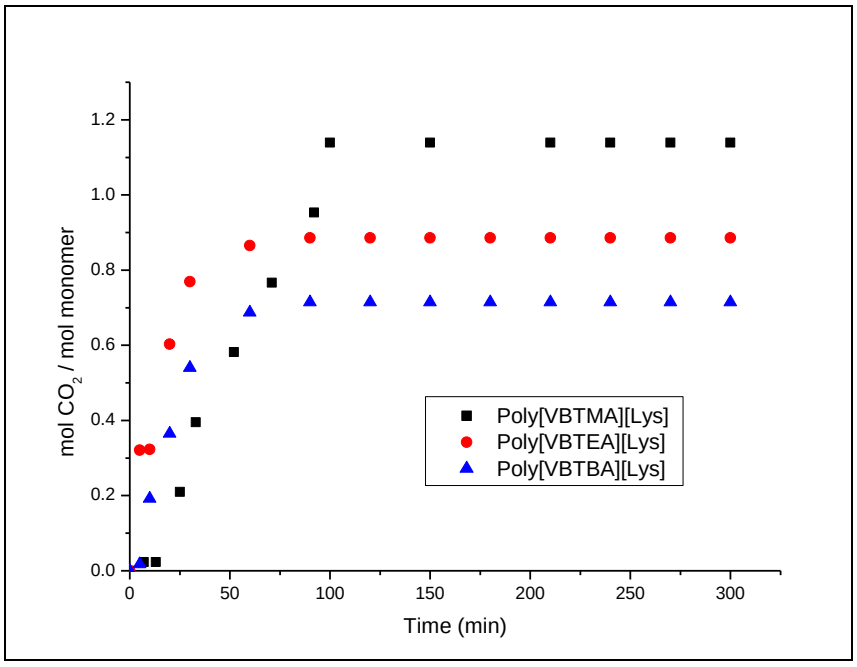

Figure 4.14: CO_2 sorption on different of alkyl chain length

From Figure 4.14, it can be seen that the trend decreases with poly[VBTMA][Lys] (1.13 mol/mol), poly[VBTEA][Lys] (0.89 mol/mol) and poly[VBTBA][Lys] with 0.72 mol/mol. The long alkyl substituents on the cation reduce the CO_2 sorption capacity. The longer alkyl chain may hinder the interaction between CO_2 and the cation due to steric effects. This trends is similar reported by Tang *et al.* (2009) [82], where poly[VBTEA][BF_4] gave lower CO_2 sorption than

poly[VBTMA][BF_4]. Osman *et al.* (2011) [3] reported that poly[VBTMA][NO_3] gave higher CO_2 uptake with 0.22 mol/mol compared to poly[VBTEA][NO_3] with 0.15 mol/mol.

4.7.4 Effect of pressure

To study the effect of pressure, the CO_2 sorption using [VBTMA] incorporating [Arg], [Lys], [Hist], [Gly] and [Ala] were studied. The CO_2 sorption was carried out at 298 K and pressures 1, 3, 5, 7 and 10 bar as shown in Figure 4.15. Table 4.10 shows the reported data.

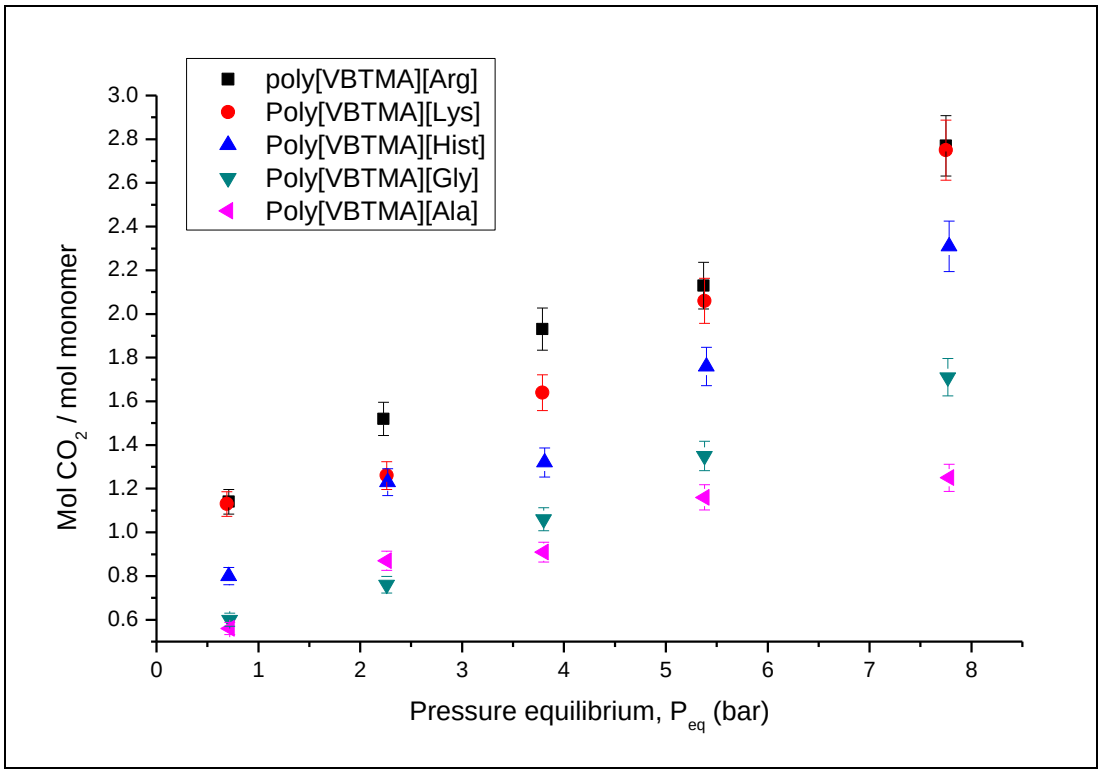

Figure 4.15: CO_2 sorption with increasing pressure at 298 K

It can be seen that the CO_2 sorption increases with increasing pressure for all five AAPILs with [VBTMA] as the cation. This is expected since when pressure increase, it will force the gas into the ILs [158]. From Figure 4.15, the CO_2 molar uptake increases continuously with increasing pressure under studied conditions. At low pressure, a large uptake of CO_2 is due to the chemical absorption process and the further increase at higher pressure is due to physical adsorption [96]. This shows how

the sorption performances of AAPILs merge the characteristics of physical adsorption with the attractive features of chemical absorption [22]. Sistla *et al*. [70] have reported that the CO_2 capacity on AAILs increases with increasing pressure which ranging from 0.32 to 0.82 mol/mol in the pressure range from 1-10 bar. They reported that the mechanism of 1:1 only achieved at 4 bar pressure. However, these reported results are lower since the latter is in monomeric form.

Table 4.10: CO_2 sorption on AAPILs at different pressure and temperature at 298 K

AAPILs	CO_2 sorption (mol/mol)				
	1 bar	3 bar	5 bar	7 bar	10 bar
Poly[VBTMA][Arg]	1.14	1.52	1.93	2.13	2.77
Poly[VBTMA][Lys]	1.13	1.26	1.64	2.06	2.75
Poly[VBTMA][Hist]	0.8	1.23	1.32	1.76	2.31
Poly[VBTMA][Gly]	0.6	0.76	1.06	1.35	1.71
Poly[VBTMA][Ala]	0.56	0.87	0.91	1.16	1.25

In general, increasing pressure is proportional to increase in gas concentration. More number of gas molecules are getting contacted with ILs, thus increases the sorption of CO_2 [92]. In a typical physisorption isotherm, the amount of CO_2 adsorbed increases with the system pressure. The gas fills the free spaces in the ILs, interacting with its ions [159], without significantly affecting the structure of the ILs [160]. To confirm the physical adsorption also involved in AAPILs at higher pressure, BET isotherm model was used to deal with adsorption process.

4.7.4.1 The Brunauer-Emmett-Teller (BET) Model

The most widely used isotherm dealing with multilayer adsorption was derived by Stephen Brunauer, Paul Emmet and Edward Teller (BET). This model mostly applied in gas-solid equilibrium system [127]. BET model was used to determine the

isotherm by plotting the CO_2 adsorb capacity, mmol/g against relative pressure, P/P^o, where P is the equilibrium pressure and P^o is the saturated vapour pressure as shown in Figure 4.16.

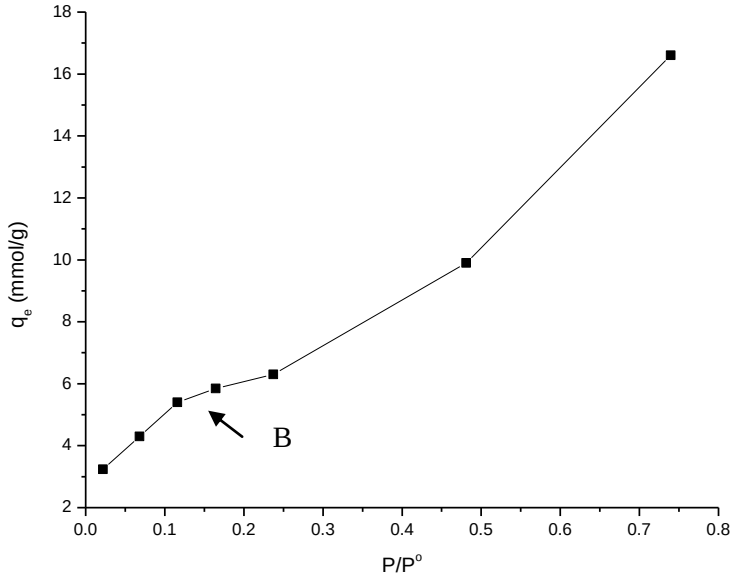

Figure 4.16: BET physisorption isotherm on poly[VBTMA][Arg] at higher pressure

In Figure 4.16, BET model shows the type II isotherm. This isotherm is produced by non-porous solid and it does not limited in the monolayer at the adsorbent surface but can also formed multilayer [161]. Kim *et al.*(2016) [162] also reported that BET model showed multilayer formation when using metal organic framework (MOFs) with CO_2 adsorption isotherm. There is a point B that shows at which monolayer coverage complete and multilayer of adsorbed is about to commence. At low relative pressure, formation of monolayer of adsorbed molecules is the prevailing process, while at high P/P^o, a multilayer adsorption take place [163] . The expression of BET model adsorption isotherm shown in equation 4.3

$$\frac{P}{n(P^o - P)} = \frac{1}{n_m C} + \frac{C-1}{n_m C}\left(\frac{P}{P^o}\right) \qquad 4.3$$

Where P is the equilibrium pressure and P^o is the saturated vapour pressure, n is the adsorption capacity and n_m is the monolayer capacity and C is the BET constant [163]. A plot of $\frac{P_e}{n(P^o-P)}$ against $\frac{P}{P^o}$ was plot and a straight line between P/P^o values from about 0.05 to 0.3 indicates monolayer formation as shown in Figure 4.17.

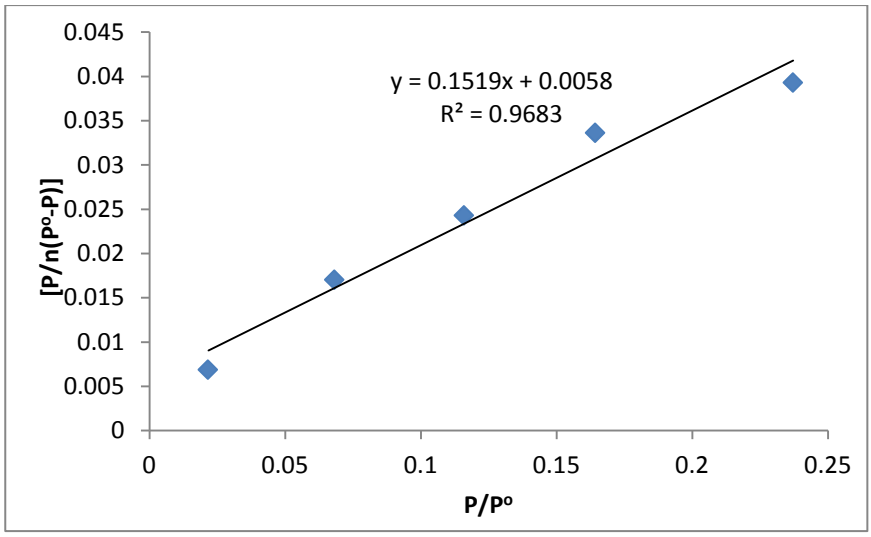

Figure 4.17: BET isotherm model plot

Figure 4.17, shows a BET plot for a given adsorption isotherm. Based on the plot, the adsorption of monolayer capacity, n_m and the BET constant, C can be calculated [162]. The calculation shows that the monolayer capacity, n_m or the quantity of gas adsorbed when the entire surface is covered with monomolecular is 4.764 mmol/g and the BET constant calculated is 3.619.

Therefore, by plotted the BET model as described above, can be concluded that physical adsorption with multilayer formation occurred in AAPILs when pressure increased.

4.7.5 Effect of Temperature

To study the effect of temperature, the CO_2 sorption of poly[VBTMA][Arg] were studied at 25, 30, 35, 40, 60 and 80 ^{o}C at 1 bar pressure as a function of time as shown in Figure 4.18 and Table 4.11 are reported data.

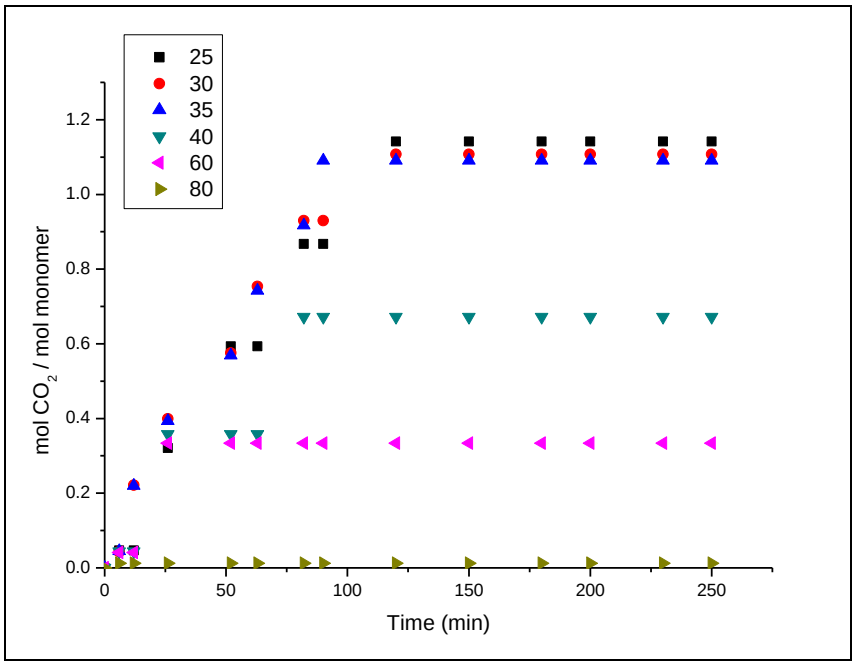

Figure 4.18: CO_2 sorption at different temperatures

Table 4.11: CO_2 sorption on poly[VBTMA][Arg] at different temperatures

Temperature (^oC)	Mol/mol	Wt %
25	1.14	14.23
30	1.10	13.95
35	1.09	13.74
40	0.69	5.40
60	0.33	4.21
80	0.01	0.16

Figure 4.18 shows at higher temperatures, 40 ^oC to 80 ^oC, it took faster to achieved equilibrium since the desorption process occurred. Hence, at Figure 4.19, it can be seen that at room temperature, the CO_2 sorption is saturated and a plateau as function of temperature exists between 25 to 35 ^oC with little effect of temperature. Temperature has a great impact on CO_2 sorption capacity. By increasing the temperature, a serious reduction in CO_2 sorption capacity can be noticed. At 40 ^oC, the adsorption capacity is much lower indicating that the adsorption equilibria is shifting towards the desorbed as expected since desorption is endothermic.

Desorption temperature as low as 30 ^{o}C have been observed previously for protic ionic liquids [88].

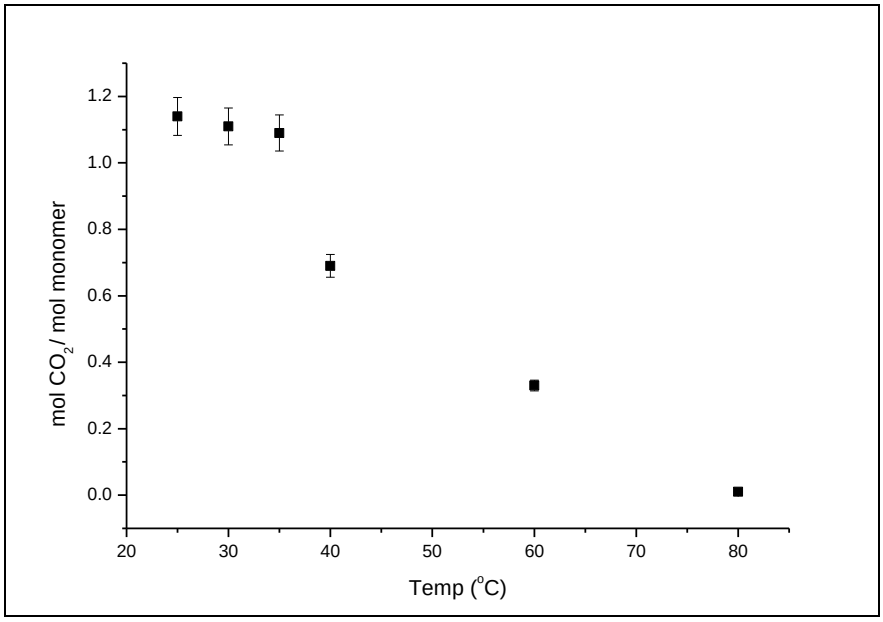

Figure 4.19: CO_2 sorption on poly[VBTMA][Arg] at different temperature

4.7.6 Recyclability of AAPILs

Environmental considerations require the recovery of ILs after their use. Since ILs are quite expensive, hence by recycling the ILs are necessary due to economic reasons. Since fully desorption of poly[VBTMA][Arg] occurred at 80 ^{o}C, therefore the recycling process carried out at 80 ^{o}C through depressurization in vacuum oven for 24 hours. The samples were run for the next cycle to see the recyclability of AAPILs. Figure 4.20 shows the recyclability of poly[VBTMA][Arg].

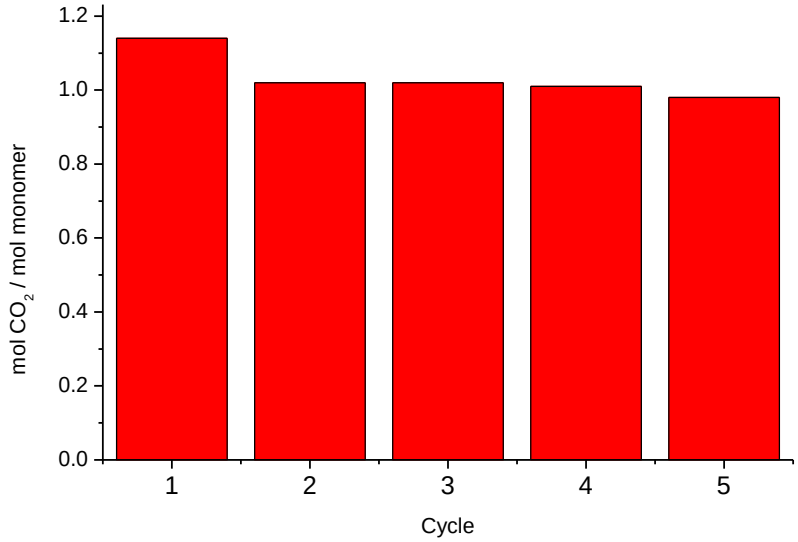

Figure 4.20: Recylability of poly[VBTMA][Arg]

In the first cycle, CO_2 capture is 1.14 mol/mol. Poly[VBTMA][Arg] was then taken out for regeneration process. After the first desorption, the CO_2 removal is not completely achieved in desorption process therefore in second cycle, the CO_2 sorption reduced slightly to 1.02 mol/mol. By repeating the procedure for 5^{th} cycle, the CO_2 sorption was still high at 0.98 mol/mol. The difference between of sorption from 1^{st} cycle to 5^{th} cycle after desorption might be due to an initial structural reorganization taking place within the ILs during the 1^{st} cycle sorption [105]. This shows that AAPILs are very stable and can be use up until 86 % sorption in 5^{th} cycle to get approximately 1 mol CO_2 captured per mole of monomer.

To study the regeneration of ILs, we studied the FTIR spectrum after the sample regenerate at 80 ^{o}C. Figure 4.21 is the FTIR spectrum before CO_2 sorption, after CO_2 sorption and after regenerate at 80 ^{o}C on poly[VBTMA][Arg].

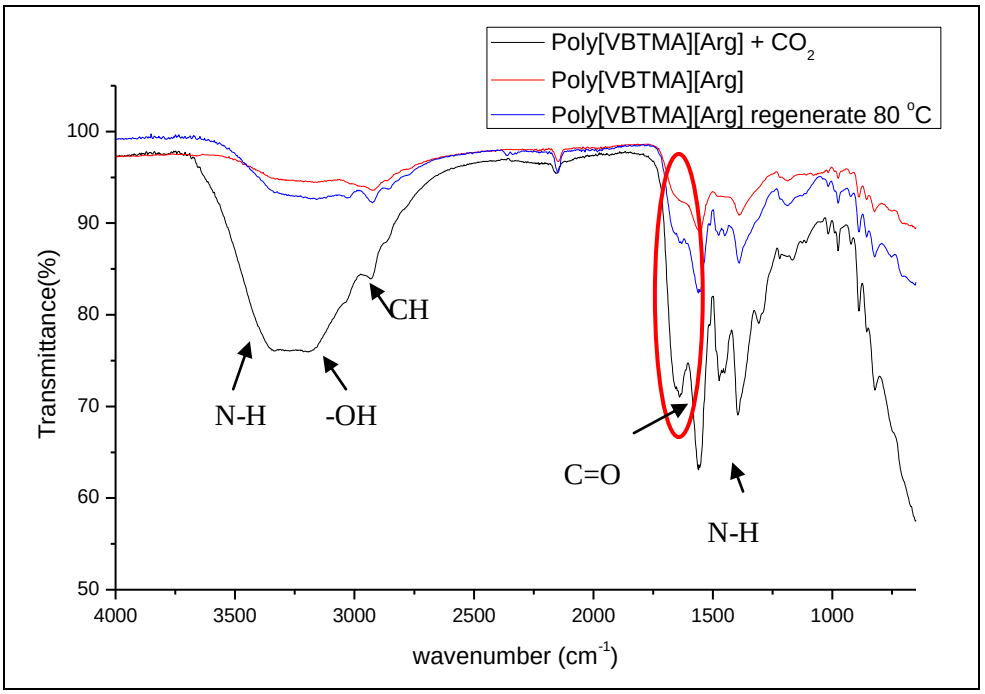

Figure 4.21: FTIR spectrum on poly[VBTMA][Arg]

After CO_2 sorption, the amine in anion reacted with CO_2 and formed carbamic acid. From Figure 4.21, after CO_2 sorption, the range 3346 – 3188 cm^{-1} shows an overlapped peak on N-H secondary and -OH formed in carbamic acid. The peak with high intensity formed in 1639 cm^{-1} and 1560 cm^{-1} corresponds to C=O in secondary amide and NH formed in carbamic acid respectively. However, after regeneration of poly[VBTMA][Arg] with CO_2 at 80 ^{o}C, the FTIR shows the intensity of C=O is reduced and the shoulder shows around 1600 cm^{-1} indicates the overlapped of COO^- and NH_2 in amino acids. After regeneration, the newly bound carbamic acid onto poly[VBTMA][Arg] would release the CO_2 molecule from poly[VBTMA][Arg]. Therefore the samples are ready for next cycle CO_2 sorption.

4.8 Adsorption Isotherm

Since the CO_2 sorption on AAPILs involved a physical adsorption at higher pressure, the study of adsorption isotherm is required. Langmuir, Freundlich, Dubinin-Radushkevich and Temkin isotherm models were applied to poly[VBTMA][Arg] at temperature 298 K, 313 K and 333 K. Figure 4.22 shows the isotherm graphs. All the parameters evaluated by linear regression. The correlation coefficient (R^2) was also used to determine the best fitting isotherm to the experimental data.

a.

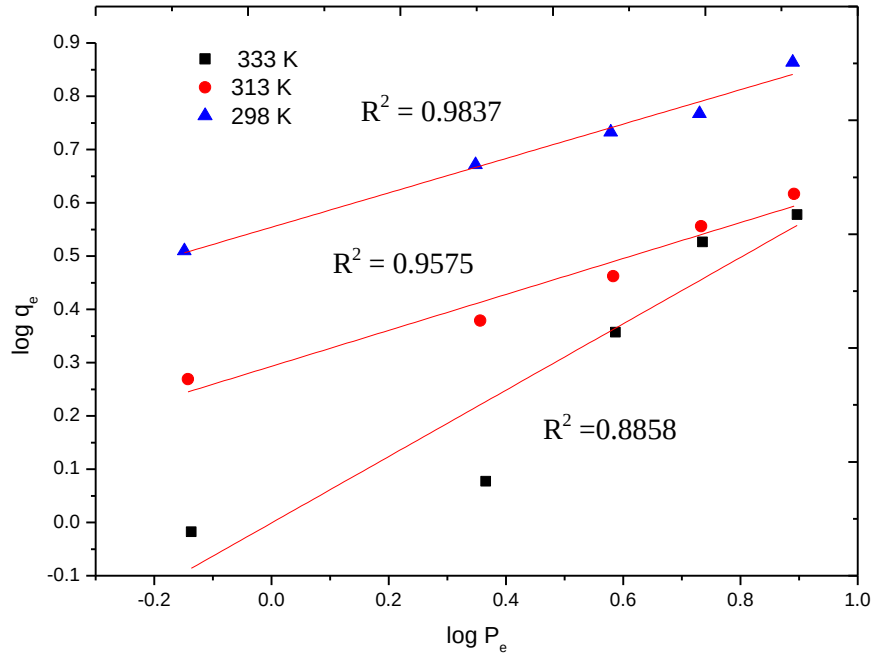
333 K
313 K
298 K
R2 = 0.9837
R2 = 0.9575
R2 =0.8858
log qe
log Pe

b.

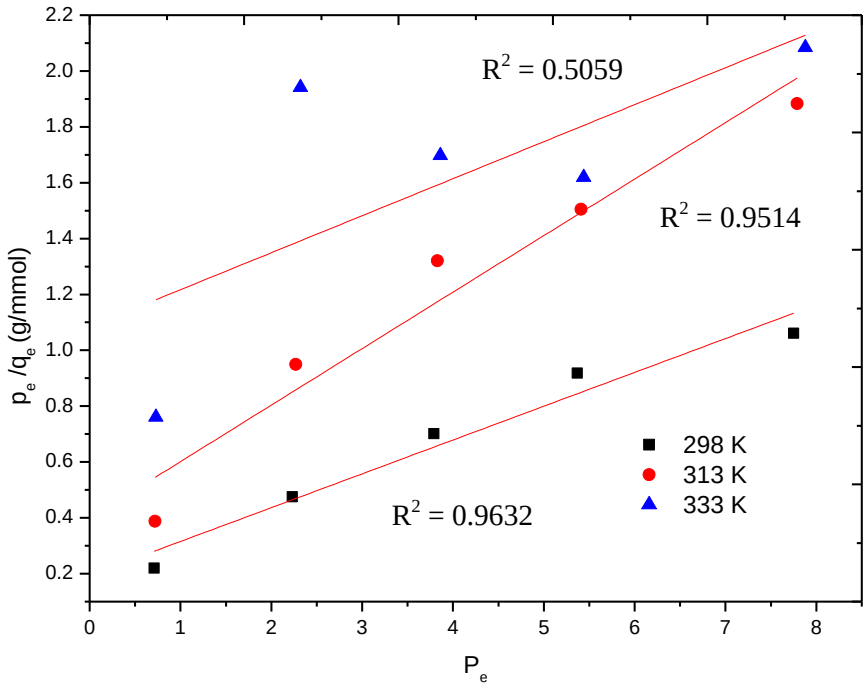
R2 = 0.5059
R2 = 0.9514
R2 = 0.9632
298 K
313 K
333 K
pe /qe (g/mmol)
Pe

c.

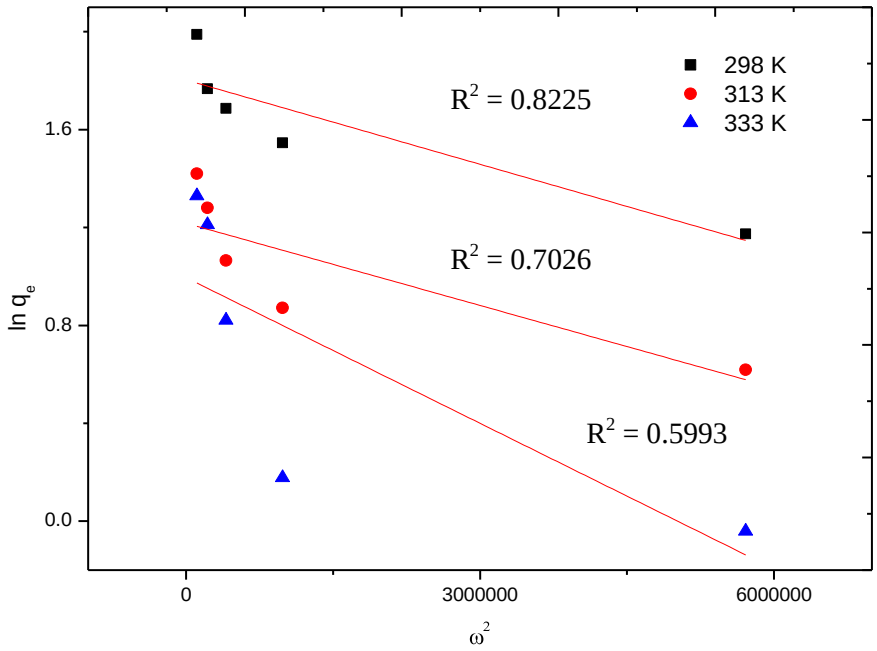

d.

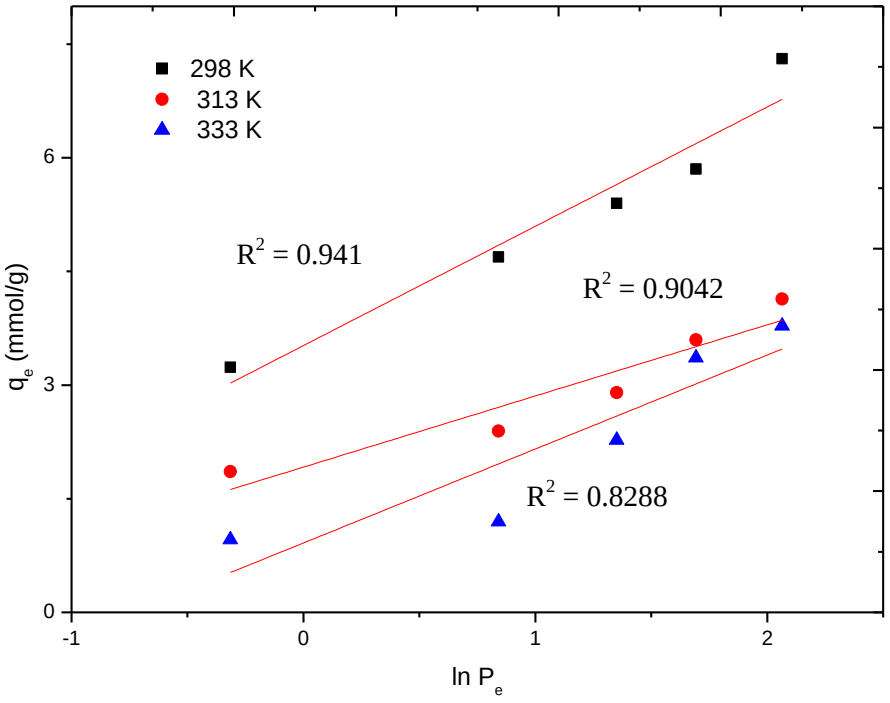

Figure 4.22: Adsorption isotherms a) Freundlich b) Langmuir c) Dabunin-Radushkevic and d) Temkin isotherm by linear regression method for poly[VBTMA][Arg] at 298 K, 313 K and 333 K.

Figure 4.22 shows the CO_2 sorption at different temperature, 298 K, 313 K and 333 K. From the isotherms graph shows that when temperature increases, the CO_2 sorption capacity decreases due to the reduction in binding strength between the CO_2

and poly[VBTMA][Arg] [164]. The reduction of CO_2 capacity shows that the sorption is exothermic thus showed that the involvement of physical adsorption process [165]. In physical adsorption, higher surface adsorption energy and molecular diffusion at elevated temperatures results instability of the CO_2 on AAPILs surface thereby promotes the desorption process at higher temperature. The increment of temperature accelerates the internal energy of the adsorbent, hence releases the CO_2 molecules from the surface [166]. The predicted isotherm constants for the CO_2 sorption and the corresponding R^2 value from the linear regression method are shown in Table 4.12.

Table 4.12: Adsorption isotherm parameters at 298 K, 313 K and 333 K

Freundlich				**Langmuir**			
Type	**298 K**	**313 K**	**333 K**	**Type**	**298 K**	**313 K**	**333 K**
K_F	3.582	1.964	0.99	q_m	8.258	4.943	7.547
n	3.09	2.966	1.605	K_L	0.6229	0.507	0.122
$1/n$	0.32	0.34	0.62	R_L	0.69	0.73	0.918
R^2	0.9837	0.9575	0.8858	R^2	0.9632	0.9514	0.5059
Dubinin Radushkevich				**Temkin**			
q_m	6.07	3.38	2.70	B	1.5635	0.9369	0.9158
λ	1.38×10^{-7}	1.25×10^{-7}	1.98×10^{-7}	K_T	9.816	7.859	2.718
E	1.9	2.003	1.588	b_T	1585	2778	3023
R^2	0.8225	0.7026	0.5993	R^2	0.941	0.9042	0.8288

Based on Table 4.12, the Langmuir constant, K_L and Freundlich constant, K_F that relates with the adsorption affinity are decreases at higher temperature. This is

because the bond strength between CO_2 and poly[VBTMA][Arg] decreased with increasing temperature thus indicate exothermic process. Le Chatelier's principle explain that desorption is favorable at elevated temperatures and caused the reduction of CO_2 sorption due to endothermic process. The maximum CO_2 capacity (q_m) is 8.258 mmol/g at 298 K and reduced at higher temperature. The essential characteristics of Langmuir equation is expressed as a dimensionless separation factor (R_L).

$$R_L = \frac{1}{1 + K_L P_o} \qquad 4.4$$

The value of R_L indicates the isotherm shape to be unfavorable (R_L>1), favorable (0<R_L<1) and irreversible R_L=1. Based on Table 4.11 the R_L values which is within the range of 0-1 suggests that the CO_2 sorption is favorable even at higher temperature [127]. The favorability of the CO_2 sorption can be supports by Freundlich isotherm.

The favourable adsorption in Freundlich isotherm is when the Freundlich constant, *n*, has the range of 1 to 10 [167]. From Table 4.11 can be seen that the *n* values are within this range thus supports the favorable sorption from Langmuir. The constant K_F is an approximate indicator of adsorption capacity, and can be seen that the K_F values decreases with increasing temperature which indicates the reduction of CO_2 capacity. The strength of adsorption process can be explain by *1/n* where *1/n* >1 is an indicative of cooperative adsorption [127] wheras *1/n* <1, indicates a normal adsorption as shows in Table 4.12.

Dubinin Radushkevich and Temkin isotherms provide a useful information related to the energy data estimation, in terms of mean free energy of adsorption (*E*), sorption energy value (*B*) and heat of adsorption (b_T) [168]. In Dubinin Radushkevich isotherm, it is used to determine the apparent energy of CO_2 sorption to poly[VBTMA][Arg]. The calculated *E* values which are within the range of 1-2 kJ/mol suggests that the CO_2 sorption is physical in nature as the magnitude of E is below 8 kJ/mol which indicate the chemisorption process [169]. The high values of q_m shows high sorption capacity at lower temperature and decreases with temperature increased. The value of the apparent energy of adsorption, also depict the physisorption process. From here can be said that the physisorption is dominant instead of chemisorption when pressure increases.

The Temkin isotherm is usually for the heterogeneous surface energy systems (non uniform distribution of sorption heat). Where *B* is constant related for heat of sorption (J/mol) and can be calculated from:

$$B = \frac{RT}{b_T} \quad 4.5$$

It decreased with increasing temperature from 1.5635 J/mol to 0.9158 J/mol indicating that the heat of adsorption of CO_2 to AAPILs decreases with increasing temperature from 298 K to 333 K, thus it is an exothermic. Besides the *E* validation test, sorption energy value (*B*) and heat of adsorption (b_T) values were lower than 20 kJ/mol thus shows a characteristic in physical adsorption [132]. This is also called non specific adsorption which occur as a result of long range weak van der Waals forces between adsorbate and adsorbent [168].

On the basis of R^2 value, the Freundlich model gives the best fit towards the experimental data over the entire temperature range. Therefore, it implies that the surface of poly[VBTMA][Arg] is heterogenous and a multi layer CO_2 sorption occurs and does not restrict to monolayer as proposed in Langmuir type. This multilayer also confirmed the BET model as reported earlier at higher pressure. This Freundlich isotherms primarily represents the physisorption process since it allows these CO_2 molecules to form a successive layer onto the surface of AAPILs. However, Dubinin Radushkevich isotherm is found to be the poorest fit of all experimental data.

4.9 Thermodynamic analysis

The thermodynamic parameters for the CO_2 sorption were estimated by van Hoff's formulation [132, 133, 169]. The change in Gibbs free energy (ΔG^o), change in enthalpy of reaction (ΔH^o) and change in entropy of adsorbent and adsorbate interaction (ΔS^o) can be estimated by following the equation 4.6 and equation 4.7.

$$ln\ K_F = \Delta S/R - \Delta H/RT \quad 4.6$$

$$\Delta G = -RT\ ln\ K_F \quad 4.7$$

Adsorption constant is the equilibrium constant, K_{eq}, therefore, they obey the van Hoff's formulation [127]. A plot of lnK_F versus $1/T$ as shown in Figure 4.23 was used to determine the ΔH^o and ΔS^o of adsorption by following Equation 4.8.

$$ln\, K_F = \frac{\Delta S}{R} - \frac{\Delta H}{RT} \qquad 4.8$$

Based on Equation 4.6 to 4.8, R represents the universal gas constant (8.314 J/mol.K), T is adsorption temperature in K and K_F is the Freundlich constant deduced from the Freundlich isotherm fit [169].

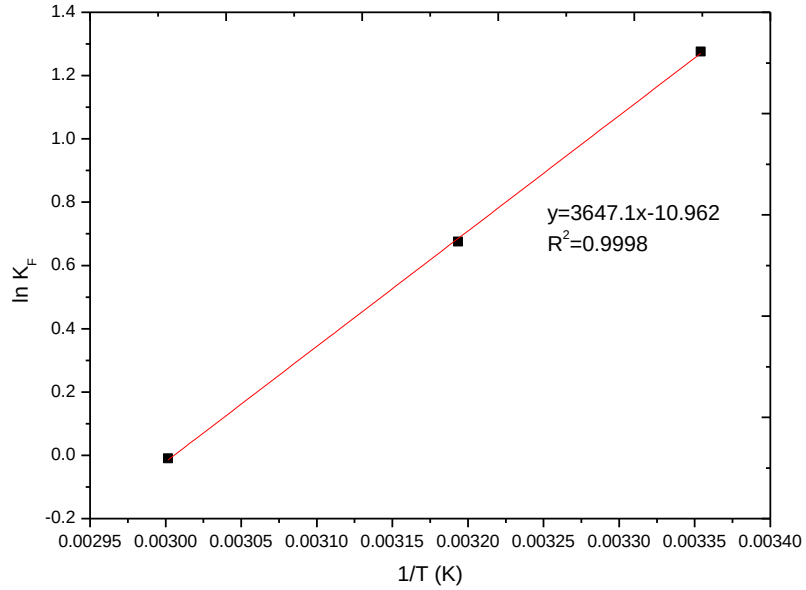

Figure 4.23: Thermodynamic parameters by using van Hoff's equation

The estimated values of thermodynamic parameters are tabulated in Table 4.13. The experimental data show the capacity of CO_2 sorption decreased with increasing temperature. This indicates that the negative sign of ΔH^o value indicates an exothermic nature of the CO_2 sorption process. In addition, for an exothermic reaction, the van Hoff's plot should always have a positive slope. The ΔS^o can be interpreted by the behavior of the CO_2 molecules upon the adsorption process, which is from randomized to an ordered form on the surface of the adsorbent. The negative value of ΔS^o suggests high orderliness of the adsorbate molecules upon adsorption.

The negative value of ΔG^o indicates the spontaneous nature of CO_2 sorption by poly[VBTMA][Arg] [133, 169-171].

Table 4.13: Thermodynamics parameters of CO_2 adsorption

Sample	ΔH^o (kJ/mol)	ΔS^o (kJ/mol.K)	ΔG^o (kJ/mol)			Ref.
			298 K	313 K	333 K	
Poly[VBTMA][Arg]	-30.3	-91.14	-3.16	-1.76	0.27	Present work
$[C_4mim][CF_3CF_2CF_2CF_2SO_3]$	-11.9	-40.0	n/a	n/a	n/a	[172]
$[C_2CNDim][DOSS]$	-12.9	-61.65	4.94	n/a	n/a	[158]
$[P_{66614}][Meth]$	-64	n/a	n/a	n/a	n/a	[68]

The magnitude of ΔH^o denotes the type of CO_2 absorption process either physical or chemical sorption. The enthalpy (ΔH^o) from experimental data is -30.3 kJ/mol which is intermediate from physical sorption (-10 to -20 kJ/mol) and chemical sorption with conventional amine (-80 to -100 kJ/mol) [173]. The calculated ΔH^o which is > -20 kJ/mol suggests that both of physisorption and chemisorption involved in the reaction. In addition, larger the negative value for enthalpy indicates stronger IL/CO_2 interaction. By comparing the experimental ΔH^o (-30 kJ/mol) with ΔH^o for $[P_{66614}][Meth]$ [68], it can be seen that the enthalpy for poly[VBTMA][Arg] is lesser. The smaller change in enthalpy on AAPILs compared to the reported AAILs [68], indicates that less energy is required for the regeneration of AAPILs, and therefore by polymerizing the AAILs can potentially impact positively on the energy balance on the recovery process.

The ΔG^o values are divided into two regions which is at low temperature (25 and 40 ^oC) with a negative value and high temperature (60 ^oC) with a positive value. The

increase of ΔG^o with increasing T indicates that the CO_2 sorption consumes more energy with increasing temperature. The negative of ΔG^o confirms the feasibility of the process and indicates an occurrence of the favorable and spontaneous adsorption [166] whilst positive value at an elevated temperature implies a non-spontaneous adsorption reaction [165]. In addition, decreased in negative ΔG^o value with increasing temperature implies that the CO_2 sorption process is more favorable at 298 K rather than 333 K. For the special condition where ΔG^o =0, the reaction is at equilibrium at standard conditions, with K_F=1. According to Table 4.12, the K_F value is 0.99 at 333 K, thus give ΔG^o with 0.27 kJ/mol. Therefore, ΔG^o is at equilibrium when temperature is almost 333 K. The negative value from the entropy ΔS^o, can be explain by the structuring effect caused by the specific interactions between the solute and the charge centers of the ILs [158].

4.10 Kinetic Studies on poly[VBTMA][Arg] at different temperature

The prediction of kinetics is necessary for the design of adsorption systems. The kinetic parameters which is helpful for the prediction of adsorption rate, gives important information for designing and modeling the processes [174]. Successful application of the adsorption demands innovation of cheap, easily available and abundant adsorbents of known kinetic parameters and sorption characteristic [175].

The kinetics studies of CO_2 adsorption into the poly[VBTMA][Arg] was studied by using various kinetic models such as pseudo-first order, pseudo second order, Elovich and intra particle model. In addition, the reliability of these kinetic models in predicting the adsorption capacity is accessed by linear regression coefficient, R^2 and relative error (ε) which is defined in Equation 4.9;

$$\varepsilon \ \% \ = \frac{q_{e\,calc} - q_{e\,act}}{q_{e\,act}} \ X \ 100\% \qquad 4.9$$

Based on Equation 4.9, $q_{e,cal}$ is refers to the measured value that is obtained from the kinetic analysis, whilst $q_{e,act}$ is the actual value of the adsorption capacity based on the experimental work [165].

4.10.1 Pseudo-first order kinetic model

The earliest work that has been reported on kinetic study was conducted by Lagergren in 1898 is given as;

$$\frac{dq_T}{dt} = k_1(q_e - q_t) \tag{4.10}$$

$$log(q_e - q_t) = log\ q_e\ - (\frac{k_1}{2.303}).t \tag{4.11}$$

Where q_t and q_e are the adsorption capacity at any particular time and at equilibrium respectively and k_1 is the pseudo first order constant with unit of 1/min. By integrating the equation results in a linearized form as Equation 4.11, hence plotting graph of *log (qe-qt)* versus time yields a linear function in which *log (qe)* and ($k_1/2.303$) is the y-intercept and slope, respectively as shown in Figure 4.24 [176]. Based on Figure 4.24 and Table 4.14, it was shown that pseudo first order fits the CO_2 sorption at all temperature with the regression coefficient values mostly greater than 0.98 and the relative error is lower, ε compared to pseudo second order model. The adsorption capacities from the experimental data and predicted by the pseudo first order has a good agreement with each other. This is because the first order of adsorption process suggests the faster diffusion of CO_2 molecules into the adsorbent surface [177]. Pseudo first order rate constant, K_1 was the highest at 333 K with 0.03155 min^{-1} suggesting the fastest adsorption kinetics among other temperatures [178]. Although the reaction rate becomes faster at a higher temperature, less CO_2 being adsorbed due to the faster desorption of CO_2 [179].

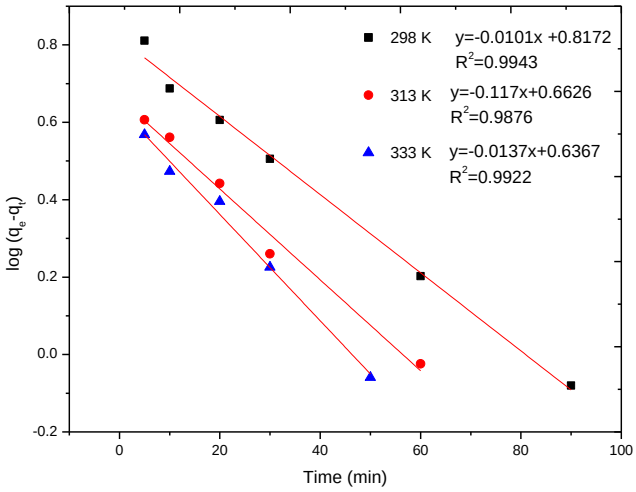

Figure 4.24: Kinetic plot of pseudo first order model at various temperatures.

Table 4.14: Kinetic parameter of Pseudo first order

Kinetic model	**Parameter**	**Temperature (K)**		
		298	**313**	**333**
	$q_{e,\,act}$ *(mmol/g)*	*7.9099*	*4.1358*	*3.7814*
Pseudo first order	K_1 (1/min)	0.0232	0.02695	0.03155
	$q_{e,\,cal}$ (mmol/g)	6.56	4.598	4.332
	R^2	0.9943	0.9876	0.9922
	Relative error, ε (%)	16.99	11.18	14.56

4.10.2 Pseudo second order kinetic model

Pseudo second order reaction also often cited in literature [180, 181]. The equation of pseudo second order is represented as below:

$$\frac{t}{q_t} = \frac{1}{k_2 . q_e^2} + \frac{t}{q_e} \qquad 4.12$$

$$h = k_2 . q_e^2 \qquad 4.13$$

Where k_2 is the pseudo second order rate constant, t is the contact time of gas-solid in min, while q_e and q_t is the adsorption capacity at equilibrium and particular time t, respectively and h is corresponds to the initial adsorption rate (mmol/g min).

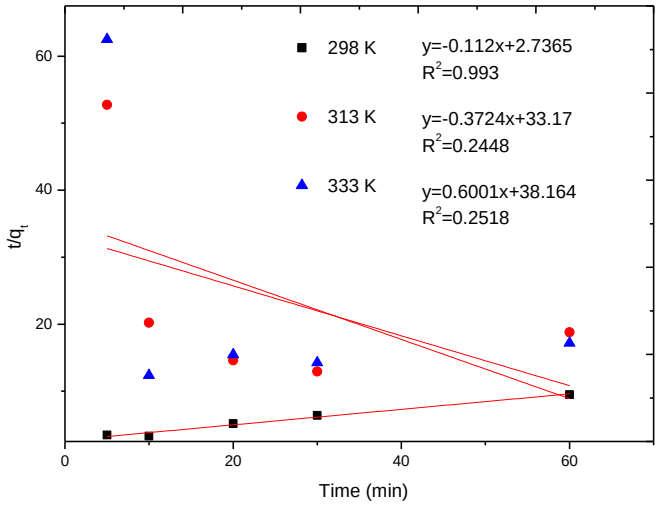

Figure 4.25: Kinetic plot of pseudo second order model at various temperatures.

Table 4.15: Kinetic parameter of Pseudo second order

Kinetic model	**Parameter**	**Temperature (K)**		
		298	**313**	**333**
	$q_{e,\,act}$ (mmol/g)	*7.9099*	*4.1358*	*3.7814*
Pseudo second order	$q_{e,cal}$ (mmol/gl)	8.9286	-2.68	1.666
	K_2 (g/mmol min)	4.58×10^{-3}	4.197×10^{-3}	9.436×10^{-3}
	h (mmol/g min)	0.3651	0.03014	0.0262
	R^2	0.993	0.2448	0.2518
	Relative error, ε (%)	11.41	164.8	55.94

From Figure 4.25 can be seen that the model poorly fit into the kinetic data. Due to its low value of R^2 value (range of 0.22 to 0.99) and large relative error as depicted in Table 4.15. This higher percentage (%) error indicates that this model is not able to describe the adsorption process of CO_2 on poly[VBTMA][Arg]. The initial

adsorption rate (*h*) that decreases with temperature verified the physisorption and exothermic behaviour during the adsorption at high pressure. From Table 4.15, the initial adsorption rate (α) decreases with an increase in temperature from 0.8193 to 0.2316 for 298 K and 333 K respectively. This is due to the higher kinetic energy of the CO_2 at a higher temperature in which the tendency of CO_2 to escape from the adsorbent also increased.

4.10.3 Elovich kinetic model

In addition with the pseudo first order and second order model, Elovich kinetic model is frequently applied in gas – solid reaction, and is expressed as follows:

$$\frac{dq_t}{dt} = \alpha\, exp(-\beta q_t) \qquad 4.14$$

Where α is the initial adsorption rate (mg/g min), while β is the extent of surface coverage and activation energy of the process. The boundary conditions in which $\alpha\beta$ is assumed ≥ 1, $q_t = 0$ at $t=0$ and $q_t = q_t$ at $t=t$ is being applied in equation, and upon integration, it results in new equation as shown in Equation 4.15.

$$q_t = \frac{1}{\beta} ln(\alpha\beta) + \frac{1}{\beta} ln\, t \qquad 4.15$$

Based on Equation 4.15, if the CO_2 sorption fits the Elovich model, the Elovich plots of q_t versus $ln(t)$ will yield a straight line with slope of $1/\beta$ and y intercept of $1/\beta\ ln\ (\alpha\beta)$. Based on Table 4.16, the initial adsorption rate (α) decreased with temperature from 0.8193 to 0.2316 for 298 K and 333 K respectively. This is similar to that of initial adsorption rate (*h*) from pseudo second order model. The Elovich model also describes the desorption process that is taking place as well as the value of β is equivalent to desorption rate [165].

As can be seen from Table 4.16, the magnitude of β which increased from 0.5217 g/mmol at 298 K to 0.8364 g/mmol at 333 K indicates that desorption was dominant at higher temperature. As shown in Figure 4.26, Elovich kinetic model does not fitted well into the experimental data with the regression coefficient within 0.96 to 0.99.

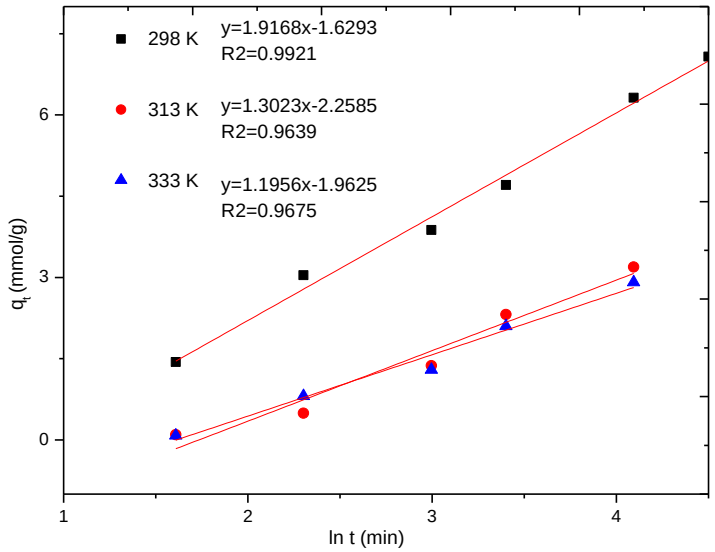

Figure 4.26: Elovich plot of CO_2 sorption at various temperatures

Table 4.16: Kinetic parameters of Elovich isotherm

Kinetic model	**Parameter**	**Temperature (K)**		
		298	**313**	**333**
	$q_{e,\,act}$ *(mmol/g)*	*7.9099*	*4.1358*	*3.7814*
Elovich	β (mmol/g)	0.5217	0.7679	0.8364
	α (mmol/g min)	0.8193	0.2299	0.2316
	R^2	0.9921	0.9639	0.9675

4.10.4 Intra-particle diffusion kinetic model

Intraparticle diffusion model provides the diffusion mechanism of the adsorption process. This model is defined by Equation 4.16.

$$q_t = kt^{\frac{1}{2}} + C \qquad 4.16$$

Where q_t is the amount adsorbed at any particular time (mmol/g), k is the intraparticle diffusion rate constant (mmol/g min ½) and C (mmol/g) relates to the thickness of boundary layer. If the adsorption process obeys the intra-particle diffusion model, a straight line plot against half power of time, $t^{1/2}$ passes through the

origin is expected, with slope of *k* and y intercept of *C*. In any adsorption process, there are multiple steps that occurs such as mass transfer of adsorbate to adsorbent surface (bulk diffusion), film diffusion (external mass transfer resistance) and followed by surface diffusion into the internal sites (intra-particle diffusion) [165, 176].

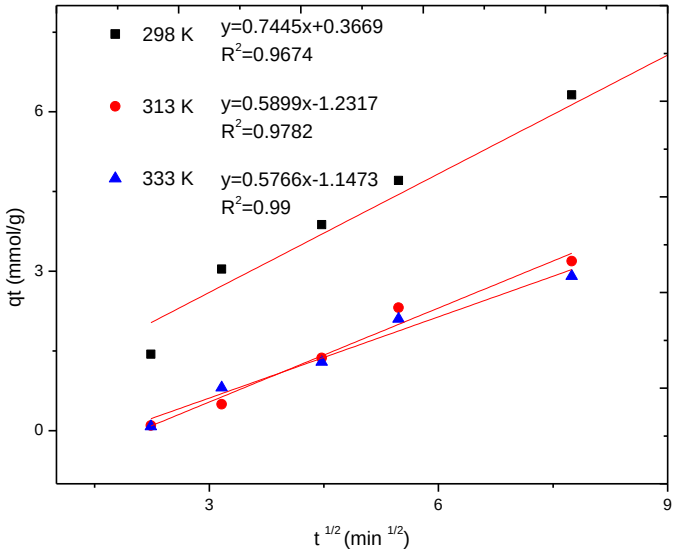

Figure 4.27: Intra-particle diffusion model at different temperatures

Table 4.17: Kinetic parameters of CO_2 sorption onto poly[VBTMA][Arg]

Kinetic model	**Parameter**	**Temperature (K)**		
		298	**313**	**333**
	$q_{e,\,act}$ (mmol/g)	*7.9099*	*4.1358*	*3.7814*
Intra-particle diffusion model	*K*(mmol/g $min^{1/2}$)	0.7445	0.5899	0.5766
	C (mmol/g)	0.3669	-1.2317	-1.1473
	R^2	0.9674	0.9782	0.99

Figure 4.27 shows the intraparticle diffusion plot for different reaction temperatures applied in this study and the corresponding kinetic parameters were tabulated in Table 4.17. From the Figure 4.27 can be seen that the kinetic parameter

plot does not fit well into the kinetic model. Kinetic parameters at different temperature and its corresponding coefficient were summarized in Table 4.17.

4.11 Evaluation of activation energy

Ease of adsorption process requires the minimum activation energy. Activation energy can be calculated by using the Arrhenius equation as shown in Equation 4.17.

$$ln\, k_1 = ln\, k_0 - \frac{E_a}{RT} \qquad 4.17$$

According to Equation 4.17, k_1 is pseudo first order constant, k_0 is the temperature impact factor, E_a is the apparent activation energy for adsorption (J/mol), R is the gas constant (8.314 J/mol K) and T is the adsorption temperature in K. By plotting ln k_1 versus the reciprocal of temperature yields a straight line with y-intercept of ln k_0 and slope of ($-E_a/R$) as shown in Figure 4.28.

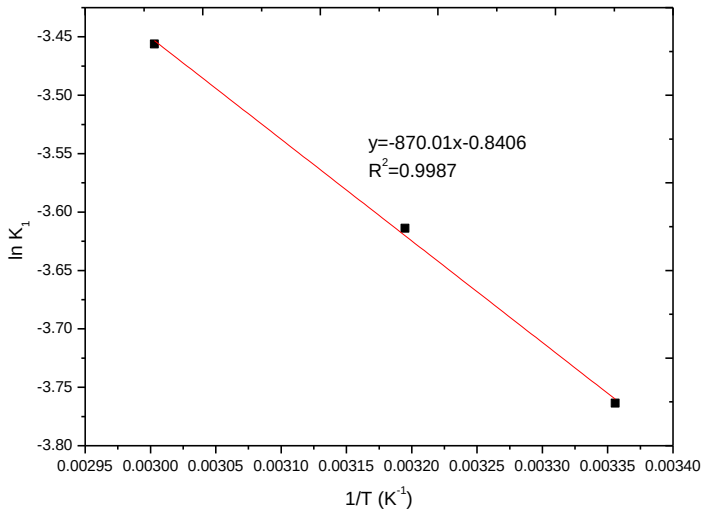

Figure 4.28: Fitting of Arrhenius equation

The activation energy of this present study was found to be approximately 7.23 kJ/mol and k_o is 0.43145. This E_a is typically low compared with the adsorption of CO_2 by using activated carbon with 17 kJ/mol [165]. The value of activation energy is low due to weak interaction forces between adsorbent and adsorbate at high pressure [165]. Thus, the lower value of the activation energy shows that the CO_2

sorption investigated falls under physisorption at these temperatures and 10 bar pressure.

4.12 Density Functional Theory (DFT) on Thermochemistry Calculation

The energy and electronic structure of the molecular systems were computed with Density Functional Theory (DFT) calculations using *Gaussian 09* with the *B3LYP* functional and *6-31G** basis set. The reaction energy of amine and CO_2 can be studied to understand the role of amine-CO_2 reaction energy by systematically different amines. In argininate structure with given multiple numbers of amines presence, it is important to understand the connection between the amine molecular structure and its reaction energy with CO_2.

The molecular modeling within the framework of DFT was carried out by co-worker. It was used to evaluate the reaction energy to form the product species associated with the amine-CO_2 system [182]. This DFT was used to relate electronic structure properties of the amines in their reactivity and to design the target amine with reactivity towards CO_2.The energies are likely to be affected by the ILs media. By following the method reported by Saravanamurugan *et al.* [105], that a solvent and the cation were not included in the calculations since the solvent-property and the diffraction data for the studied ILs structures were not available. Therefore, without inclusion of such experimental data (*i.e.*, cations with specific conformations) the model would most likely to be improved [105]. Table 4.18 below shows the molecular structure of different conformations of argininate with CO_2 and the electronic energy and enthalpy for each conformation.

Table 4.18: Molecular structures and enthalpy reaction of argininate and CO_2

Molecular structure (3D)	Molecular structure (1D)	electronic energy + enthalpy (kcal/mol)	ΔH (kJ/mol)
1 mol CO_2 + 1 mol argininate			
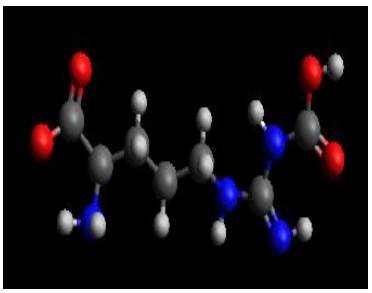	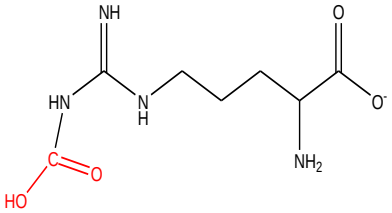	-498431.15	-30.42
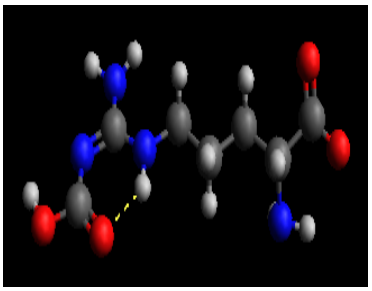	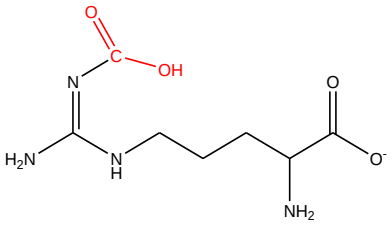	-498440.01	-32.61
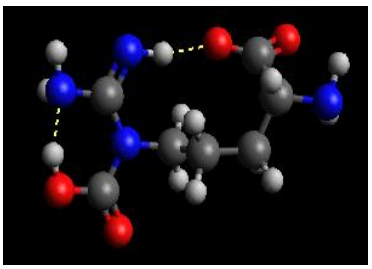	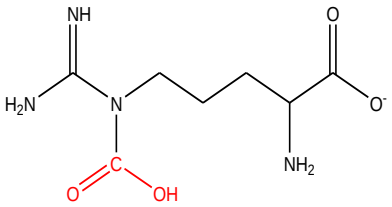	-498453.90	-89.75
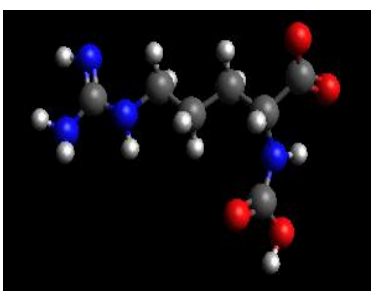	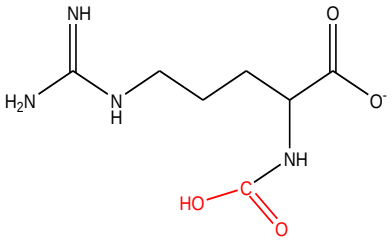	-498443.21	-59.14

2 mole CO_2 + 1 mole argininate			
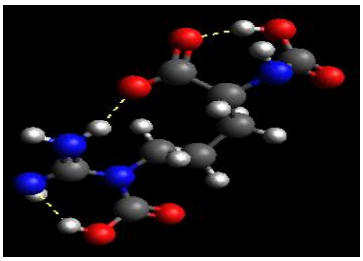	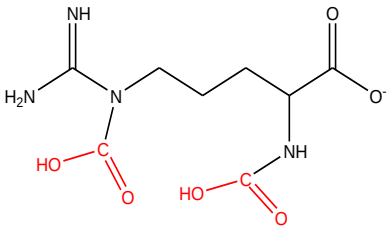	-616771.49	-110.27
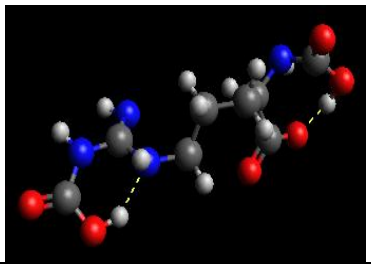	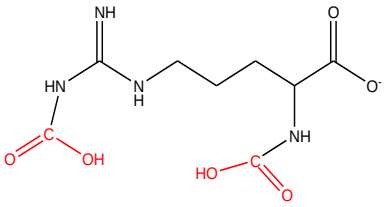	-616762.29	-92.68
3 mol CO_2 + 1 mol argininate			
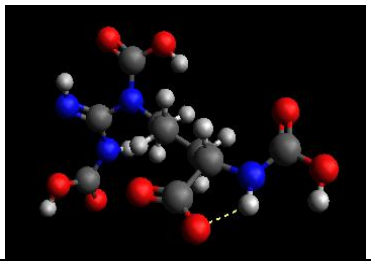	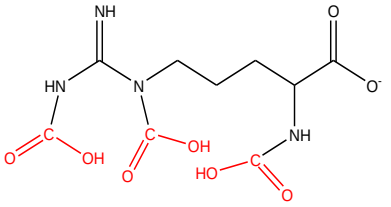	-735077.49	-14.30

Table 4.18 shows the electronic molecular structure and electronic enthalpy and enthalpy reaction for the argininate complex with CO_2. Since in argininate structure has two primary and two secondary amines functional, there are various composition where 1 mol of CO_2 could be attached to 1 mol of argininate. The enthalpy reaction for 1 mol of CO_2 reacts with 1 mol of argininate is from -30 kJ/mol to -90 kJ/mol. When 2 mol of CO_2 attached with 1 mol of argininate, the enthalpy higher from -92 kJ/mol to -110 kJ/mol showing that strong chemical bonding between CO_2 and amine, hence more CO_2 could be absorb. However, when 3 mol of CO_2 attached with 1 mole of argininate, the enthalpy of reaction drop to -14.30 kJ/mol. This might be caused by the steric repulsion dominated when CO_2 crowded in argininate. In our experiment, the enthalpy of reaction is -30.3 kJ/mol. This result has a good agreement with enthalpy calculated by DFT with -30.42 kJ/mol when 1 mol of CO_2 reacts with 1 mol argininate. Thus, the mechanism 1:1 is achieved. The CO_2 sorption

capacities in [VBTMA][Arg] with 0.83 mol/mol and poly[VBTMA][Arg] with 1.14 mol/mol proved the mechanism 1:1.

4.13 Proposed Mechanism of poly[VBTMA][Arg] with CO_2

The mechanism of CO_2 with TSILs proposed by Bates *et al.* [67] stated when the amine is attached to the cation, the carbamate formation is favoured. However when the amine bound to the anion, the formation of carbamic acid is the favoured one [68].

By using amino acid as anions, many researchers [68, 70, 96] have proposed a new mechanism with the formation of carbamic acid. It was shown that 1 mol ILs can absorb 1 mol of CO_2 (1:1 mechanism). The proposed mechanism as in literature reported for AAILs with CO_2 is shown in Figure 4.29.

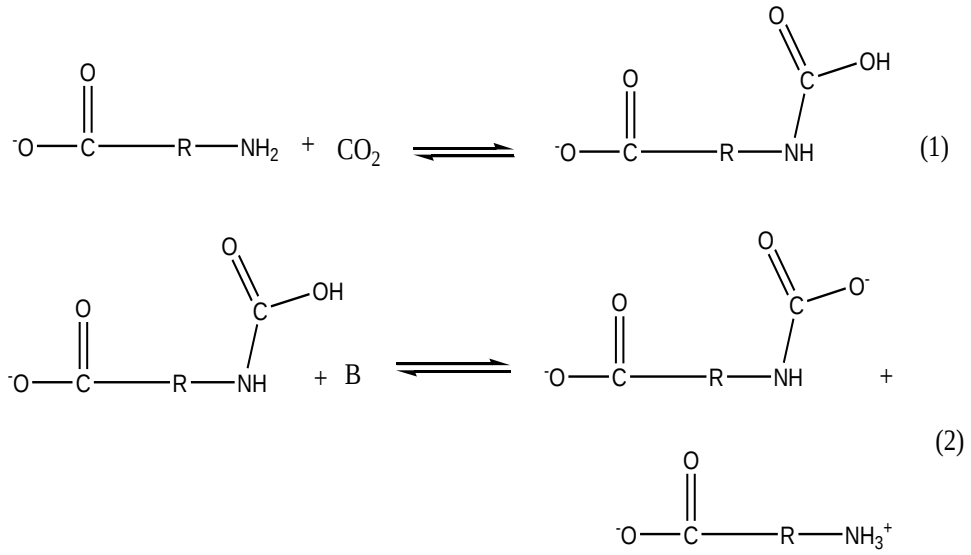

Figure 4.29: Proposed mechanism of AAILs with CO_2 [68]

In Figure 4.29, when amino acid anion reacts with CO_2, carbamic acid was formed as shown in first formation (1). When this carbamic acid react with any base, or in non aqueous medium (amino acid itself act as base), dianion are formed as shown in second (2) formations. This is supported by Gurkan *et al.* [68] that the reaction between AAILs and CO_2 terminates at formation of carbamic acid (1) without forming a carbamate species (2). The dianion formed in the second formation (2) is chemically unstable therefore the reaction would expect to terminate

at first formation upon addition of CO_2 to AAILs. This indicates a potential absorption stoichiometry of 1:1 (CO_2: IL).

Therefore, the maximum capacity can be achieved is 1 mol/mol. However, for polymerized AAPILs, the CO_2 sorption capacities can be more than 1 mol/mol due to involvement of physical adsorption [105]. Figure 4.30 below shows the proposed mechanism of AAPILs which is poly[VBTMA][Arg] with CO_2.

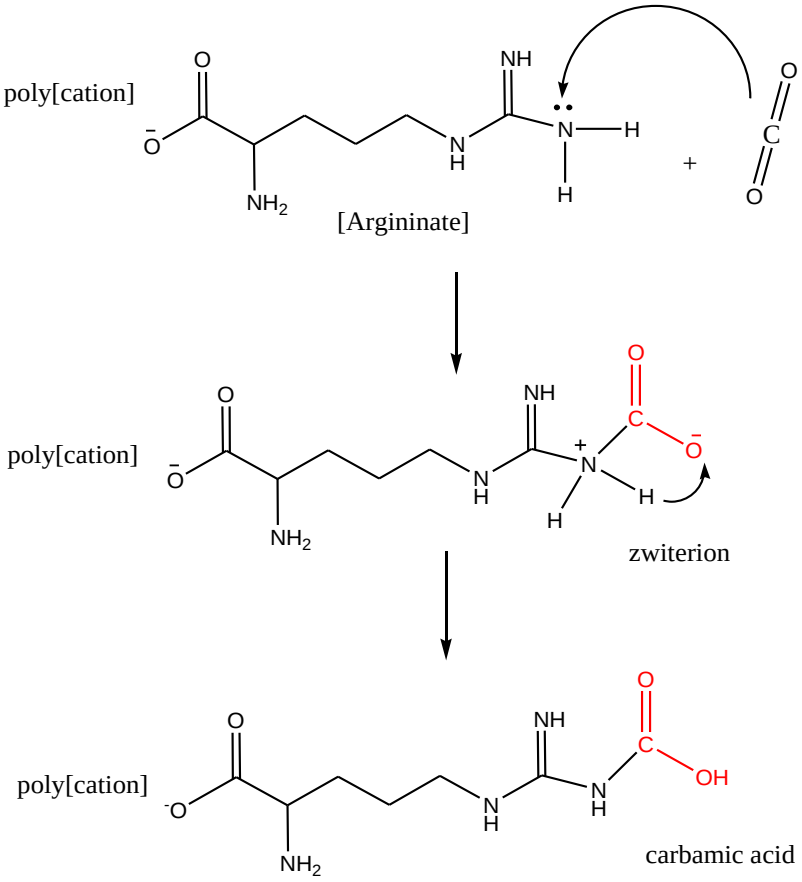

Figure 4.30: Proposed mechanism of poly[VBTMA][Arg] with CO_2

Figure 4.30 shows the proposed mechanism of one mol of CO_2 react with one mol of argininate and formed carbamic acid. Initially, the addition of CO_2 to nitrogen in amine functionalized in argininate would form a carbamate bond with the formation of zwiterion. The reaction proceeds with the proton shifting from the amine onto the newly bound of CO_2 thus form a carbamic acid.

In the simple route, the chemisorptions of CO_2 to the amine group is an elemental reaction where the proton migrates from the amine to an oxygen atom of the

incoming CO_2 molecules [105]. From DFT calculation, only one primary amine react with one mole of CO_2 as shown in Figure 4.30 giving ΔH^o is -30.42 kJ/mol. This theoretical ΔH^o is similar with experimental ΔH^o which is -30.3 kJ/mol. Therefore, the proposed mechanism followed the 1:1 mechanism where 1 mol CO_2 reacts with 1 mol argininate, which only 1 amine reacted with CO_2 at ambient pressure. However, in higher pressure, the possibility of CO_2 to react with one or more amines is higher since argininate comprises of two primary and two secondary amine sites. Therefore, more CO_2 capacities can be achieved in high pressure.

4.14 Characterization of AAPILs after CO_2 sorption

The characterization of AAPILs after CO_2 absorption can be characterized by using FTIR before and after CO_2 absorption. FTIR before and after CO_2 absorption of poly[VBTMA][Arg] are shown in Figure 4.31. All of FTIR spectrum can be found in Appendix B.

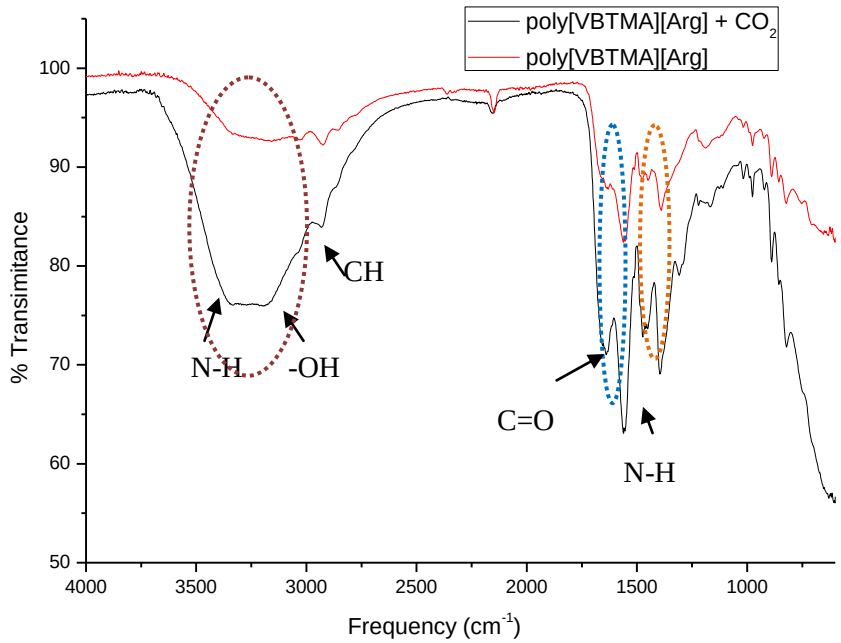

Figure 4.31: FTIR before and after CO_2 sorption of poly[VBTMA][Arg]

Figure 4.31 shows a FTIR spectrum of poly[VBTMA][Arg] before and after CO_2 sorption to see any peak changes and Figure 4.32 shows a carbamic formed at argininate.

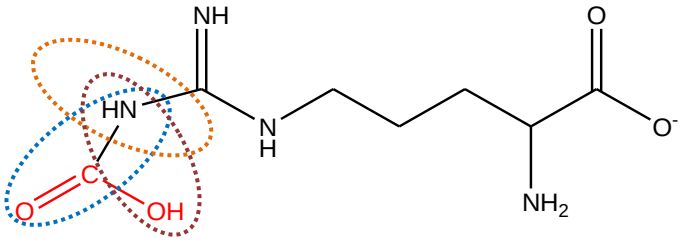

Figure 4.32: Carbamic acid formed at argininate

For poly[VBTMA][Arg], the reaction CO_2 and amine shows a broad peak in range 3346 – 3188 cm^{-1} corresponds to –NH in secondary amides and OH overlapped in carbamic acid formed. A peak with high intensity at 1639 cm^{-1} corresponds to the C=O and the peaks at 1560 cm^{-1} and 1476 cm^{-1} corresponds to –NH in secondary amides that were formed in carbamic acid species as shown in Figure 4.32. The reaction of CO_2 and NH_2 was confirmed in poly[VBTMA][Arg].

For poly[VBTMA][Lys], poly[VBTEA][Lys], poly[VBTBA][Lys], poly[VBMI][Lys] and poly[VBPPN][Lys], the intensity for all peaks increased after CO_2 absorption. Peak at 3344 cm^{-1} increased and became broader, which corresponds to –NH in secondary and overlapped with -OH. The increasing peak intensity at 1581 cm^{-1} indicated the –C=O overlaps with the –NH after formation of carbamic acid species.

For poly[VBTMA][Hist], high intensity for all peaks are observed after CO_2 absorption and new peak is observed at 1631 cm^{-1}, indicating the formation of carbamic acid species. The broad peak and high intensity are observed in range 3200 to 3350 cm^{-1} indicating the –NH secondary peak after reaction with CO_2. For poly[VBTMA][Tau], the increased of intensity for all peaks can be observed after CO_2 absorption, especially in range of 3200 to 3350 cm^{-1} for the -NH peaks. The new peak is observed at 1641 cm^{-1} indicating the formation of carbamic acid.

In poly[VBTMA][Pro], the new peak is also observed at 1643 cm^{-1} after CO_2 absorption showing the formation of carbamic acid. For poly[VBTMA][Ser], the increasing of intensity for all peaks can be observed especially in the range 3200 to 3400 cm^{-1} showing broad peaks of –NH secondary. Peak at 1571 cm^{-1} indicating the carbamic acid species been overlapped with –C=O from carbonyl salts. In poly[VBTMA][Ala] and poly[VBTMA][Gly] ,increasing intensity is observed after CO_2 absorption especially in –NH region and –C=O region.

From all the FTIR spectrums it can be shown that after CO_2 absorption, some of the samples clearly show the formation of carbamic acid species *i.e.* poly[VBTMA][Arg], poly[VBTMA][Hist], poly[VBTMA][Tau] and poly[VBTMA][Pro]. But for other AAPILs like poly[VBTMA][Lys], poly[VBTEA][Lys], poly[VBTBA][Lys], poly[VBMI][Lys], poly[VBPPN][Lys], poly[VBTMA][Ser], poly[VBTMA][Ala] and poly[VBTMA][Gly], it showed the overlapping of carbamic acid species with $–COO^-$ from carbonyl salts. Generally, it was observed the increasing of intensity for all samples after CO_2 been absorbed. This showed those both chemical and physical adsorptions are involved in AAPILs after reaction with CO_2.

4.15 Effect of water to AAPILs

A study on effect of water to AAPILs for CO_2 capture is needed since in natural gas contains impurities of moisture. The solubility measurement was made by using dry ice method as follows the method by Vijayraghavan *et al.* [88]. The CO_2 sorption of ILs is substantially sensitive to their water content [89, 183-185]. The presence of water can even produce chemical instability of the ILs [186-188]. However, there are cases where the presence of water improves the level of absorption [17, 97].

Figure 4.33 shows the effect of water with additional of 2 mol and 4 mol of water to AAPILs (poly[VBTMA][[Gly], poly[VBTMA][Ala], poly[VBTMA][Ser] and poly[VBTMA][Pro]. A huge increment in sorption capacity of AAPILs was achieved with addition of water. It can be seen that with additional 4 mole of water the CO_2 sorption increased up to 12 w/w% for poly[VBTMA][Gly].

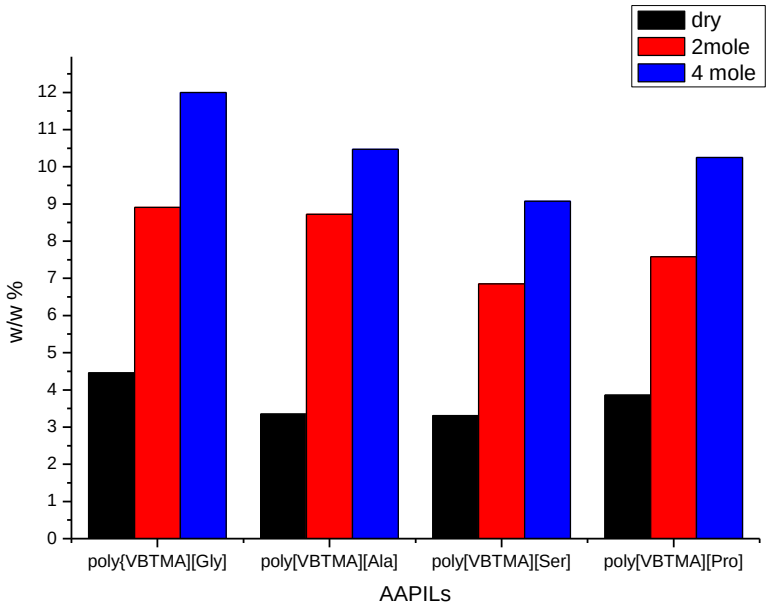

Figure 4.33: Effect of water to AAPILs

Hu *et al.* [118] have studied the effect of water to the sorption of CO_2 capacity. The results indicate that presence of water promotes the absorption of CO_2. The absorption capacity increases from 0.96 mol/mol to 1.91 mol/mol when water content increases from 0 % to 30 %. Therefore shown that water content of ILs has direct effect on their CO_2 sorption capacity [118].

Water promotes ionization of the ILs. This suggests that the water makes the ILs generate more H^+ and any other ions after absorbing with CO_2 [43]. The hydration reaction occurred between water and CO_2 formed carbonic acid as shown in 4.18 [118].

$$CO_2 + H_2O \leftrightarrow H_2CO_3 \quad 4.18$$

$$H_2CO_3 + NH_2\text{-}R\text{-}COO^- \leftrightarrow HCO_3^- + NH_2\text{-}R\text{-}COOH \quad 4.19$$

$$H_2CO_3 + H_2O \leftrightarrow HCO_3^- + H_3O^+ \quad 4.20$$

$$HCO_3^- + H_2O \leftrightarrow HCO_3^{2-} + H_3O^+ \quad 4.21$$

A reaction as shown in equation 4.19 is a proton transfer from carbonic acid to amino acid anion. Since CO_2 is a weaker acid than amino acid, the proton transfer would not supply enough thermodynamic driving force for chemisorption. Therefore any hydrogen bond acceptors present in CO_2 loaded absorbents such as amino acid and bicarbonate anion are candidates for hydrogen bond partners for amino acid as

shown in 4.22 [189]. The amino acid anions also may react with amino acid that formed in reaction 4.19 to form hydrogen bond.

$$HCO_3^- + NH_2\text{-}R\text{-}COOH \leftrightarrow [HO(CO)O\text{---}H\text{---}OOC\text{-}R\text{-}NH_2]^- \quad 4.22$$

$$NH_2\text{-}R\text{-}COO^- + NH_2\text{-}R\text{-}COOH \leftrightarrow [NH_2\text{-}R\text{-}COO\text{---}H\text{---}OOC\text{-}R\text{-}NH_2]^- \quad 4.23$$

Hence, more reaction capability between CO_2, H_2O and amino acid anion are formed. Thus, the CO_2 sorption capacity also increases. In view, these stoichiometry of chemisorption is most reasonably represented by the following equation [189]:

$$CO_2 + H_2O + NH_2\text{-}R\text{-}COO^- \leftrightarrow HCO_3^- + NH_2\text{-}R\text{-}COOH \quad 4.24$$

With the addition water, the hydration reaction between water in ILs and CO_2 makes the absorption capacity higher compared to dry ILs [118]. The significant increment of CO_2 sorption can be explained by swelling behavior. Since the AAPILs are in solid form, the water content plays a major role in increasing the surface area due to swelling behaviour. This will offer a great surface area for CO_2 to be hosted. Secondly, the water itself consists of H^+ and OH^- anion and they may act as standalone cation and anion enhancing the CO_2 sorption [3]. Therefore, these AAPILs can be considered as highly feasible for industrial application.

4.16 Comparison of gas solubility in poly[VBTMA][Lys]

Natural gas contains a large number of impurities and selectivities like CO_2/CH_4, CO_2/SO_x, CO_2/H_2S which might also become important. Besides CO_2, methane (CH_4) is largely contained in natural gas with 40-50 % and nitrogen (N_2) with 0-5 %. Thus, reliable knowledge on their solubility in ILs is needed for developing process models.

Separation processes involve mixtures of two or more components are important hence solubility data only is not enough for the performance of AAPILs. Nevertheless, for CO_2 capture from natural gas, the CO_2/CH_4 and CO_2/N_2 is mainly relevant. The solubility measurements were made using a single gas of CO_2, CH_4 and

N_2. Figure 4.34 shows the comparison of gas solubility on poly[VBTMA][Lys] with CO_2 , CH_4 and N_2 gases at 1 bar, 303 K.

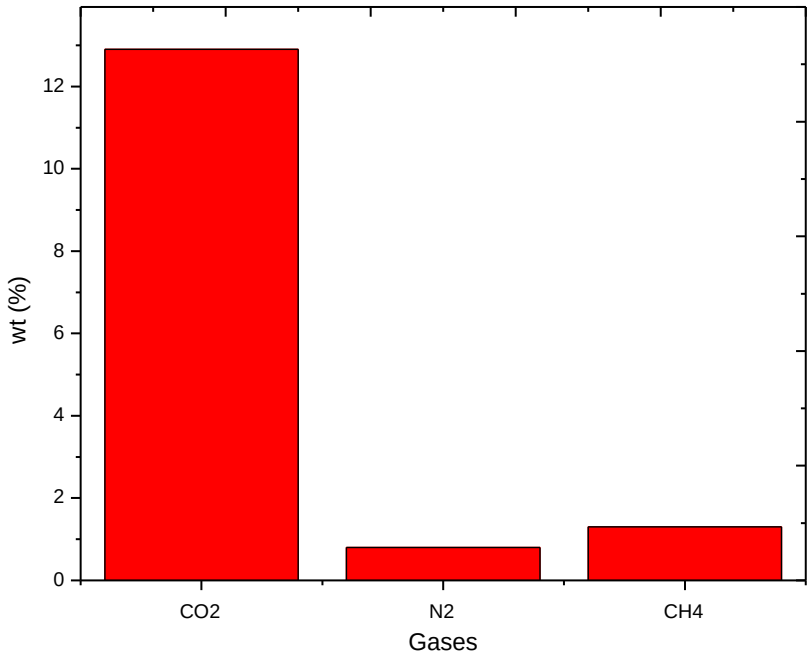

Figure 4.34: Comparison of gases on poly[VBTMA][Lys] at 1 bar, 303 K

From Figure 4.34 can be seen that the sorption of CO_2 gas is higher as compared to N_2 and CH_4 gases. CH_4 sorption has much lower solubility than CO_2 but higher than N_2. Since the sorption of gases in AAPILs is governed by the interaction between the gas molecules and polymer molecules, it is worth to look at these gases polarizabilities. Table 4.19 shows the values of polarizabilities and gas sorption for each gas.

Table 4.19: Polarizabilities (α) and gas sorption of each gas

Gas	α x 10^{24}, [cm^3]	Gas sorption (wt%)
Carbon dioxide, CO_2	2.64	12.9
CH_4	2.6	1.3
Nitrogen, N_2	1.74	0.8

The most important property that determines these interactions is the polarizabilities, α [190]. The capabilities AAPILs to capture CO_2 is higher with 12 wt% followed with CH_4 (1.3 wt%) and N_2 (0.8 wt%). This trend correlates well with

their polarizabilities as shown in Table 4.19. It is seen that these energies are nearly proportional to α thus contribute on higher sorption.

The molar selectivities toward CO_2 was calculated based on the single gas absorption measurements for CO_2 and N_2 as expressed in below Equation 4.25.

$$S_{CO_2/N_2} = \frac{(\frac{wt\ CO_2}{wt\ ILs})}{(\frac{wt\ N_2}{wt\ ILs})} = [\frac{\text{wt CO}_2}{wt\ N_2}] \quad 4.25$$

The selectivities of S_{CO_2/N_2} calculated is 9.92 and selectivities of S_{CO_2/CH_4} is 16.13. This is showed that the selectivity of CO_2 from CO_2+CH_4 is higher than N_2+CO_2.

CHAPTER 5

CONCLUSIONS AND RECOMENDATIONS

5.1 Conclusions

Eight anions have been used to synthesize the AAPILs *i.e.* [Arg], [Lys], [Hist], [Tau], [Pro], [Ser], [Ala] and [Gly] with ammonium based, [VBTMA], as cation. The studied shows that [Arg] and [Lys] which have greater numbers of amines in the structure have higher CO_2 absorption than other anions because of greater chance of amines to react with CO_2. COSMO-RS also was carried out to study the chemical potential on activity coefficient of CO_2 towards the ILs. The trends of activity coefficients are similar with experimental results and the interaction between anions and CO_2 also are explained further by σ-profile and σ-potential. By polymerizing the monomers, AAILs, the CO_2 absorption increased to almost double from the monomeric forms.

To study the effects of different cation, ammonium based [VBTMA] gave higher CO_2 sorption and [VBMI] gave the least sorption. By changing the alkyl chain length in cation, methyl, [VBTMA], gives the highest CO_2 sorption. The CO_2 sorption decreases with longer alkyl chain as it may hinder the interaction between CO_2 and the cation due to steric effects.

The FTIR results after CO_2 absorption shows the formation of carbamic acid species which confirms the chemical absorption. When pressure increase, the CO_2 sorption increased due to the physical adsorption. At low pressure, a large uptake of CO_2 can be expected to be due to the chemical absorption process and the further increase at higher pressure is in part of physical adsorption. BET isotherm model shows type II which attributed to the multilayer formation of CO_2 on AAPILs thus explained the increasing of CO_2 adsorption at higher pressure.

By increasing the temperature to 80 ^{o}C, almost fully desorption occurred. The recyclability of AAPILs been studied where the pressure and temperature swing applied. The result shows that AAPILs are very stable and can be use up until 86 % sorption in 5th cycle to get approximately 1 mol CO_2 captured per mole of monomer. This shows that these AAPILs can be reuse more than 5 times.

The adsorption isotherm follows Freundlich isotherm and thermodynamic analysis gives the ΔH^o is -30.3 kJ/mol. The kinetics studies of CO_2 sorption showed that the CO_2 sorption follows pseudo first order by using the best fitted in correlation coefficient (R^2).

DFT calculation showed that the mechanism of 1:1 is achieved when one mol of CO_2 react with one mole of argininate with $\Delta H^o is$ -30.42 kJ/mol. This is similar with change of enthalpy in experimental with -30.3 kJ/mol. Therefore, the mechanism between CO_2 and argininate can be proposed with formation of carbamic acid.

With the addition water, the hydration reaction between water in ILs and CO_2 makes the absorption capacity higher compared to dry ILs. In hydration reaction, the reaction between CO_2 and H_2O formed the carbonic acid where this carbonic acid may form a hydrogen bond with amino acids anion. The addition of water also plays a major role in increasing the surface area due to swelling behavior since AAPILs are in solid form. This will offer a great surface area for CO_2 to be hosted. The water itself consists of H^+ and OH^- anion and they may act as standalone cation and anion enhancing the CO_2 sorption.

In thermal stability, the degradation temperature (T_d) and glass transition temperature (T_g) also increase after polymerization. From these results, we can see that the polymerization of AAILs enhanced CO_2 absorption as well as thermal stability. In thermal stability shows that anion plays a key role in thermal stability. By changing the anion type, thermal stability shows a great significant followed with cation type while cation modification has the least effect.

Therefore, these AAPILs can be considered as highly feasible for industrial application for CO_2 sorption in natural gas.

5.2 Recommendations

Functionalized ILs promising the higher CO_2 sorption and more research is need to further studies and understand their capabilities. In this research, by using amino acid as anions and polymerized the amino acid ionic liquids are the key factor of novelty to capture CO_2.

However, there are some recommendations which it could be useful to improve the progress of using ILs for CO_2 capture by modifying the existing ILs to enhance their properties.

- Functionalized PILs with diamino are tethered in cation and anion can be developed. These diamino properties would give higher CO_2 sorption. Literature has showed that with diamino ILs would give higher CO_2 sorption, however there were drawbacks due to higher viscosity of ILs. To overcome this, polymerizing the diamino ILs and converty to solid form would overcome this disadvantage.

- In CO_2 sorption, both chemisorption and physisorption are involved in AAPILs. In low pressure, the chemisorption took place and in higher pressure, the physisorption become the pririority. These phenomena of increases of CO_2 sorption, needs to be investigated in more depth by taking into account the mechanism and type of anions in AAPILs.

- With the addition of water, the CO_2 sorption showed higher CO_2 sorption than dry AAPILs. This CO_2 sorption capacity should be investigated at higher pressure. The swelling behavior of AAPILs in the presence of water should be studied in depth accounting for all parameters that could influence the swelling. *i.e.* pressure, temperature, amount of water, density, volume of sample

- The absorption of AAPILs with CO_2 in low pressure involves chemisorptions where a new peak around 1600 to 1700 cm^{-1} are formed showing a carbamic peak is formed. The forming of new peak should be studied by using *in-situ* of FTIR where the reaction of AAPILs and CO_2 can be study deeply.

- Natural gas consists largely of methane, ethane, propane, nitrogen, carbon dioxide, hydrogen sulphide, etc. Therefore selectivity of gases should be taking

into account. This is to study the capabilities of AAPILs to capture CO_2 in mixture of gases instead of in a single line gas.

BIBLIOGRAPHY

[1] W. A. W. A. Bakar and R. Ali, "Natural gas," in *Natural Gas*, P. Potocnik, Ed., ed Croatia: Intech, 2014, pp. 1-38.

[2] R. Baciocchi, G. Storti, and M. Mazzotti, "Process design and energy requirements for the capture of carbon dioxide from air," *Chemical Engineering and Processing: Process Intensification*, vol. 45, pp. 1047-1058, 2006.

[3] M. O. H. A. Ali, "Design of novel polymerized ionic liquids for carbon dioxide capture from natural gas," Chemical Engineering Department, Universiti Teknologi PETRONAS, 2011.

[4] T. E. Rufford, S. Smart, G. C. Y. Watson, B. F. Graham, J. Boxall, J. C. Diniz da Costa, "The removal of CO_2 and N_2 from natural gas: A review of conventional and emerging process technologies," *Journal of Petroleum Science and Engineering*, vol. 94-95, pp. 123-154, 2012.

[5] D. A. Eimer, *Gas Treating: Absorption Theory and Practice*. United Kingdom: John Wiley & Sons, Ltd, 2014.

[6] B. P. Spigarelli and S. K. Kawatra, "Opportunities and challenges in carbon dioxide capture," *Journal of CO_2 Utilization*, vol. 1, pp. 69-87, 2013.

[7] L. C. Tomé, D. Mecerreyes, C. S. R. Freire, L. P. N. Rebelo, and I. M. Marrucho, "Pyrrolidinium-based polymeric ionic liquid materials: New perspectives for CO_2 separation membranes," *Journal of Membrane Science*, vol. 428, pp. 260-266, 2013.

[8] L. Peters, A. Hussain, M. Follmann, T. Melin, and M. B. Hägg, "CO_2 removal from natural gas by employing amine absorption and membrane technology—A technical and economical analysis," *Chemical Engineering Journal*, vol. 172, pp. 952-960, 2011.

[9] J. Wilday, M. Wardman, M. Johnson, and M. Haines, "Hazards from carbon dioxide capture, transport and storage," *Process Safety and Environmental Protection,* vol. 89, pp. 482-491, 2011.

[10] H. N. A. Halim, A. M. Shariff, and M. A. Bustam, "High pressure CO_2 absorption from natural gas using piperazine promoted 2-amino-2-methyl-1-propanol in a packed absorption column," *Separation and Purification Technology,* vol. 152, pp. 87-93, 2015.

[11] F. Karadas, M. Atilhan, and S. Aparicio, "Review on the Use of Ionic Liquids (ILs) as Alternative Fluids for CO_2Capture and Natural Gas Sweetening," *Energy & Fuels,* vol. 24, pp. 5817-5828, 2010.

[12] Y. Wu and C. W. Chan, "Analysis of data for the carbon dioxide capture domain," *Engineering Applications of Artificial Intelligence,* vol. 24, pp. 154-163, 2011.

[13] B. Li, Y. Duan, D. Luebke, and B. Morreale, "Advances in CO_2 capture technology: A patent review," *Applied Energy,* vol. 102, pp. 1439-1447, 2013.

[14] A. Dibenedetto, M. Aresta, and M. Narracci, "Carbon dioxide capture by amines: Increasing the efficiency by amine structure modification," *Fuel Chemistry Division Preprints,* vol. 47, pp. 53-54, 2002.

[15] Y. E. Kim, J. A. Lim, S. K. Jeong, Y. I. Yoon, S. T. Bae, and S. C. Nam, "Comparison of Carbon Dioxide Absorption in Aqueous MEA, DEA, TEA, and AMP Solutions," *Bulletin of the Korean Chemical Society,* vol. 34, pp. 783-787, 2013.

[16] R. C. Atkins, F. A. Carey, and C. W. Ong, *Organic Chemistry: A Brief Course*, 3rd ed. New York: Mc Graw-Hill, 2013.

[17] F. Zhang, C.-G. Fang, Y.-T. Wu, Y.-T. Wang, A.-M. Li, and Z.-B. Zhang, "Absorption of CO_2 in the aqueous solutions of functionalized ionic liquids and MDEA," *Chemical Engineering Journal,* vol. 160, pp. 691-697, 2010.

[18] B. Li, Y. Duan, D. Luebke, and B. Morreale, "Advances in CO_2 capture technology A patent review," *Applied Energy*, vol. 102, pp. 1439-1447, 2013.

[19] D. M. D'Alessandro, B. Smit, and J. R. Long, "Carbon dioxide capture: prospects for new materials," *Angew Chem Int Ed Engl*, vol. 49, pp. 6058-82, Aug 16 2010.

[20] C.-H. Yu, C.-H. Huang, and C.-S. Tan, "A Review of CO_2 Capture by Absorption and Adsorption," *Aerosol and Air Quality Research*, vol. 12, pp. 745-769, 2012.

[21] J. Huang and T. Ruther, "Why are ionic liquids attractive for CO_2 absorption? An overview," *Australia Journal of Chemistry*, vol. 62, pp. 298-308, 2009.

[22] E. Torralba-Calleja, J. Skinner, and D. Gutierrez-Tauste, "CO_2 Capture in Ionic Liquids A Review of Solubilities and Experimental Methods," *Journal of Chemistry*, vol. 2013, p. 16, 2013.

[23] J. Huang and T. Ruther, "Why are Ionic Liquids Attractive for CO_2 absorption?," *Australia Journal of Chemistry*, vol. 62, p. 298, 2009.

[24] C. A. Scholes, G. W. Stevens, and S. E. Kentish, "Membrane gas separation applications in natural gas processing," *Fuel*, vol. 96, pp. 15-28, 2012.

[25] H. B. Al-saffar, B. Ozturk, and R. Hughes, "A Comparison of Porous and Non-Porous Gas-Liquid Membrane Contactors for Gas Separation," *Chemical Engineering Research and Design*, vol. 75, pp. 685-692, 1997/10/01 1997.

[26] S. Kasahara, E. Kamio, T. Ishigami, and H. Matsuyama, "Effect of water in ionic liquids on CO_2 permeability in amino acid ionic liquid-based facilitated transport membranes," *Journal of Membrane Science*, vol. 415-416, pp. 168-175, 2012.

[27] M. G. Plaza, S. García, F. Rubiera, J. J. Pis, and C. Pevida, "Post-combustion CO_2 capture with a commercial activated carbon: Comparison of different

regeneration strategies," *Chemical Engineering Journal,* vol. 163, pp. 41-47, 9/15/ 2010.

[28] P. J. E. Harlick and A. Sayari, "Applications of pore-expanded mesoporous silicas. 3. Triamine silane grafting for enhanced CO_2 adsorption," *Industrial & Engineering Chemistry Research,* vol. 45, pp. 3248-3255, 2006.

[29] Q. Wang, J. Luo, Z. Zhong, and A. Borgna, "CO_2 capture by solid adsorbents and their applications: current status and new trends," *Energy & Environmental Science,* vol. 4, pp. 42-55, 2011.

[30] A. Sayari, Y. Belmabkhout, and R. Serna-Guerrero, "Flue gas treatment via CO_2 adsorption," *Chemical Engineering Journal,* vol. 171, pp. 760-774, 7/15/ 2011.

[31] B. Feng, H. An, and E. Tan, "Screening of CO_2 Adsorbing Materials for Zero Emission Power Generation Systems†," *Energy & Fuels,* vol. 21, pp. 426-434, 2007/03/01 2007.

[32] T. Yamaguchi, T. Niitsuma, B. N. Nair, and K. Nakagawa, "Lithium silicate based membranes for high temperature CO_2 separation," *Journal of Membrane Science,* vol. 294, pp. 16-21, 5/15/ 2007.

[33] A. R. Millward and O. M. Yaghi, "Metal−Organic Frameworks with Exceptionally High Capacity for Storage of Carbon Dioxide at Room Temperature," *Journal of the American Chemical Society,* vol. 127, pp. 17998-17999, 2005/12/01 2005.

[34] Z. Zhang, W. Liu, H. Xie, and Z. K. Zhao, "An unexpected reaction between 5-hydroxymethylfurfural and imidazolium-based ionic liquids at high temperatures," *Molecules,* vol. 16, pp. 8463-74, 2011.

[35] J. A. Lazzús, "A group contribution method to predict the glass transition temperature of ionic liquids," *Thermochimica Acta,* vol. 528, pp. 38-44, 2012.

[36] J. Lu, F. Yan, and J. Texter, "Advanced applications of ionic liquids in polymer science," *Progress in Polymer Science,* vol. 34, pp. 431-448, 2009.

[37] A. Berthod and S. C. Broch, "Uses of Ionic Liquids in Analytical Chemistry.pdf."

[38] A. B. K. Z. Taha, "Thermophysical Properties and Carbon Dioxide Solubility of Novel Room Temperature Ionic Liquids," p. 280, 2011.

[39] J. Yuan, H. Schlaad, C. Giordano, and M. Antonietti, "Double hydrophilic diblock copolymers containing a poly(ionic liquid) segment: Controlled synthesis, solution property, and application as carbon precursor," *European Polymer Journal*, vol. 47, pp. 772-781, 2011.

[40] O. Green, S. Grubjesic, S. Lee, and M. A. Firestone, "The Design of Polymeric Ionic Liquids for the Preparation of Functional Materials," *Polymer Reviews*, vol. 49, pp. 339-360, 2009.

[41] L. Vidal, M. L. Riekkola, and A. Canals, "Ionic liquid-modified materials for solid-phase extraction and separation: a review," *Anal Chim Acta*, vol. 715, pp. 19-41, Feb 17 2012.

[42] D. Han and K. H. Row, "Recent applications of ionic liquids in separation technology," *Molecules*, vol. 15, pp. 2405-26, Apr 2010.

[43] J. W. Ma, Z. Zhou, F. Zhang, C. G. Fang, Y. T. Wu, Z. B. Zhang, "Ditetraalkylammonium amino acid ionic liquids as CO_2 absorbents of high capacity," *Environ Sci Technol*, vol. 45, pp. 10627-33, Dec 15 2011.

[44] M. Galinski, A. Lewandowski, and I. Stepniak, "Ionic liquids as electrolytes," *Electrochimica Acta*, vol. 51, pp. 5567-5580, Aug 2006.

[45] B. Scrosati and J. Garche, "Lithium batteries: Status, prospects and future," *Journal of Power Sources*, vol. 195, pp. 2419-2430, May 2010.

[46] M. J. Earle and K. R. Seddon, "Ionic liquids. Green solvents for the future," *Pure and Applied Chemistry*, vol. 72, pp. 1391-1398, Jul 2000.

[47] R. P. Swatloski, S. K. Spear, J. D. Holbrey, and R. D. Rogers, "Dissolution of cellose with ionic liquids," *Journal of the American Chemical Society*, vol. 124, pp. 4974-4975, May 2002.

[48] J. E. Bara, T. K. Carlisle, C. J. Gabriel, D. Camper, A. Finotello, D. L. Gin, "Guide to CO_2 Separations in Imidazolium-Based Room-Temperature Ionic Liquids," *Industrial & Engineering Chemistry Research,* vol. 48, pp. 2739-2751, Mar 2009.

[49] E. D. Bates, R. D. Mayton, I. Ntai, and J. H. Davis, "CO_2 capture by a task-specific ionic liquid," *Journal of the American Chemical Society,* vol. 124, pp. 926-927, Feb 2002.

[50] O. A. El Seoud, A. Koschella, L. C. Fidale, S. Dorn, and T. Heinze, "Applications of ionic liquids in carbohydrate chemistry: A window of opportunities," *Biomacromolecules,* vol. 8, pp. 2629-2647, Sep 2007.

[51] G. Viswanathan, S. Murugesan, V. Pushparaj, O. Nalamasu, P. M. Ajayan, and R. J. Linhardt, "Preparation of biopolymer fibers by electrospinning from room temperature ionic liquids," *Biomacromolecules,* vol. 7, pp. 415-418, Feb 2006.

[52] N. M. Yunus, M. I. A. Mutalib, Z. Man, M. A. Bustam, and T. Murugesan, "Solubility of CO_2 in pyridinium based ionic liquids " *Chemical Engineering Journal,* vol. 189-190, pp. 94-100, 2012.

[53] K. A. Kurnia, F. Harris, C. D. Wilfred, M. I. A. Mutalib, and T. Murugesan, "Thermodynamic properties of CO_2 absorption in hydroxyl ammonium ionic liquids at pressure of (100-1600)kPa," *The Journal of Chemical Thermodynamics,* vol. 41, pp. 1069-1073, 2009.

[54] A. K. Ziyada, "Thermophysical properties and carbon dioxide solubility of novel room temperature ionic liquids," Chemical Engineering, Universiti Teknologi PETRONAS, Malaysia, 2011.

[55] J. G. Huddleston, H. D. Willauer, R. P. Swatloski, A. E. Visser, and R. D. Rogers*, "Room temperature ionic liquids as novel media for 'clean' liquid–liquid extraction," *Chemistry Communication,* pp. 1765-1766, 1998.

[56] W. Wang, S. Wang, H. Liu, and Z. Wang, "Desulfurization of gasoline by a new method of electrochemical catalytic oxidation," *Fuel*, vol. 86, pp. 2747-2753, 12// 2007.

[57] Y. C. Pei, J. J. Wang, X. P. Xuan, J. Fan, and M. Fan, "Factors Affecting Ionic Liquids Based Removal of Anionic Dyes from Water," *Environmental Science & Technology*, vol. 41, pp. 5090-5095, 2007/07/01 2007.

[58] P. Wasserscheid, T. Welton, and E. Corporation, *Ionic Liquids in Synthesis* vol. 2: Wiley Online Library, 2003.

[59] M. J. Muldoon, S. N. V. K. Aki, J. L. Anderson, J. K. Dixon, and J. F. Brennecke, "Improving Carbon Dioxide Solubility in Ionic Liquids," *Jounal of Physical Chemistry B*, vol. 111, pp. 9001-9009, 2007.

[60] B. F. Goodrich, J. C. de la Fuente, B. E. Gurkan, Z. K. Lopez, E. A. Price, Y. Huang, "Effect of water and temperature on absorption of CO_2 by amine-functionalized anion-tethered ionic liquids," *J Phys Chem B*, vol. 115, pp. 9140-50, Jul 28 2011.

[61] B. Lv, Y. Shi, C. Sun, N. Liu, W. Li, and S. Li, "CO_2 capture by a highly-efficient aqueous blend of monoethanolamine and a hydrophilic amino acid ionic liquid [C_2OHmim][Gly]," *Chemical Engineering Journal*, vol. 270, pp. 372-377, 2015.

[62] L. A. Blanchard and J. F. Brennecke, "Recovery of Organic Products from Ionic Liquids Using Supercritical Carbon Dioxide," *Ind. Eng. Chem. Res*, vol. 40, pp. 287-292, 2001.

[63] L. A. Blanchard, D. Hancu, E. J. Beckman, and J. F. Brennecke, "Green processing using ionic liquids and CO_2," *Nature*, vol. 399, pp. 28-29, 05/06/print 1999.

[64] J. L. Anthony, J. L. Anderson, E. J. Maginn, and J. F. Brennecke, "Anion Effects on Gas Solubility in Ionic Liquids," *Jounal of Physical Chemistry B*, vol. 109, pp. 6366-6374, 2005.

[65] C. Wang, X. Luo, X. Zhu, G. Cui, D.-e. Jiang, D. Deng, *et al.*, "The strategies for improving carbon dioxide chemisorption by functionalized ionic liquids," *RSC Advances*, vol. 3, p. 15518, 2013.

[66] A. Yokozeki, M. B. Shiflett, C. P. Junk, L. M. Grieco, and T. Foo, "Physical and Chemical Absorptions of Carbon Dioxide in Room-Temperature Ionic Liquids," *Jounal of Physical Chemistry B*, vol. 112, pp. 16654-16663, 2008.

[67] E. D. Bates, R. D. Mayton, l. Ntai, and J. H. D. Jr, "CO_2 Capture by a Task-Specific Ionic Liquid," *Journal of American Chemical Society*, vol. 124, p. 2, 2002.

[68] B. E. Gurkan, J. C. d. l. Fuente, E. M. Mindrup, L. E. Ficke, B. F. Goodrich, E. A. Price, *et al.*, "Equimolar CO_2 Absorption by Anion-Functionalized Ionic Liquids.," *Journal of American Chemical Society*, vol. 2010, 2010.

[69] Y. Gao, F. Zhang, K. Huang, J.-W. Ma, Y.-T. Wu, and Z.-B. Zhang, "Absorption of CO_2 in amino acid ionic liquid (AAIL) activated MDEA solutions," *International Journal of Greenhouse Gas Control*, vol. 19, pp. 379-386, 2013.

[70] Y. S. Sistla and A. Khanna, "CO_2 Absorption Studies in Amino Acid-Anion Based Ionic Liquids," *Chemical Engineering Journal*, 2014.

[71] Y. Zhang, S. Zhang, X. Lu, Q. Zhou, W. Fan, and X. Zhang, "Dual amino-functionalised phosphonium ionic liquids for CO_2 capture," *Chemistry A European Journal*, vol. 15, pp. 3003-11, 2009.

[72] K. Fukumoto, H. Ohno, and M. Yoshizawa, "Room Temperature Ionic Liquids from 20 Natural Amino Acids," *J. Am. Chem. Soc*, vol. 2005, p. 2, 2005.

[73] H. Ohno and K. Fukumoto, "Amino Acid Ionic Liquids," *Accounts of Chemical Research*, vol. 40, pp. 1122-1129, 2007.

[74] R. S. Bhavsar, S. C. Kumbharkar, and U. K. Kharul, "Polymeric ionic liquids (PILs): Effect of anion variation on their CO_2 sorption," *Journal of Membrane Science,* vol. 389, pp. 305-315, 2012.

[75] A. Blasig, J. Tang, X. Hu, Y. Shen, and M. Radosz, "Magnetic suspension balance study of carbon dioxide solubility in ammonium-based polymerized ionic liquids: Poly(p-vinylbenzyltrimethyl ammonium tetrafluoroborate) and poly([2-(methacryloyloxy)ethyl] trimethyl ammonium tetrafluoroborate)," *Fluid Phase Equilibria,* vol. 256, pp. 75-80, 2007.

[76] Y.-B. Xiong, H. Wang, Y.-J. Wang, and R.-M. Wang, "Novel imidazolium-based poly(ionic liquid)s: preparation, characterization, and absorption of CO_2," *Polymers for Advanced Technologies,* vol. 23, pp. 835-840, 2012.

[77] J. Yuan and M. Antonietti, "Poly(ionic liquid)s: Polymers expanding classical property profiles," *Polymer,* vol. 52, pp. 1469-1482, 2011.

[78] G. Yu, Z. Man, Q. Li, N. Li, X. Wu, C. Asumana, "New crosslinked-porous poly-ammonium microparticles as CO_2 adsorbents," *Reactive and Functional Polymers,* vol. 73, pp. 1058-1064, 2013.

[79] E. I. Privalova, E. Karjalainen, M. Nurmi, P. Maki-Arvela, K. Eranen, H. Tenhu, "Imidazolium-based poly(ionic liquid)s as new alternatives for CO_2 capture," *ChemSusChem,* vol. 6, pp. 1500-9, Aug 2013.

[80] J. Tang, W. Sun, H. Tang, M. Radosz, and Y. Shen, "Enhanced CO_2 Absorption of Poly(ionic liquid)s," *Macromolecules,* vol. 38, pp. 2037-2039, 2005.

[81] J. Tang, H. Tang, W. Sun, M. Radosz, and Y. Shen, "Low pressure CO_2 sorption in ammonium-based poly(ionic liquid)s," *Polymer,* vol. 46, pp. 12460-12467, 2005.

[82] J. Tang, Y. Shen, M. Radosz, and W. Sun, "Isothermal Carbon Dioxide Sorption in Poly(ionic liquid)s," *Ind. Eng. Chem. Res,* vol. 48, pp. 9113-9118, 2009.

[83] J. Yuan, D. Mecerreyes, and M. Antonietti, "Poly(ionic liquid)s: An update," *Progress in Polymer Science,* vol. 38, pp. 1009-1036, 2013.

[84] M. Erbeldinger, M. A. J., and R.A.J, "Enzymatic catalysis of formation of Z-aspertame in ionic liquid -An alternative to enzymatic catalysis in organic solvents," *Biotechnol. Prog.,* vol. 16, pp. 1129-1131, 2000.

[85] P. Wasserscheid and W.T., *Ionic Liquids in Synthesis*. weinheim Germany: Wiley-VCH, 2003.

[86] W. J.S., "A short history of ionic liquids from molten salts to neoteric solvents," *Green Chemistry,* vol. 4, pp. 73-80, 2004.

[87] I. a. V. Chemical. *Technical summaries on ionic liquids in chemical processing,* .

[88] R. Vijayraghavan, S. J. Pas, E. I. Izgorodina, and D. R. MacFarlane, "Diamino protic ionic liquids for CO_2 capture," *Phys Chem Chem Phys,* vol. 15, p. 19994, 2013.

[89] J. G. Huddleston, A. E. Visser, W. M. Reichert, H. D. Willauer, G. A. Broker, and R. D. Rogers, "Characterization and comparison of hydrophilic and hydrophobic room temperature ionic liquids incorporating the imidazolium cation," *Green Chemistry,* vol. 3, pp. 156-164, 2001.

[90] J. Kagimoto, S. Taguchi, K. Fukumoto, and H. Ohno, "Hydrophobic and low-density amino acid ionic liquids," *Journal of Molecular Liquids,* vol. 153, pp. 133-138, 2010.

[91] J. L. McDonald, R. E. Sykora, P. Hixon, A. Mirjafari, and J. H. Davis, "Impact of water on CO_2 capture by amino acid ionic liquids," *Environmental Chemistry Letters,* vol. 12, pp. 201-208, 2014.

[92] Y. S. Sistla and A. Khanna, "Carbon dioxide absorption studies using amine-functionalized ionic," *Journal of Industrial and Engineering Chemistry,* vol. 20, p. 2497, 2014.

[93] Abobakr K. Ziyada, Cecilia D. Wilfred, and T. Murugesan, "Densities, viscosities and refractive indices of 1-alkyl-3-propanenitrile imidazolium chloride ionic liquids," *Physics and Chemistry of Liquids,* vol. 50, p. 8, 2012.

[94] A. Muhammad, M. I. A. Mutalib, T. Murugesan, Z. Man, and A. Bustam, "Density and viscosity estimation of 1-hexyl-3-methyl imidazolium based ionic liquids with [BF_4] and [PF_6] anions at high pressures," *Journal of Applied Sciences,* vol. 11, pp. 2452-2455, 2011.

[95] Y. Zhang, T. Li, Z. Wu, P. Yu, and Y. Luo, "Synthesis and thermophysical properties of imidazolate-based ionic liquids: Influences of cations and anions," *The Journal of Chemical Thermodynamics,* 2013.

[96] B. F. Goodrich, J. C. d. l. Fuente, B. E. Gurkan, D. J. Zadigian, E. A. Price, Y. Huang, "Experimental Measurements of Amine-Functionalized Anion-Tethered Ionic Liquids with Carbon Dioxide," *Ind. Eng. Chem. Res,* vol. 2011, p. 111, 2011.

[97] Y. Zhang, P. Yu, and Y. Luo, "Absorption of CO_2 by amino acid-functionalized and traditional dicationic," *Chemical Engineering Journal,* vol. 214, pp. 355-363, 2013.

[98] N. Muhammad, Z. B. Man, M. A. Bustam, M. I. A. Mutalib, C. D. Wilfred, and S. Rafiq, "Synthesis and Thermophysical Properties of Low Viscosity Amino Acid-Based Ionic Liquids," *Journal of Chemical & Engineering Data,* vol. 56, pp. 3157-3162, 2011.

[99] H. Chen, J.-H. Choi, D. Salas-de la Cruz, K. I. Winey, and Y. A. Elabd, "Polymerized Ionic Liquids: The Effect of Random Copolymer Composition on Ion Conduction," *Macromolecules,* vol. 42, pp. 4809-4816, 2009.

[100] L. Chanceliera, O. Boyrona, T. Gutelb, and C. C. Santinia, "Thermal stability of imidazolium-based ionic liquids," *French-Ukrainian Journal of Chemistry,* vol. 4, pp. 51-64, 2016.

[101] C. Nwaoha, T. Supap, R. Idem, C. Saiwan, P. Tontiwachwuthikul, M. J. Al-Marri,"Advancement and new perspectives of using formulated reactive

amine blends for post-combustion carbon dioxide (CO_2) capture technologies," *Petroleum,* vol. 3, pp. 10-36, 2017.

[102] C. Nwaoha, C. Saiwan, T. Supap, R. Idem, P. Tontiwachwuthikul, W. Rongwong, *et al.*, "Carbon dioxide (CO_2) capture performance of aqueous tri-solvent blends containing 2-amino-2-methyl-1-propanol (AMP) and methyldiethanolamine (MDEA) promoted by diethylenetriamine (DETA)," *International Journal of Greenhouse Gas Control,* vol. 53, pp. 292-304, 2016.

[103] C.-H. Yu, C.-H. Huang, and C.-S. Tan, "A Review of CO_2 Capture by Absorption and Adsorption."

[104] J. Yang, H. Y. Tan, Q. X. Low, B. P. Binks, and J. M. Chin, "CO_2 capture by dry alkanolamines and an efficient microwave regeneration process," *Journal of Materials Chemistry A,* vol. 3, pp. 6440-6446, 2015.

[105] S. Saravanamurugan, A. J. Kunov-Kruse, R. Fehrmann, and A. Riisager, "Amine-functionalized amino acid-based ionic liquids as efficient and high-capacity absorbents for CO_2," *ChemSusChem,* vol. 7, pp. 897-902, Mar 2014.

[106] P. Sharma, S. D. Park, K. T. Park, S. C. Nam, S. K. Jeong, and Y. I. Yoon, "Solubility of carbon dioxide in amine-functionalized ionic liquids Role of the anions " *Chemical Engineering Journal,* vol. 193-194, pp. 267-275, 2012.

[107] Z. Zhao, H. Dong, and X. Zhang, "The research progress of CO_2 capture with ionic liquids.," *Chinese Journal of Chemical Engineering,* vol. 20, 2012.

[108] P. Sharma, S. D. Park, I. H. Baek, K. T. Park, Y. I. Yoon, and S. K. Jeong, "Effects of anions on absorption capacity of carbon dioxide in acid functionalized ionic liquids," *Fuel Processing Technology,* vol. 100, pp. 55-62, 2012.

[109] M. Wang, L.-q. Zhang, H. Liu, J.-y. Zhang, and C.-g. Zheng, "Studies on CO_2 absorption performance by imidazole-based ionic liquid mixtures," *Journal of Fuel Chemistry and Technology,* vol. 40, pp. 1264-1268, 2012.

[110] W. Mei, Z. Li-qi, L. Hao, Z. Jun-ying, and Z. Chu-guang, "Studies on CO_2 absorption performance by imidazole-based ionic liquid mixtures," *Journal of Fuel Chemistry and Technology*, vol. 40, pp. 1264-1268, 2012.

[111] J. Blath, N. Deubler, T. Hirth, and T. Schiestel, "Chemisorption of carbon dioxide in imidazolium based ionic liquids with carboxylic anions," *Chemical Engineering Journal*, vol. 181-182, pp. 152-158, 2012.

[112] N. M. Yunus, M. I. A. Mutalib, Z. Man, M. A. Bustam, and T. Murugesan, "Solubility of CO_2 in pyridinium based ionic liquids," *Chemical Engineering Journal*, vol. 189-190, pp. 94-100, 2012.

[113] P. Husson, L. Pison, J. Jacquemin, and M. F. C. Gomes, "Influence of water on the carbon dioxide absorption by 1-ethyl-3-methylimidazolium bis(trifluoromethylsulfonyl)amide," *Fluid Phase Equilibria*, vol. 294, pp. 98-104, 2010.

[114] Y. Zhang, P. Yu, and Y. Luo, "Absorption of CO_2 by amino acid-functionalized and traditional dicationic ionic liquids: Properties, Henry's law constants and mechanisms," *Chemical Engineering Journal*, vol. 214, pp. 355-363, 2013.

[115] Z. Zhou, G. Jing, and L. Zhou, "Characterization and absorption of carbon dioxide into aqueous solution of amino acid ionic liquid $[N_{1111}]$[Gly] and 2-amino-2-methyl-1-propanol," *Chemical Engineering Journal*, vol. 204-206, pp. 235-243, 2012.

[116] K. A. Mumford, S. J. Pas, T. Linseisen, T. M. Statham, N. Johann Nicholas, A. Lee, *et al.*, "Evaluation of the protic ionic liquid, N,N-dimethyl-aminoethylammonium formate for CO_2 capture," *International Journal of Greenhouse Gas Control*, vol. 32, pp. 129-134, 2015.

[117] P. Sharma, S.-H. Choi, S.-D. Park, I.-H. Baek, and G.-S. Lee, "Selective chemical separation of carbondioxide by ether functionalized imidazolium cation based ionic liquids," *Chemical Engineering Journal*, vol. 181–182, pp. 834-841, 2/1/ 2012.

[118] H. Hu, F. Li, Q. Xia, X. Li, L. Liao, and M. Fan, "Research on influencing factors and mechanism of CO_2 absorption by poly-amino-based ionic liquids," *International Journal of Greenhouse Gas Control*, vol. 31, pp. 33-40, 2014.

[119] Z. Xue, Z. Zhang, J. Han, Y. Chen, and T. Mu, "Carbon dioxide capture by a dual amino ionic liquid with amino-functionalized imidazolium cation and taurine anion," *International Journal of Greenhouse Gas Control*, vol. 5, p. 628, 2011.

[120] Y. Chen, X.-q. Zhou, Y. Cao, Z. Xue, and T. Mu, "Quantitative investigation on the physical and chemical interactions between CO_2 and amine-functionalized ionic liquid [aEMMIM][BF_4] by NMR," *Chemical Physics Letters*, vol. 574, pp. 124-128, 2013.

[121] Z. Feng, M. Jing-Wen, Z. Zheng, W. You-Ting, and Z. Zhi-Bing, "Study on the absorption of carbon dioxide in high concentrated MDEA and ILs solutions," *Chemical Engineering Journal*, vol. 181-182, pp. 222-228, 2012.

[122] D. M. Muñoz, A. F. Portugal, A. E. Lozano, J. G. de la Campa, and J. de Abajo, "New liquid absorbents for the removal of CO_2 from gas mixtures," *Energy & Environmental Science*, vol. 2, p. 883, 2009.

[123] X. Wang, N. G. Akhmedov, Y. Duan, D. Luebke, D. Hopkinson, and B. Li, "Amino acid-functionalized ionic liquid solid sorbents for post-combustion carbon capture," *ACS Appl Mater Interfaces*, vol. 5, pp. 8670-7, Sep 11 2013.

[124] B. E. Gurkan, J. C. d. l. Fuente, E. M. Mindrup, L. E. Ficke, B. F. Goodrich, E. A. Price, "Equimolar CO_2 absorption by anion-functionalized ionic liquids," *Journal of American Chemical Society*, vol. 132, pp. 2116-2117, 2010.

[125] M. Hasib-ur-Rahman, M. Siaj, and F. Larachi, "Ionic liquids for CO_2 capture—Development and progress," *Chemical Engineering and Processing: Process Intensification*, vol. 49, pp. 313-322, 2010.

[126] A. Wilke, J. Yuan, M. Antonietti, and J. Weber, "Enhanced Carbon Dioxide Adsorption by a Mesoporous Poly(ionic liquid)," *ACS Macro Letters,* vol. 1, pp. 1028-1031, 2012.

[127] K. Y. Foo and B. H. Hameed, "Insights into the modeling of adsorption isotherm systems," *Chemical Engineering Journal,* vol. 156, pp. 2-10, 2010.

[128] M. N. Safiah, B. M. Azmi, and M. Y. Normawati, "CO_2 Capture Using Silica and Molecular Sieve Impregnated with [hmim][Tf_2N]," *International Journal of Chemical Engineering and Applications,* vol. 5, pp. 342-346, 2014.

[129] A. Mittal, L. Kurup, and J. Mittal, "Freundlich and Langmuir adsorption isotherms and kinetics for the removal of Tartrazine from aqueous solutions using hen feathers," *J Hazard Mater,* vol. 146, pp. 243-8, Jul 19 2007.

[130] B. Subramanyam and A. Das, "Linearized and non-linearized isotherm models comparative study on adsorption of aqueous phenol solution in soil," *International Journal of Environment Science and technologies,* vol. 6, pp. 633-640, 2009.

[131] X. Chen, "Modeling of Experimental Adsorption Isotherm Data," *Information,* vol. 6, pp. 14-22, 2015.

[132] A. O. Dada, A. Olalekan, A. Olatunya, and O. DADA, "Langmuir, Freundlich, Temkin and Dubinin–Radushkevich Isotherms Studies of Equilibrium Sorption of Zn^{2+} Unto Phosphoric Acid Modified Rice Husk," *Journal of Applied Chemistry,* vol. 3, pp. 38-45, 2012.

[133] M. Erhayem, F. Al-Tohami, R. Mohamed, and K. Ahmida, "Isotherm, Kinetic and Thermodynamic Studies for the Sorption of Mercury (II) onto Activated Carbon from Rosmarinus officinalis Leaves," *American Journal of Analytical Chemistry,* vol. 06, pp. 1-10, 2015.

[134] A. Klamt, "COSMO-RS for aqueous solvation and interfaces," *Fluid Phase Equilibria,* vol. 407, pp. 152-158, 2016.

[135] E. Ali, M. K. Hadj-Kali, and I. Alnashef, "Modeling of $_2$Solubility in Selected Imidazolium-Based Ionic Liquids," *Chemical Engineering Communications*, vol. 204, pp. 205-215, 2016.

[136] V. Losetty, P. Matheswaran, and C. D. Wilfred, "Synthesis, thermophysical properties and COSMO-RS study of DBU based protic ionic liquids," *The Journal of Chemical Thermodynamics*, vol. 105, pp. 151-158, 2017.

[137] M. Diedenhofen and A. Klamt, "COSMO-RS as a tool for property prediction of IL mixtures—A review," *Fluid Phase Equilibria*, vol. 294, pp. 31-38, 2010.

[138] K. A. Kurnia, S. P. Pinho, and J. A. P. Coutinho, "Evaluation of the Conductor-like Screening Model for Real Solvents for the Prediction of the Water Activity Coefficient at Infinite Dilution in Ionic Liquids," *Industrial & Engineering Chemistry Research*, vol. 53, pp. 12466-12475, 2014.

[139] J. Ochterski. (2000). *Thermochemistry in Gaussian*. Available: http://www.gaussian.com/g_whitepap/thermo.htm

[140] A. D. Becke, "Density-functional thermochemistry. IV. A new dynamical correlation functional and implications for exact-exchange mixing," *Journal of Chemistry Physic*, vol. 104, pp. 1040-1046, 1995.

[141] Y. Zhao, B. J. Lynch, and D. G. Truhlar, "Multi-coefficient extrapolated density functional theory for thermochemistry and thermochemical kinetics," *Physical Chemistry Chemical Physics*, vol. 7, p. 43, 2005.

[142] D. S. Sholl and J. A. Steckel, *Density Functional Theory: A Practical Introduction*. USA: John Wiley & Sons, 2009.

[143] M. L. Laury and A. K. Wilson, "Performance of Density Functional Theory for Second Row (4d) Transition Metal Thermochemistry," *J Chem Theory Comput*, vol. 9, pp. 3939-46, Sep 10 2013.

[144] C. J. Cramer, *Essentials of Computational Chemistry*, Secoond Edition ed. England: John Wiley & Sons, Ltd, 2004.

[145] S. E. Wheeler, A. Moran, S. N. Pieniazek, and K. N. Houk, "Accurate reaction enthalpies and sources of error in DFT thermochemistry for Aldol, Mannich, and a- Aminoxylation reaction " *Journal of physical Chemistry A,* vol. 113, pp. 10376-10384, 2009.

[146] R. O. Ebewele, *Polymer Science and Technology*, 1 edition ed. United States of America: CRC Press, 2000.

[147] Y. Cao and T. Mu, "Comprehensive Investigation on the Thermal Stability of 66 Ionic Liquids by Thermogravimetric Analysis," *Industrial & Engineering Chemistry Research,* vol. 53, pp. 8651-8664, 2014.

[148] N. Muhammad, Z. Man, Y. A. Elsheikh, M. A. Bustam, and M. I. A. Mutalib, "Synthesis and Thermophysical Properties of Imidazolium-Based Bronsted Acidic Ionic Liquids," *Journal of Chemical & Engineering Data,* vol. 59, pp. 579-584, 2014.

[149] W. H. Awad, J. W. Gilman, M. Nyden, R. H. Harris, T. E. Sutto, J. Callahan, "Thermal degradation studies of alkyl-imidazolium salts and their application in nanocomposites," *Thermochimica Acta,* vol. 409, pp. 3-11, 2004.

[150] W. H. Awad, J. W. Gilman, M. Nyden, R. H. Harris, T. E. Sutto, J. Callahan, "Thermal degradation studies of alkyl-imidazolium salts and their application in nanocomposites," *Thermochimica Acta,* vol. 409, pp. 3-11, 2004.

[151] H. L. Ngo, K. LeCompte, L. Hargens, and A. B. McEwen, "Thermal properties of imidazolium ionic liquids," *Thermochimica Acta,* vol. 357-358, pp. 97-102, 2000.

[152] J. Leys, M. Wubbenhorst, C. Preethy Menon, R. Rajesh, J. Thoen, C. Glorieux, *et al.*, "Temperature dependence of the electrical conductivity of imidazolium ionic liquids," *J Chem Phys,* vol. 128, p. 064509, Feb 14 2008.

[153] J. M. Pringle, J. Golding, K. Baranyai, C. M. Forsyth, G. B. Deacon, J. L. Scott, *et al.*, "The effects of anion fluorination in ionic liquids-physical properties of a range of bis(methanesulfonyl)amide salts," *New J. Chem,* vol. 27, pp. 1504-1510, 2003.

[154] A. Klamt, "Prediction of the mutual solubilities of hydrocarbons and water with COSMO-RS," *Fluid Phase Equilibria*, vol. 206, pp. 223-235, 2003.

[155] D. M. Eike, J. F. Brennecke, and E. J. Maginn, "Predicting Infinite-Dilution Activity Coefficients of Organic Solutes in Ionic Liquids," *Ind. Eng. Chem. Res*, vol. 2004, pp. 1039-1048, 2004.

[156] P. Matheswaran, C. D. Wilfred, K. A. Kurnia, and A. Ramli, "Overview of Activity Coefficient of Thiophene at Infinite Dilution in Ionic Liquids and their Modeling Using COSMO-RS," *Industrial & Engineering Chemistry Research*, vol. 55, pp. 788-797, 2016.

[157] M. Gonzalez-Miquel, M. Talreja, A. L. Ethier, K. Flack, J. R. Switzer, E. J. Biddinger, *et al.*, "COSMO-RS Studies: Structure–Property Relationships for CO_2Capture by Reversible Ionic Liquids," *Industrial & Engineering Chemistry Research*, vol. 51, pp. 16066-16073, 2012.

[158] A. K. Ziyada, "Thermophysical properties and carbon dioxide solubility of novel room temperature ionic liquids," Doctor of Phylosophy, Chemical Engineering Department, Universiti Teknologi PETRONAS, Malaysia, 2011.

[159] C. Cadena, J. L. Anthony, J. K. Shah, T. I. Morrow, J. F. Brennecke, and E. J. Maginn, "Why Is CO_2 So Soluble in Imidazolium Based Ionic Liquids?," *Journal of American Chemical Society*, vol. 126, pp. 5300-5308, 2003.

[160] F. Jutz, J.-M. Andanson, and A. Baiker, "Ionic Liquids and Dense Carbon Dioxide: A Beneficial Biphasic System for Catalysis," *Chemical Reviews*, vol. 111, pp. 322-353, 2011.

[161] R. J. Aguerre, C. Suarez, and P. E. Viollaz, "New BET type multilayer sorption isotherms. Part I. Theoretical deviation of the model " *Lebensm.-Wiss. u.-Technol.*, vol. 22, pp. 188-191, 1989.

[162] K. C. Kim, T.-U. Yoon, and Y.-S. Bae, "Applicability of using CO_2 adsorption isotherms to determine BET surface areas of microporous materials," *Microporous and Mesoporous Materials*, vol. 224, pp. 294-301, 2016.

[163] A. Hussain, N. K. M. Saiyudi, and Z. A. Majid, *Introduction to Surface and Colloid Chemistry*. Malaysia: UTM, 2008.

[164] V. K. Singh and E. A. Kumar, "Measurement and Analysis of Adsorption Isotherms of CO_2 on Activated Carbon," *Applied Thermal Engineering,* 2015.

[165] N. A. Rashidi, S. Yusup, and B. H. Hameed, "Kinetic studies on carbon dioxide capture using lignocellulosic based activated carbon," *Energy*, vol. 61, pp. 440-446, 2013.

[166] L. Hauchhum and P. Mahanta, "Kinetic, Thermodynamic and Regeneration Studies for CO_2 Adsorption onto Activated Carbon," *International Journal of Advanced Mechanical Engineering*, vol. 4, 2014.

[167] A. O. Dada, A. Olalekan, A. M. Olatunya, and O. DADA, "Langmuir, Freundlich, Temkin and Dubinin–Radushkevich Isotherms Studies of Equilibrium Sorption of Zn^{2+} Unto Phosphoric Acid Modified Rice Husk," *Journal of Applied Chemistry*, vol. 3, pp. 38-45, 2012.

[168] A. U. Itodo and H. U. Itodo, "Sorption Energies Estimation Using Dubinin-Radushkevich and Temkin Adsorption Isotherms " *Life Science Journal*, vol. 7, pp. 31-39, 2010.

[169] N. A. Rashidi, S. Yusup, and A. Borhan, "Isotherm and Thermodynamic Analysis of Carbon Dioxide on Activated Carbon," *Procedia Engineering*, vol. 148, pp. 630-637, 2016.

[170] L. Hauchhum and P. Mahanta, "Kinetic, Thermodynamic and Regeneration Studies for CO_2 Adsorption onto Activated Carbon," *International Journal of Advanced Mechanical Engineering*, vol. 4, pp. 27-32, 2014.

[171] P. S. Kumar and K. Kirthika, "Equilibrium and kinetic Study of Adosrption of Nickel from aqueous solution onto Bael Tree Leaf powder," *Journal of Engineering Science and Technology*, vol. 4, pp. 351-363, 2009.

[172] L. Zhou, J. Fan, and X. Shang, "CO_2 Capture and Separation Properties in the Ionic Liquid 1-n-Butyl-3-Methylimidazolium Nonafluorobutylsulfonate," *Materials,* vol. 7, pp. 3867-3880, 2014.

[173] M. Ramdin, T. W. de Loos, and T. J. H. Vlugt, "State-of-the-Art of CO_2Capture with Ionic Liquids," *Industrial & Engineering Chemistry Research,* vol. 51, pp. 8149-8177, 2012.

[174] S. Azizian, "Kinetic models of sorption: a theoretical analysis," *J Colloid Interface Sci,* vol. 276, pp. 47-52, Aug 1 2004.

[175] A. S. Alzaydien and W. Manasreh, "Equilibrium, kinetic and thermodynamic studies on the adsorption of phenol onto activated phosphate rock," *International Journal of Physical Sciences,* vol. 4, pp. 172-181, 2009.

[176] K. V. Kumar, "Linear and non-linear regression analysis for the sorption kinetics of methylene blue onto activated carbon," *Journal of Hazardous Materials B137,* vol. 137, pp. 1538-44, Oct 11 2006.

[177] C. Goel, H. Bhunia, and P. K. Bajpai, "Novel nitrogen enriched porous carbon adsorbents for CO_2 capture: Breakthrough adsorption study," *Journal of Environmental Chemical Engineering,* vol. 4, pp. 346-356, 2016.

[178] C. Goel, H. Kaur, H. Bhunia, and P. K. Bajpai, "Carbon dioxide adsorption on nitrogen enriched carbon adsorbents: Experimental, kinetics, isothermal and thermodynamic studies," *Journal of CO_2 Utilization,* vol. 16, pp. 50-63, 2016.

[179] Q. Liu, J. Shi, S. Zheng, M. Tao, Y. He, and Y. Shi, "Kinetics Studies of CO_2 Adsorption/Desorption on Amine Functionalized Multiwalled Carbon Nonotubes," *Industrial & Engineering Chemistry Research,* vol. 53, pp. 11677-11683, 2014.

[180] K. V. Kumar, "Linear and non-linear regression analysis for the sorption kinetics of methylene blue onto activated carbon," *Journal of Hazardous Materials B137,* vol. 137, pp. 1538-1544, Oct 11 2006.

[181] Y. S. Ho and G. McKay, "Pseudo-second order model for sorption processes," *Process Biochemistry,* vol. 34, pp. 451-465, 1999.

[182] D. Bakowies, "Assessment of density functional theory for thermochemical approaches based on bond separation reactions," *J Phys Chem A,* vol. 117, pp. 228-43, Jan 10 2013.

[183] L. A. Blanchard, Z. Gu, and J. F. Brennecke, "High Pressure Phase Behavior of Ionic Liquid CO_2 Systems," *Journal of Physical Chemistry B.,* vol. 105, pp. 2437-2444, 2001.

[184] K. R. Seddon, A. Stark, and M.-J. Torres, "Influence of chloride, water, and organic solvents on the physical properties of ionic liquids," *Pure Applied Chemistry,* vol. 72, pp. 2275-2287, 2000.

[185] P. Hussona, L. Pisona, J. Jacquemina, and M. F. C. Gomes, "Influence of water on the carbon dioxide absorption by 1-ethyl-3-methylimidazolium bis(trifluoromethylsulfonyl)amid," *Fluid Phase Equilibria,* vol. 294, pp. 98-104.

[186] L. E. Ficke, H. Rodriguez, and J. F. Brennecke, "Heat capacities and excess enthalpies of 1-ethyl-3-methylimidazolium-based ionic liquids and water," *Journal of Chemical and Engineering Data,* vol. 53, pp. 2112-2119, 2008.

[187] R. P. Swatloski, R. D. Rogers, and J. Holbrey, "Ionic Liquids are Not Always Green: Hydrolysis of 1-Butyl-3-Methylimidazolium Hexafluorophosphate," *Green Chemistry,* vol. 5, pp. 361-363, 2003.

[188] M. E. Van Valkenburg, R. L. Vaughn, M. Williams, and J. S. Wilkes, "Thermochemistry of ionic liquid heat-transfer fluids," *Thermochimica Acta,* vol. 425, pp. 181-188, 2005.

[189] Y. Yasaka and Y. Kimura, "Effect of Temperature and Water Concentration on CO_2Absorption by Tetrabutylphosphonium Formate Ionic Liquid," *Journal of Chemical & Engineering Data,* vol. 61, pp. 837-845, 2016.

[190] R. T. Yang, *Adsorbents - fundamentals and applications.* University of Michigan: John Wiley & Sons, 2003.

PUBLICATIONS AND ACHIEVEMENTS

1. **Maisara Shahrom Raja Shahrom** and Cecilia Devi Wilfred. Synthesis and Thermal Properties of Amino Acids Ionic Liquids (AAILs). *Journal of Applied Sciences* 14 (10): 1067-1072, 2014

2. **Maisara Shahrom Raja Shahrom**, Cecilia Devi Wilfred and Chong Fai Kait. Synthesis and Characterization of poly[VBTMA][Ala]. *AIP Conference Proceeding*. 1621: 237-243, 2014

3. **Maisara Shahrom Raja Shahrom**, Cecilia Devi Wilfred, AboBakr Khidir Ziyada Taha. CO_2 Capture by Task Specific Ionic Liquids (TSILs) and Polymerized Ionic Liquids (PILs and AAPILs). *Journal of Molecular Liquids* 219 (2016): 306-312

4. Animesh Pal**, Maisara Shahrom Raja Shahrom**, Muhammad Moniruzzaman, Cecilia Devi Wilfred, Bidyut Baran Saha. Ionic Liquid as a new binder for activated carbon based consolidated composite adsorbents. *Chemical Engineering Journal* 326 (2017):980-986

5. Patent filed **PI2015703179.** Aqua Amino Acid Polymerized Ionic Liquids (Aqua-AAPILs) for CO_2 Capture.

6. Patent filed **PI2014701103.** Amino Acid Polymerized Ionic Liquids (AAPILs) for CO_2 Capture**.**

7. Patent filed **PI2016701603.** Polymerized Amino Acid Ionic Liquids (PAAILs) for CO_2 Capture.

8. ITEX 2014, KLCC, Malaysia: Amino Acid Polymerized Ionic Liquids (aPILs) for CO_2 Capture: **GOLD**

9. INNOVA 2014, Brussels, France: Amino Acid Polymerized Ionic Liquids (aPILs) for CO_2 Capture: **GOLD**

10. ITEX 2015, KLCC, Malaysia: Aqua-Amino Acid Polymerized Ionic Liquids (Aqua-aPILs) for CO_2 Capture: **SILVER**

11. PECIPTA 2015, KLCC, Malaysia: Aqua-Amino Acid Polymerized Ionic Liquids (Aqua-aPILs) for CO_2 Capture: **BRONZE**

12. ITEX 2016, KLCC, Malaysia: Polymerized Amino Acid Ionic Liquids (PAAILs) for CO_2 Capture, **GOLD**

APPENDIX A

NMR SPECTRUMS OF ALL AAPILS AND THEIR MONOMERS

The ^{1}H-NMR includes all synthesized AAPILs and their monomers

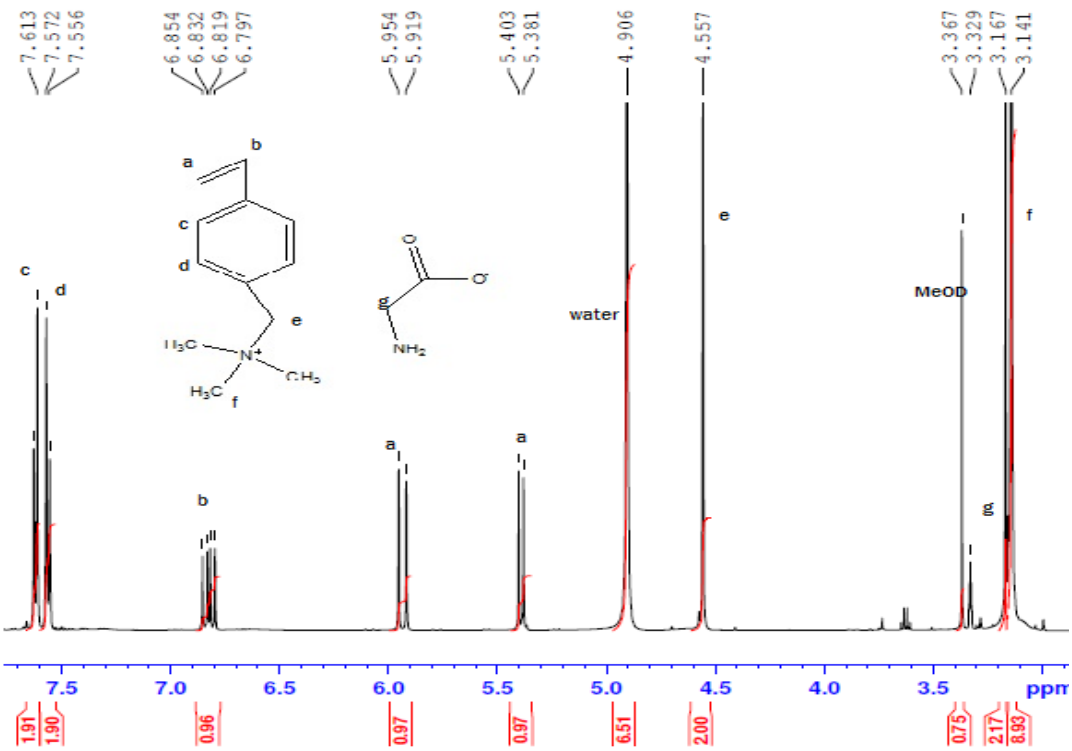

Fig. A-1 ^{1}H-NMR [VBTMA][Gly]

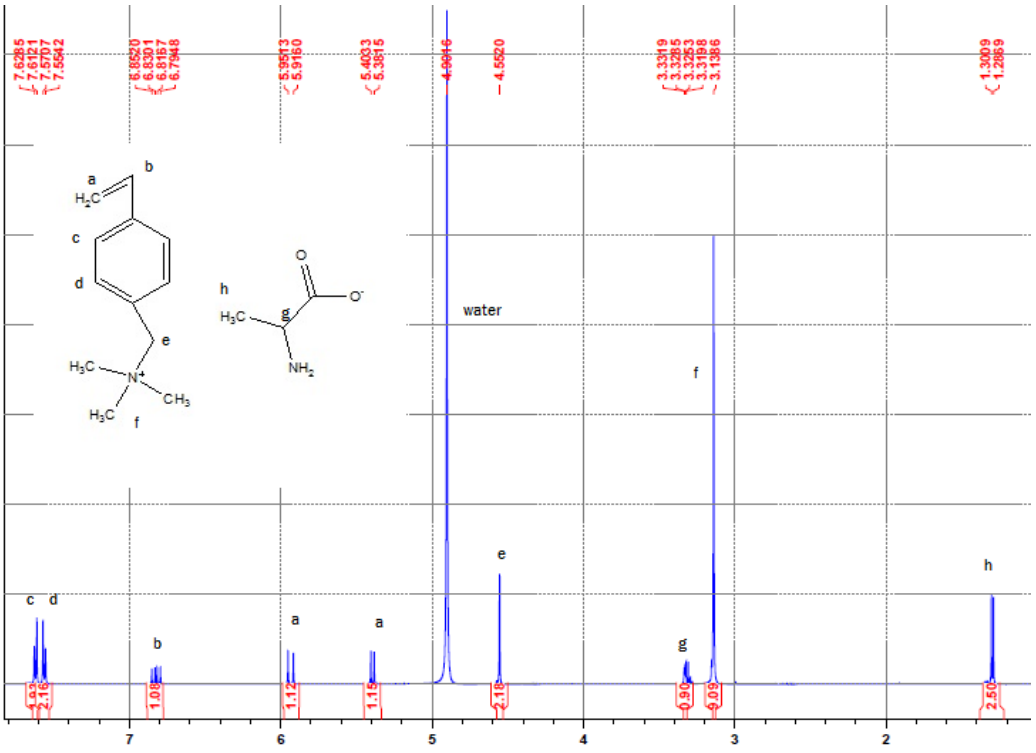

Fig. A-2 ^{1}H-NMR [VBTMA][Ala]

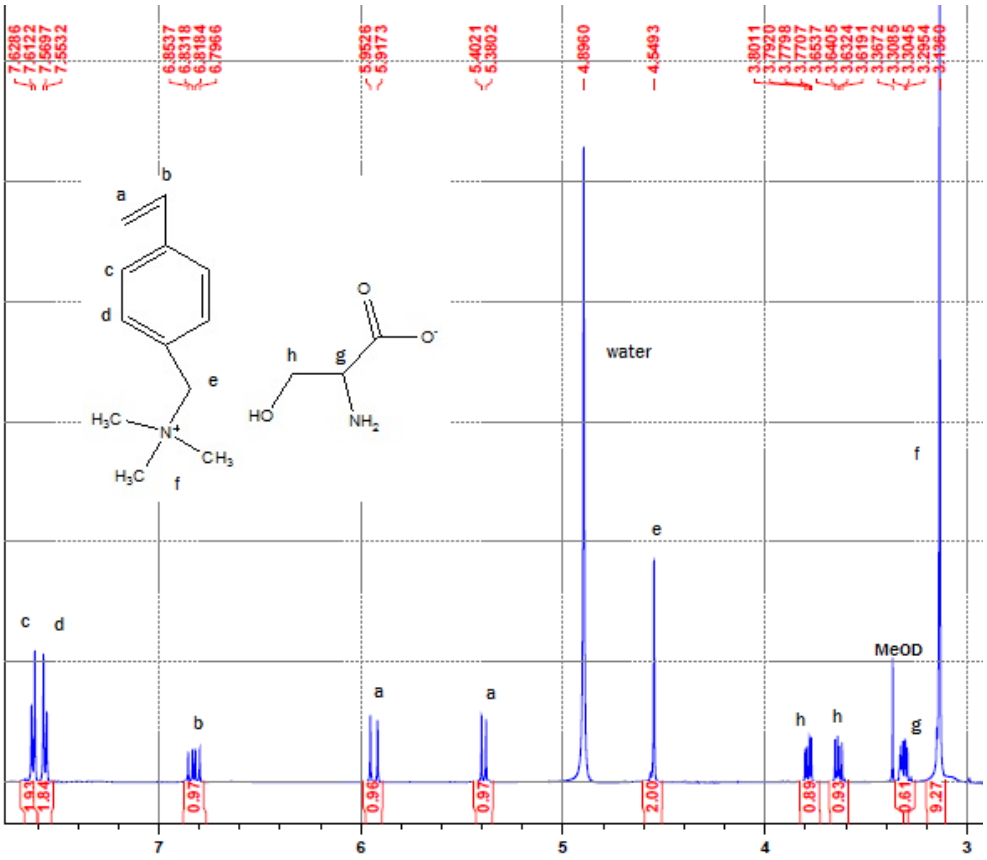

Fig. A-3 ^{1}H-NMR [VBTMA][Ser]

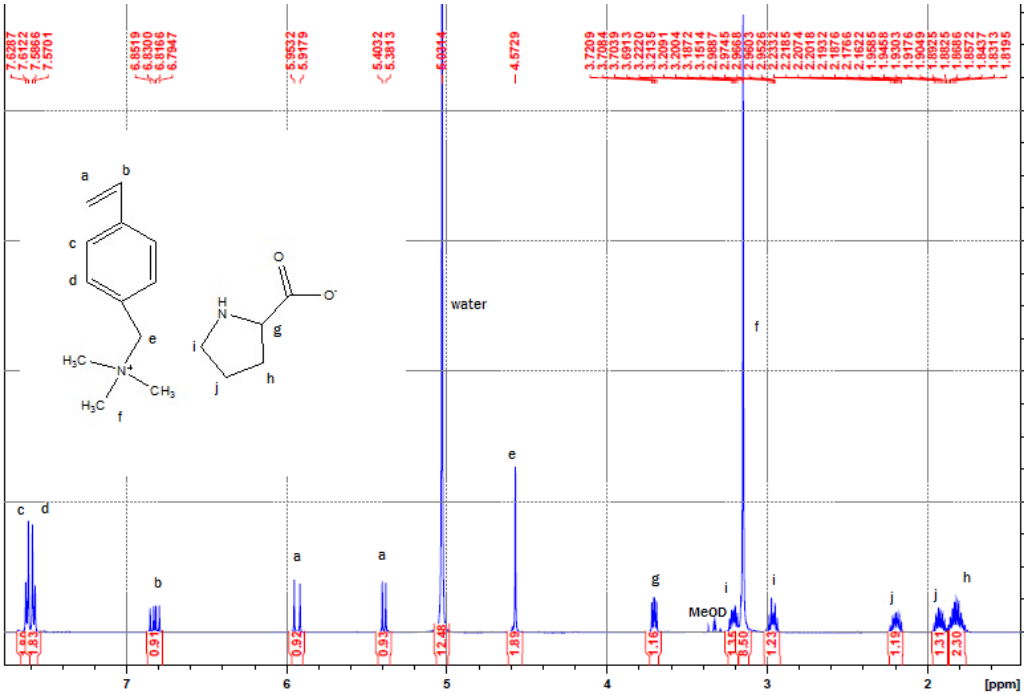

Fig. A-4 ^{1}H-NMR [VBTMA][Pro]

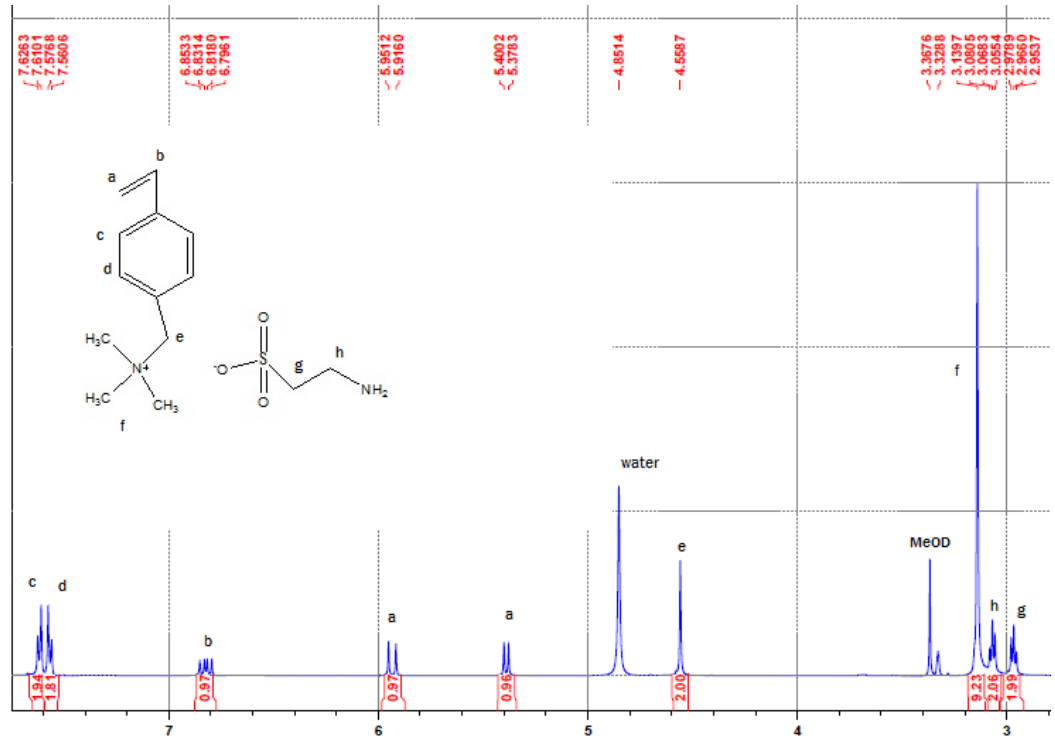

Fig. A-5 ^{1}H-NMR [VBTMA][Tau]

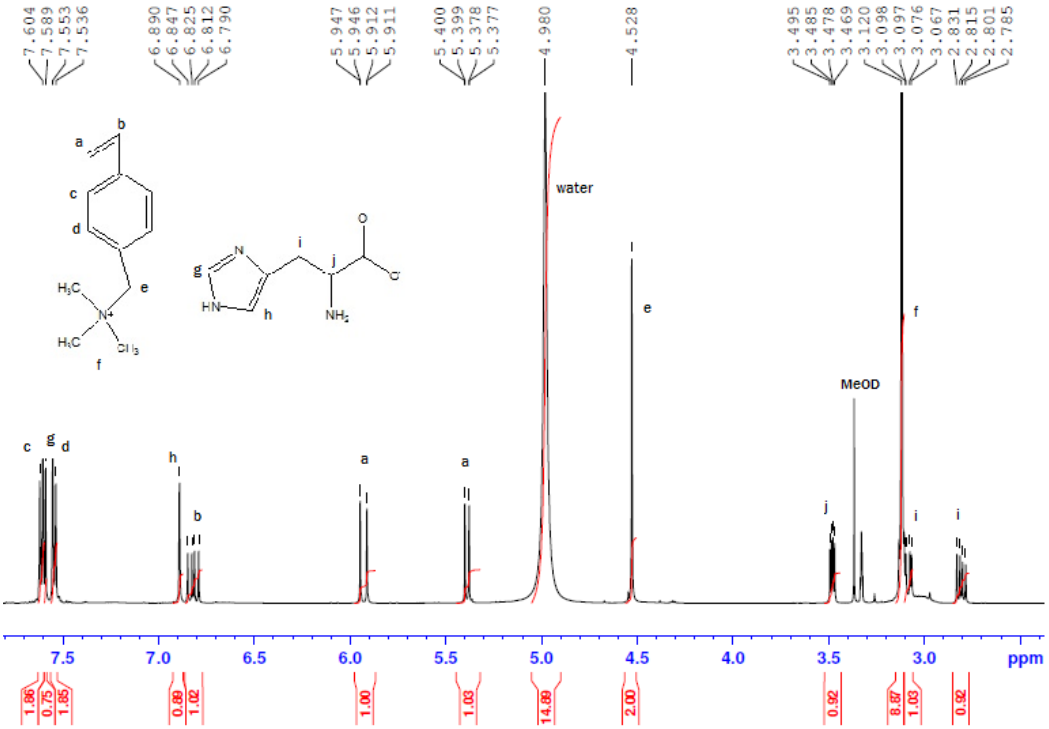

Fig. A-6 ^{1}H-NMR spectrum [VBTMA][Hist]

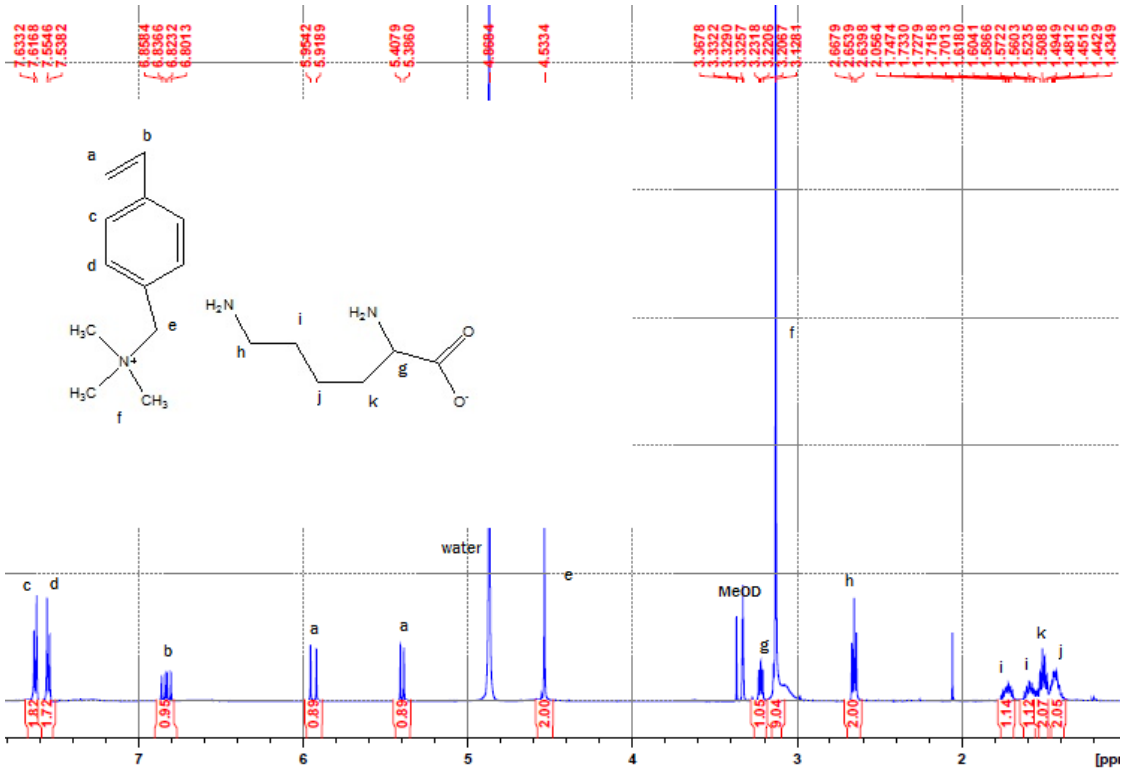

Fig. A-7 ^{1}H-NMR spectrum [VBTMA][Lys]

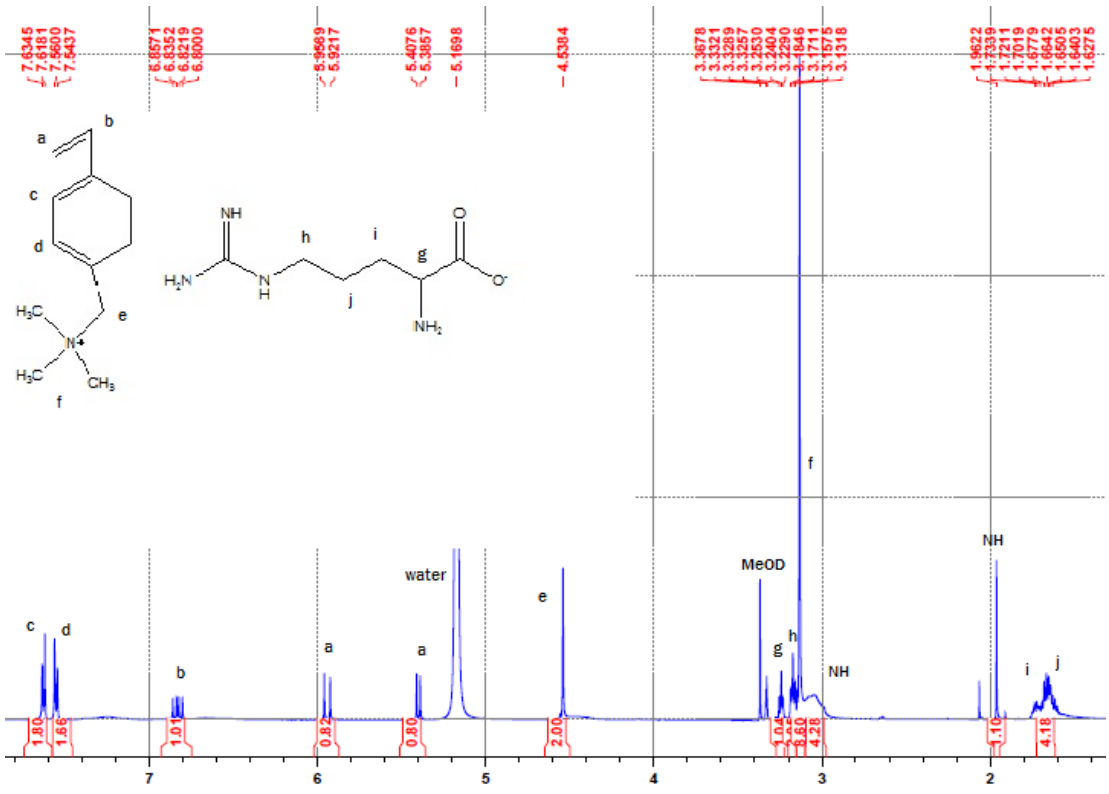

Fig. A-8. ^{1}H-NMR spectrum [VBTMA][Arg]

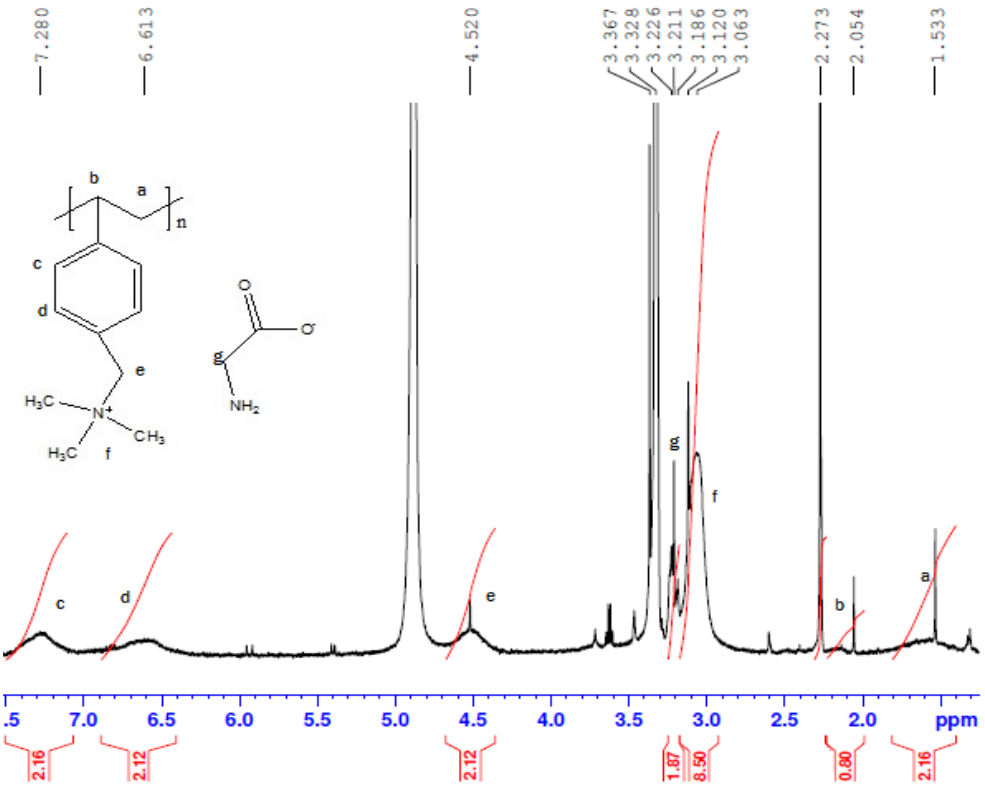

Fig. A-9. ^{1}H-NMR spectrum Poly[VBTMA][Gly]

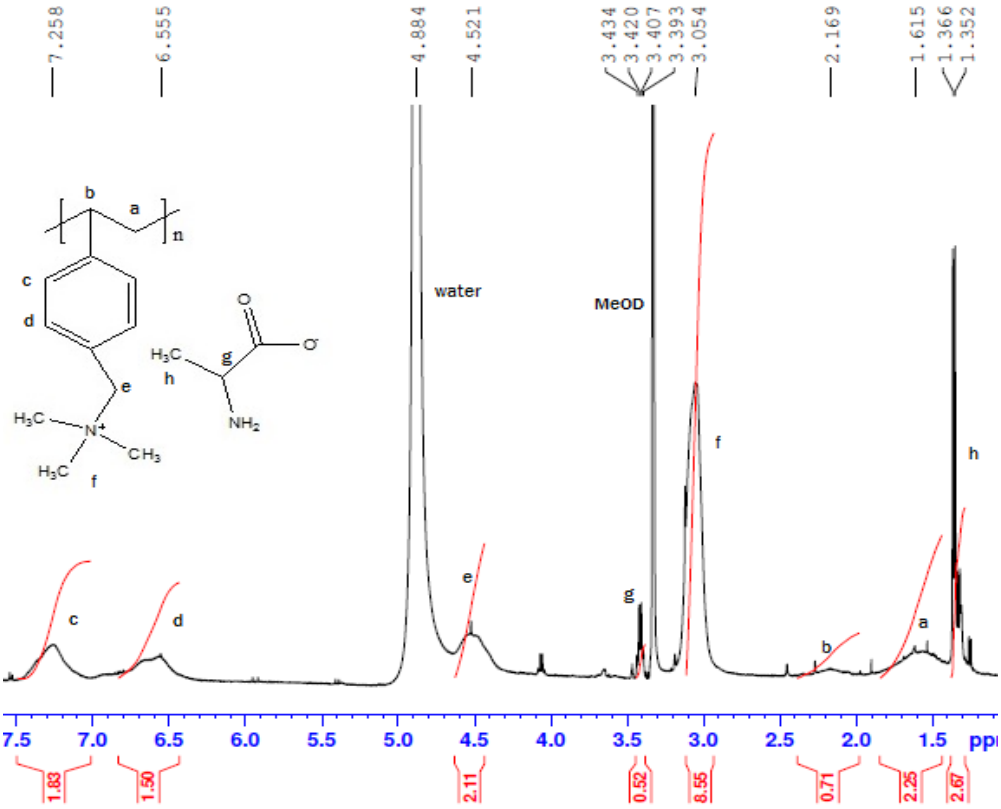

Fig. A-10 ^{1}H-NMR spectrum Poly[VBTMA][Ala]

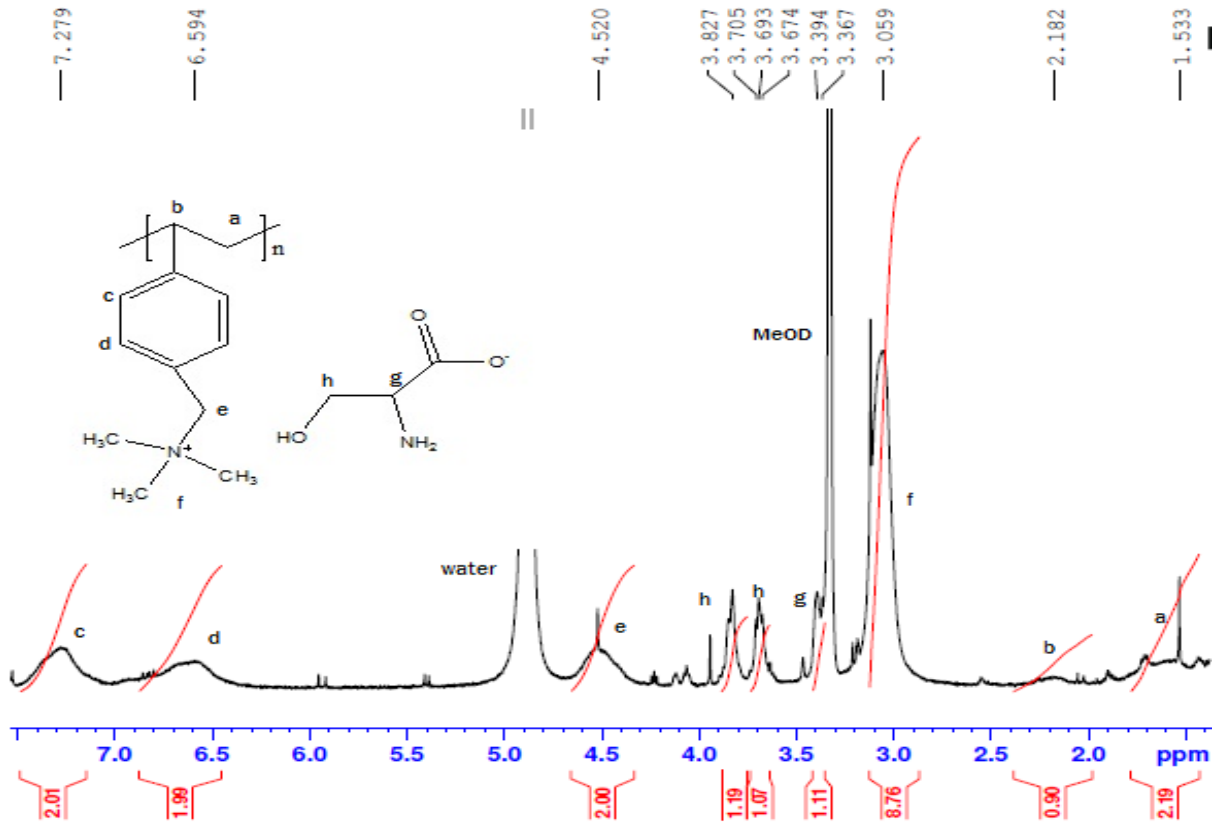

Fig. A-11. [1]H-NMR spectrum Poly[VBTMA][Ser]

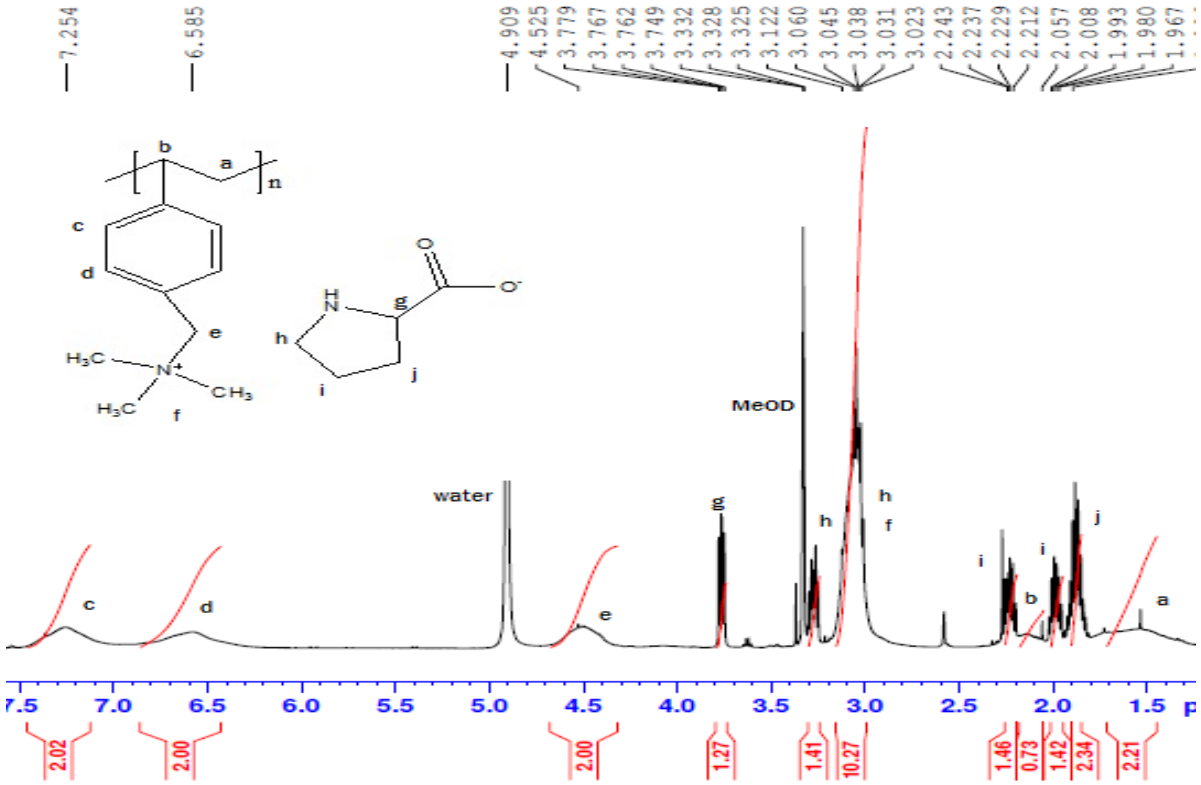

Fig. A-12 [1]H-NMR spectrum Poly[VBTMA][Pro]

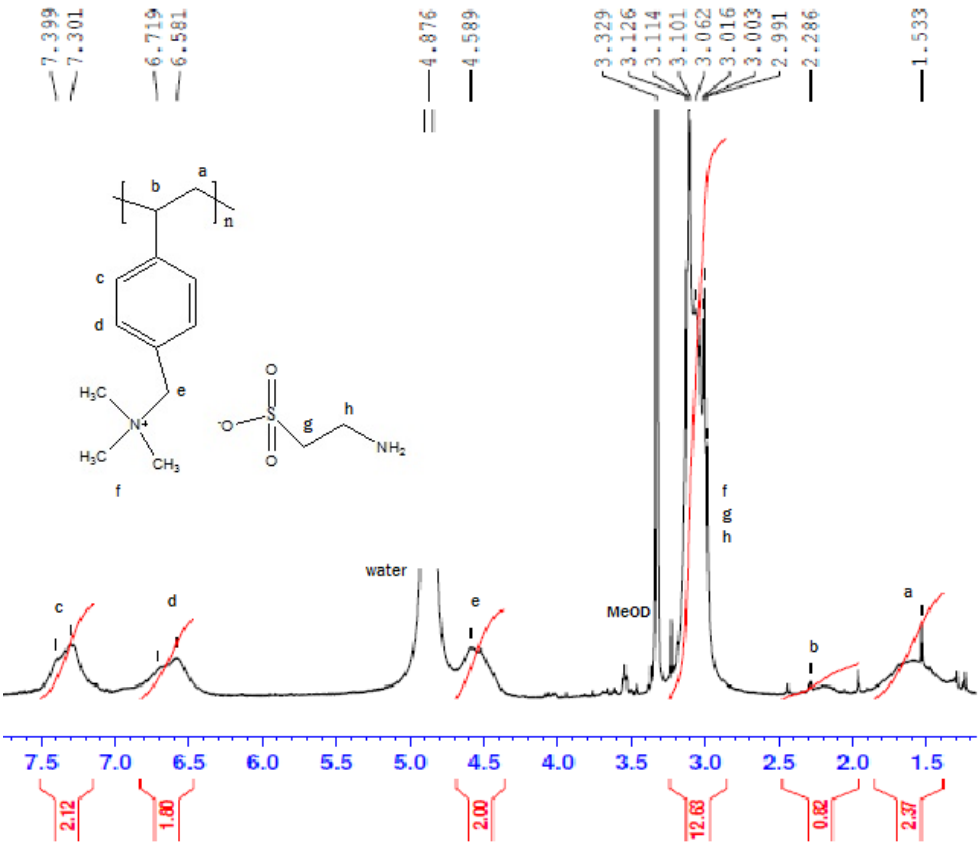

Fig. A-13 ^{1}H-NMR spectrum Poly[VBTMA][Tau]

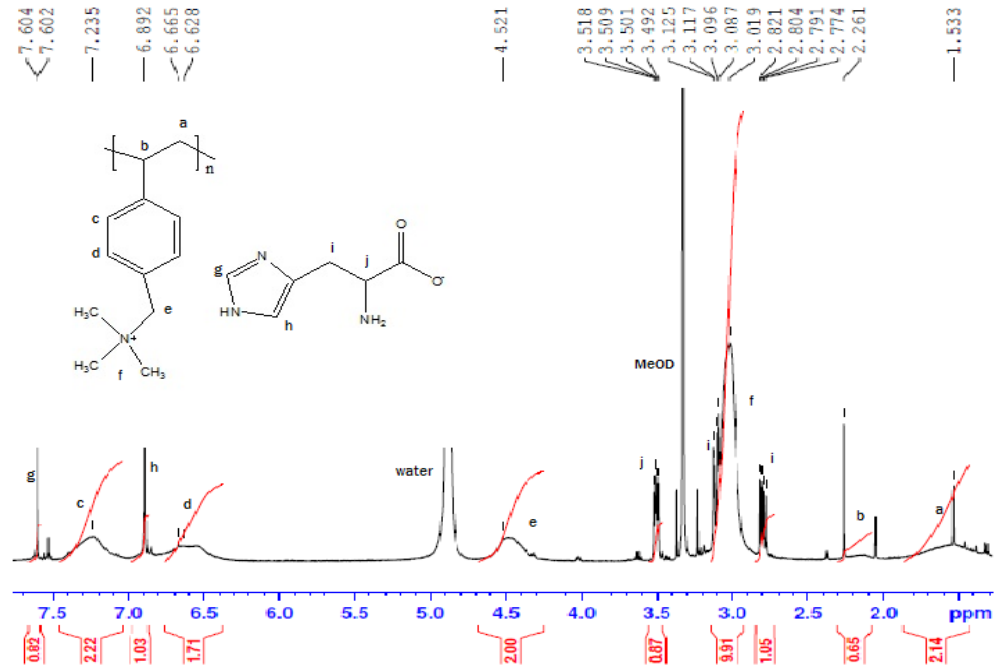

Fig. A-14 ^{1}H-NMR spectrum Poly[VBTMA][Hist]

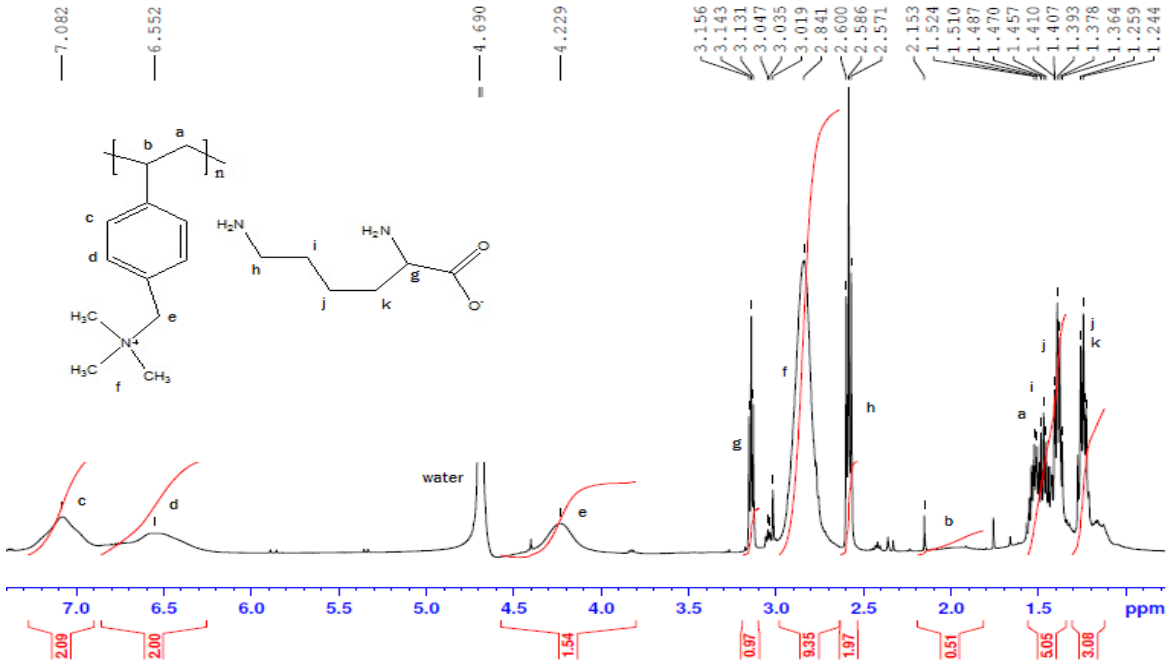

Fig. A-15 ^{1}H-NMR spectrum Poly[VBTMA][Lys]

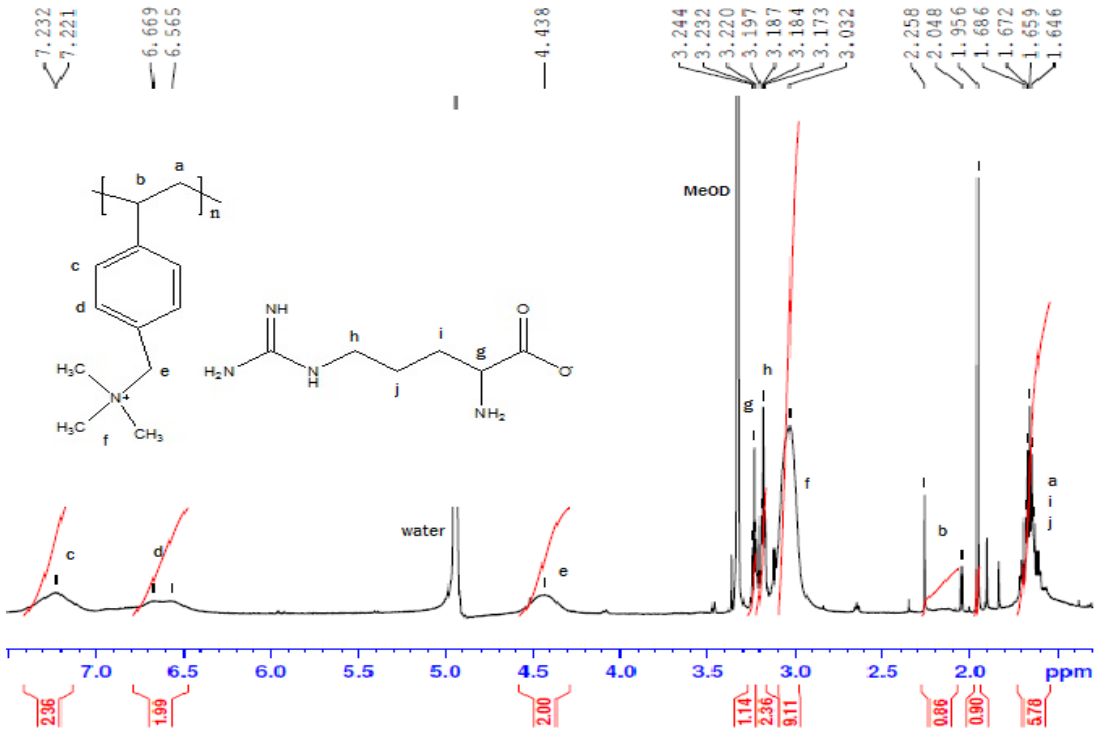

Fig.A-16 ^{1}H-NMR spectrum Poly[VBTMA][Arg]

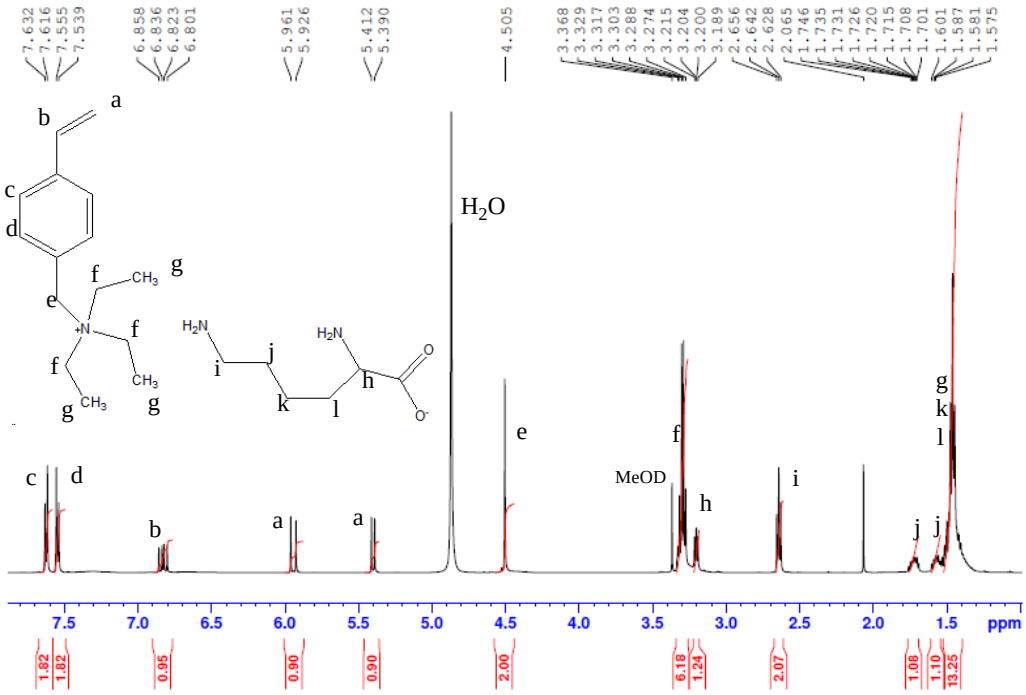

Fig. A-17 [1]H-NMR spectrum [VBTEA][Lys]

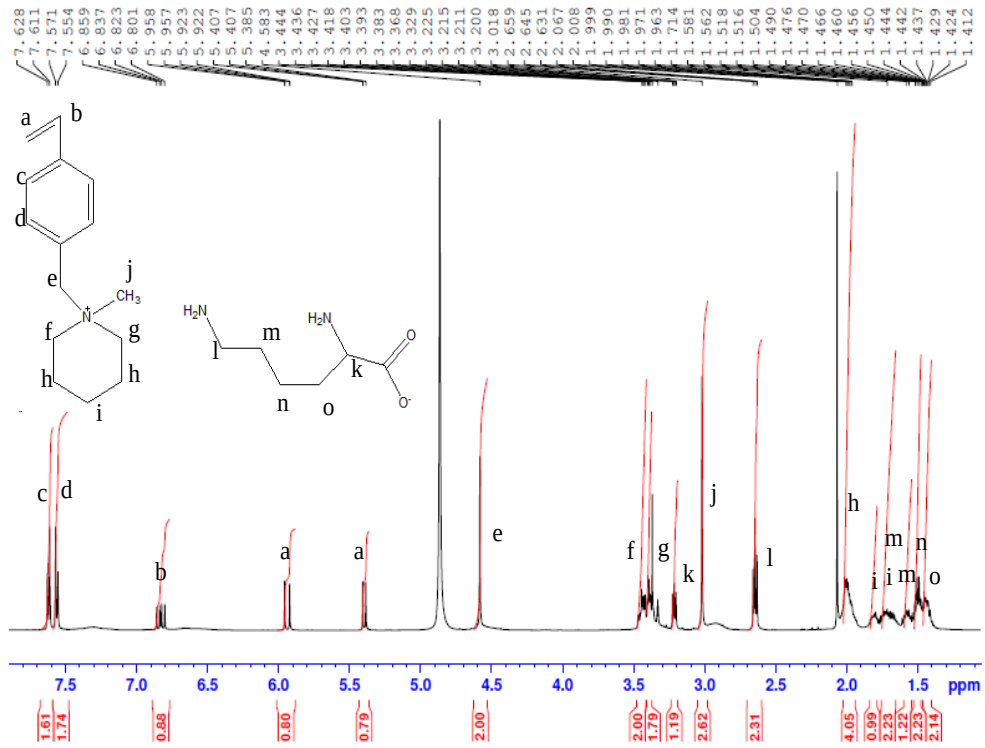

Fig. A-18. [1]H-NMR [VBPPN][Lys]

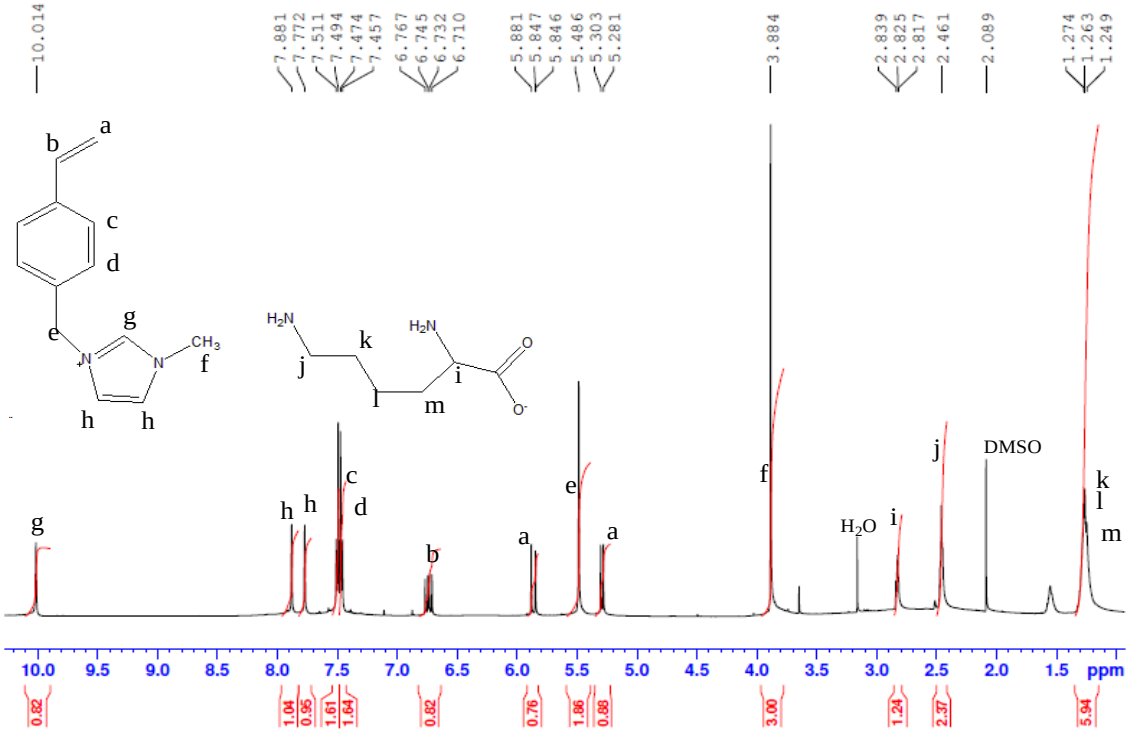

Fig. A-19 ^{1}H-NMR spectrum [VBMI][Lys]

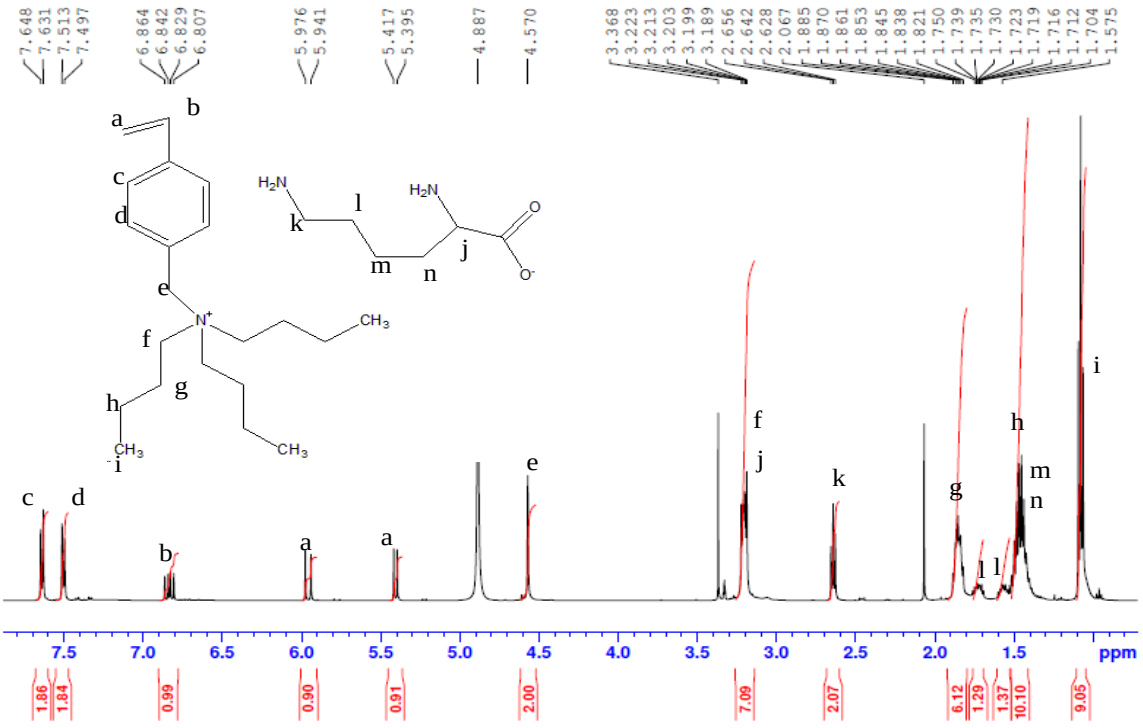

Fig. A-20 ^{1}H-NMR spectrum [VBTBA][Lys]

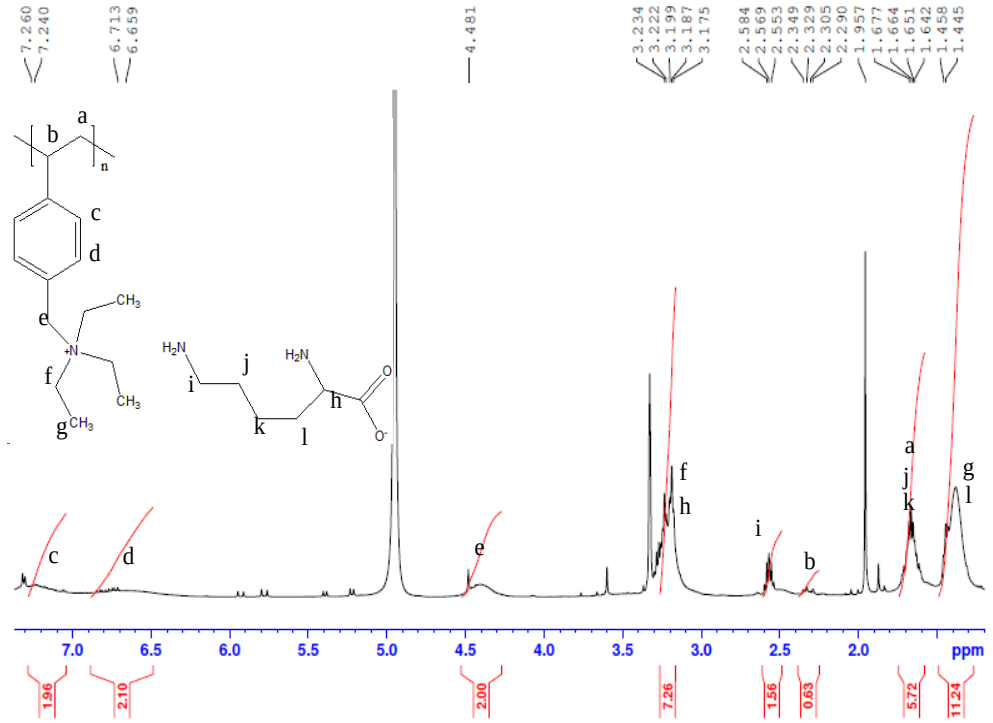

Fig. A-21 ^{1}H-NMR spectrum Poly[VBTEA][Lys]

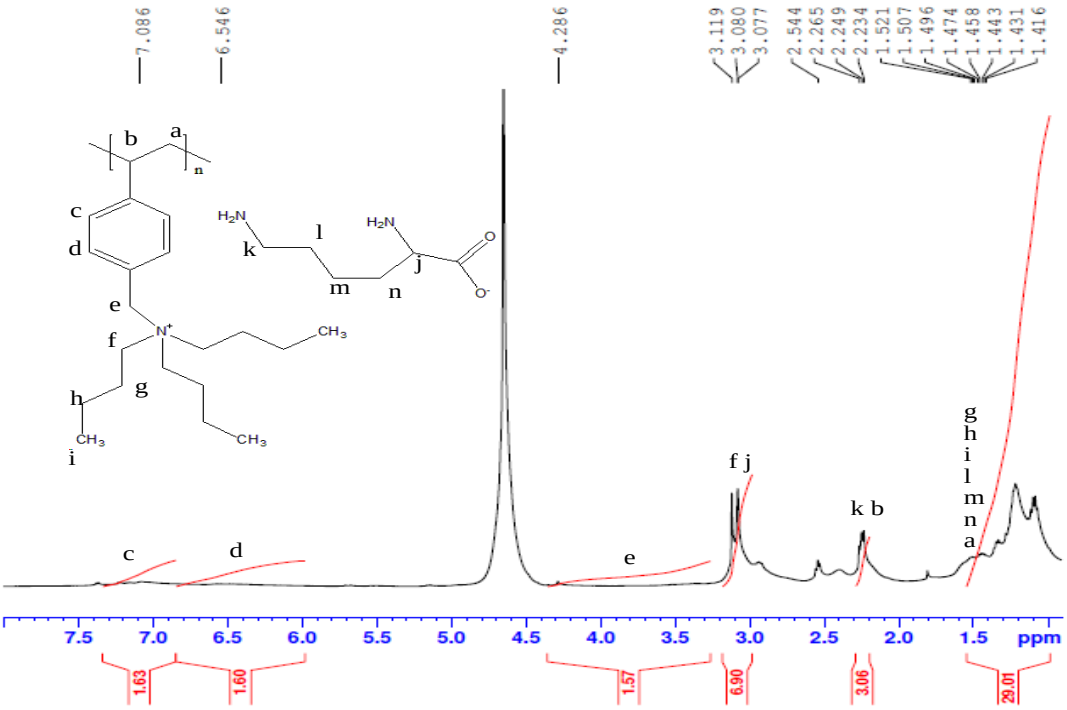

Fig. A-22 ^{1}H-NMR spectrum poly[VBTBA][Lys]

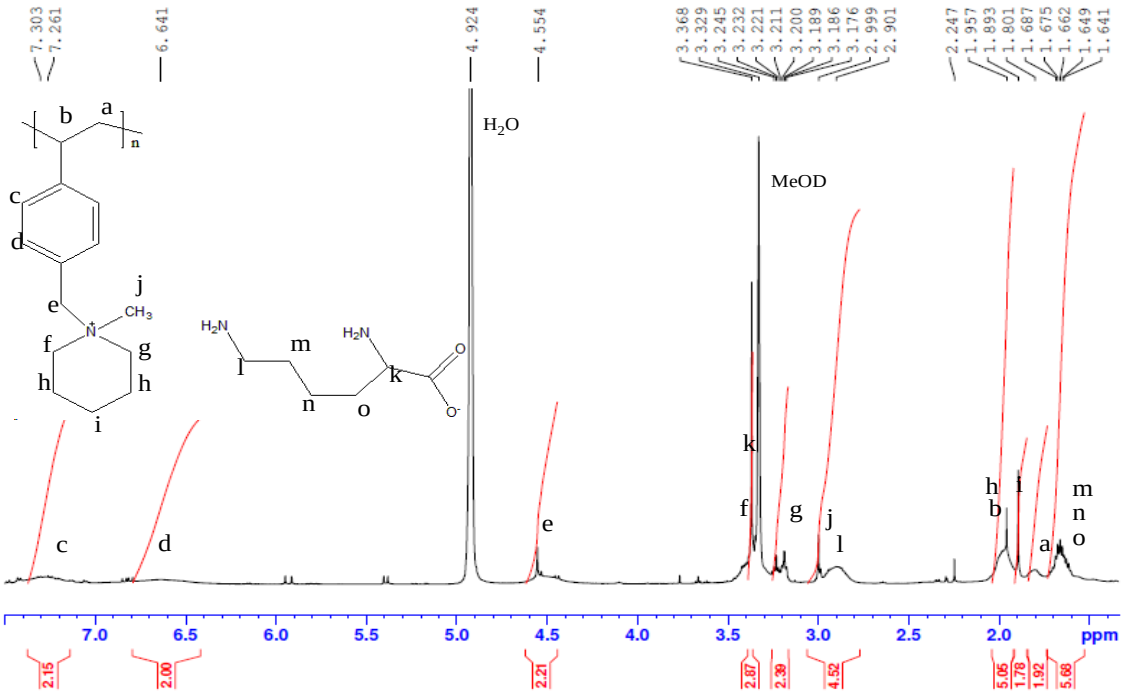

Fig. A-23 ^{1}H-NMR spectrum Poly[VBPPN][Lys]

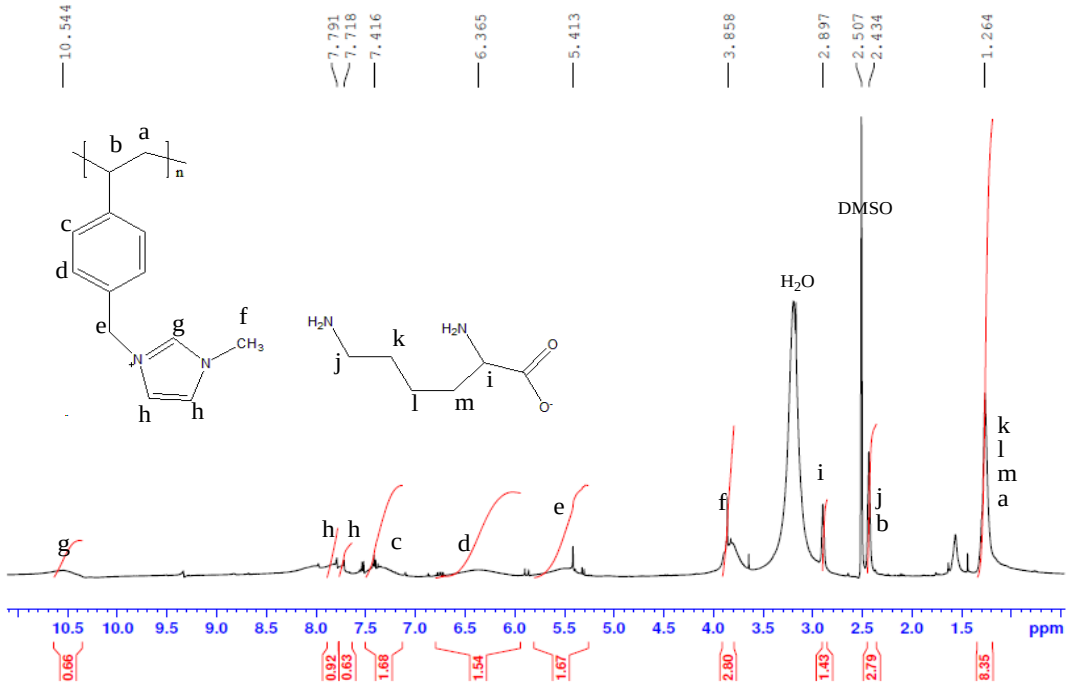

Fig. A-24 ^{1}H-NMR spectrum Poly[VBMI][Lys]

APPENDIX B

FTIR SPECTRUMS OF ALL AAPIL SYNTHESIZED AND CALIBRATION CURVE FOR CHLORIDE CONTENT

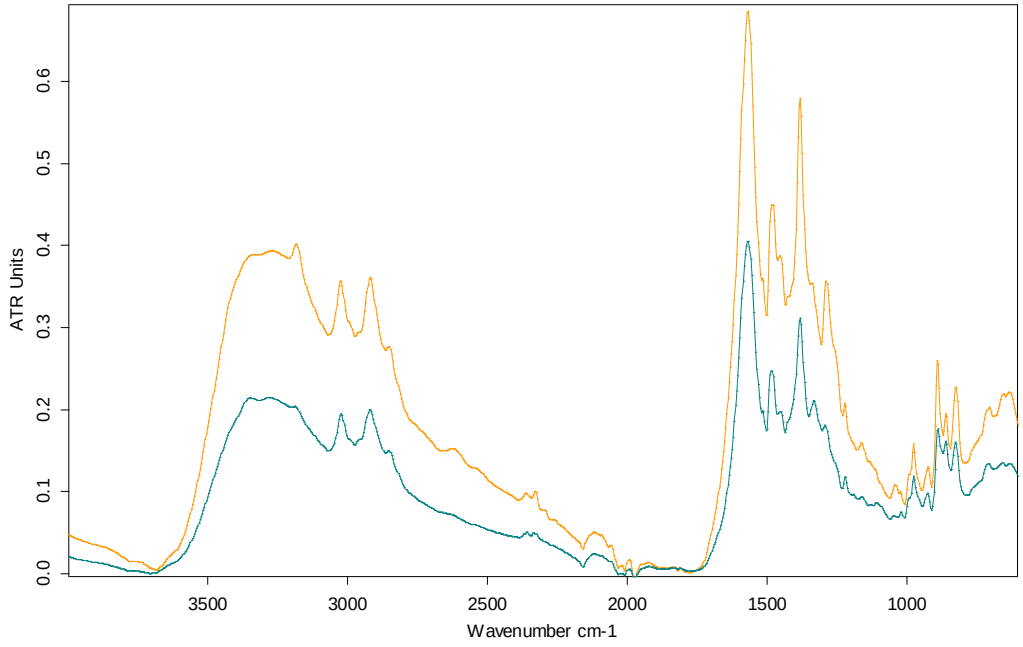

C:\Userdata\Maisara 2014New\PolyVBTMAGly2.0	polyVBTMAGly	Solid	06/06/14
C:\Userdata\Maisara 2014New\PolyVBTMAGly CO2.0	PolyVBTMAGly CO2	Solid	06/06/14

Page 1/1

Fig. B-1 FTIR spectrum Poly[VBTMA][Gly] and Poly[VBTMA][Gly] with CO_2

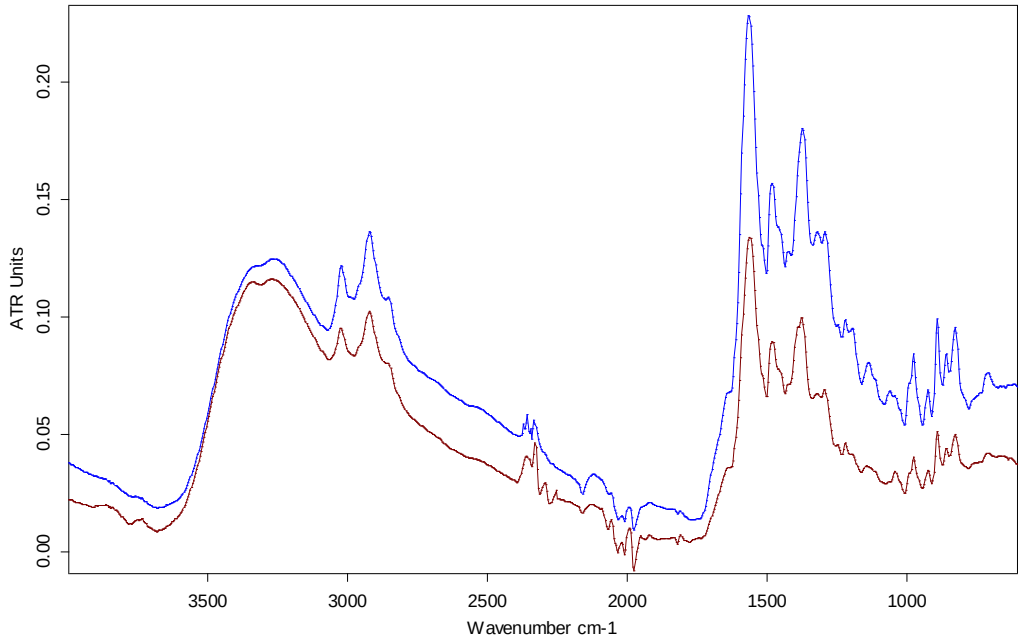

C:\Userdata\Maisara 2014New\PolyVBTMAAla.0	polyVBTMAAla	Solid	06/06/14
C:\Userdata\Maisara 2014New\PolyVBTMAAla CO2.0	PolyVBTMAAla CO2	Solid	06/06/14

Page 1/1

Fig. B-2 FTIR spectrum Poly[VBTMA][Ala] and Poly[VBTMA][Ala] with CO_2

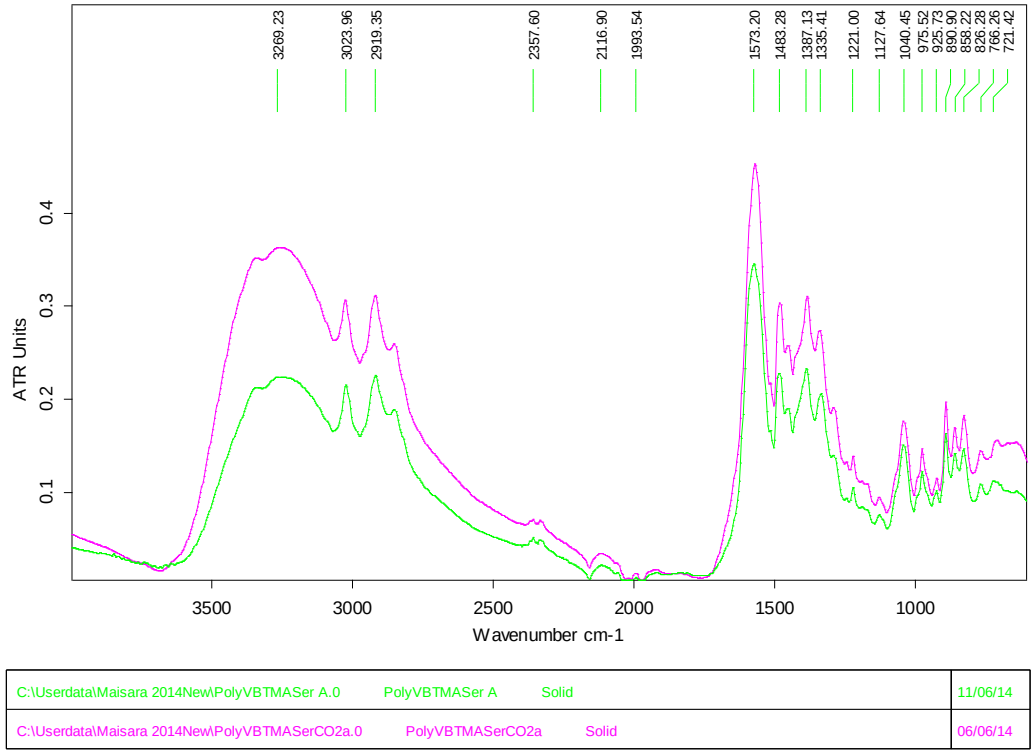

C:\Userdata\Maisara 2014New\PolyVBTMASer A.0	PolyVBTMASer A	Solid	11/06/14
C:\Userdata\Maisara 2014New\PolyVBTMASerCO2a.0	PolyVBTMASerCO2a	Solid	06/06/14

Page 1/1

Fig. B-3 FTIR spectrum Poly[VBTMA][Ser] and Poly[VBTMA][Ser] with CO_2

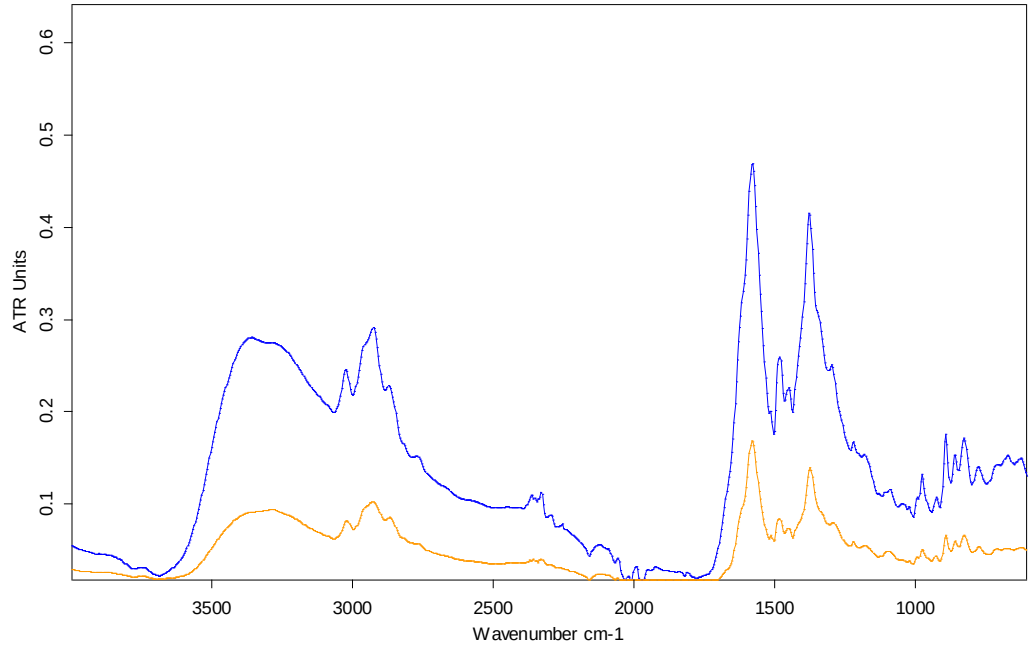

C:\Userdata\Maisara 2014New\PolyVBTMAPro A.0	PolyVBTMAPro A	Solid	11/06/14
C:\Userdata\Maisara 2014New\PolyVBTMAProCO2.0	PolyVBTMAProCO2	Solid	06/06/14

Page 1/1

Fig. B-4 FTIR spectrum Poly[VBTMA][Pro] and Poly[VBTMA][Pro with CO_2

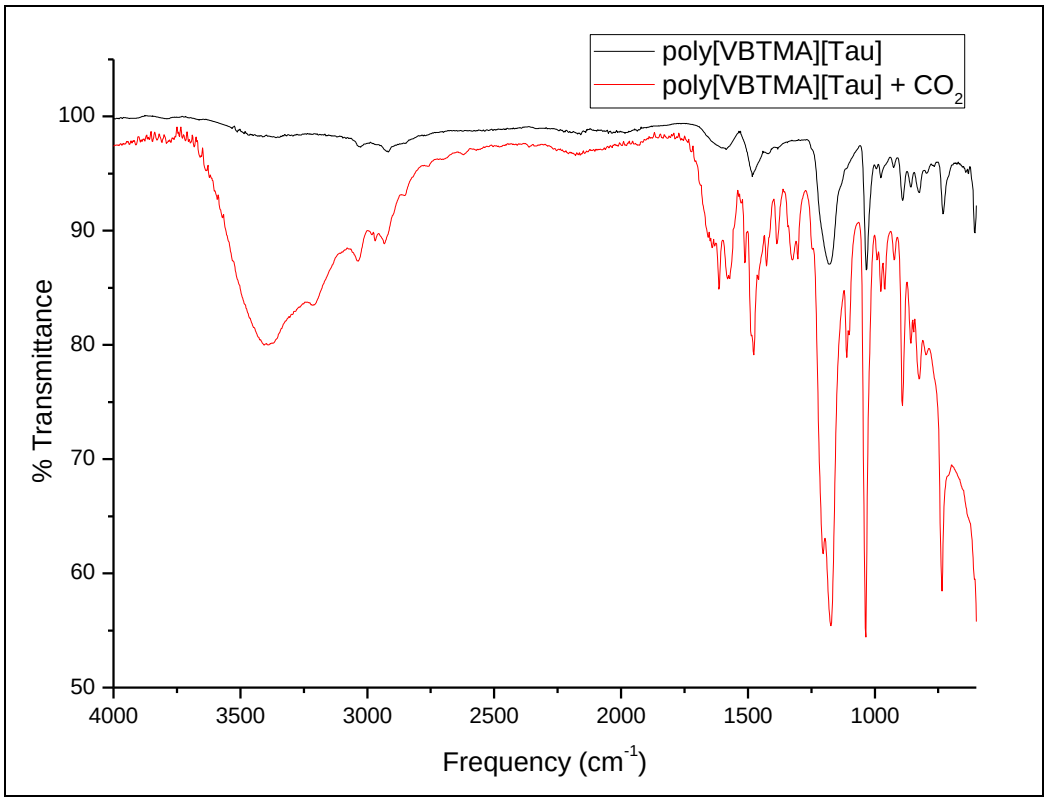

Fig. B-5 FTIR spectrum Poly[VBTMA][Tau] and Poly[VBTMA][Tau] with CO_2

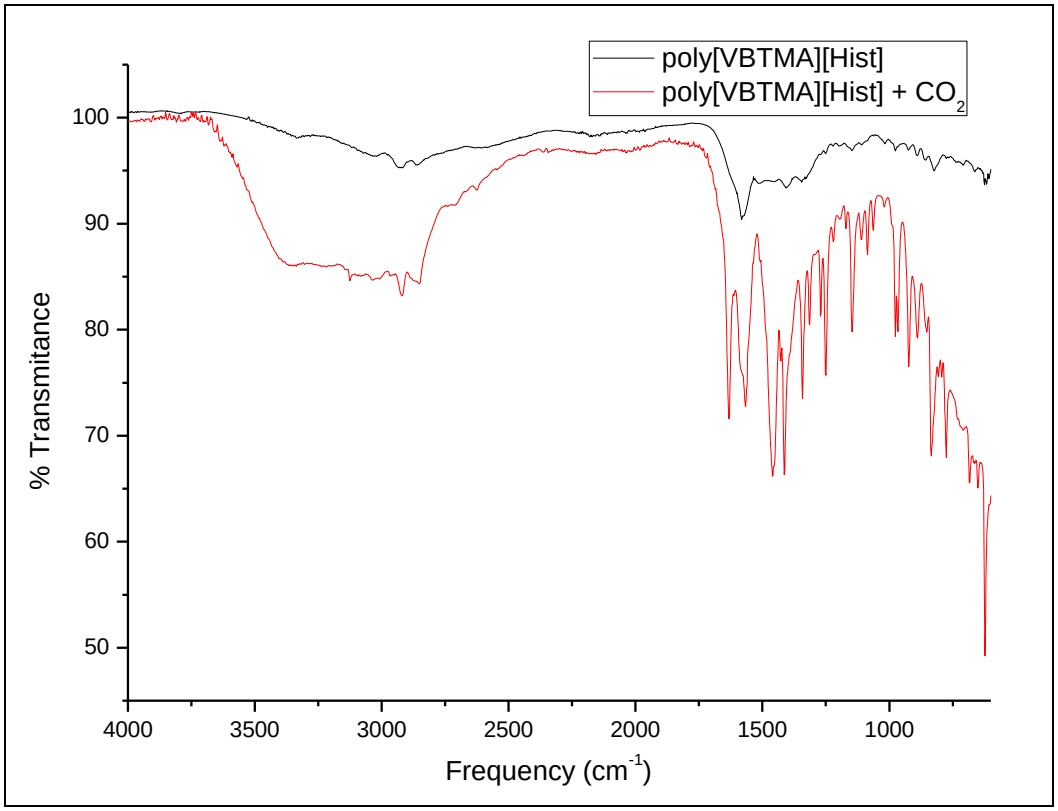

Fig. B-6 FTIR spectrum Poly[VBTMA][Hist] and Poly[VBTMA][Hist] with CO_2

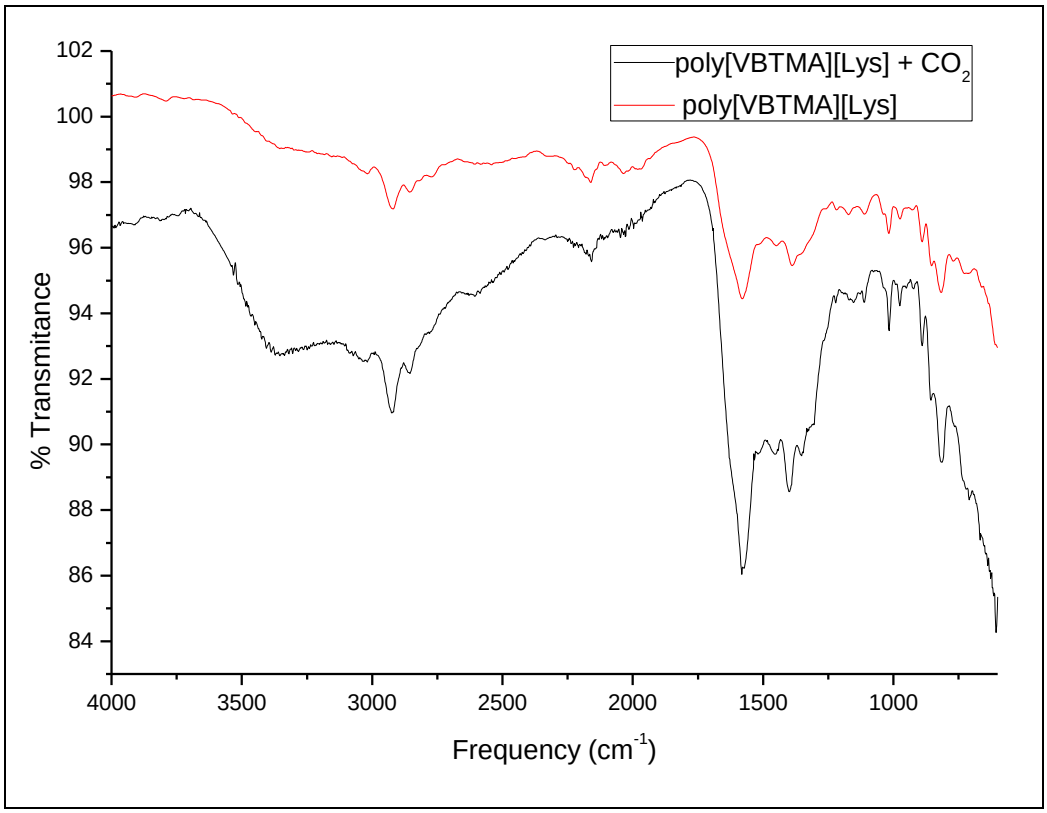

Fig. B-7 FTIR spectrum Poly[VBTMA][Lys] and Poly[VBTMA][Lys] with CO_2

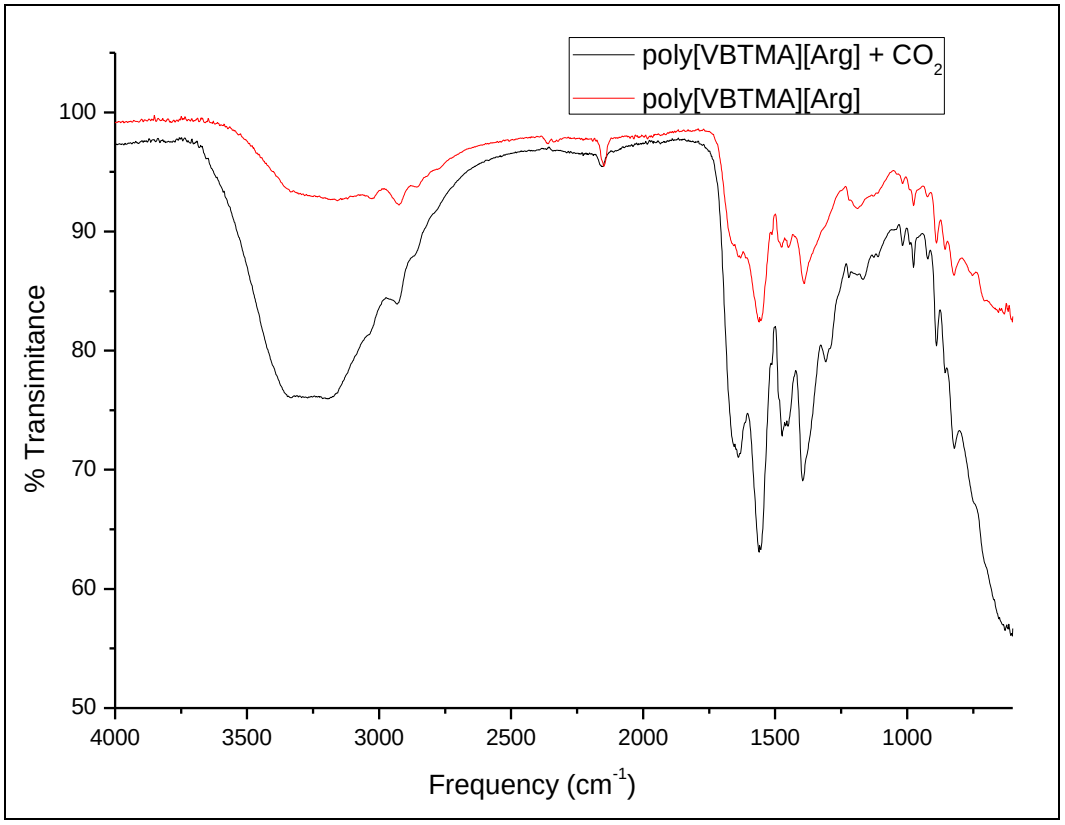

Fig. B-8 FTIR spectrum Poly[VBTMA][Arg] and Poly[VBTMA][Arg] with CO_2

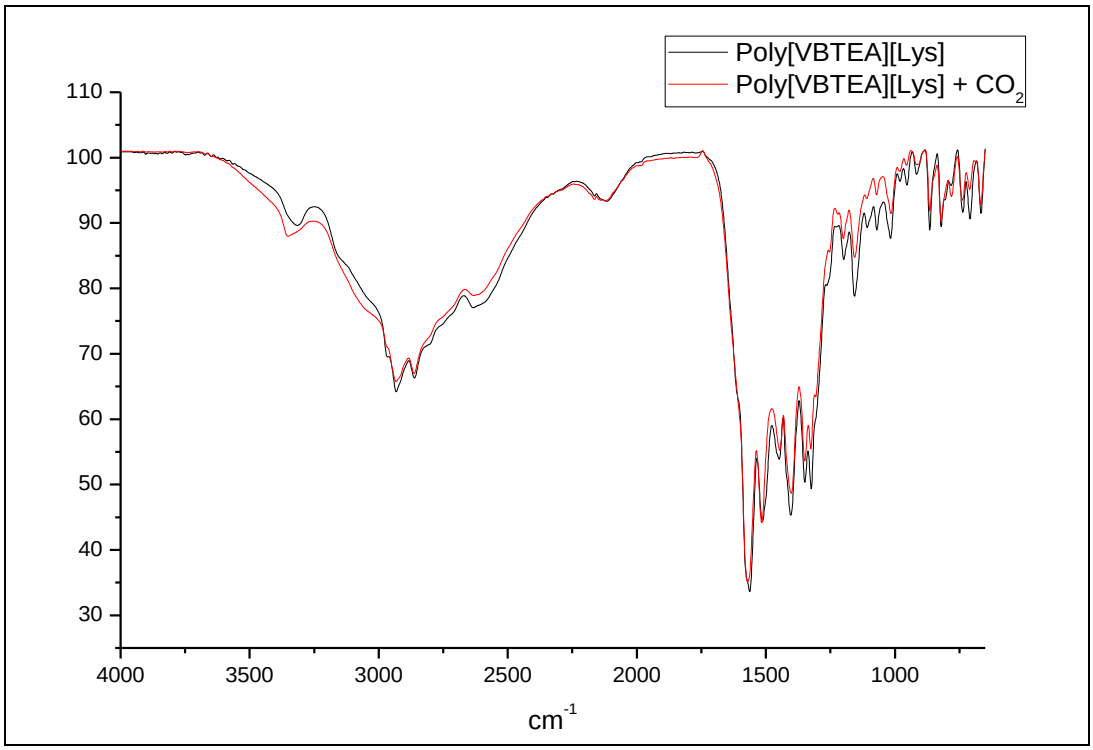

Fig. B-9 FTIR spectrum Poly[VBTEA][Lys] and Poly[VBTEA][Lys] with CO_2

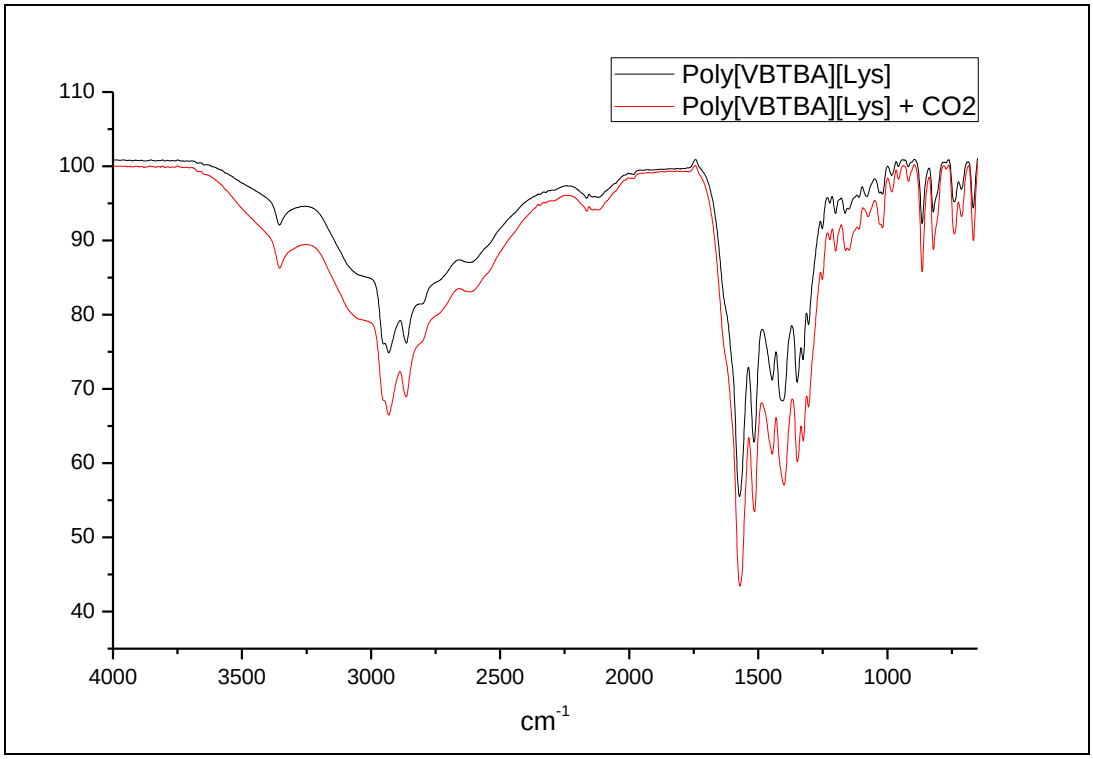

Fig. B-10 FTIR spectrum Poly[VBTBA][Lys] and Poly[VBTBA][Lys] with CO_2

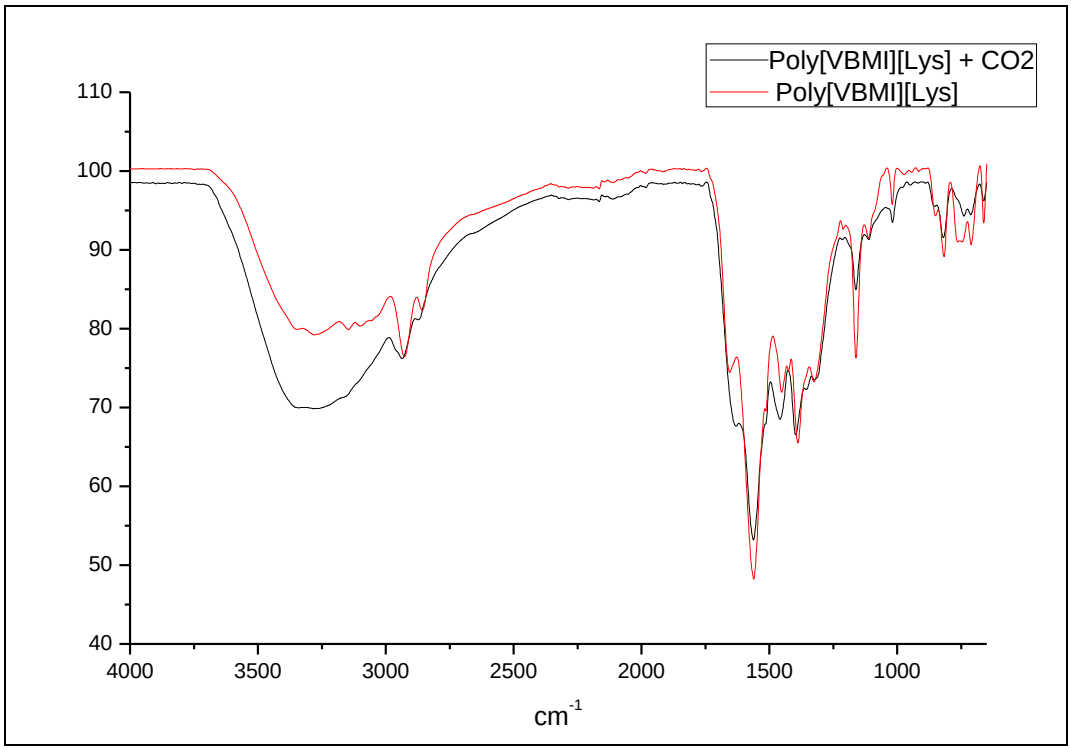

Fig B-11 FTIR spectrum Poly[VBMI][Lys] and Poly[VBMI][Lys] with CO_2

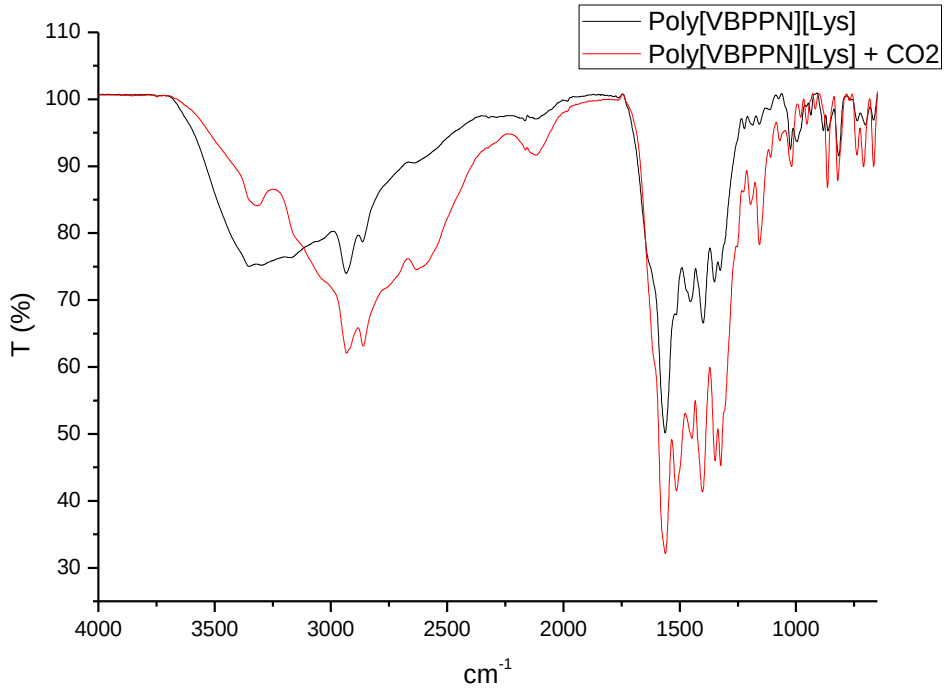

Fig B-12 FTIR spectrum Poly[VBMI][Lys] and Poly[VBMI][Lys] with CO_2

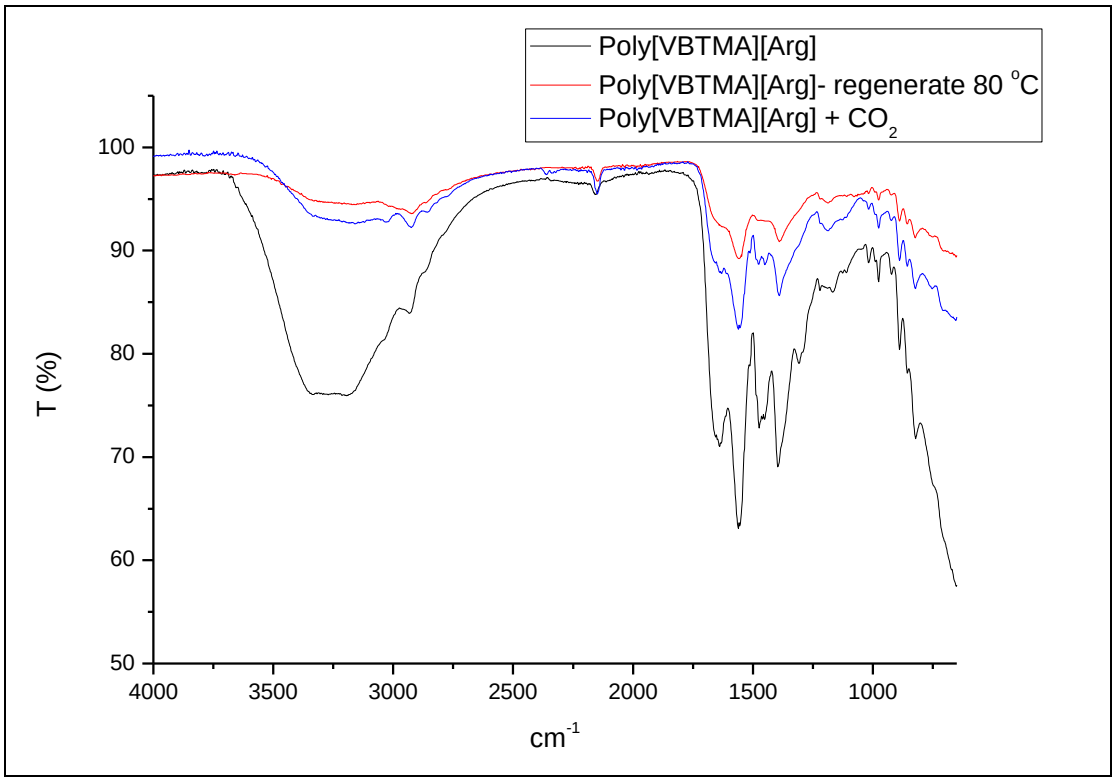

Fig. B-13 FTIR spectrum Poly[VBTMA][Arg], after, regenerate of CO_2.

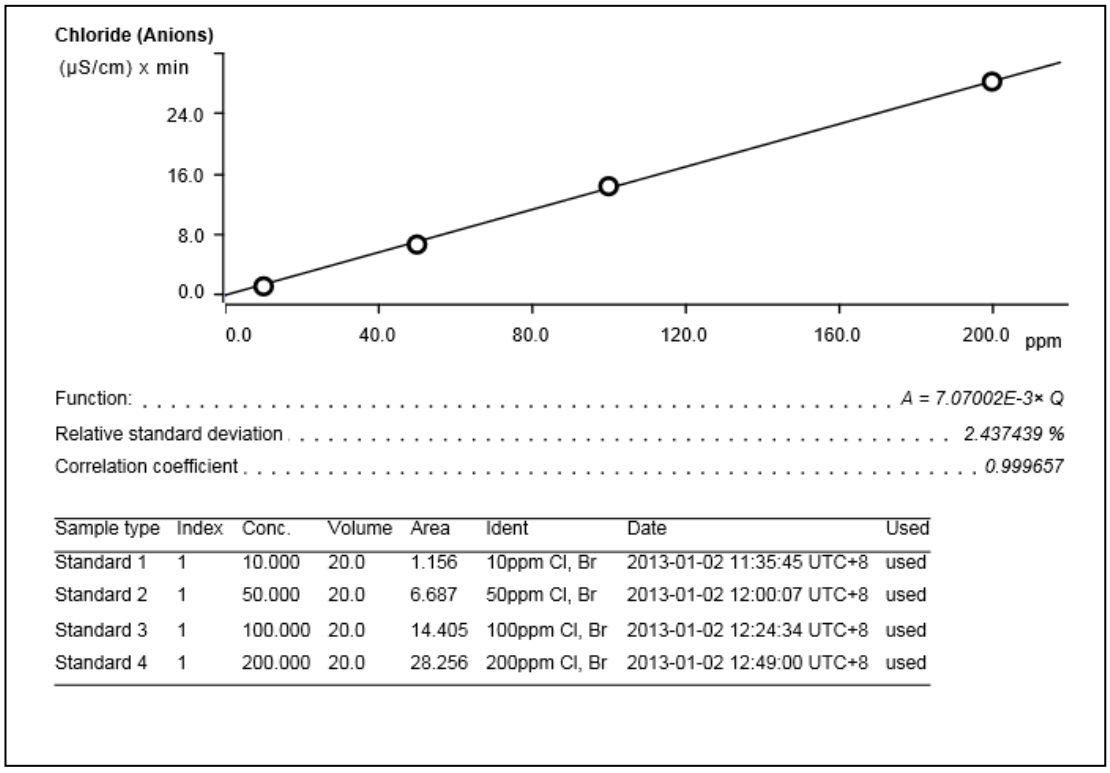

Function: . . . . . A = 7.07002E-3× Q

Relative standard deviation . . . . . 2.437439 %

Correlation coefficient 0.999657

Sample type	Index	Conc.	Volume	Area	Ident	Date	Used
Standard 1	1	10.000	20.0	1.156	10ppm Cl, Br	2013-01-02 11:35:45 UTC+8	used
Standard 2	1	50.000	20.0	6.687	50ppm Cl, Br	2013-01-02 12:00:07 UTC+8	used
Standard 3	1	100.000	20.0	14.405	100ppm Cl, Br	2013-01-02 12:24:34 UTC+8	used
Standard 4	1	200.000	20.0	28.256	200ppm Cl, Br	2013-01-02 12:49:00 UTC+8	used

Fig B-14 Calibration curve for ion chromatography

APPENDIX C

TGA AND DSC THERMOGRAM

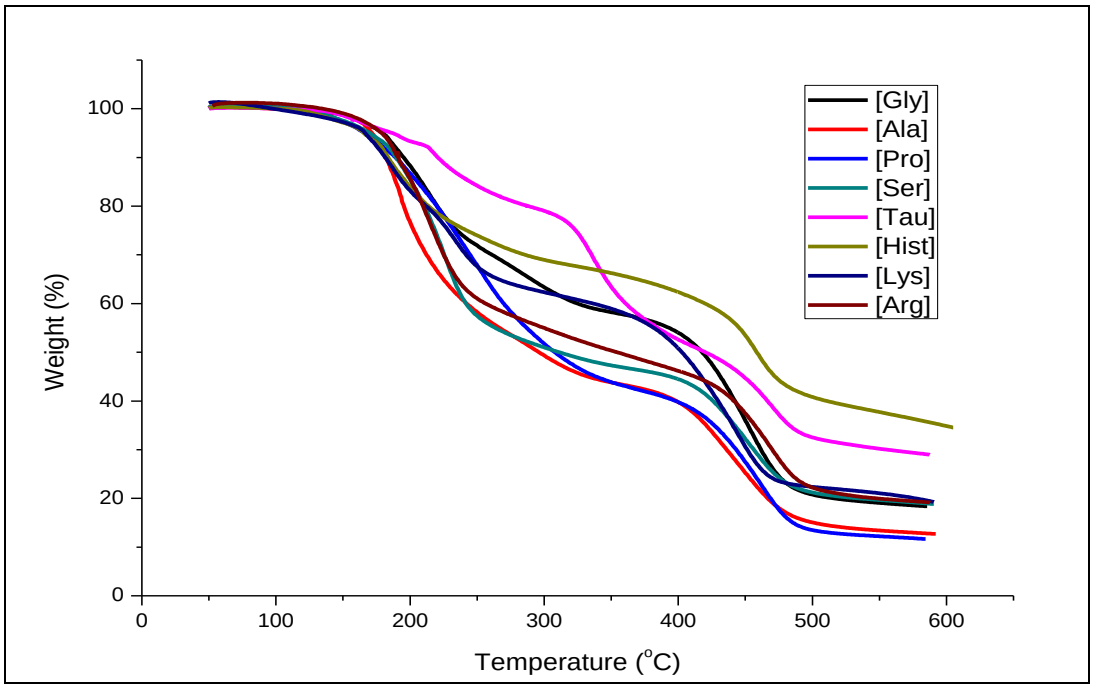

Fig. C-1. TGA thermogram on AAILs with different anions and fixed cation [VBTMA]

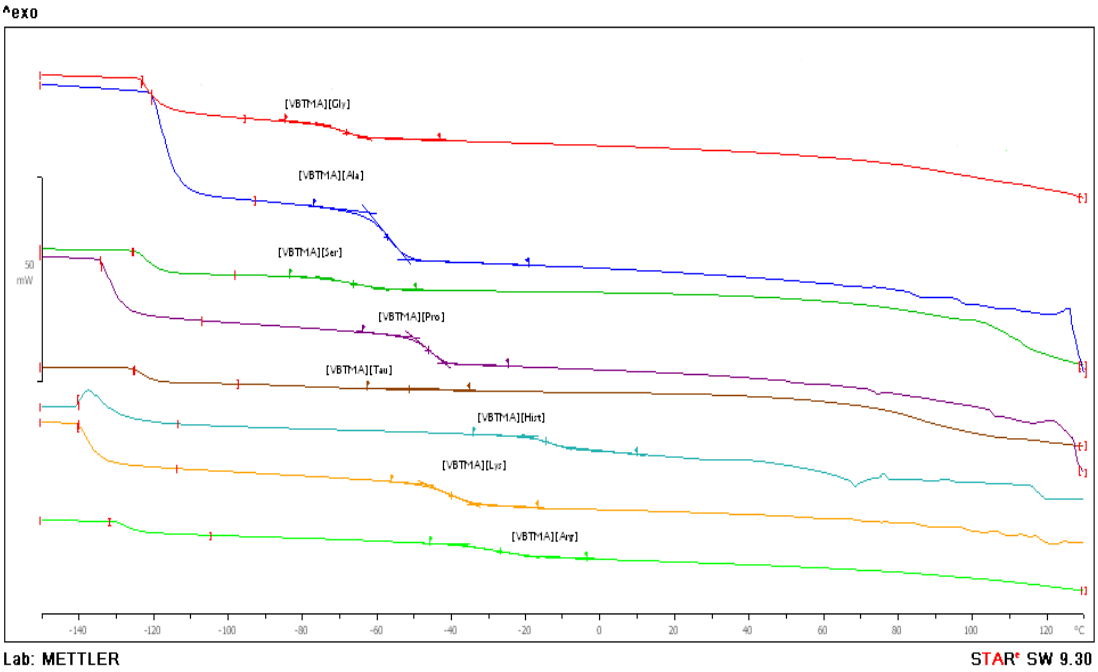

Fig. C-2. DSC Thermogram on AAILs with different anions and fixed cation, [VBTMA]

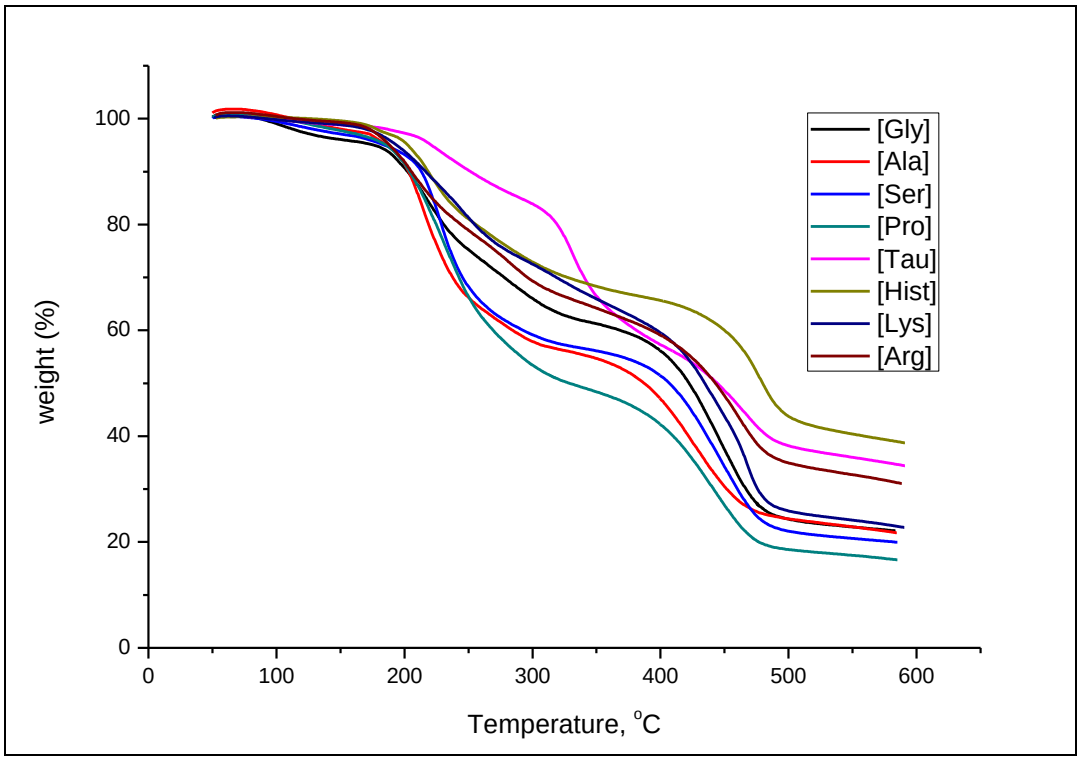

Fig. C-3. TGA thermogram on AAPILs with different anions and fixed [VBTMA] cation

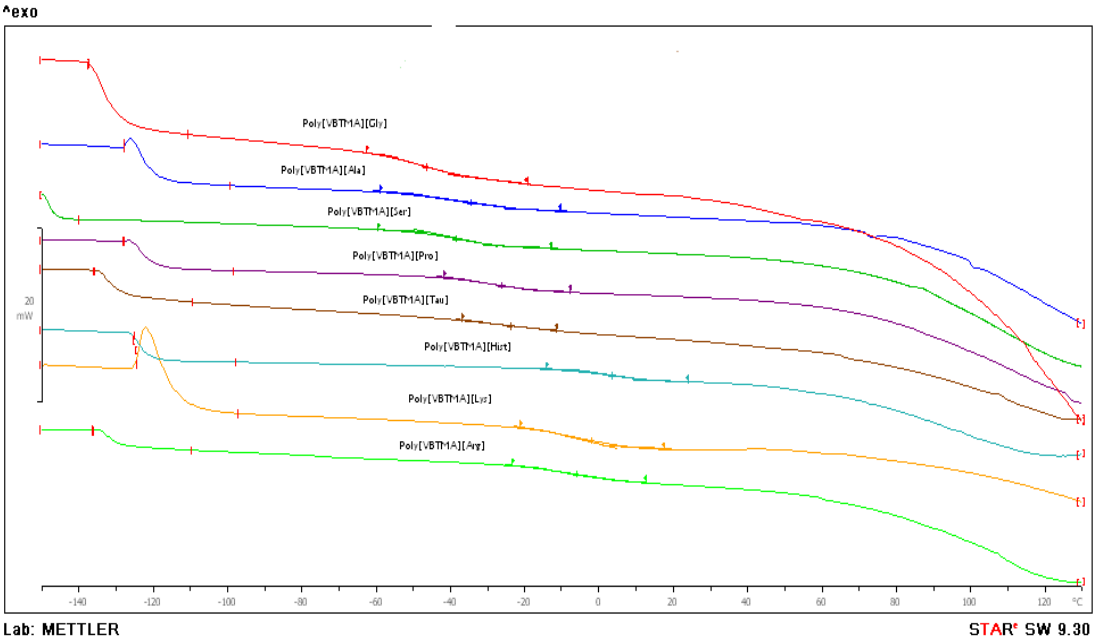

Fig. C-4. DSC thermogram on AAPILs with different anions and fixed cation

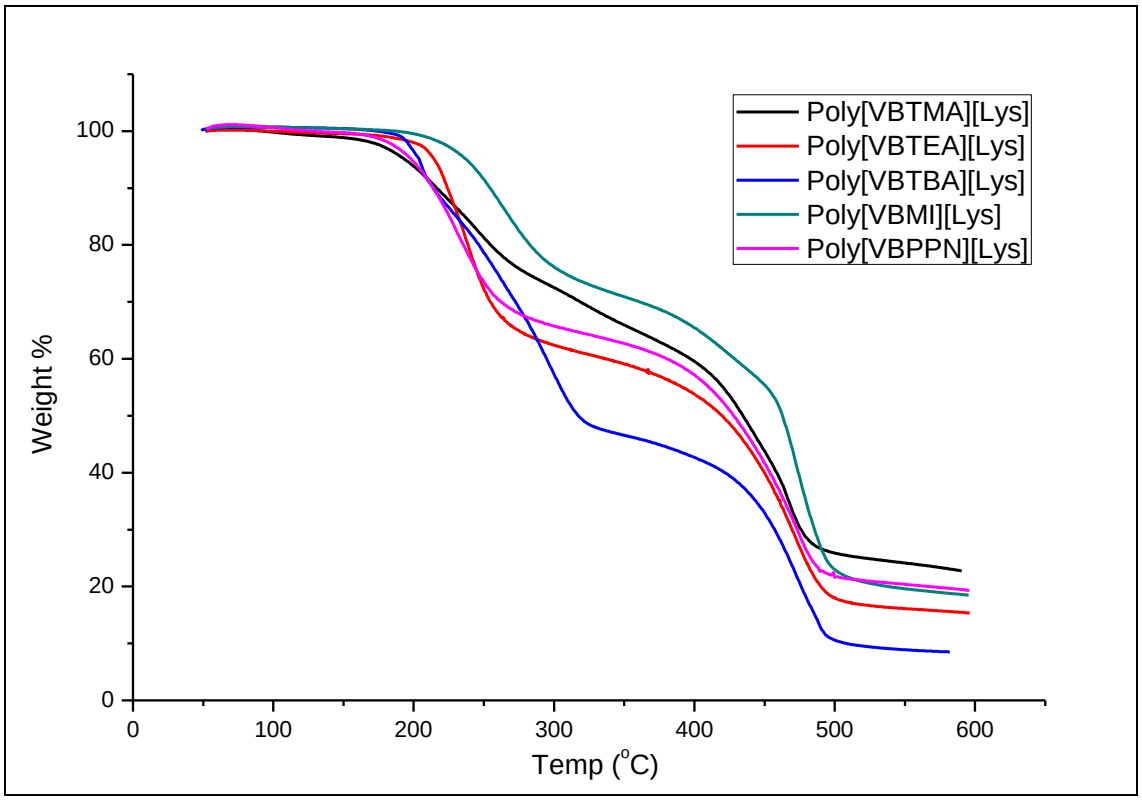

Fig. C-5. TGA thermogram on AAPILs with different cations and fixed anion

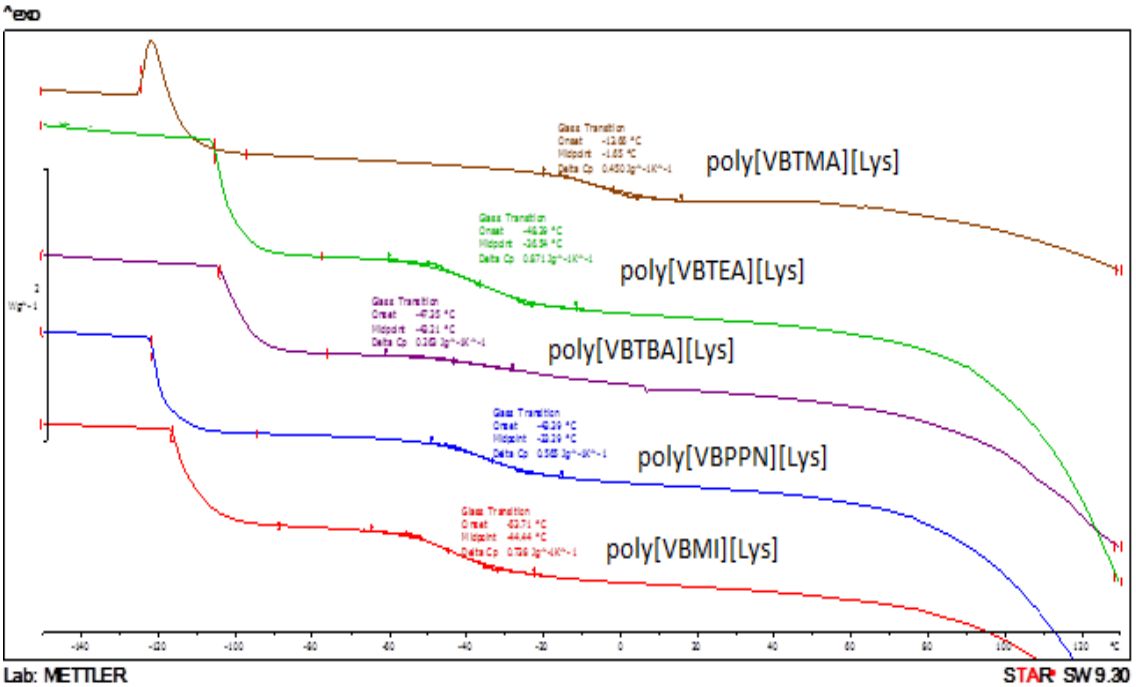

Fig. C-6. DSC thermogram on AAPILs with different cations and fixed anion

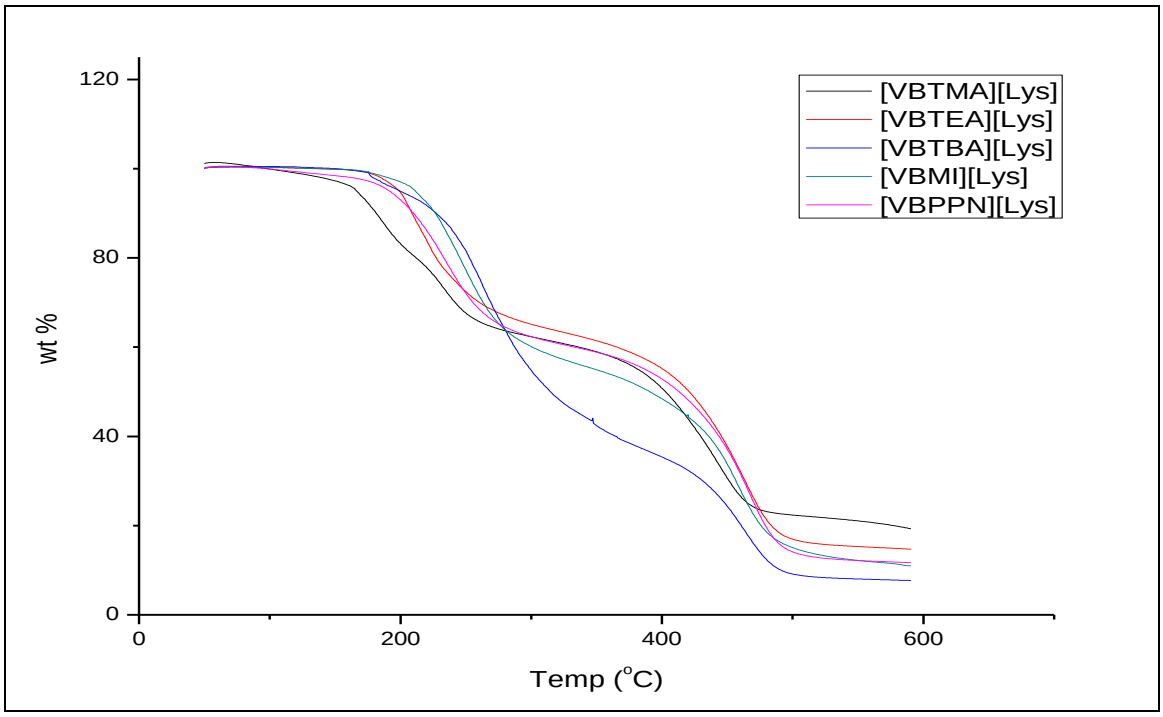

Fig. C-7. TGA thermogram on AAILs with different cation and fixed anion

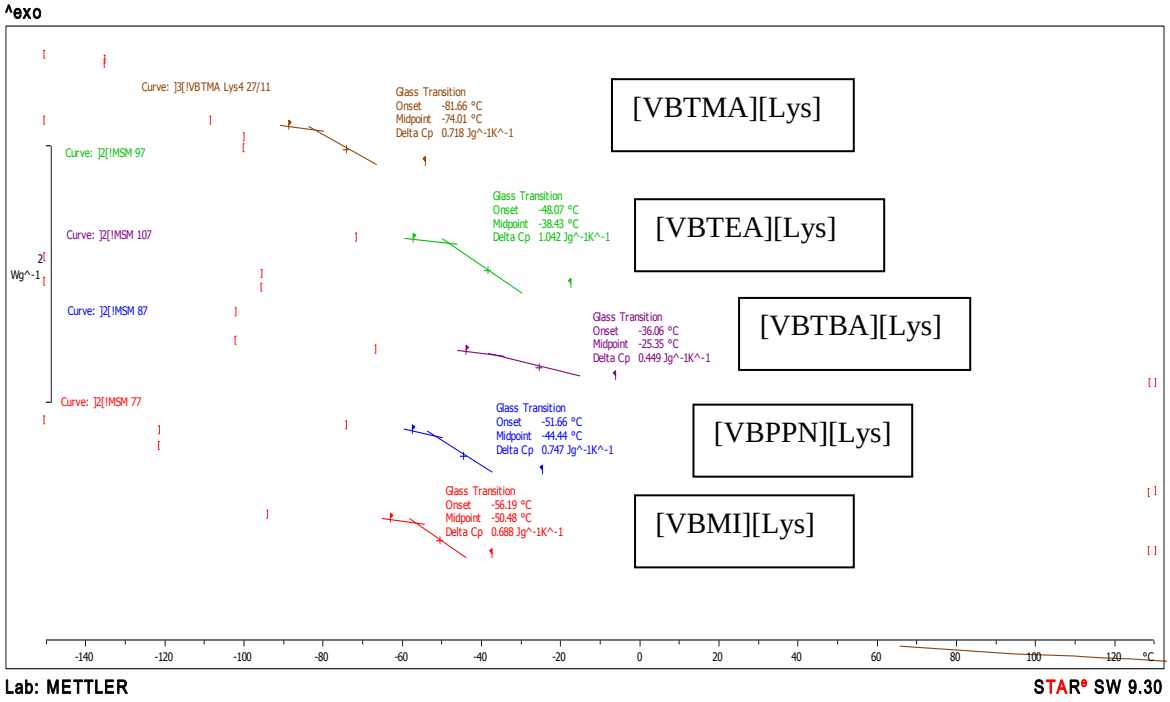

Fig C-8. DSC thermogram on AAILs with different cations and fixed anion

APPENDIX D

SEM MICROGRAPHS

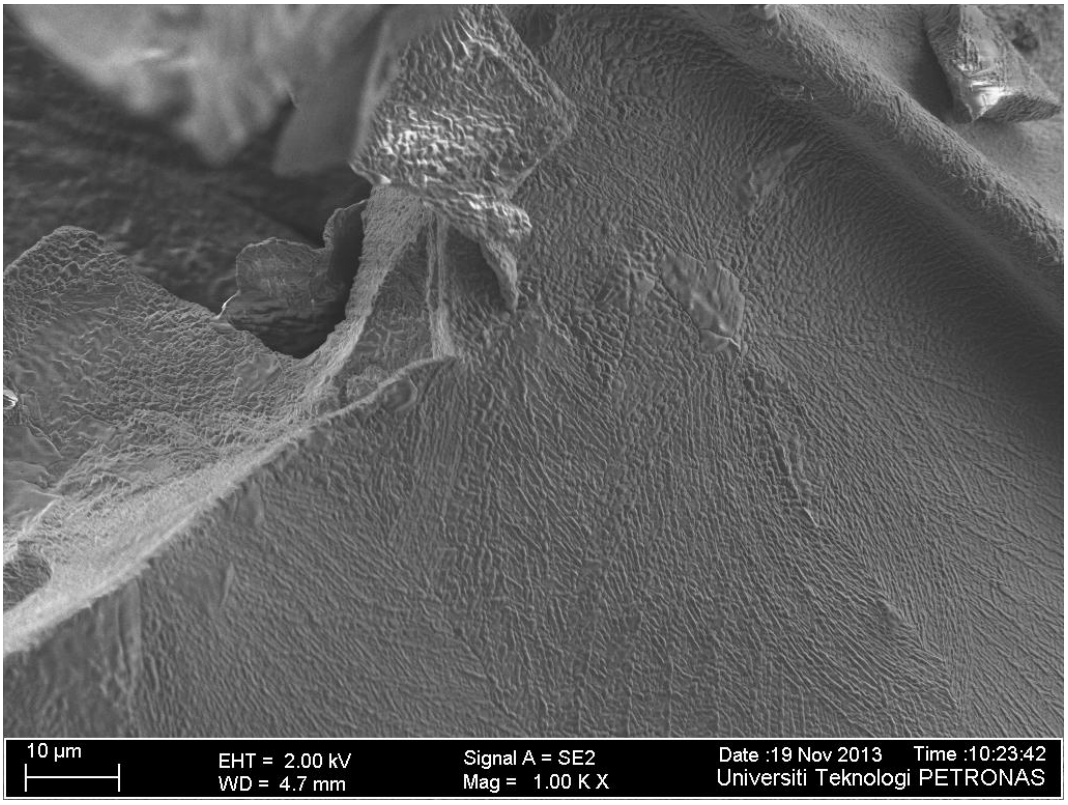

Fig. D-1. SEM micrograph for poly[VBTMA][Gly]

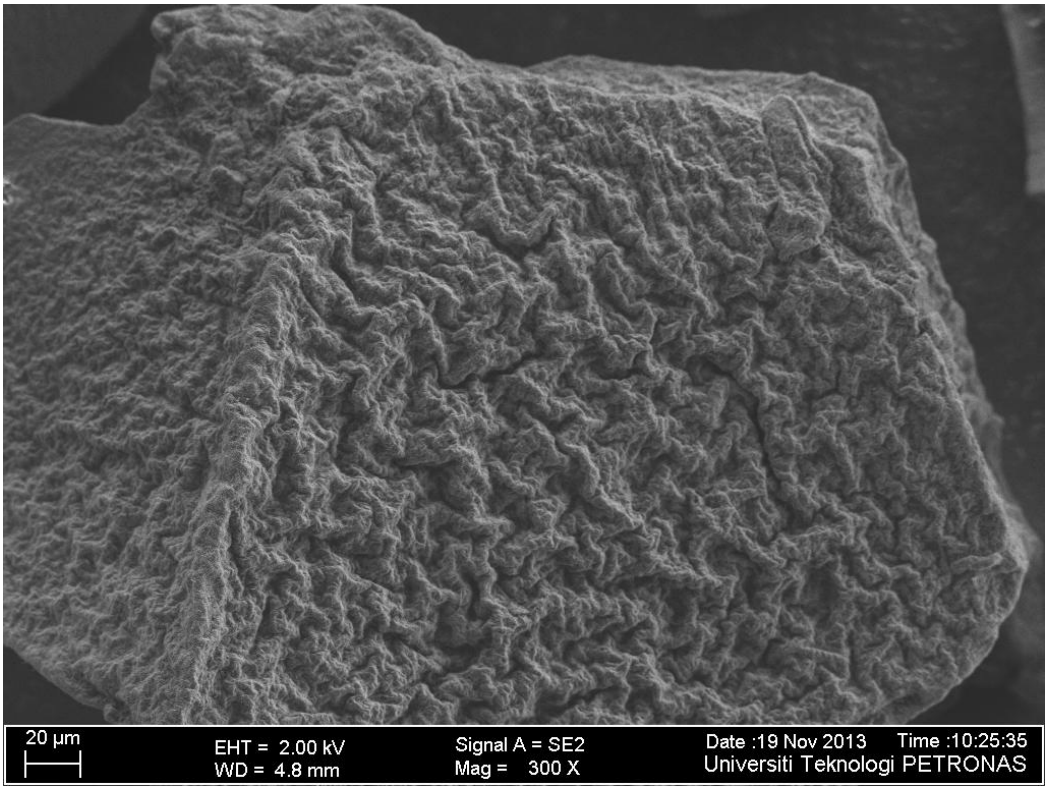

Fig. D-2. SEM micrograph for poly[VBTMA][Ala]

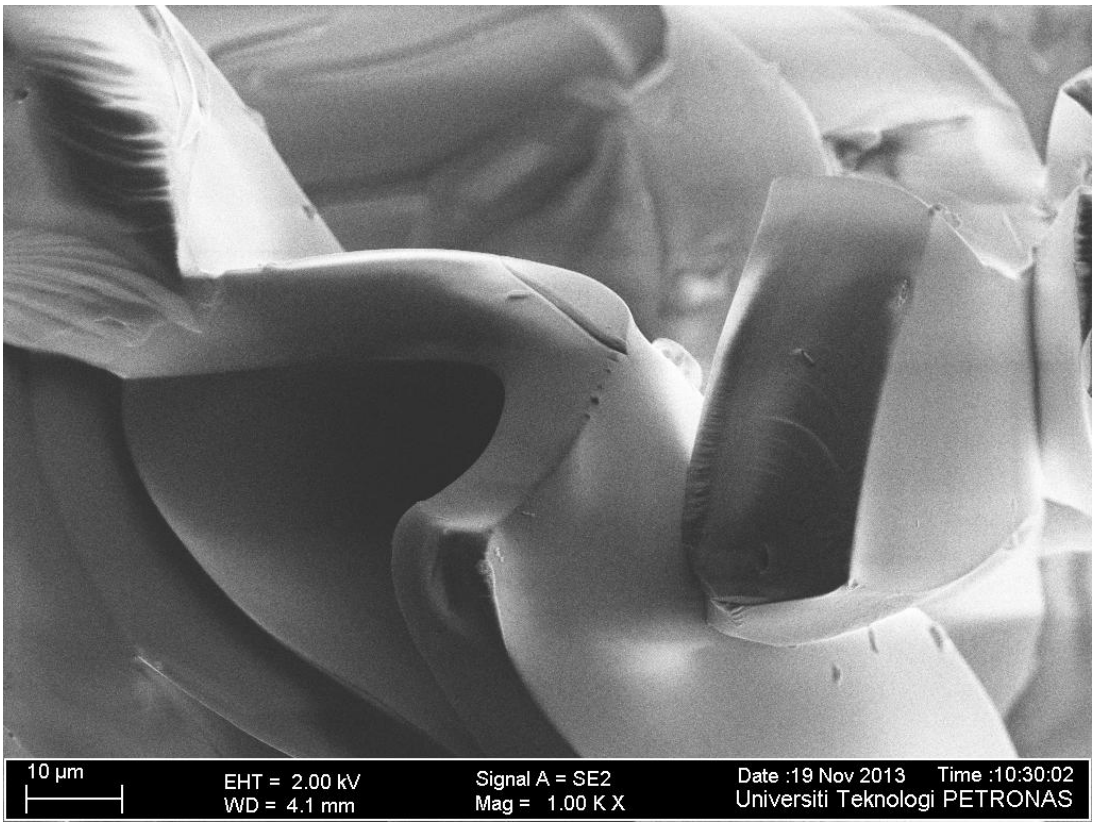

Fig. D-3. SEM micrograph for poly[VBTMA][Ser]

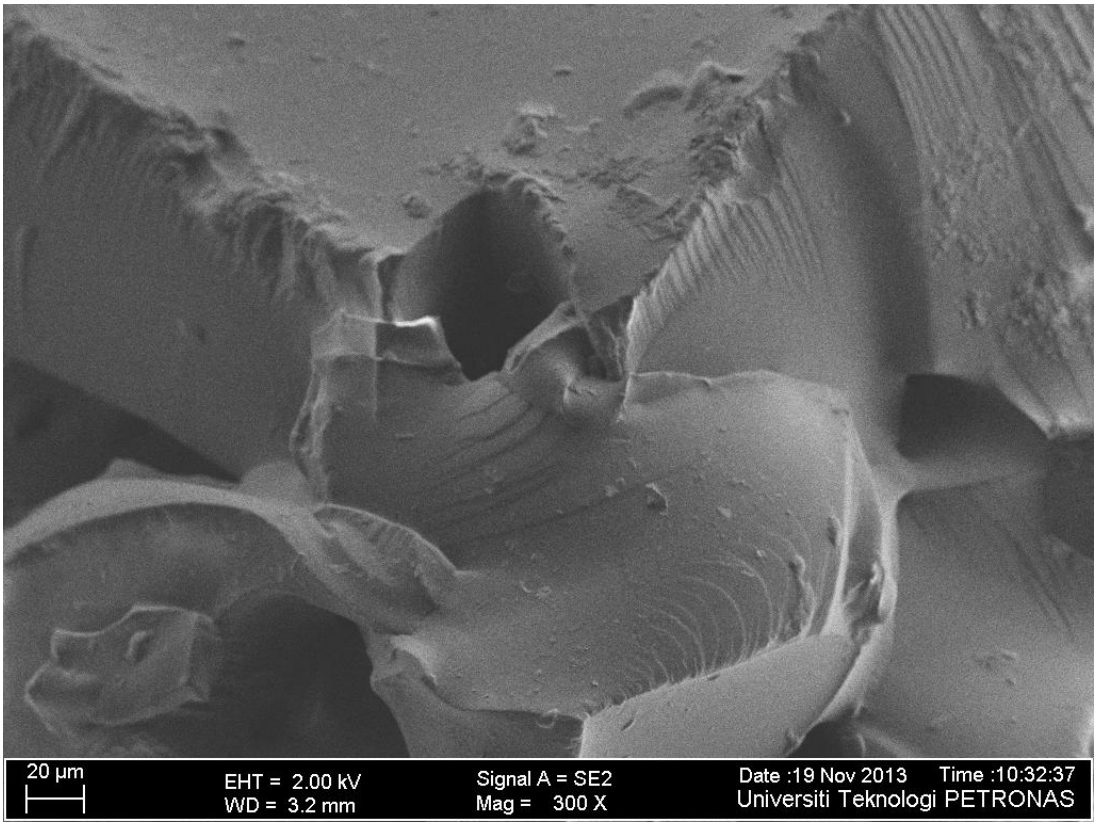

Fig. D-4. SEM micrograph for poly[VBTMA][Pro]

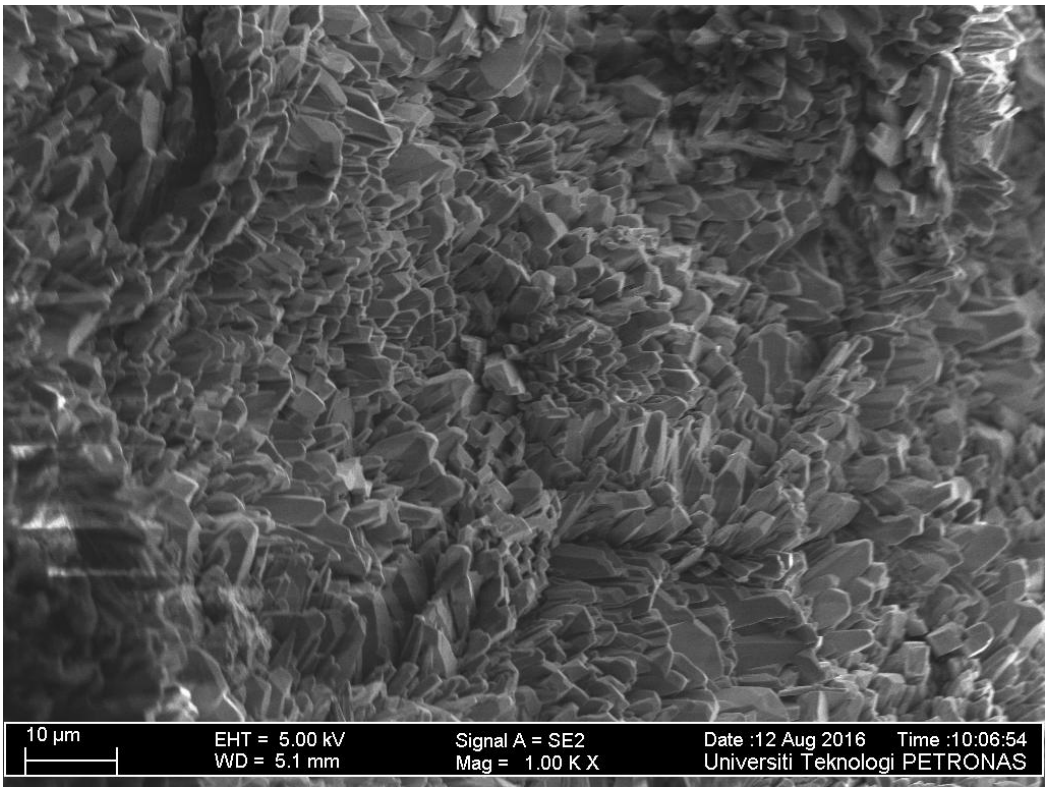

Fig. D-5. SEM micrograph for poly[VBTMA][Tau]

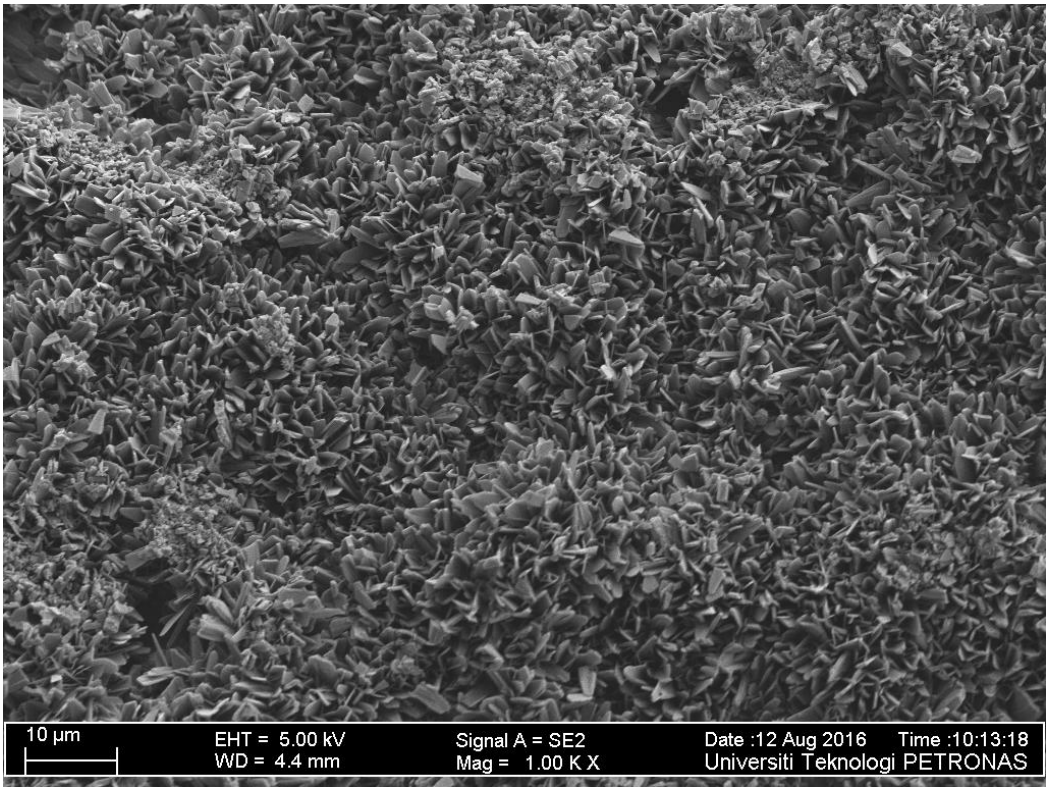

Fig. D-6. SEM micrograph for poly[VBTMA][Hist]

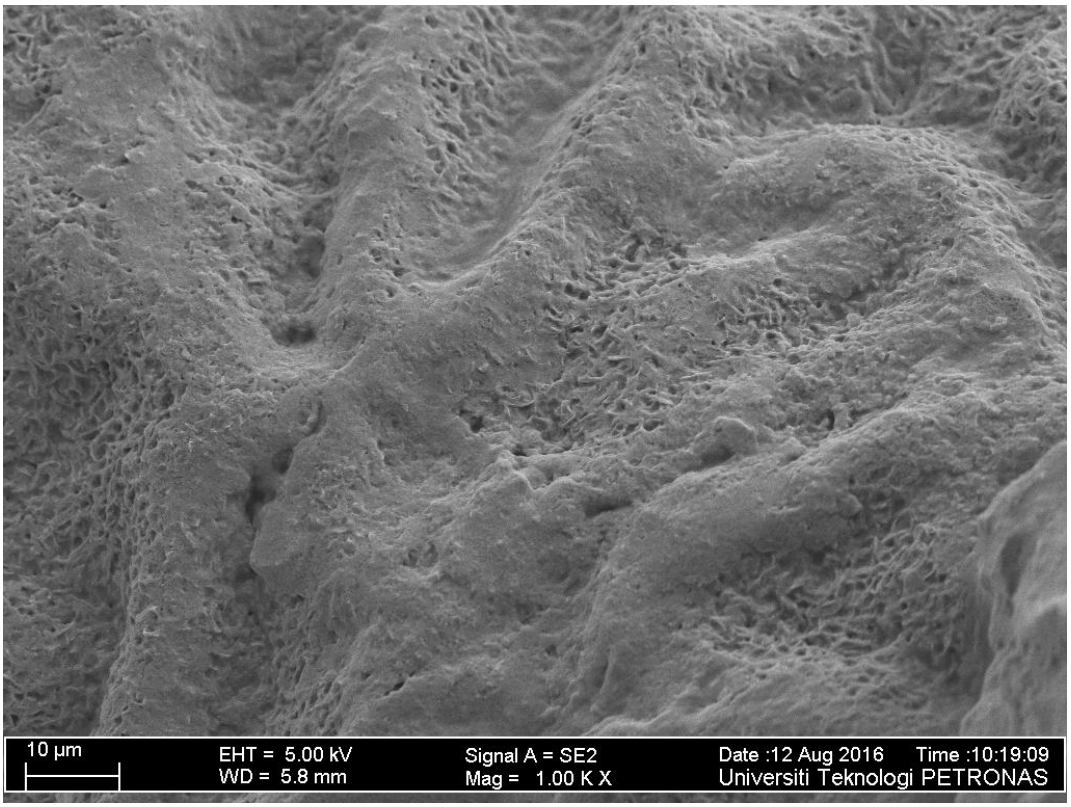

Fig. D-7. SEM micrograph for poly[VBTMA][Lys]

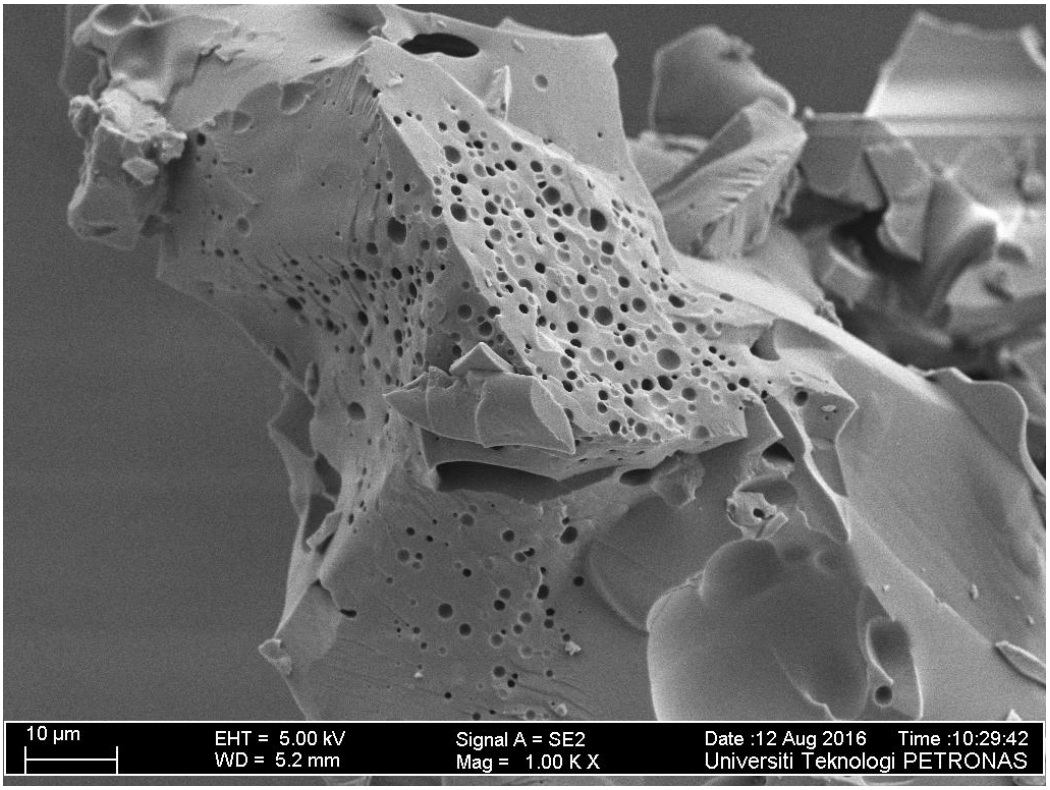

Fig. D-8. SEM micrograph for poly[VBTMA][Arg]

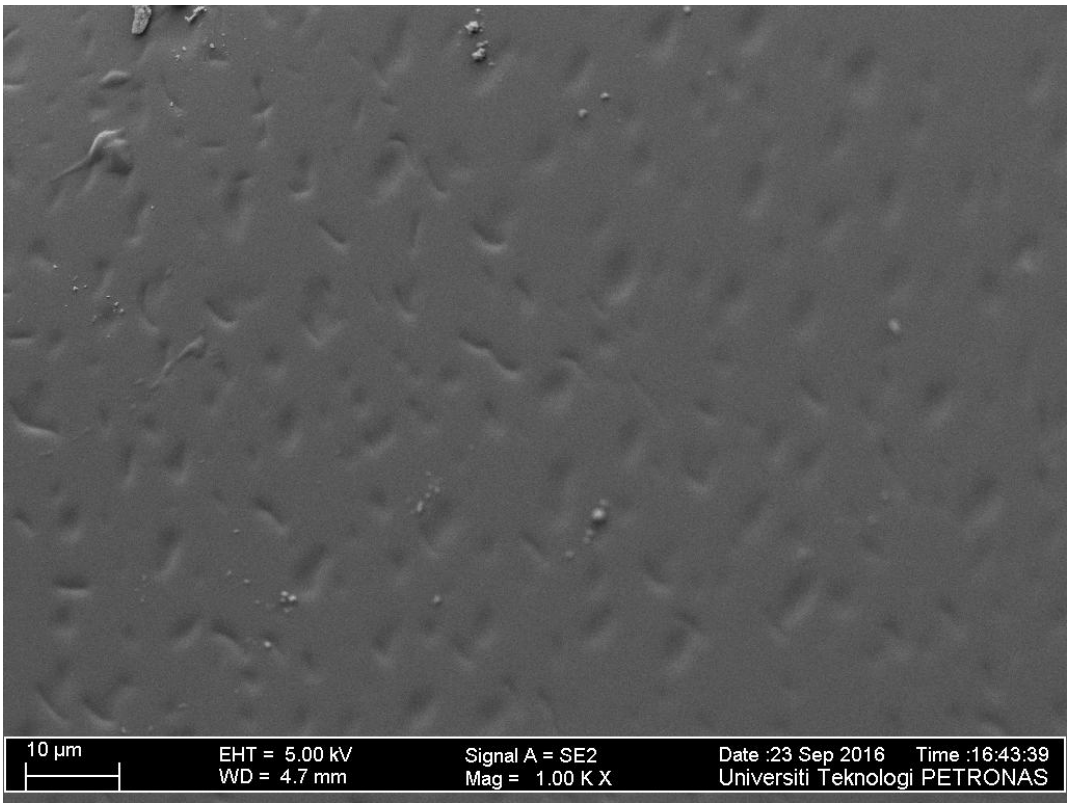

Fig. D-9. SEM micrograph for poly[VBMI][Lys]

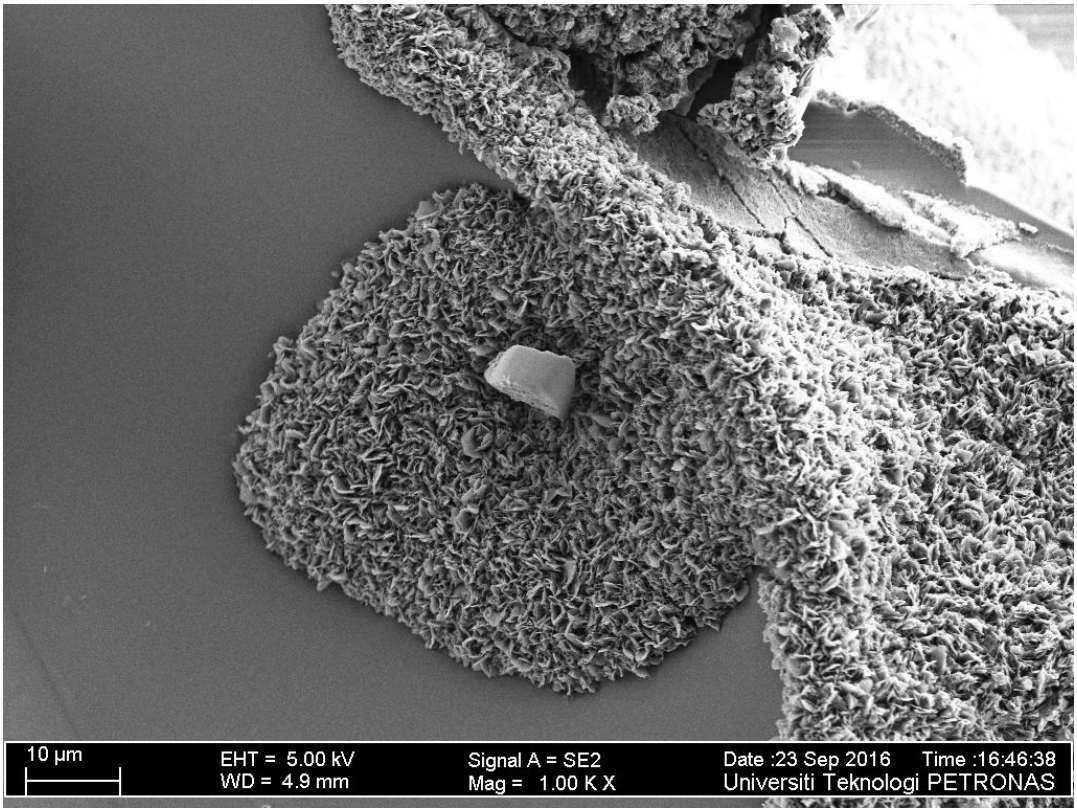

Fig. D-10. SEM micrograph for poly[VBPPN][Lys]

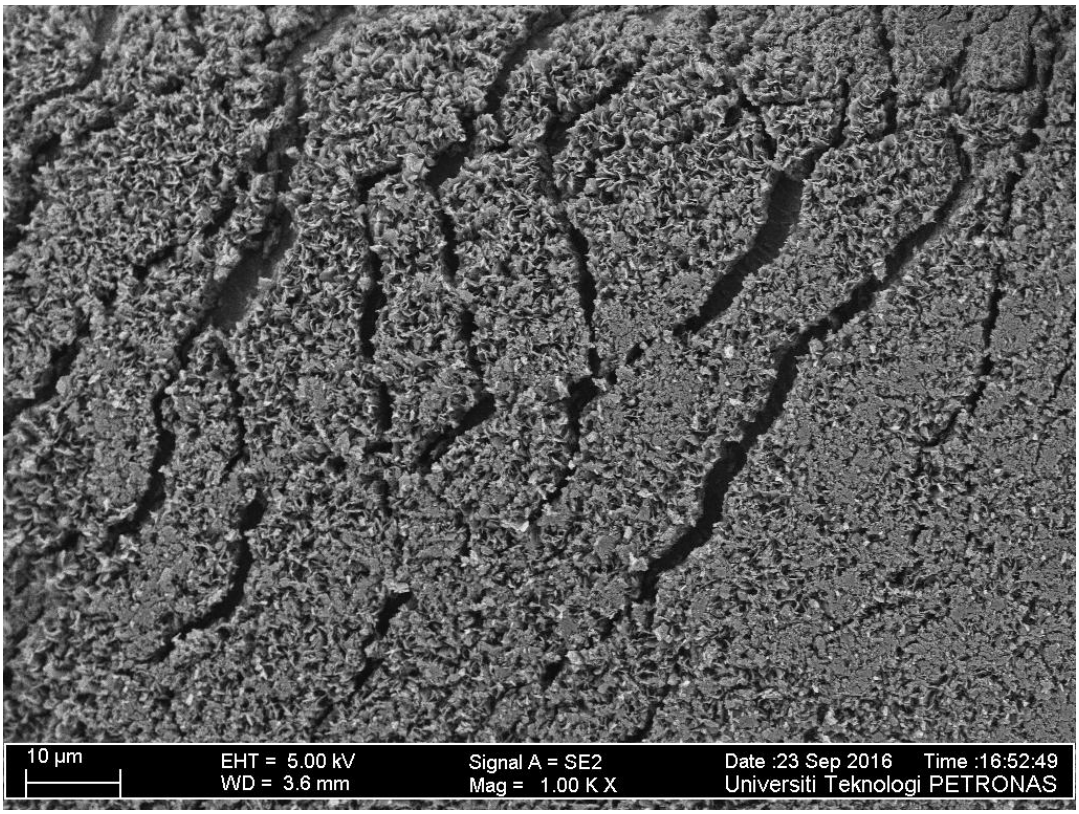

Fig. D-11. SEM micrograph for poly[VBTEA][Lys]

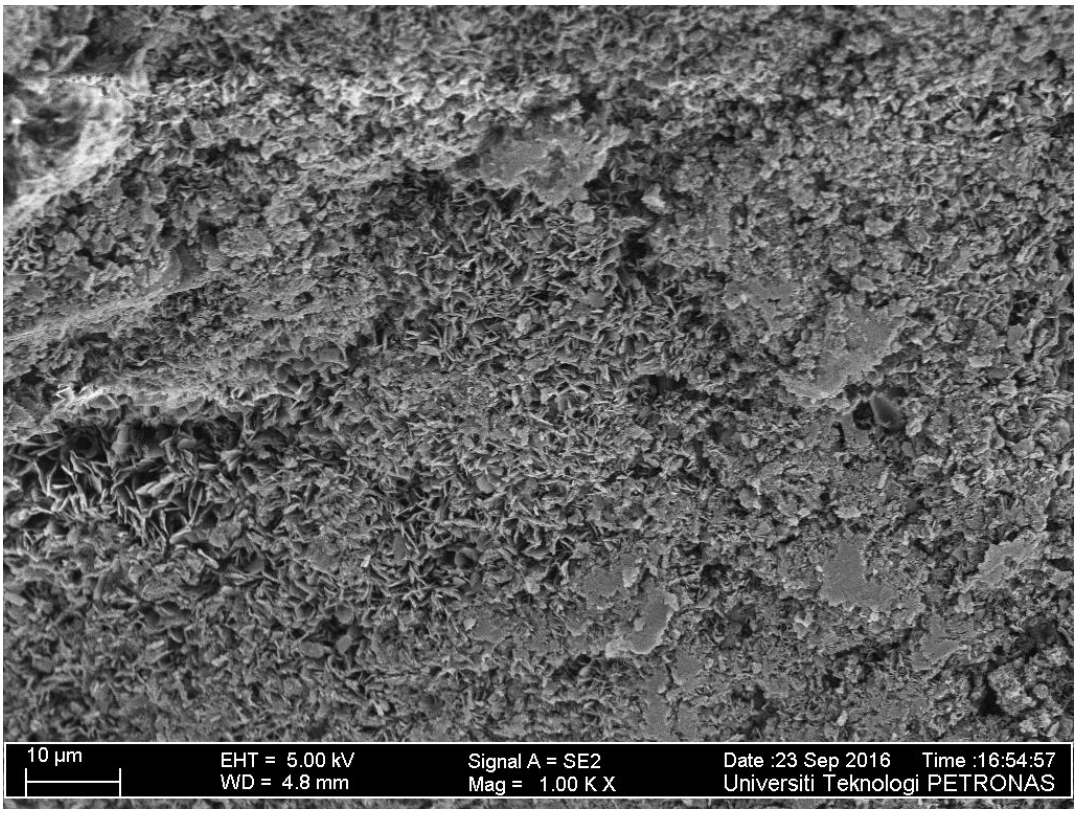

Fig. D-12. SEM micrograph for poly[VBTBA][Lys]

APPENDIX E

CO_2 SORPTION DATA

Table E-1. CO_2 sorption on poly[VBTMA][Gly], 1 bar, 298 K

Time (min)	P (bar)	P (atm)	Zeq	mol	mol/mol
0	0	0	0	0	0
5	0.75	0.74025	0.9958	5.47E-06	0.022789
13	0.74	0.73038	0.9959	5.21E-05	0.217103
25	0.73	0.72051	0.9959	9.84E-05	0.409965
38	0.72	0.71064	0.996	0.000145	0.604221
60	0.72	0.71064	0.996	0.000145	0.604221
90	0.72	0.71064	0.996	0.000145	0.604221
120	0.72	0.71064	0.996	0.000145	0.604221
150	0.72	0.71064	0.996	0.000145	0.604221
180	0.72	0.71064	0.996	0.000145	0.604221

Table E-2. CO_2 sorption on poly[VBTMA][Ala], 1 bar, 298 K

Time (min)	P (bar)	P (atm)	Zeq	mol	mol/mol
0	0	0	0	0	0
6	0.75	0.74025	0.9958	4.79E-06	0.018437
14	0.74	0.73038	0.9959	5.14E-05	0.197829
18	0.73	0.72051	0.9959	9.77E-05	0.375881
31	0.72	0.71064	0.996	0.000144	0.55522
60	0.72	0.71064	0.996	0.000144	0.55522
90	0.72	0.71064	0.996	0.000144	0.55522
120	0.72	0.71064	0.996	0.000144	0.55522
150	0.72	0.71064	0.996	0.000144	0.55522
180	0.72	0.71064	0.996	0.000144	0.55522

Table E-3. CO_2 sorption on poly[VBTMA][Ser], 1 bar, 298 K

Time (min)	P (bar)	P (atm)	Zeq	mol	mol/mol
0	0	0	0	0	0
4	0.75	0.74025	0.9958	4.24E-06	0.020197
9	0.74	0.73038	0.9959	5.09E-05	0.242309
18	0.73	0.72051	0.9959	9.72E-05	0.462762
29	0.72	0.71064	0.996	0.000144	0.684808
60	0.72	0.71064	0.996	0.000144	0.684808
90	0.72	0.71064	0.996	0.000144	0.684808
120	0.72	0.71064	0.996	0.000144	0.684808
150	0.72	0.71064	0.996	0.000144	0.684808
180	0.72	0.71064	0.996	0.000144	0.684808
210	0.72	0.71064	0.996	0.000144	0.684808
240	0.72	0.71064	0.996	0.000144	0.684808

Table E-4 CO_2 sorption on poly[VBTMA][Pro] , 1 bar, 298 K

Time (min)	P (bar)	P (atm)	Zeq	mol	mol/mol
0	0	0	0	0	0
6	0.75	0.74025	0.9958	8.69E-06	0.036205
18	0.74	0.73038	0.9959	5.53E-05	0.230429
26	0.73	0.72051	0.9959	0.000102	0.423201
31	0.72	0.71064	0.996	0.000148	0.617367
60	0.72	0.71064	0.996	0.000148	0.617367
90	0.72	0.71064	0.996	0.000148	0.617367
120	0.72	0.71064	0.996	0.000148	0.617367
150	0.72	0.71064	0.996	0.000148	0.617367
180	0.72	0.71064	0.996	0.000148	0.617367
210	0.72	0.71064	0.996	0.000148	0.617367

Table E-5. CO_2 sorption on poly[VBTMA][Tau], 1 bar, 298 K

Time (min)	P (bar)	P (atm)	Zeq	mol	mol/mol
0	0	0	0	0	0
7	0.75	0.74025	0.9958	5.18E-06	0.01725
12	0.74	0.73038	0.9959	5.18E-05	0.172708
21	0.73	0.72051	0.9959	9.81E-05	0.327003
32	0.72	0.71064	0.996	0.000145	0.482414
52	0.72	0.71064	0.996	0.000145	0.482414
80	0.71	0.70077	0.9961	0.000191	0.637794
120	0.71	0.70077	0.9961	0.000191	0.637794
150	0.71	0.70077	0.9961	0.000191	0.637794
180	0.71	0.70077	0.9961	0.000191	0.637794
210	0.71	0.70077	0.9961	0.000191	0.637794
240	0.71	0.70077	0.9961	0.000191	0.637794
270	0.71	0.70077	0.9961	0.000191	0.637794
300	0.71	0.70077	0.9961	0.000191	0.637794

Table E-6. CO_2 sorption on poly[VBTMA][Hist], 1 bar, 298 K

Time (min)	P (bar)	P (atm)	Zeq	mol	mol/mol
0	0	0	0	0	0
4	0.75	0.74025	0.9958	6.85E-06	0.028556
11	0.75	0.74025	0.9958	6.85E-06	0.028556
22	0.74	0.73038	0.9959	5.35E-05	0.222831
31	0.73	0.72051	0.9959	9.98E-05	0.415654
55	0.72	0.71064	0.996	0.000146	0.609871
87	0.72	0.71064	0.996	0.000146	0.609871
99	0.71	0.70077	0.996	0.000193	0.802674
150	0.71	0.70077	0.996	0.000193	0.802674
180	0.71	0.70077	0.9961	0.000193	0.804048
210	0.71	0.70077	0.9961	0.000193	0.804048
240	0.71	0.70077	0.9961	0.000193	0.804048
270	0.71	0.70077	0.9961	0.000193	0.804048
300	0.71	0.70077	0.9961	0.000193	0.804048

Table E-7. CO_2 sorption on Poly[VBTMA][Lys], 1 bar, 298 K

Time (min)	P (bar)	P (atm)	Zeq	mol	mol/mol
0	0	0	0	0	0
7	0.75	0.74025	0.9958	5.86E-06	0.023426
13	0.75	0.74025	0.9958	5.86E-06	0.023426
25	0.74	0.73038	0.9959	5.25E-05	0.209957
33	0.73	0.72051	0.9959	9.88E-05	0.395094
52	0.72	0.71064	0.996	0.000145	0.581569
71	0.71	0.70077	0.996	0.000192	0.766687
92	0.7	0.6909	0.9961	0.000238	0.953106
100	0.69	0.68103	0.9962	0.000285	1.139488
150	0.69	0.68103	0.9962	0.000285	1.139488
210	0.69	0.68103	0.9962	0.000285	1.139488
240	0.69	0.68103	0.9962	0.000285	1.139488
270	0.69	0.68103	0.9962	0.000285	1.139488
300	0.69	0.68103	0.9962	0.000285	1.139488

Table E-8. CO_2 sorption on Poly[VBTMA][Arg], 1 bar, 298 K

Time (min)	P(bar)	P(atm)	Zeq	mol	mol/mol
0	0	0	0	0	0
6	0.75	0.74025	0.9958	7.97E-06	0.046871
12	0.75	0.74025	0.9958	7.97E-06	0.046871
26	0.74	0.73038	0.9959	5.46E-05	0.321098
52	0.73	0.72051	0.9959	0.000101	0.593276
63	0.73	0.72051	0.9959	0.000101	0.593276
90	0.72	0.71064	0.996	0.000147	0.867421
102	0.72	0.71064	0.996	0.000147	0.867421
110	0.71	0.70077	0.9961	0.000194	1.141511
180	0.71	0.70077	0.9961	0.000194	1.141511
210	0.71	0.70077	0.9961	0.000194	1.141511
240	0.71	0.70077	0.9961	0.000194	1.141511
270	0.71	0.70077	0.9961	0.000194	1.141511
300	0.71	0.70077	0.9961	0.000194	1.141511

Table E-9 CO_2 sorption on monomers, AAILs, 1 bar, 298 K

Time (min)	[VBTMA][Gly]		[VBTMA][Ala]		[VBTMA][Ser]		[VBTMA][Pro]	
	mol	mol/mol	mol	mol/mol	mol	mol/mol	mol	Mol/mol
0	0	0	0	0	0	0	0	0
5	3.21E-06	0.008039	2.67E-05	0.022049	3.58E-06	0.014331	3.49E-06	0.009208
10	4.99E-05	0.124808	7.33E-05	0.060541	5.02E-05	0.201142	5.01E-05	0.132321
20	9.65E-05	0.241553	7.33E-05	0.060541	5.02E-05	0.201142	9.64E-05	0.254513
30	0.000143	0.357438	0.000119	0.098745	9.65E-05	0.386557	0.000143	0.377589
60	0.000189	0.474148	0.000166	0.137226	9.65E-05	0.386557	0.000143	0.377589
90	0.000189	0.474148	0.000213	0.175699	9.65E-05	0.386557	0.000143	0.377589
120	0.000189	0.474148	0.000213	0.175699	9.65E-05	0.386557	0.000143	0.377589
150	0.000189	0.474148	0.000213	0.175699	9.65E-05	0.386557	0.000143	0.377589
180	0.000189	0.474148	0.000259	0.213895	9.65E-05	0.386557	0.000143	0.377589
210	0.000189	0.474148	0.000259	0.213895	9.65E-05	0.386557	0.000143	0.377589
240	0.000189	0.474148	0.000259	0.213895	9.65E-05	0.386557	0.000143	0.377589
270	0.000189	0.474148	0.000305	0.252356	9.65E-05	0.386557	0.000143	0.377589
300	0.000189	0.474148	0.000305	0.252356	9.65E-05	0.386557	0.000143	0.377589

Table E-10 CO_2 sorption on monomer AAILs, 1 bar, 298 K

	[VBTMA][Tau]		[VBTMA][Hist]		[VBTMA][Lys]		[VBTMA][Arg]	
Time (min)	mol	Mol/mol	mol	Mol/mol	mol	Mol/mol	mol	mol/mol
	0	0	0	0	0	0	0	0
0	5.94E-06	0.013723	4.13E-06	0.019492	4.497E-06	0.0206484	3.18E-06	0.018503
5	5.26E-05	0.121463	4.13E-06	0.019492	5.114E-05	0.2347933	4.98E-05	0.290185
10	9.89E-05	0.228397	5.08E-05	0.23961	9.743E-05	0.4473373	9.61E-05	0.559836
20	0.000145	0.336104	5.08E-05	0.23961	9.743E-05	0.4473373	9.61E-05	0.559836
30	0.000192	0.443789	5.08E-05	0.23961	9.743E-05	0.4473373	9.61E-05	0.559836
60	0.000192	0.443789	9.71E-05	0.458084	0.0001441	0.6614178	0.000143	0.831436
90	0.000192	0.443789	9.71E-05	0.458084	0.0001441	0.6614178	0.000143	0.831436
120	0.000192	0.443789	9.71E-05	0.458084	0.0001441	0.6614178	0.000143	0.831436
150	0.000192	0.443789	9.71E-05	0.458084	0.0001441	0.6614178	0.000143	0.831436
180	0.000192	0.443789	9.71E-05	0.458084	0.0001441	0.6614178	0.000143	0.831436
210	0.000192	0.443789	9.71E-05	0.458084	0.0001441	0.6614178	0.000143	0.831436
240	0.000192	0.443789	9.71E-05	0.458084	0.0001441	0.6614178	0.000143	0.831436
270	0.000192	0.443789	9.71E-05	0.458084	0.0001441	0.6614178	0.000143	0.831436

Table E-11 CO_2 sorption on poly[VBTMA][Arg], 3 bar, 298 K

Time (min)	P (bar)	P (atm)	Zeq	mol	mol/mol
0	0	0	0	0	0
5	2.3	2.2701	0.9872	-6.87515E-05	-0.40442
10	2.29	2.26023	0.9872	-2.26883E-05	-0.13346
18	2.28	2.25036	0.9873	2.44387E-05	0.143757
22	2.27	2.24049	0.9874	7.15562E-05	0.420919
33	2.26	2.23062	0.9874	0.00011761	0.691824
46	2.26	2.23062	0.9874	0.00011761	0.691824
57	2.25	2.22075	0.9875	0.000164713	0.968902
68	2.25	2.22075	0.9875	0.000164713	0.968902
79	2.25	2.22075	0.9875	0.000164713	0.968902
88	2.24	2.21088	0.9875	0.000210763	1.23978
97	2.24	2.21088	0.9875	0.000210763	1.23978
102	2.24	2.21088	0.9875	0.000210763	1.23978
110	2.23	2.20101	0.9876	0.000257852	1.516774
150	2.23	2.20101	0.9876	0.000257852	1.516774
200	2.23	2.20101	0.9876	0.000257852	1.516774
250	2.23	2.20101	0.9876	0.000257852	1.516774

Table E-12 CO_2 sorption on poly[VBTMA][Arg], 5 bar, 298 K

Time (min)	P (bar)	P (atm)	Zeq	mol	mol/mol
0	0	0	0	0	0
7	3.84	3.79008	0.9785	3.45779E-05	0.246985
10	3.83	3.78021	0.9786	8.23753E-05	0.588395
15	3.83	3.78021	0.9786	8.23753E-05	0.588395
20	3.82	3.77034	0.9786	0.000128368	0.916914
28	3.82	3.77034	0.9786	0.000128368	0.916914
35	3.82	3.77034	0.9786	0.000128368	0.916914
40	3.82	3.77034	0.9786	0.000128368	0.916914
48	3.82	3.77034	0.9786	0.000128368	0.916914
50	3.81	3.76047	0.9787	0.000176151	1.258221
55	3.81	3.76047	0.9787	0.000176151	1.258221
60	3.81	3.76047	0.9787	0.000176151	1.258221

69	3.81	3.76047	0.9787	0.000176151	1.258221
74	3.81	3.76047	0.9787	0.000176151	1.258221
81	3.81	3.76047	0.9787	0.000176151	1.258221
89	3.8	3.7506	0.9787	0.000222139	1.586706
97	3.8	3.7506	0.9787	0.000222139	1.586706
101	3.8	3.7506	0.9787	0.000222139	1.586706
106	3.8	3.7506	0.9787	0.000222139	1.586706
110	3.8	3.7506	0.9787	0.000222139	1.586706
150	3.79	3.74073	0.9788	0.000269907	1.92791
200	3.79	3.74073	0.9788	0.000269907	1.92791
250	3.79	3.74073	0.9788	0.000269907	1.92791
300	3.79	3.74073	0.9788	0.000269907	1.92791

Table E-13 CO_2 sorption on Poly[VBTMA][Arg], 7 bar, 298 K

Time (min)	P (bar)	P (atm)	Zeq	mol	mol/mol
0	0	0	0	0	0
5	5.43	5.35941	0.9695	-4.79573E-05	-0.43598
10	5.42	5.34954	0.9695	-1.81604E-06	-0.01651
20	5.41	5.33967	0.9696	4.68997E-05	0.426361
35	5.4	5.3298	0.9696	9.30362E-05	0.845784
40	5.39	5.31993	0.9696	0.000139173	1.265206
45	5.39	5.31993	0.9696	0.000139173	1.265206
50	5.39	5.31993	0.9696	0.000139173	1.265206
57	5.39	5.31993	0.9696	0.000139173	1.265206
60	5.38	5.31006	0.9697	0.000187869	1.707899
70	5.38	5.31006	0.9697	0.000187869	1.707899
75	5.38	5.31006	0.9697	0.000187869	1.707899
88	5.38	5.31006	0.9697	0.000187869	1.707899
90	5.38	5.31006	0.9697	0.000187869	1.707899
100	5.38	5.31006	0.9697	0.000187869	1.707899
110	5.37	5.30019	0.9697	0.000234001	2.127278
130	5.37	5.30019	0.9697	0.000234001	2.127278
150	5.37	5.30019	0.9697	0.000234001	2.127278
200	5.37	5.30019	0.9697	0.000234001	2.127278

Table E-14 CO_2 sorption on Poly[VBTMA][Arg], 10 bar, 298 K

Time (min)	P (bar)	P (atm)	Zeq	mol	mol/mol
0	0	0	0	0	0
5	7.83	7.72821	0.9556	8.63812E-05	0.502801
10	7.81	7.70847	0.9557	0.000182529	1.062452
20	7.8	7.6986	0.9557	0.000228711	1.331265
30	7.79	7.68873	0.9558	0.000278657	1.621987
60	7.77	7.66899	0.9559	0.000374765	2.181404
90	7.76	7.65912	0.956	0.000424685	2.471976
120	7.75	7.64925	0.9561	0.000474595	2.762487
150	7.75	7.64925	0.9561	0.000474595	2.762487
180	7.75	7.64925	0.9561	0.000474595	2.762487
210	7.75	7.64925	0.9561	0.000474595	2.762487
240	7.75	7.64925	0.9561	0.000474595	2.762487
270	7.75	7.64925	0.9561	0.000474595	2.762487
300	7.75	7.64925	0.9561	0.000474595	2.762487

Table E-15 CO_2 sorption on Poly[VBTMA][Lys], 3 bar, 298 K

		3 bar			
Time (min)	P (bar)	P (atm)	Zeq	mol	mol/mol
0	0	0	0	0	0
5	2.32	2.28984	0.9871	-7.97824E-05	-0.51274
10	2.31	2.27997	0.9871	-3.4085E-05	-0.21906
15	2.3	2.2701	0.9872	1.26771E-05	0.081472
20	2.29	2.26023	0.9872	5.83699E-05	0.375128
25	2.29	2.26023	0.9872	5.83699E-05	0.375128
30	2.28	2.25036	0.9873	0.000105118	0.675565
40	2.28	2.25036	0.9873	0.000105118	0.675565
50	2.27	2.24049	0.9874	0.000151856	0.975941
60	2.27	2.24049	0.9874	0.000151856	0.975941
70	2.27	2.24049	0.9874	0.000151856	0.975941
90	2.26	2.23062	0.9874	0.00019754	1.269537
100	2.26	2.23062	0.9874	0.00019754	1.269537
200	2.26	2.23062	0.9874	0.00019754	1.269537
330	2.26	2.23062	0.9874	0.00019754	1.269537

Table E-16 CO_2 sorption on Poly[VBTMA][Lys], 5 bar, 298 K

Time (min)	P (bar)	P (atm)	Zeq	mol	mol/mol
0	0	0	0	0	0
5	3.84	3.79008	0.9785	1.9057E-05	0.122475
10	3.83	3.78021	0.9786	6.68747E-05	0.429786
15	3.82	3.77034	0.9786	0.000112887	0.725492
20	3.81	3.76047	0.9787	0.00016069	1.03271
30	3.81	3.76047	0.9787	0.00016069	1.03271
40	3.8	3.7506	0.9787	0.000206697	1.328387
60	3.8	3.7506	0.9787	0.000206697	1.328387
80	3.8	3.7506	0.9787	0.000206697	1.328387
100	3.79	3.74073	0.9788	0.000254486	1.635512
150	3.79	3.74073	0.9788	0.000254486	1.635512
200	3.79	3.74073	0.9788	0.000254486	1.635512
270	3.79	3.74073	0.9788	0.000254486	1.635512
300	3.79	3.74073	0.9788	0.000254486	1.635512
330	3.79	3.74073	0.9788	0.000254486	1.635512

Table E-17 CO2 sorption on Poly[VBTMA][Lys], 7 bar, 298 K

Time (min)	P (bar)	P (atm)	Zeq	mol	mol/mol
0	0	0	0	0	0
5	5.43	5.35941	0.9695	2.17475E-05	0.174819
10	5.42	5.34954	0.9695	6.77347E-05	0.544491
20	5.41	5.33967	0.9696	0.000116288	0.934789
35	5.41	5.33967	0.9696	0.000116288	0.934789
50	5.4	5.3298	0.9696	0.00016227	1.304423
55	5.4	5.3298	0.9696	0.00016227	1.304423
60	5.4	5.3298	0.9696	0.00016227	1.304423
70	5.39	5.31993	0.9696	0.000208253	1.674056
80	5.39	5.31993	0.9696	0.000208253	1.674056
100	5.39	5.31993	0.9696	0.000208253	1.674056
120	5.38	5.31006	0.9697	0.000256786	2.064197
170	5.38	5.31006	0.9697	0.000256786	2.064197
200	5.38	5.31006	0.9697	0.000256786	2.064197
330	5.38	5.31006	0.9697	0.000256786	2.064197
360	5.38	5.31006	0.9697	0.000256786	2.064197
390	5.38	5.31006	0.9697	0.000256786	2.064197

Table E-18 CO_2 sorption on Poly[VBTMA][Lys], 10 bar, 298 K

Time (min)	P (bar)	P (atm)	Zeq	mol	mol/mol
0	0	0	0	0	0
5	7.84	7.73808	0.9556	-6.38227E-06	-0.04102
10	7.83	7.72821	0.9556	3.99992E-05	0.257064
20	7.82	7.71834	0.9557	8.99969E-05	0.578386
30	7.81	7.70847	0.9557	0.000136208	0.875373
50	7.8	7.6986	0.9558	0.00018619	1.196597
60	7.79	7.68873	0.9559	0.000236162	1.517753
70	7.78	7.67886	0.9559	0.000282364	1.814679
90	7.77	7.66899	0.956	0.000332321	2.135737
100	7.76	7.65912	0.956	0.000378517	2.432631
110	7.76	7.65912	0.956	0.000378517	2.432631
130	7.75	7.64925	0.9561	0.000428459	2.753591
170	7.75	7.64925	0.9561	0.000428459	2.753591
200	7.75	7.64925	0.9561	0.000428459	2.753591
300	7.75	7.64925	0.9561	0.000428459	2.753591
360	7.75	7.64925	0.9561	0.000428459	2.753591
390	7.75	7.64925	0.9561	0.000428459	2.753591

Table E-19 CO2 sorption on Poly[VBTMA][Gly], 3 bar, 298 K

Time (min)	P (bar)	P (atm)	Zeq	mol	mol/mol
0	0	0	0	0	0
5	2.3	2.2701	0.9872	1.40862E-05	0.070537
10	2.3	2.2701	0.9872	1.40862E-05	0.070537
20	2.29	2.26023	0.9872	5.97729E-05	0.299313
30	2.29	2.26023	0.9872	5.97729E-05	0.299313
60	2.28	2.25036	0.9873	0.000106515	0.533373
90	2.28	2.25036	0.9873	0.000106515	0.533373
120	2.27	2.24049	0.9874	0.000153247	0.767385
150	2.27	2.24049	0.9874	0.000153247	0.767385
180	2.27	2.24049	0.9874	0.000153247	0.767385
210	2.27	2.24049	0.9874	0.000153247	0.767385
240	2.27	2.24049	0.9874	0.000153247	0.767385
270	2.27	2.24049	0.9874	0.000153247	0.767385
300	2.27	2.24049	0.9874	0.000153247	0.767385

Table E-20 CO_2 sorption on Poly[VBTMA][Gly], 5 bar, 298 K

Time (min)	P (bar)	P (atm)	Zeq	mol	mol/mol
0	0	0	0	0	0
5	3.84	3.79008	0.9785	2.3763E-05	0.118993
10	3.83	3.78021	0.9786	7.15742E-05	0.358409
20	3.83	3.78021	0.9786	7.15742E-05	0.358409
30	3.83	3.78021	0.9786	7.15742E-05	0.358409
50	3.82	3.77034	0.9786	0.00011758	0.588783
60	3.82	3.77034	0.9786	0.00011758	0.588783
70	3.81	3.76047	0.9787	0.000165377	0.828126
80	3.81	3.76047	0.9787	0.000165377	0.828126
90	3.8	3.7506	0.9787	0.000211378	1.058476
110	3.8	3.7506	0.9787	0.000211378	1.058476
180	3.8	3.7506	0.9787	0.000211378	1.058476
270	3.8	3.7506	0.9787	0.000211378	1.058476
300	3.8	3.7506	0.9787	0.000211378	1.058476

Table E-21 CO_2 sorption on Poly[VBTMA][Gly], 7 bar, 298 K

Time (min)	P (bar)	P (atm)	Zeq	mol	mol/mol
0	0	0	0	0	0
5	5.43	5.35941	0.9695	3.39048E-05	0.169779
10	5.42	5.34954	0.9695	7.98807E-05	0.400004
20	5.41	5.33967	0.9696	0.000128422	0.643074
30	5.4	5.3298	0.9696	0.000174393	0.873275
60	5.4	5.3298	0.9696	0.000174393	0.873275
90	5.39	5.31993	0.9697	0.00022292	1.116272
100	5.39	5.31993	0.9697	0.00022292	1.116272
120	5.38	5.31006	0.9697	0.000268886	1.34645
180	5.38	5.31006	0.9697	0.000268886	1.34645
210	5.38	5.31006	0.9697	0.000268886	1.34645
240	5.38	5.31006	0.9697	0.000268886	1.34645
270	5.38	5.31006	0.9697	0.000268886	1.34645
300	5.38	5.31006	0.9697	0.000268886	1.34645

Table E-22 CO_2 sorption on Poly[VBTMA][Gly], 10 bar, 298 K

Time (min)	P (bar)	P (atm)	Zeq	mol	mol/mol
0	0	0	0	0	0
5	7.83	7.72821	0.9556	4.95632E-05	0.248188
10	7.82	7.71834	0.9557	9.95544E-05	0.49852
20	7.81	7.70847	0.9557	0.00014576	0.729893
30	7.8	7.6986	0.9558	0.000195736	0.980148
60	7.79	7.68873	0.9559	0.000245701	1.230351
70	7.79	7.68873	0.9559	0.000245701	1.230351
80	7.78	7.67886	0.9559	0.000291897	1.461675
90	7.78	7.67886	0.9559	0.000291897	1.461675
110	7.77	7.66899	0.956	0.000341847	1.711801
210	7.77	7.66899	0.956	0.000341847	1.711801
240	7.77	7.66899	0.956	0.000341847	1.711801
270	7.77	7.66899	0.956	0.000341847	1.711801
300	7.77	7.66899	0.956	0.000341847	1.711801

Table E-23 CO_2 sorption on Poly[VBTMA][Hist], 3 bar, 298 K

Time (min)	P (bar)	P (atm)	Zeq	mol	mol/mol
0	0	0	0	0	0
5	2.3	2.2701	0.9872	1.05412E-05	0.087045
10	2.29	2.26023	0.9872	5.62356E-05	0.464373
20	2.29	2.26023	0.9872	5.62356E-05	0.464373
30	2.28	2.25036	0.9873	0.000102985	0.850415
60	2.28	2.25036	0.9873	0.000102985	0.850415
90	2.27	2.24049	0.9874	0.000149725	1.236379
120	2.27	2.24049	0.9874	0.000149725	1.236379
150	2.27	2.24049	0.9874	0.000149725	1.236379
180	2.27	2.24049	0.9874	0.000149725	1.236379
210	2.27	2.24049	0.9874	0.000149725	1.236379
240	2.27	2.24049	0.9874	0.000149725	1.236379
270	2.27	2.24049	0.9874	0.000149725	1.236379
300	2.27	2.24049	0.9874	0.000149725	1.236379

Table E-24 CO_2 sorption on Poly[VBTMA][Hist], 5 bar, 298 K

Time (min)	P (bar)	P (atm)	Zeq	mol	mol/mol
0	0	0	0	0	0
5	3.84	3.79008	0.9785	1.7771E-05	0.146747
10	3.83	3.78021	0.9786	6.55904E-05	0.541621
20	3.82	3.77034	0.9786	0.000111604	0.921585
30	3.82	3.77034	0.9786	0.000111604	0.921585
60	3.82	3.77034	0.9786	0.000111604	0.921585
90	3.81	3.76047	0.9787	0.000159409	1.31634
120	3.81	3.76047	0.9787	0.000159409	1.31634
150	3.81	3.76047	0.9787	0.000159409	1.31634
180	3.81	3.76047	0.9787	0.000159409	1.31634
210	3.81	3.76047	0.9787	0.000159409	1.31634
240	3.81	3.76047	0.9787	0.000159409	1.31634
270	3.81	3.76047	0.9787	0.000159409	1.31634
300	3.81	3.76047	0.9787	0.000159409	1.31634

Table E-25 CO_2 sorption on Poly[VBTMA][Hist], 7 bar, 298 K

Time (min)	P (bar)	P (atm)	Zeq	mol	mol/mol
0	0	0	0	0	0
5	5.44	5.36928	0.9694	-2.69517E-05	-0.29682
10	5.43	5.35941	0.9695	2.16188E-05	0.238092
20	5.43	5.35941	0.9695	2.16188E-05	0.238092
30	5.42	5.34954	0.9695	6.76084E-05	0.744586
60	5.41	5.33967	0.9696	0.000116164	1.279341
90	5.4	5.3298	0.9696	0.000162149	1.785782
120	5.4	5.3298	0.9696	0.000162149	1.785782
150	5.4	5.3298	0.9696	0.000162149	1.785782
180	5.4	5.3298	0.9696	0.000162149	1.785782
210	5.4	5.3298	0.9696	0.000162149	1.785782
240	5.4	5.3298	0.9696	0.000162149	1.785782
270	5.4	5.3298	0.9696	0.000162149	1.785782
300	5.4	5.3298	0.9696	0.000162149	1.785782

Table E-26 CO_2 sorption on Poly[VBTMA][Hist], 10 bar, 298 K

Time (min)	P (bar)	P (atm)	Zeq	mol	mol/mol
0	0	0	0	0	0
5	7.83	7.72821	0.9556	3.71015E-05	0.306371
10	7.82	7.71834	0.9557	8.71014E-05	0.719252
20	7.81	7.70847	0.9557	0.000133315	1.100864
30	7.8	7.6986	0.9558	0.000183299	1.513619
60	7.8	7.6986	0.9558	0.000183299	1.513619
90	7.79	7.68873	0.9559	0.000233273	1.926287
120	7.79	7.68873	0.9559	0.000233273	1.926287
150	7.78	7.67886	0.9559	0.000279477	2.307819
180	7.78	7.67886	0.9559	0.000279477	2.307819
210	7.78	7.67886	0.9559	0.000279477	2.307819
240	7.78	7.67886	0.9559	0.000279477	2.307819
270	7.78	7.67886	0.9559	0.000279477	2.307819
300	7.78	7.67886	0.9559	0.000279477	2.307819

Table E-27 CO_2 sorption on Poly[VBTMA][Ala], 3 bar, 298 K

Time (min)	P (bar)	P (atm)	Zeq	mol	mol/mol
0	0	0	0	0	0
5	2.3	2.2701	0.9872	1.18567E-05	0.052232
10	2.29	2.26023	0.9872	5.75482E-05	0.253516
20	2.28	2.25036	0.9873	0.000104295	0.459449
30	2.27	2.24049	0.9874	0.000151032	0.66534
60	2.27	2.24049	0.9874	0.000151032	0.66534
90	2.26	2.23062	0.9874	0.000196714	0.866583
120	2.26	2.23062	0.9874	0.000196714	0.866583
150	2.26	2.23062	0.9874	0.000196714	0.866583
180	2.26	2.23062	0.9874	0.000196714	0.866583
210	2.26	2.23062	0.9874	0.000196714	0.866583
240	2.26	2.23062	0.9874	0.000196714	0.866583
270	2.26	2.23062	0.9874	0.000196714	0.866583
300	2.26	2.23062	0.9874	0.000196714	0.866583

Table E-28 CO_2 sorption on Poly[VBTMA][Ala], 5 bar, 298 K

Time (min)	P (bar)	P (atm)	Zeq	mol	mol/mol
0	0	0	0	0	0
5	3.84	3.79008	0.9785	1.99674E-05	0.087962
10	3.83	3.78021	0.9786	6.77837E-05	0.298607
20	3.82	3.77034	0.9786	0.000113794	0.501297
30	3.82	3.77034	0.9786	0.000113794	0.501297
60	3.81	3.76047	0.9787	0.000161596	0.711877
90	3.8	3.7506	0.9787	0.000207602	0.914547
120	3.8	3.7506	0.9787	0.000207602	0.914547
150	3.8	3.7506	0.9787	0.000207602	0.914547
180	3.8	3.7506	0.9787	0.000207602	0.914547
210	3.8	3.7506	0.9787	0.000207602	0.914547
240	3.8	3.7506	0.9787	0.000207602	0.914547
270	3.8	3.7506	0.9787	0.000207602	0.914547
300	3.8	3.7506	0.9787	0.000207602	0.914547

Table E-29 CO_2 sorption on Poly[VBTMA][Ala], 7 bar, 298 K

Time (min)	P (bar)	P (atm)	Zeq	mol	mol/mol
0	0	0	0	0	0
5	5.43	5.35941	0.9695	2.85138E-05	0.125611
10	5.42	5.34954	0.9695	7.44947E-05	0.32817
20	5.41	5.33967	0.9696	0.000123041	0.542031
30	5.4	5.3298	0.9696	0.000169017	0.744569
60	5.39	5.31993	0.9697	0.000217549	0.958365
90	5.39	5.31993	0.9697	0.000217549	0.958365
120	5.38	5.31006	0.9697	0.00026352	1.160882
150	5.38	5.31006	0.9697	0.00026352	1.160882
180	5.38	5.31006	0.9697	0.00026352	1.160882
210	5.38	5.31006	0.9697	0.00026352	1.160882
240	5.38	5.31006	0.9697	0.00026352	1.160882
270	5.38	5.31006	0.9697	0.00026352	1.160882
300	5.38	5.31006	0.9697	0.00026352	1.160882

Table E-30 CO_2 sorption on Poly[VBTMA][Ala], 10 bar, 298 K

Time (min)	P (bar)	P (atm)	Zeq	mol	mol/mol
0	0	0	0	0	0
5	7.83	7.72821	0.9556	4.16961E-05	0.183683
10	7.82	7.71834	0.9557	9.16927E-05	0.403933
20	7.81	7.70847	0.9557	0.000137903	0.607502
30	7.8	7.6986	0.9558	0.000187884	0.827684
60	7.8	7.6986	0.9558	0.000187884	0.827684
90	7.79	7.68873	0.9559	0.000237855	1.04782
120	7.79	7.68873	0.9559	0.000237855	1.04782
150	7.78	7.67886	0.9559	0.000284056	1.251347
180	7.78	7.67886	0.9559	0.000284056	1.251347
210	7.78	7.67886	0.9559	0.000284056	1.251347
240	7.78	7.67886	0.9559	0.000284056	1.251347
270	7.78	7.67886	0.9559	0.000284056	1.251347
300	7.78	7.67886	0.9559	0.000284056	1.251347

Table E-31 CO_2 sorption on Poly[VBTMA][Arg], 1 bar, 313.15 K

Time (min)	P (bar)	P (atm)	Zeq	mol	mol/mol
0	0	0	0	0	0
5	0.75	0.74025	0.9964	-3.83762E-05	-0.26818
10	0.74	0.73038	0.9964	6.25966E-06	0.043743
20	0.73	0.72051	0.9965	5.12225E-05	0.357949
30	0.73	0.72051	0.9965	5.12225E-05	0.357949
60	0.73	0.72051	0.9965	5.12225E-05	0.357949
90	0.72	0.71064	0.9966	9.61763E-05	0.672092
120	0.72	0.71064	0.9966	9.61763E-05	0.672092
150	0.72	0.71064	0.9966	9.61763E-05	0.672092
180	0.72	0.71064	0.9966	9.61763E-05	0.672092
210	0.72	0.71064	0.9966	9.61763E-05	0.672092
240	0.72	0.71064	0.9966	9.61763E-05	0.672092
270	0.72	0.71064	0.9966	9.61763E-05	0.672092
300	0.72	0.71064	0.9966	9.61763E-05	0.672092

Table E-32 CO_2 sorption on Poly[VBTMA][Arg], 3 bar, 313.15 K

Time (min)	P (bar)	P (atm)	Zeq	mol	mol/mol
0	0	0	0	0	0
5	2.3	2.2701	0.989	-2.40877E-05	-0.16833
10	2.29	2.26023	0.989	1.95041E-05	0.136297
20	2.28	2.25036	0.9891	6.41008E-05	0.447944
30	2.28	2.25036	0.9891	6.41008E-05	0.447944
60	2.27	2.24049	0.9891	0.000107688	0.752538
90	2.27	2.24049	0.9891	0.000107688	0.752538
120	2.27	2.24049	0.9891	0.000107688	0.752538
150	2.27	2.24049	0.9891	0.000107688	0.752538
180	2.27	2.24049	0.9891	0.000107688	0.752538
210	2.27	2.24049	0.9891	0.000107688	0.752538
240	2.27	2.24049	0.9891	0.000107688	0.752538
270	2.27	2.24049	0.9891	0.000107688	0.752538
300	2.27	2.24049	0.9891	0.000107688	0.752538

Table E-33 CO_2 sorption on Poly[VBTMA][Arg], 5 bar, 313.15 K

Time (min)	P (bar)	P (atm)	Zeq	mol	mol/mol
0	0	0	0	0	0
5	3.85	3.79995	0.9815	3.30374E-05	0.230869
10	3.85	3.79995	0.9815	3.30374E-05	0.230869
20	3.84	3.79008	0.9816	7.82864E-05	0.547075
30	3.84	3.79008	0.9816	7.82864E-05	0.547075
60	3.83	3.78021	0.9816	0.000121828	0.851345
90	3.83	3.78021	0.9816	0.000121828	0.851345
120	3.83	3.78021	0.9816	0.000121828	0.851345
150	3.83	3.78021	0.9816	0.000121828	0.851345
180	3.83	3.78021	0.9816	0.000121828	0.851345
210	3.83	3.78021	0.9816	0.000121828	0.851345
240	3.83	3.78021	0.9816	0.000121828	0.851345
270	3.83	3.78021	0.9816	0.000121828	0.851345
300	3.83	3.78021	0.9816	0.000121828	0.851345

Table E-34 CO_2 sorption on Poly[VBTMA][Arg], 7 bar, 313.15 K

Time (min)	P (bar)	P (atm)	Zeq	mol	mol/mol
0	0	0	0	0	0
5	5.44	5.36928	0.9738	4.70985E-05	0.32913
10	5.43	5.35941	0.9738	9.05862E-05	0.633028
20	5.42	5.34954	0.9739	0.000136494	0.953838
30	5.42	5.34954	0.9739	0.000136494	0.953838
60	5.41	5.33967	0.9739	0.000179977	1.257704
90	5.41	5.33967	0.9739	0.000179977	1.257704
120	5.41	5.33967	0.9739	0.000179977	1.257704
150	5.41	5.33967	0.9739	0.000179977	1.257704
180	5.41	5.33967	0.9739	0.000179977	1.257704
210	5.41	5.33967	0.9739	0.000179977	1.257704
240	5.41	5.33967	0.9739	0.000179977	1.257704
270	5.41	5.33967	0.9739	0.000179977	1.257704
300	5.41	5.33967	0.9739	0.000179977	1.257704

Table E-35 CO_2 sorption on Poly[VBTMA][Arg], 10 bar, 313.15 K

Time (min)	P (bar)	P (atm)	Zeq	mol	mol/mol
0	0	0	0	0	0
5	7.84	7.73808	0.9621	4.74E-06	0.033135
10	7.83	7.72821	0.9621	2.47416E-05	0.172897
20	7.82	7.71834	0.9622	7.20378E-05	0.503409
30	7.81	7.70847	0.9622	0.000115774	0.809046
60	7.8	7.6986	0.9622	0.000159511	1.114683
90	7.79	7.68873	0.9623	0.000206788	1.445063
120	7.79	7.68873	0.9623	0.000206788	1.445063
150	7.79	7.68873	0.9623	0.000206788	1.445063
180	7.79	7.68873	0.9623	0.000206788	1.445063
210	7.79	7.68873	0.9623	0.000206788	1.445063
240	7.79	7.68873	0.9623	0.000206788	1.445063
270	7.79	7.68873	0.9623	0.000206788	1.445063
300	7.79	7.68873	0.9623	0.000206788	1.445063

Table E-36 CO_2 sorption on Poly[VBTMA][Arg], 1 bar, 333.15 K

Time (min)	P (bar)	P (atm)	Zeq	mol	mol/mol
0	0	0	0	0	0
5	0.75	0.74025	0.9971	-3.6047E-05	-0.2519
10	0.74	0.73038	0.9971	5.87975E-06	0.041088
20	0.73	0.72051	0.9971	4.78065E-05	0.334078
30	0.73	0.72051	0.9971	4.78065E-05	0.334078
60	0.73	0.72051	0.9971	4.78065E-05	0.334078
90	0.73	0.72051	0.9971	4.78065E-05	0.334078
120	0.73	0.72051	0.9971	4.78065E-05	0.334078
150	0.73	0.72051	0.9971	4.78065E-05	0.334078
180	0.73	0.72051	0.9971	4.78065E-05	0.334078
210	0.73	0.72051	0.9971	4.78065E-05	0.334078
240	0.73	0.72051	0.9971	4.78065E-05	0.334078
270	0.73	0.72051	0.9971	4.78065E-05	0.334078
300	0.73	0.72051	0.9971	4.78065E-05	0.334078

Table E-37 CO_2 sorption on Poly[VBTMA][Arg], 3 bar, 333.15 K

Time (min)	P (bar)	P (atm)	Zeq	mol	mol/mol
0	0	0	0	0	0
5	2.34	2.30958	0.9908	-2.15679E-05	-0.15072
10	2.33	2.29971	0.9908	1.86296E-05	0.130186
20	2.33	2.29971	0.9908	1.86296E-05	0.130186
30	2.32	2.28984	0.9909	5.97683E-05	0.417668
60	2.32	2.28984	0.9909	5.97683E-05	0.417668
90	2.32	2.28984	0.9909	5.97683E-05	0.417668
120	2.32	2.28984	0.9909	5.97683E-05	0.417668
150	2.32	2.28984	0.9909	5.97683E-05	0.417668
180	2.32	2.28984	0.9909	5.97683E-05	0.417668
210	2.32	2.28984	0.9909	5.97683E-05	0.417668
240	2.32	2.28984	0.9909	5.97683E-05	0.417668
270	2.32	2.28984	0.9909	5.97683E-05	0.417668
300	2.32	2.28984	0.9909	5.97683E-05	0.417668

Table E-38 CO_2 sorption on Poly[VBTMA][Arg], 5 bar, 333.15 K

Time (min)	P (bar)	P (atm)	Zeq	mol	mol/mol
0	0	0	0	0	0
5	3.88	3.82956	0.9847	3.12013E-05	0.218039
10	3.88	3.82956	0.9847	3.12013E-05	0.218039
20	3.87	3.81969	0.9847	7.16845E-05	0.50094
30	3.87	3.81969	0.9847	7.16845E-05	0.50094
60	3.86	3.80982	0.9848	0.000113754	0.79493
90	3.86	3.80982	0.9848	0.000113754	0.79493
120	3.86	3.80982	0.9848	0.000113754	0.79493
150	3.86	3.80982	0.9848	0.000113754	0.79493
180	3.86	3.80982	0.9848	0.000113754	0.79493
210	3.86	3.80982	0.9848	0.000113754	0.79493
240	3.86	3.80982	0.9848	0.000113754	0.79493
270	3.86	3.80982	0.9848	0.000113754	0.79493
300	3.86	3.80982	0.9848	0.000113754	0.79493

Table E-39 CO_2 sorption on Poly[VBTMA][Arg], 7 bar, 333.15 K

Time (min)	P (bar)	P (atm)	Zeq	mol	mol/mol
0	0	0	0	0	0
5	5.47	5.39889	0.9784	4.42683E-05	0.309352
10	5.46	5.38902	0.9784	8.47281E-05	0.59209
20	5.46	5.38902	0.9784	8.47281E-05	0.59209
30	5.45	5.37915	0.9785	0.000127442	0.890577
60	5.45	5.37915	0.9785	0.000127442	0.890577
90	5.44	5.36928	0.9785	0.000167897	1.173286
120	5.44	5.36928	0.9785	0.000167897	1.173286
150	5.44	5.36928	0.9785	0.000167897	1.173286
180	5.44	5.36928	0.9785	0.000167897	1.173286
210	5.44	5.36928	0.9785	0.000167897	1.173286
240	5.44	5.36928	0.9785	0.000167897	1.173286
270	5.44	5.36928	0.9785	0.000167897	1.173286
300	5.44	5.36928	0.9785	0.000167897	1.173286

Table E-40 CO_2 sorption on Poly[VBTMA][Arg], 10 bar, 333.15 K

Time (min)	P (bar)	P (atm)	Zeq	mol	mol/mol
0	0	0	0	0	0
5	7.93	7.82691	0.9687	0.000004	0.027952
10	7.92	7.81704	0.9687	0.0000404	0.28232
20	7.91	7.80717	0.9687	6.47E-05	0.45196
30	7.9	7.7973	0.9687	0.000105045	0.734068
50	7.89	7.78743	0.9687	0.000145415	1.016175
90	7.88	7.77756	0.9687	0.000185784	1.298282
120	7.88	7.77756	0.9688	0.000189068	1.321228
150	7.88	7.77756	0.9688	0.000189068	1.321228
180	7.88	7.77756	0.9688	0.000189068	1.321228
210	7.88	7.77756	0.9688	0.000189068	1.321228
240	7.88	7.77756	0.9688	0.000189068	1.321228
270	7.88	7.77756	0.9688	0.000189068	1.321228
300	7.88	7.77756	0.9688	0.000189068	1.321228

Table E-41 CO_2 sorption on [VBMI][Lys], 1 bar, 298 K

Time (min)	P (bar)	P (atm)	Zeq	mol	mol/mol
0	0	0	0	0	0
5	0.75	0.74025	0.9958	5.83619E-06	0.013401
10	0.74	0.73038	0.9959	5.24533E-05	0.120444
20	0.73	0.72051	0.9959	9.87219E-05	0.226686
30	0.73	0.72051	0.9959	9.87219E-05	0.226686
60	0.72	0.71064	0.996	0.000145325	0.333697
90	0.72	0.71064	0.996	0.000145325	0.333697
120	0.71	0.70077	0.9961	0.000191919	0.440686
150	0.71	0.70077	0.9961	0.000191919	0.440686
180	0.71	0.70077	0.9961	0.000191919	0.440686
210	0.71	0.70077	0.9961	0.000191919	0.440686
240	0.71	0.70077	0.9961	0.000191919	0.440686
270	0.71	0.70077	0.9961	0.000191919	0.440686
300	0.71	0.70077	0.9961	0.000191919	0.440686

Table E-42 CO_2 sorption on [VBPPN][Lys], 1 bar, 298 K

Time (min)	P (bar)	P (atm)	Zeq	mol	mol/mol
0	0	0	0	0	0
5	0.75	0.74025	0.9958	2.0665E-06	0.009338
10	0.74	0.73038	0.9959	4.87342E-05	0.220218
20	0.73	0.72051	0.9959	9.50531E-05	0.429521
30	0.73	0.72051	0.9959	9.50531E-05	0.429521
60	0.72	0.71064	0.996	0.000141707	0.640338
90	0.72	0.71064	0.996	0.000141707	0.640338
120	0.72	0.71064	0.996	0.000141707	0.640338
150	0.72	0.71064	0.996	0.000141707	0.640338
180	0.72	0.71064	0.996	0.000141707	0.640338
210	0.72	0.71064	0.996	0.000141707	0.640338
240	0.72	0.71064	0.996	0.000141707	0.640338
270	0.72	0.71064	0.996	0.000141707	0.640338
300	0.72	0.71064	0.996	0.000141707	0.640338

Table E-43 CO_2 sorption on [VBTEA][Lys], 1 bar, 298 K

Time (min)	P (bar)	P (atm)	Zeq	mol	mol/mol
0	0	0	0	0	0
5	0.75	0.74025	0.9958	9.01433E-06	0.01927
10	0.74	0.73038	0.9959	5.5624E-05	0.118906
20	0.73	0.72051	0.9959	0.000101885	0.217797
30	0.72	0.71064	0.996	0.000148481	0.317403
60	0.71	0.70077	0.9961	0.000195067	0.416989
90	0.7	0.6909	0.9961	0.000241319	0.51586
120	0.7	0.6909	0.9961	0.000241319	0.51586
150	0.69	0.68103	0.9962	0.000287892	0.615416
180	0.69	0.68103	0.9962	0.000287892	0.615416
210	0.69	0.68103	0.9962	0.000287892	0.615416
240	0.69	0.68103	0.9962	0.000287892	0.615416
270	0.69	0.68103	0.9962	0.000287892	0.615416
300	0.69	0.68103	0.9962	0.000287892	0.615416

Table E-44 CO_2 sorption on [VBTBA][Lys], 1 bar, 298 K

Time (min)	P (bar)	P (atm)	Zeq	mol	mol/mol
0	0	0	0	0	0
5	0.75	0.74025	0.9958	8.6637E-06	0.027469
10	0.74	0.73038	0.9959	5.52775E-05	0.175262
20	0.74	0.73038	0.9959	5.52775E-05	0.175262
30	0.73	0.72051	0.9959	0.000101543	0.321949
60	0.73	0.72051	0.9959	0.000101543	0.321949
90	0.72	0.71064	0.996	0.000148143	0.469698
120	0.72	0.71064	0.996	0.000148143	0.469698
150	0.71	0.70077	0.9961	0.000194733	0.617416
180	0.71	0.70077	0.9961	0.000194733	0.617416
210	0.71	0.70077	0.9961	0.000194733	0.617416
240	0.71	0.70077	0.9961	0.000194733	0.617416
270	0.71	0.70077	0.9961	0.000194733	0.617416
300	0.71	0.70077	0.9961	0.000194733	0.617416

Table E-45 CO_2 sorption poly[VBMI][Lys], 1 bar, 298 K

Time (min)	P (bar)	P (atm)	Zeq	mol	mol/mol
0	0	0	0	0	0
5	0.75	0.74025	0.9958	4.7747E-06	0.016447
10	0.74	0.73038	0.9959	5.14136E-05	0.177105
20	0.73	0.72051	0.9959	9.77039E-05	0.336562
30	0.72	0.71064	0.996	0.000144329	0.497171
60	0.72	0.71064	0.996	0.000144329	0.497171
90	0.71	0.70077	0.9961	0.000190944	0.657748
120	0.71	0.70077	0.9961	0.000190944	0.657748
150	0.7	0.6909	0.9961	0.000237225	0.817173
180	0.7	0.6909	0.9961	0.000237225	0.817173
210	0.7	0.6909	0.9961	0.000237225	0.817173
240	0.7	0.6909	0.9961	0.000237225	0.817173
270	0.7	0.6909	0.9961	0.000237225	0.817173
300	0.7	0.6909	0.9961	0.000237225	0.817173
330	0.7	0.6909	0.9961	0.000237225	0.817173
360	0.7	0.6909	0.9961	0.000237225	0.817173
390	0.7	0.6909	0.9961	0.000237225	0.817173

Table E-46 CO_2 sorption poly[VBPPN][Lys], 1 bar, 298 K

Time (min)	P (bar)	P (atm)	Zeq	mol	mol/mol
0	0	0	0	0	0
5	0.75	0.74025	0.9958	4.63412E-06	0.023887
10	0.74	0.73038	0.9959	5.12648E-05	0.264252
20	0.73	0.72051	0.9959	9.9542E-05	0.513103
30	0.72	0.71064	0.996	0.000146131	0.753253
60	0.71	0.70077	0.9961	0.000192711	0.993356
90	0.71	0.70077	0.9961	0.000192711	0.993356
120	0.71	0.70077	0.9961	0.000192711	0.993356
150	0.71	0.70077	0.9961	0.000192711	0.993356
180	0.71	0.70077	0.9961	0.000192711	0.993356
210	0.71	0.70077	0.9961	0.000192711	0.993356
240	0.71	0.70077	0.9961	0.000192711	0.993356
270	0.71	0.70077	0.9961	0.000192711	0.993356
300	0.71	0.70077	0.9961	0.000192711	0.993356
330	0.71	0.70077	0.9961	0.000192711	0.993356
360	0.71	0.70077	0.9961	0.000192711	0.993356
390	0.71	0.70077	0.9961	0.000192711	0.993356

Table E-47 CO_2 sorption on poly[VBTEA][Lys], 1bar, 298 K

Time (min)	P (bar)	P (atm)	Zeq	mol	mol/mol
0	0	0	0	0	0
5	0.74	0.73038	0.9958	5.29135E-05	0.320688
10	0.74	0.73038	0.9959	5.32572E-05	0.322771
20	0.73	0.72051	0.9959	9.95124E-05	0.603106
30	0.72	0.71064	0.996	0.000146102	0.885467
60	0.72	0.71064	0.996	0.000146102	0.885467
90	0.72	0.71064	0.996	0.000146102	0.885467
120	0.72	0.71064	0.996	0.000146102	0.885467
150	0.72	0.71064	0.996	0.000146102	0.885467
180	0.72	0.71064	0.996	0.000146102	0.885467
210	0.72	0.71064	0.996	0.000146102	0.885467
240	0.72	0.71064	0.996	0.000146102	0.885467
270	0.72	0.71064	0.996	0.000146102	0.885467
300	0.72	0.71064	0.996	0.000146102	0.885467
330	0.72	0.71064	0.996	0.000146102	0.885467
360	0.72	0.71064	0.996	0.000146102	0.885467
390	0.72	0.71064	0.996	0.000146102	0.885467

Table E-48 CO_2 sorption on poly[VBTBA][Lys], 1 bar, 298 K

Time (min)	P (bar)	P (atm)	Zeq	mol	mol/mol
0	0	0	0	0	0
5	0.75	0.74025	0.9958	4.67967E-06	0.017527
10	0.74	0.73038	0.9959	5.13098E-05	0.192171
20	0.73	0.72051	0.9959	9.75913E-05	0.36551
30	0.72	0.71064	0.996	0.000144207	0.540103
60	0.71	0.70077	0.9961	0.000190814	0.71466
90	0.71	0.70077	0.9961	0.000190814	0.71466
120	0.71	0.70077	0.9961	0.000190814	0.71466
150	0.71	0.70077	0.9961	0.000190814	0.71466
180	0.71	0.70077	0.9961	0.000190814	0.71466
210	0.71	0.70077	0.9961	0.000190814	0.71466
240	0.71	0.70077	0.9961	0.000190814	0.71466
270	0.71	0.70077	0.9961	0.000190814	0.71466
300	0.71	0.70077	0.9961	0.000190814	0.71466
330	0.71	0.70077	0.9961	0.000190814	0.71466
360	0.71	0.70077	0.9961	0.000190814	0.71466
390	0.71	0.70077	0.9961	0.000190814	0.71466